PEPTIDE TARGETED DRUG DELIVERY TO NON-SMALL CELL LUNG CANCER

APPROVED BY SUPERVISORY COMMITTEE

Kathlynn Brown, Ph.D.

Jinming Gao, Ph.D.

Philip Thorpe, Ph.D.

Jennifer Kohler, Ph.D.

DEDICATION

I wish to thank the numerous people who contributed to helping me complete this work. First and foremost, I would like to thank my mentor, Dr. Kathlynn Brown, for her guidance throughout the entirety of this project. Her constant optimism and enthusiasm about results made it possible for me to continue through the discouragements and challenges of research. She has been a continual source of support and ideas. I am incredibly grateful for her willingness to take me in to her lab even though I had very little knowledge of biology.

I owe much, as well, to Dr. Michael McGuire, who always so patiently put up with my endless questions and concerns. Thank you Mike, for your constant support, help, and sharing of knowledge. I owe a significant portion of my education to your guidance. I am going to miss having "Mikeapedia" around.

I would also like to thank the members of my dissertation committee, Drs. Jinming Gao, Phil Thorpe, and Jennifer Kohler, for their helpful advice and guidance.

Many thanks to former lab members who continually taught and helped me and who made the lab an enjoyable working environment. Our lab has been a place of friendship in addition to a place of work. I would especially like to thank Dr. Shunzi (Susan) Li for patiently teaching me so many lab techniques and for always being willing to listen and offer experimental ideas. Susan became a great friend and I still miss her presence in lab. Additionally, Lei Wu and Ying-Horng (Steve) Liu both taught me many important lab techniques. I would also like to thank Tracy Diaz for being such a great co-worker and for her support throughout this process.

Many other individuals taught me how to perform a variety of techniques that were crucial for my experiments including, Dr. Erik Bey, Dr. Chase Kessinger, and Dr. Gang Huang. I could not have performed these studies without their help.

A special thanks to my undergraduate research advisor, Dr. Perry Reeves, who has always supported me and who worked so hard to help me succeed.

I have been surrounded by an extensive support system of friends and family throughout my graduate career and am very grateful for all of their support and encouragement. In particular, I wish to thank my parents for all of their love and support. I have the unique privilege of being the daughter of two scientists and realize how lucky I am to have parents who understand graduate school and the challenges, frustrations, and joys of research. Thank you Mom and Dad for your endless support! After writing this dissertation, I am particularly thankful for all of the many papers of my youth that you edited in your attempts to teach me how to write.

Finally, I wish to thank my husband, Nathan. He has supported, encouraged, and helped me throughout this entire process. Despite his own crazy work schedule, he has been willing to run up to lab to open containers or bring me dinner. He has also been an invaluable source of medical knowledge and is always willing to answer my naïve questions. In addition, he has been a source of sanity and stability in my life and has taught me to relax, laugh, and enjoy the craziness of life.

PEPTIDE TARGETED DRUG DELIVERY TO NON-SMALL CELL LUNG CANCER

by

BETHANY POWELL GRAY

DISSERTATION

Presented to the Faculty of the Graduate School of Biomedical Sciences

The University of Texas Southwestern Medical Center at Dallas

In Partial Fulfillment of the Requirements

For the Degree of

DOCTOR OF PHILOSOPHY

The University of Texas Southwestern Medical Center at Dallas

Dallas, Texas

August, 2012

PEPTIDE TARGETED DRUG DELIVERY TO NON-SMALL CELL LUNG CANCER

Bethany Powell Gray

The University of Texas Southwestern Medical Center at Dallas, 2012

Kathlynn C. Brown, Ph.D.

Non-small cell lung cancer (NSCLC) is a notoriously deadly disease. The integrin $\alpha_v\beta_6$ is emerging as a viable target for NSCLC; it is expressed in more than half of NSCLC patient tumor samples and only rarely expressed in normal tissue. Importantly, $\alpha_v\beta_6$ is "turned on" early in the disease progression of NSCLC, indicating that it may be a good biomarker for early cancer detection and treatment. The phage display selected H2009.1 peptide exhibits high affinity for $\alpha_v\beta_6$, specifically binding and internalizing into $\alpha_v\beta_6$-expressing cells.

Tumor targeting therapies that specifically deliver drugs to the tumor, reducing accumulation and toxicity in non-target tissues, are a promising niche of cancer

therapeutics, and the H2009.1 peptide is anticipated to have great utility as a targeting ligand for the delivery of therapeutics to $\alpha_v\beta_6$-positive NSCLC tumors. To examine the ability of the H2009.1 peptide to specifically deliver drugs to NSCLC cells, it was used as a targeting ligand for three different drug platforms: liposomal doxorubicin and direct drug conjugates of both doxorubicin and paclitaxel. Conjugation of the H2009.1 peptide to all three of these drug platforms led to $\alpha_v\beta_6$-specific targeting and toxicity *in vitro*.

In vitro studies determined the ideal construct for H2009.1 peptide targeting of liposomal doxorubicin. Liposomes displaying the higher affinity multivalent H2009.1 tetrameric peptide demonstrated higher specificity and greater toxicity towards $\alpha_v\beta_6$-expressing cells than liposomes displaying the lower affinity monomeric H2009.1 peptide. All H2009.1 peptide liposomal doxorubicin formulations exhibited greater toxicity towards $\alpha_v\beta_6$-expressing cells than control non-targeted liposomes. Both the H2009.1-doxorubicin and paclitaxel conjugates demonstrated $\alpha_v\beta_6$-specific toxicity *in vitro*, although they were less toxic than the respective free drugs and exerted their effects on a later time frame.

Neither H2009.1 peptide-targeted liposomal doxorubicin nor the H2009.1 direct drug conjugates improved *in vivo* efficacy compared to the non-targeted drugs. The liposomes suffered from poor tumor penetration and the *in vitro* studies with the drug conjugates suggest that they suffered from poor intracellular drug release. These results highlight the complexity of drug delivery and targeting *in vivo* and provide a basis for the design of optimized H2009.1 targeting therapies.

TABLE OF CONTENTS

PRIOR PUBLICATIONS

Li S, **Gray BP**, McGuire MJ, Brown KC. Synthesis and Biological Evaluation of a Peptide-Paclitaxel Conjugate which Targets the Integrin αvβ6. Bioorganic & Medicinal Chemistry. 2011;19(18):5480-5489.

Powell BD, Powell GL, Reeves PC. Phosphonium Ionic Liquids as Solvents for Nitration Reactions of Arenes. Letters in Organic Chemistry. 2005;2(6):550-553.

LIST OF FIGURES

LIST OF TABLES

LIST OF SCHEMES

LIST OF ABBREVIATIONS

Ac – Acetylated

Acm – Acetamidomethyl

AD – Adenocarcinoma

ALK – Anaplastic lymphoma kinase

BCIP – Bromo-chloro-indolyl-phosphate

BMPH - *N*-β-maleimidopropionic acid hydrazide trifluoroacetic acid salt

CDT – Covalent DNA display

CMC – Critical micelle concentration

DCC - *N*,*N*'-Dicyclohexyl-carbodiimide

DiI - 1,1'-Dioctadecyl-3,3,3',3'-Tetramethylindocarbocyanine Perchlorate

DiR - 1,1'-Dioctadecyl-3,3,3',3'-Tetramethylindotricarbocyanine Iodide

DSPE-PEG_{2000}-maleimide - 1,2-distearoyl-*sn*-glycero-3-phosphoethanolamine-N-[maleimide(polyethylene glycol)-2000]

DSPE-PEG_{20000} - 1,2-distearoyl-*sn*-glycero-3-phosphoethanolamine-N-[methoxy(polyethylene glycol)-2000]

DTT – dithiothreitol

E. coli – Escherichia coli

EDT – Ethanedithiol

EGFR – Epidermal growth factor receptor

ER - Endoplasmic reticulum

FACS – Fluorescence-activated cell sorting

FBS – Fetal bovine serum

FDA – Food and Drug Administration

FITC – Fluorescein

FMDV – Foot-and-mouth disease virus

GFP – Green fluorescent protein

GMP – Good Manufacturing Practices

Golgi - Golgi apparatus

HBS – HEPES buffered saline

HBTU - 2-(1*H*-benzotriazole-1-yl)-1,1,3,3-tetramethyluronium hexafluorophosphate

HDAC – Histone deacetylase

HL – Hodgkin's lymphoma

HOBt – Hydroxybenzotriazole

HPLC – High-performance liquid chromatography

HSPC - Hydrogenated soy L-α-phophatidylcholine

kDa – Kilodaltons

Lab – Laboratory

LC – Large-cell

LCM – Laser capture microdissection

LHRH – Luteinizing-hormone-releasing hormone

MALDI - Matrix-assisted laser desorption/ionization

MFI – Mean fluorescence intensity

MPM – Malignant pleural mesothelioma

NMM - *N*-Methylmorpholine

NSCLC - Non-small cell lung cancer

OBOC – One-bead one-compound

Panning - Biopanning

PBS – Phosphate buffered saline

PEG – Polyethylene glycol

PET – Positron emission tomography

Phage – Bacteriophage

Phage display – Bacteriophage display

PI – Propidium iodide

PNA – Peptide nucleic acid

PS-SPCL – Positional scanning synthetic peptide library

R5 – RPMI 1640 supplemented with 5% fetal bovine serum

rGel - Gelonin

RT – Radiation therapy

SABR – Stereotactic ablative radiotherapy

sALCL – Systemic anaplastic large cell lymphoma

SBRT – Stereotactic body radiation therapy

SCLC – Small cell lung cancer

SPIO – Superparamagnetic iron oxide

SQ – Squamous carcinoma

TFA – Trifluoroacetic acid

TKI – Tyrosine kinase inhibitor

U.S. – United States

UV – Ultraviolet

VEGF – Vascular endothelial growth factor

VEGFR – Vascular endothelial growth factor receptor

CHAPTER ONE

INTRODUCTION AND LITERATURE REVIEW

1.1 Problem of and Significance of Lung Cancer

Lung cancer is the leading cause of cancer incidence and death worldwide, affecting 1.6 million people and killing 1.4 million yearly.[1] In the United States (U.S.) alone, lung cancer is the second leading cause of death, behind heart disease,[2] and more people die of lung and bronchial cancer than prostate, breast, and pancreatic cancers combined.[3] Unfortunately, lung cancer often remains undetected until patients experience symptoms common to late stage disease,[4] resulting in more than half of patients receiving an initial diagnosis of metastatic disease with a very poor prognosis.[3] Significantly, only 16% of lung cancer patients live to 5 years after diagnosis, and only 4% of these surviving patients were originally diagnosed with metastatic disease.[3] Despite many advances in scientific knowledge and an increase in therapeutic options, patient survival has changed little since 1975.[3] Clearly new treatments are needed for this deadly disease.

The major risk factor for developing lung cancer is exposure to smoking tobacco; 85% of lung cancer deaths are smoking related,[5] attributed either to current or former smokers, or to secondhand smoke. While smoking cessation could prevent the majority of lung cancer cases, the 15% of lung cancer cases not related to smoking are by themselves the 6th leading cause of cancer death in the U.S. Even if future public health initiatives successfully reduce smoking incidence, lung cancer will remain a treatment challenge.

1.1.1 *Pathology of Lung Cancer*

Lung cancer is a complex and diverse disease that encompasses different tumor types arising from the lung. Based on underlying biology, therapeutic options, and patient prognosis, lung cancer is divided into 2 main histologic classes: non-small cell lung cancer (NSCLC) and small cell lung cancer (SCLC).[6] Over 85% of lung cancers are categorized as NSCLC, and NSCLC is further subdivided into either non-squamous carcinoma or squamous cell carcinoma.[6] Non-squamous carcinoma encompasses several different types of lung cancer, including adenocarcinoma, large-cell carcinoma and other less common cancers.[6] Smokers are more likely to develop small cell or squamous cell carcinoma, while most non-smokers develop adenocarcinoma.[7] Adenocarcinoma is also the most common type of lung cancer in the U.S.[6] The different types of NSCLC typically derive from different cell types. While squamous cell carcinoma arises from lung epithelium, adenocarcinoma often arises from glandular cells.[8] Large cell carcinomas do not have a distinguishing feature and are categorized by a lack of the hallmarks of squamous carcinoma or adenocarcinoma.[8] One of the challenges of lung cancer treatment arises from the large heterogeneity of lung tumors. There are great variations even among each lung cancer subtype. For example, a recent mRNA expression profiling of patient lung tumors revealed that adenocarcinoma comprises four distinct biological subclasses and that one of these subclasses, distinct for high expression of neuroendocrine genes, is associated with poor patient survival.[9] Approximately half of all tumors comprise more than one of the major histopathological types,[8] making it difficult to classify tumors for later therapy decisions. The distinction between SCLC and NSCLC is of particular importance, as treatments differ greatly between the two classes.

1.1.2 NSCLC Staging

While pathological analysis determines the NSCLC subtype, lung cancer staging is based upon tumor anatomy and location. The International Association of the Study of Lung Cancer recently revised the lung cancer staging system, which is based upon the TNM system commonly used for cancers.[10] In this system, three separate parameters determine tumor stage: T, the magnitude and location of the primary tumor; N, the infection of regional lymph nodes and location of these nodes; and M, the extent of distant metastasis.[11] Different combinations of T, N, and M stages combine to give an overall stage of 0-IV, (with stages I-III further subdividing into A or B subtypes).[10, 12] The staging process is complex and not easily generalized. Stage O refers to carcinoma in situ, a grouping of abnormal cells with the potential to form lung cancer. Stage I lung cancers are isolated tumors no larger than 5 cm with no metastasis to regional lymph nodes. Stage II includes tumors greater than 5 cm without lymph node metastasis or less than 7 cm with metastasis into lymph nodes in the same side of the lung or bronchus as the primary tumor. Patients with stage II cancer can also have multiple tumors in the same lobe of the lung. Stage III is a broad category encompassing 15 different combinations of T, N, and M states. In general terms, stage III tumors can be any size and can spread into any of the regional lymph nodes – including lymph nodes on the same side or the opposite side of the chest as the primary tumor. Patients can also have multiple tumors in the same lobe or in different lobes of the same lung. Significantly, the stage III classification also includes tumor that have metastasized into nearby structures such as the heart, trachea, esophagus, major blood vessels, and sternum. Stage IV tumors

are the most advanced tumors and can be any size and have any type of lymph node metastasis. However, all stage IV tumors either involve one or more tumor in both lungs; a malignant pleural effusion, in which cancer cells are found in the fluid surrounding the heart or lungs; or metastasis to distant organs such as the brain or bone. Unfortunately, most NSCLC cases are detected at the later metastasized stages III and IV, and not at the earlier more treatable stages of 0-II.

1.2 Current NSCLC Therapies and Limitations

There are three forms of primary treatment currently available for NSCLC: surgery, radiation therapy (RT), and chemotherapy. Each treatment can be used alone or in combination, and varying regimens are used depending on the patient's tumor type and stage.

1.2.1 *Surgery for NSCLC*

The ideal treatment for patients with stage I or II NSCLC is surgery.[13] Resection of lung tumors offers these patients their best chance for a complete cure.[13] However, surgery is not limited to those with early stage disease and may also be an appropriate part of the treatment plan for select patients with stage III disease, although it is only rarely performed on patients with stage IV disease.[13] The preferred surgical procedure is a lobectomy, in which the infected lobe of the lung is removed.[14] If necessary, the entire infected lung can be removed in a surgery known as a pneumonectomy.[14] Patients ineligible for a lobectomy due to limited lung function or comorbid disease can undergo a wedge resection or segmentectomy, in which a wedge or section of the infected lobe of

the lung is removed.[14] However, despite all of these available surgerical interventions, many patients with early stage disease relapse after surgery. Depending on the initial site of the lung tumor and the type of surgical procedure used, anywhere from 35-63% of stage I patients succumb to the disease by 5 years after diagnosis.[15] Clearly other treatment options are needed for patients.

1.2.2 *Radiation Therapy for NSCLC*

Radiation therapy (RT) is the best option for stage I NSCLC patients who are medically unfit for surgery, older in age, or resistant to surgery.[13] RT works by exposing tissue to ionizing radiation, which damages the DNA of exposed cells, leading to cell death. Traditionally, low doses of radiation are administered over a period of several months. However, the more precise stereotactic ablative radiotherapy (SABR), or stereotactic body RT (SBRT), technique is recommended for stage I patients.[13] SABR precisely delivers high doses of radiation to a patient-tailored region of interest over a period of several weeks.[16] Thanks to advances in RT such as SABR, RT alone now cures approximately 15% of early stage patients.[4]

In addition to its use as a primary treatment, RT is used as an adjuvant therapy for some stage II and III patients post-surgery.[13] RT is also commonly used in conjunction with chemotherapy, for a treatment termed chemoradiotherapy. Chemoradiotherapy is the first line of treatment for patients with stage II or III tumors that are inoperable, and if the patient's health allows, the RT and chemotherapy are administered concurrently.[17] For patients with advanced Stage IV NSCLC, RT is primarily used as a palliative treatment to relieve symptoms and is directed at either the

site of the tumor or at metastases.[13] While these many uses make RT an important part of NSCLC treatment, the poor prognosis of NSCLC patients indicates that RT alone or in combination with other currently available treatments is insufficient to offer the majority of NSCLC patients a cure. Additionally, RT is not entirely selective for cancer cells. Ionizing radiation primarily kills dividing cells; faster growing cancer cells are therefore more susceptible to RT but slower growing normal cells are also affected. The location of the lung tumor must be carefully considered before beginning RT as normal tissues can be extensively damaged by treatment.[18] The use of SABR for centrally located tumors or for those located near the chest wall or the brachial plexus can lead to severe injuries, including paralysis or death.[18-20] Therefore, certain tumor locations are not amenable to such RT. In particular, patients with lung tumors near the central airways should not be treated with SBRT due to risk of radiation-induced death.[19]

1.2.3 *Chemotherapy for NSCLC*

Chemotherapy was first used against lung cancer in the 1940s, in the form of nitrogen mustard.[4] Subsequent studies with other chemotherapy drugs failed to show any significant survival or tumor growth inhibition benefit for single-agent chemotherapies[21] and chemotherapy was largely considered ineffective for patients with NSCLC.[22] However, in the late 1970s-1980s, studies first demonstrated that combinations of chemotherapy drugs, primarily combinations of cisplatin with either an etoposide or a vinca alkaloid - such as vindesine or vinblastine - showed activity against NSCLC.[4, 21, 23] Additional studies conducted during the following decades demonstrated that doublet chemotherapy regimens (two chemotherapy drugs given in combination) modestly

improve patient survival and decrease unwanted symptoms.[4, 21, 22] These doublet chemotherapy treatments always center around a platinum-based chemotherapeutic – cisplatin or carboplatin – with the addition of a second chemotherapeutic.[4, 21, 22]

Currently, chemotherapy for early stage NSCLC treatment is generally given either as an adjuvant therapy to surgery or as part of a chemoradiotherapy treatment.[13] Patients with stage I or II disease often receive adjuvant chemotherapy post-surgery.[13] Treatment of stage III disease is more complex and controversial, with patients receiving some combination of chemotherapy, surgery, and RT.[13] Stage IV NSCLC patients also benefit from combination chemotherapy, which produces 1-year survival rates of 30-40%.[13] Platinum-based regimens are also primarily used for these patients.[13] Despite the variety of chemotherapy drugs and regimens available for NSCLC, patient response to these drugs is only modest. Significantly, despite the more recent use of various drug combinations, patient survival has changed little since 1975, and the 5-year survival rate is still only 16%.[3]

1.2.4 *Moleculary Targeted Therapies for NSCLC*

Recently, molecularly targeted therapies have garnered significant attention and much of the focus on new therapies for NSCLC lies in these tailored treatments. Increased knowledge of the biology behind lung cancer has led to the identification of different pathways and molecules that drive cells to transform from normal to cancerous. Frequently, known oncogenes or tumor suppressors undergo either genetic changes, such as gene amplification or deletion, or epigenetic changes, leading to aberrant activation of signaling pathways that maintain the cancerous cellular state.[4] If the cancer cells are

dependent on one or a few of these altered genes, and unable to survive once these genes are inhibited, drugs can be designed to specifically target the cancer-driving gene or genes.[4] These specific drugs are commonly referred to as molecularly targeted therapies, or simply, as targeted therapies.

There are a large variety of molecularly targeted therapies currently in clinical trials for NSCLC, including oncogenic tyrosine kinase inhibitors (such as EGFR and VEGR pathway inhibitors), angiogenic tyrosine kinase inhibitors, tumor suppressor therapies, proteasome inhibitors, histone deacetylase (HDAC) inhibitors, and telomerase inhibitors.[4] Several therapies are already used clinically. The recombinant monoclonal antibody bevacizumab (Avastin®) inhibits the vascular endothelial growth factor (VEGF)/ VEGF receptor (VEGFR) pathway important for lung tumor angiogenesis by binding the VEGF-A ligand important for this pathway.[4] Bevacizumab was approved by the Food and Drug Administration (FDA) in 2006 for select patients with nonsquamous NSCLC, including those unable to undergo surgery with advanced disease.[13] Many targeted inhibitors have been directed against the epidermal growth factor receptor (EGFR) pathway, which is commonly dysregulated in cancer, and is of particular importance in NSCLC. Approximately 70% of all NSCLC tumors overexpress EGFR and its ligands.[4, 24] Several EGFR pathway inhibitors are used clinically, including the tyrosine kinase inhibitors (TKIs), erlotinib (Tarceva®) and gefitinib (Iressa™), and the monoclonal antibody cetuximab (Erbitux®).[13] The FDA approved erlotinib in 2004 as a treatment for patients with advanced or metastatic NSCLC who failed previous chemotherapy treatments. Additionally, erlotinib or gefitinib are used as a first-line therapy for advanced disease patients with an EGFR mutation or gene amplification.[13]

Patients with advanced disease can also be treated with cetuximab in combination with vinorelbine and cisplatin, regardless of whether they have EGFR aberrancy.[13] Recently, the small molecule oncogene inhibitor crizotinib (Xalkori®) has created much excitement. Crizotinib targets the anaplastic lymphoma kinase (ALK) fusion gene and was FDA approved based on an ongoing phase II clinical trial; an impressive >80% of patients with previous therapy-resistant disease responded to treatment.[13] Crizotinib is now recommended as a first-line treatment for patients with advanced disease who are ALK positive.[13]

While advances in targeted molecular therapies for NSCLC are exciting and may greatly benefit those patients whose cancers are driven by gene mutations or translocations, they are not sufficient to successfully treat most NSCLC patients. Although treatment with the EGFR inhibitor gefitinib significantly increased 1-year progression-free survival from 6.7% for patients receiving traditional chemotherapy to 24.9% for patients receiving gefitinib, this means that 75% of patients still progressed after EGFR inhibitor treatment.[25] Additionally, even though the ALK inhibitor crizotinib looks very promising for patients with the ALK fusion gene, only 6.7% of NSCLC patients have this translocation.[26] Clearly new methods of NSCLC treatment are needed.

1.3 The Case for Targeting Therapies

At the beginning of the 20th century, Paul Ehrlich first introduced the concept of a "magic bullet" drug that would demonstrate high affinity and toxicity against a causative agent without causing any harmful side effects.[27] More than 100 years later, scientists and clinicians alike still search for such a cancer-specific drug. One method for

developing magic bullet therapies is to use tumor-specific ligands for targeting therapies. As opposed to molecularly targeted therapies that seek to inhibit a particular gene or pathway upon which cancer growth is dependent, targeting therapies seek to use ligands that bind tumor cells to specifically deliver drugs to the cancer cells. Ideal tumor targeting ligands are cancer cell specific and can be modified with drugs or toxins; they can then deliver their cargo exclusively to cancer cells, preventing the cargo from accumulating in normal cells.

Targeting therapies are particularly attractive for cancer treatment due to the inherent toxicity and unwanted side effects of chemotherapy drugs. Most chemotherapy drugs are small molecules with little selectivity for tumor tissue. Once in the bloodstream, these drugs distribute throughout the body and only a small fraction of the drug actually reaches the site of the tumor. As most chemotherapeutics are active against any rapidly dividing cells, cells in other areas of the body undergoing division are also sensitive to the drug. Therefore, the inherent distribution of chemotherapeutics to normal organs often results in unwanted and potentially life-threatening toxicities. The therapeutic window for chemotherapies is particularly small, such that the dose required for efficacy often results in such unwanted toxicities.[28] Conjugation of chemotherapeutics to targeting ligands has the potential to avert this unwanted cell death by preventing the drugs from entering normal cells while maintaining specificity for tumor cells.

1.3.1 *Antibody Targeting Therapies*

Antibodies have traditionally been the gold standard of targeting reagents. As antibodies are inherently very selective for their targets, they are ideal ligands for specific

delivery. There are currently 12 monoclonal antibodies approved for clinical use for cancer patients in different countries around world.[29, 30] However, most of these antibodies are not conjugated to any drugs or toxins, and therefore fall into the category of molecularly targeted therapies, like the bevacizumab and cetuximab antibodies approved for NSCLC patients. Such antibodies function passively by either blocking the activity of tumor-required receptors or by activating the immune system to destroy the antibody target.[29] Significantly, there are 3 radiolabeled antibodies and 1 immunotoxin that are clinically approved for cancer and all but 1 are approved in the U.S.[29] Radiolabeled antibodies carry destructive radioactive isotopes while immunotoxins are antibodies conjugated to toxins such as proteins or traditional chemotherapeutics. Two of the radiolabeled antibodies, Zevalin® (ibritumomab tiuxetan) and Bexxar® (Iodine-131 tositumomab), are approved in the U.S.; both are anti-CD20 antibodies used for select patients with non-Hodgkin's lymphoma. A third radiolabeled antibody against DNA associated antigens is approved in China for patients with advanced stage lung cancer. The only approved immunotoxin is also used clinically in the U.S. Adcetris™ (brentuximab vedotin) is an anti-CD30 antibody conjugated to the microtubule-disrupting agent monomethyl auristatin E and is approved for certain patients with Hodgkin's lymphoma (HL) or systemic anaplastic large cell lymphoma (sALCL).[30] Despite the small number of approved antibody conjugates, 44% of the 206 antibodies that entered clinical trials between 1980 and 2005 were either radiolabeled antibodies or immunotoxicins.[29] There is clearly large clinical interest in pursuing antibodies as cancer targeting agents.

Antibody targeting reagents offer many advantages, primarily in their high affinity and specificity for their targets. However, it is also important to note that antibody conjugates can also take advantage of the more passive roles of antibody therapies. Just like their unconjugated counterparts, antibody conjugates are also capable of activating the immune system or of blocking receptor function. Therefore, antibody conjugates may benefit from multiple mechanisms working in conjunction to inhibit tumor growth; both the isotope or toxin conjugated to the antibody and the more passive roles of the antibody may contribute to the efficacy of such conjugates. Despite these advantages, antibodies suffer from several disadvantages. Significantly, it is difficult to chemically modify antibodies and is particularly difficult to manufacture antibody conjugates.[29] The size of immunoconjugates also inhibits their tumor penetration, making it difficult for the conjugates to reach the entirety of the tumor.[31, 32] Additionally, nonspecific clearance of antibodies by the reticuloendothelial system can lead to accumulation of any conjugated drugs or toxins in unwanted sites such as the liver and bone, damaging these organs.[33, 34]

1.3.2 *Peptide Targeting Therapies*

Peptides are an attractive alternative to antibody targeting therapies. Unlike antibodies, peptides are easy to synthesize in large quantities[35] and their smaller size improves tissue penetration while preventing nonspecific uptake by the reticuloendothelial system. Additionally, peptides can be chemically modified to alter affinity, charge, hydrophobicity, stability, and solubility and can be optimized for *in vivo* use through reiterative modifications. Importantly, peptides can display antibody-like

affinities for their receptors. Several naturally occurring peptides, such as Luteinizing-hormone-releasing hormone (LHRH) and somatostatin and their derivatives, are useful for tumor targeting, due to overexpression of their receptors on many cancer cells.[36] However, these peptides bind a minute fraction of the receptors overexpressed on neoplastic cells. Therefore, peptide libraries have been used to select additional peptides that bind to cancerous cells.

Peptide libraries have been used to select a wide variety of peptides that bind to various cell types. These libraries can be divided into two main categories: biological libraries and chemical libraries (Table 1-1). Biological libraries have a genotype, or DNA encoding the peptide sequence, that is linked to the phenotype, or expression of the peptide as part of the library's normal structure. This genotype-phenotype link was first demonstrated for bacteriophage display (phage display),[37] which still remains the major type of combinatorial library in use for the isolation of cell binding peptides. Other types of biological libraries include bacterial, ribosome, mRNA, yeast, cDNA, retrovirus, baculovirus, and mammalian cell display. While all of these library types are promising, only phage, bacterial, and ribosome display have been used to isolate cell binding peptides. Among the numerous types of non-biological combinatorial libraries, one-bead one-compound libraries (OBOC) and positional scanning synthetic peptide libraries (PS-SPCL) are the only types that have been used to isolate peptides that bind to cells. Other types of combinatorial libraries such as microarrays, self-assembled peptide nucleic acid (PNA)-encoded chemical microarrays, CIS display, multipin, SPOT, nanoken, iterative approach, orthogonal partition, recursive deconvolution,

Table 1-1. Comparison of Peptide Libraries

Library Type	Format	Strengths	Weaknesses
Biological Libraries	Phage display	library sizes of 10^8-10^9 different peptides	typically only display natural, L-amino acid peptides
		accommodates large peptide sequences	complicated structures cannot be incorporated
		simply grow the phage in bacteria to produce the library	clone screening is not quantitative
		inexpensive	two hosts, the phage and bacterium
		libraries are commercially available	library amplification requires reinfection
		libraries can be recycled and reused	
		library aliquots can be stored at -80°C for years	
		peptide selection can be done on whole cells *in vitro* or *ex vivo* or *in vivo* in living animals or patients	
	Bacterial display	library sizes of 10^{11} different peptides for *E. coli* libraries	complex bacterial cell surface can interfere with binding of displayed peptide
		easily manipulated both genetically and physically	bacteria other than *E. coli* are limited to a library size of 10^5
		E. coli grows quickly	limited to the rate of the flow cytometer for quantitative results
		large size of bacteria allows for quantitative and high throughput screening using fluorescence-activated cell sorting (FACS)	limited to *in vitro* panning and screening studies
		only one host (the bacterium itself)	
		library amplification does not require reinfection	
		bacteria can be fluorescently labeled for ease of selection	
		commercially available	
Chemical Libraries	Positional Scanning Synthetic Peptide Combinatorial Library (PS-SPCL)	peptides are their own entity (not bound to support), allowing them to interact in solution for use in any assay	libraries are not commercially available
		large number of peptides can be synthesized and used for relatively quick screening (a 6-mer peptide library would contain 64 million different	assumes that each amino acid independently contributes to binding

		peptides)	
		library can be aliquoted for use in multiple assays	requires additional peptide synthesis and testing after the initial screening
	One-bead one-compound (OBOC)	library sizes of 10^6-10^8 compounds	peptides are connected to the beads by linkers, with the potential for steric hindrance between the cellular receptor and peptide
		libraries can be synthesized easily and screened rapidly	chemical structures of identified beads have to be determined
		display of peptides that contain L-amino acids, D-amino acids, or unnatural amino acids	libraries are not commercially available
		peptide selection can be done on whole cells *in vitro* or *ex vivo*	cannot be used to select peptides that internalize *in vitro*
			not available for *in vivo* screening in living animals or patients

affinity selection, *in vitro* compartmentalization, STABLE, and covalent DNA display (CDT) have not been used for cell binding peptide selections.

1.4 Peptide Libraries Used to Select Cancer Cell Targeting Peptides

1.4.1 *Phage Display Peptide Libraries*

Bacteriophage (phage) is a single-stranded DNA virus that infects bacteria and is widely used to generate biological ligand libraries, known as phage display. The field of phage display began with George Smith's discovery in 1985 that foreign DNA sequences could be inserted into coat proteins of filamentous phage without altering phage function.[37] Since that time, phage protein manipulation has allowed for display of numerous ligand types, including peptides, antibodies, and receptors.[38-40] Phage coat proteins are accommodating and allow display of both linear and cyclic, cysteine-disulfide linked peptides. DNA sequences encoding a unique peptide are inserted into the DNA for a phage coat protein such that as the phage assembles, it expresses the protein-peptide fusions and incorporates them into the normal phage structure. The result is a phage that displays a unique peptide on the surface of one of its coat proteins, allowing this peptide to direct phage binding to a target of interest. Peptide phage libraries usually have a diversity of 10^8-10^{10} different phage displaying different peptide sequences. Importantly, phage manipulation is relatively straightforward; phage are easy to grow and amplify by infecting the bacteria *Escherichia coli* (*E. coli*). Additionally, the unique peptide encoded by a phage is easily determined using DNA sequencing.

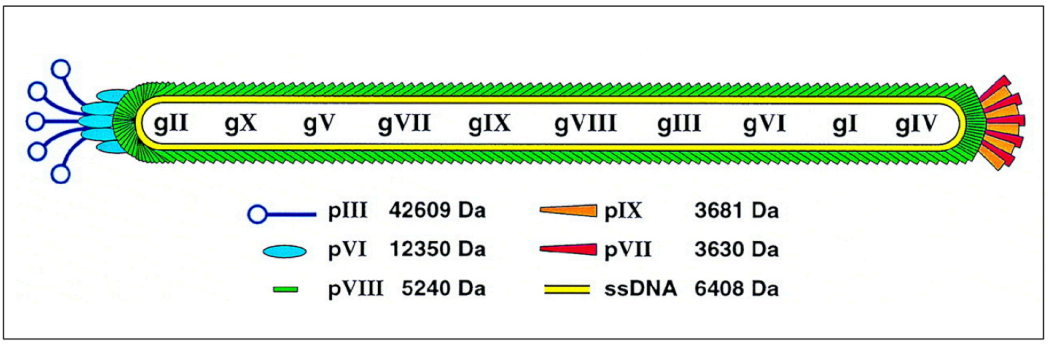

Figure 1-1. Structure of a filamentous phage. Figure from reference 41, copyright PNAS.

1.4.1.1 *Types of Phage Display Libraries*

Nonlytic filamentous phage, which assemble in and secrete from their bacterial hosts without bacterial cell lysis, are commonly used for library construction. The filamentous phage is a flexible rod composed of five capsid protein types encasing a large, circular single strand of DNA (Figure 1-1).[40] The majority of the phage body is comprised of 2700 copies of the major coat protein pVIII, encoded by a single pVIII gene.[40] Both ends of the phage body are composed of minor coat proteins; one end displays 5 copies of both the minor coat proteins pIII and pVI and the other end displays 5 copies of both the minor coat proteins pVII and pIX.[40] While all of the phage proteins can accommodate a foreign peptide sequence, peptides are generally displayed at the N-terminus of the pIII or pVIII proteins.[42] There are two different ways that peptides can be displayed from coat proteins: either every copy of the coat protein can display the peptide or the peptide-displaying coat protein can exist as a hybrid with the normal, wild-type coat protein.[40] As only 5 copies of the pIII protein exist, all pIII peptide libraries

express the peptide on every copy of the pIII protein.[43-46] As the pVIII coat protein exists in so many copies, pVIII display libraries are frequently used in the hybrid form in which only a fraction of the pVIII protein expresses peptides.[47] However, some groups have used a "landscape" display in which all of the pVIII proteins express peptide.[48]

The filamentous phage M13 was the first phage used for polypeptide display[37] and is still attractive due to its ease of replication and ability to accommodate large pieces of foreign DNA. M13 phage displaying peptides from the N-terminus of their pIII protein are widely used due to the commercial availability of 7-mer, 12-mer, and cyclic 7-mer libraries from New England Biolabs®.[46] Dyax Corp also sells M13 pIII display libraries,[49] and a CLIO M13 pIII display library has also been used.[45] The fd filamentous phage is also commonly used for library construction and fd phages are used for pIII,[43] pVIII hybrid,[47] and pVIII landscape display,[48] largely due to vectors generated by George Smith's laboratory (lab). His lab makes available the fuse5 pIII display phage, the f88 pVIII hybrid display phage, and the f8 pVIII landscape display phage.[50]

Filamentous phage based phagemid libraires are also used for peptide display. A phagemid is a plasmid encoding the recombinant peptide-phage protein that contains origins of replication for both bacteria and phage, in addition to an antibiotic resistance gene.[42] While a phagemid can replicate in *E. coli* using its bacterial origin of replication, it does not produce phage unless the bacterium is also infected with a helper phage.[40] This helper phage rescues the expression of the phagemid by producing a phage replication protein that can act on the phagemid vector at the phage origin of replication.[40] Thus, after helper phage infection, the *E. coli* produces two types of phage viruses: one type contains helper phage DNA and the other type contains phagemid

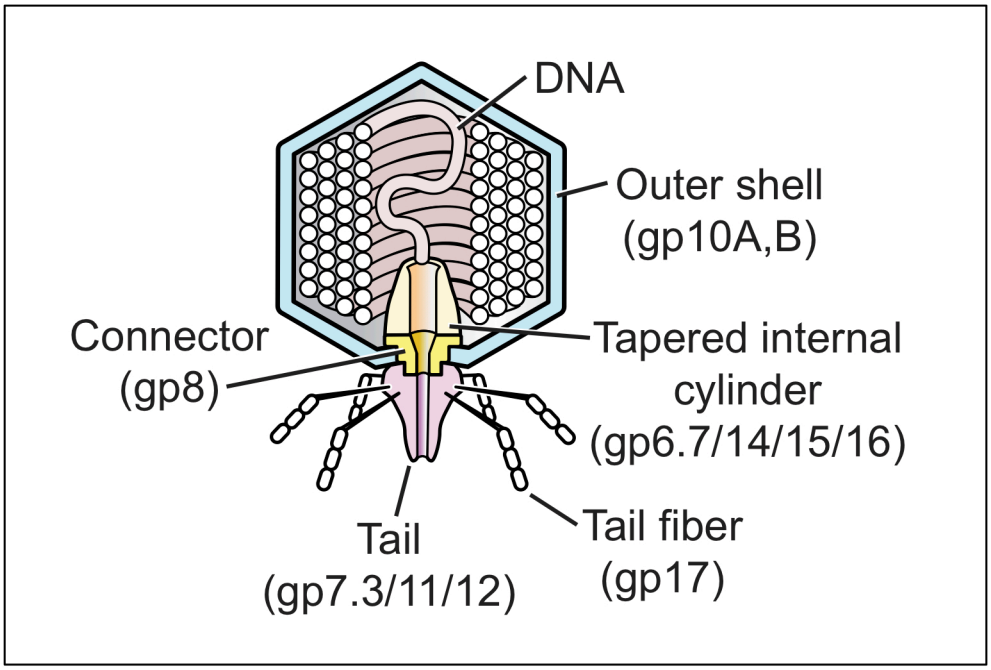

Figure 1-2. Structure of a lytic phage. Figure from reference 51.

DNA.[40] The phagemid DNA usually predominates,[42] generating phage bearing the peptide library-phage coat protein fusions in a hybrid format with the wild-type coat proteins. Two different types of phagemids have been used to select peptides that bind to cancer cells. The first type is a pVIII hybrid display type based on the f1 phage using the phagemid PC89,[52] and the second type is a pCGMT vector phagemid based on the fd phage in which each virus displays a unique peptide on the pVII coat protein and a second unique protein on the pIX coat protein.[53]

Although less common, lytic phages that lyse their bacterial hosts as they exit are also used for phage display of peptides**.** The lytic phage structure is very different from filamentous phage; lytic phages have an icosahedral head and a short tail (Figure 1-2).

The T7 lytic phage species is typically used for phage display. The outer shell of the T7 phage head is comprised of the 10A and 10B capsid proteins, at a total of 415 proteins per head.[54] In the wild-type phage, approximately 10% of the total capsid protein is the 10B form.[55] However, the T7 phage can be modified to express different amounts of 10B verses 10A protein.[56] Novagen's T7Select® Phage Display System, commercially available from EMD Millipore, takes advantage of the ability to change the amount of 10B verses 10A protein, displaying peptide sequences as C-terminal fusions of the 10B protein in 1-415 copies.[56] The T7Select® system has been used by several labs for selection of cancer-cell binding peptides.

1.4.1.2 *Advantages and Disadvantages of Phage Display Libraries*

There are a number of advantages to using biological peptide libraries such as phage display (Table 1-1). Phage display libraries are inexpensive, commercially available, and easy to amplify and reuse by simply allowing the phage to replicate in bacteria. In addition, they can be aliquoted and stored at -80°C for years. Importantly, phage can accommodate large peptide sequences, including cyclic peptides, and typical libraries display from 10^8-10^9 different peptide sequences. Peptide selection can also occur *in vitro*, *ex vivo*, or *in vivo*, as described in more detail later. Phage libraries are tolerant of a variety of selection conditions and can endure harsh washing conditions. Despite these many advantages, phage display is not without disadvantages. While phage are ideal for displaying linear peptides and simple cyclic peptides, they cannot accommodate more complicated chemical structures, such as branched or bicyclic compounds.[38] Additionally, D-amino acids are traditionally difficult to incorporate,[38]

although a recent study demonstrated the ability to incorporate D-amino acids into phage libraries.[57]

1.4.2 *Bacterial Display Peptide Libraries*

1.4.2.1 *Types of Bacterial Display Libraries*

Peptide libraries can also be displayed on the surface of bacteria. The Gram-negative bacterium *E. coli* is the most commonly used bacterium for display libraries[58] and is the only bacterium that has been used for the selection of cell binding peptides. As *E. coli* is easy to manipulate both genetically and physically and grows quickly, it is ideal for display libraries.[58] Typical libraries incorporate up to 10^{11} different peptides.[58] Once libraries are made, they are amplified by growth in typical bacterial liquid culture and specific clones can be isolated by plating the bacteria on agar.[59] *E. coli* libraries are made by genetically incorporating peptides into the membrane flagella and fimbriae proteins. While a variety of different bacterial proteins can be used for these libraries,[58] peptide libraries have been incorporated into FliTrx, OmpA, CPX, and invasin proteins. For all of these display formats, the peptide can be fused to the N or C-terminus of the bacterial protein or inserted into the middle of the protein.[58]

Insertional libraries, where the peptide library is inserted into the middle of the bacterial membrane protein such that it forms a loop that sticks out of the membrane with the N and C terminus of the membrane protein inside the bacterium, include the FliTrx and OmpA libraries. The FliTrx library is particularly convenient as it is commercially available from Life Technologies™. In this type of library, developed by McCoy and colleagues, peptides are inserted in the active site of the *E. coli* thioredoxin protein, and

the entire peptide-thioredoxin protein fusion is subsequently inserted into the *E. coli* flagellin protein.[60] Thioredoxin is used because the active site forms a disulfide bond constrained loop that can accommodate foreign sequences and still fold properly.[60] As the flagellin protein is the major component of the bacteria's flagella, the peptide-thioredoxin-flagellin fusion protein ends up displayed on the cell surface as a partially functional flagella.[60] The unique peptide is displayed in a disulfide bond constrained loop that extends out of the body of the thioredoxin protein, allowing it to bind selectively to the target protein or cell type.[60] Similarly, the OmpA library was created by inserting peptides into a flexible exposed loop of the outer membrane protein A (OmpA).[61]

N-terminal libraries, such as the CPX library, involve fusion of the peptide to the N-terminus of an outer membrane protein. The CPX library involves a rearrangement of the OmpX outer membrane protein such that its N and C-terminus stick outside of the cell membrane.[62] This allows for peptide fusion at either the OmpX N-terminus, C-terminus, or both,[62] although most applications have used the N-terminus of the protein for peptide display.

C-terminal libraries have also been used, such as the invasin library. This library was created by expressing a modified form of the invasin protein from the pathogenic bacterium *Yersinia pseudotuberculosis* in non-pathogenic *E. coli*.[63] Invasin is a bacterial membrane protein that binds to integrins, allowing the *Yersinia pseudotuberculosis* to penetrate mammalian cells.[63] Replacing its integrin-binding C-terminus with a random peptide library and subsequent transformation into *E. coli* results in *E. coli* displaying invasin-peptide fusions at the outer membrane.[63]

1.4.2.2 *Advantages and Disadvantages of Bacterial Display*

Bacterial display libraries also have a number of advantages and disadvantages (Table 1-1). *E. coli* grows quickly and is easy to manipulate both genetically and physically.[58] Significantly, unlike phage libraries, which require both phage and bacteria, bacterial libraries only have one component: the bacteria. This allows for easy library growth and amplification using typical bacterial liquid culture and for the selection of specific clones by plating the bacteria on agar.[59] Another major advantage of bacterial libraries is the ability to use fluorescence-activated cell sorting (FACS) for library screening, allowing for the quantification of clone binding.[64] This screening is relatively straightforward as the bacteria can easily be modified to incorporate a fluorescent label such as green fluorescent protein (GFP).[64] However, the screening process is then limited to the rate of the flow cytometer, which can significantly slow the selection process.[59] Other disadvantages include the complexity of the bacterial surface, which may interfere with binding of the displayed peptide.[59] Additionally, while typical *E. coli* libraries can incorporate up to 10^{11} different peptides,[58] other bacteria can only incorporate a library size of approximately 10^{5}.[59] Significantly, bacterial display libraries can only be screened *in vitro* and *ex vivo* and cannot be used for *in vivo* screening.

1.4.3 *One-Bead-One-Compound (OBOC) Peptide Libraries*

1.4.3.1 *Synthesis of OBOC Libraries*

OBOC libraries are combinatorial peptide libraries synthesized on 80-100 μm beads so that each bead displays approximately 10^{13} copies of a single peptide.[38, 65] The OBOC approach using the "split-mix" synthesis method (Figure 1-3) was first described

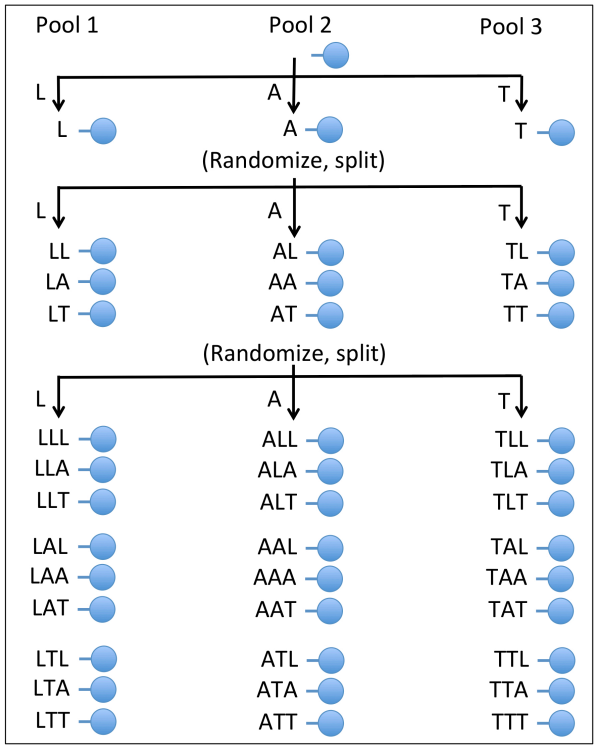

Figure 1-3. OBOC peptide library generation using "split-mix" synthesis. This diagram shows an example of "split-mix" synthesis for tripepetides composed of leucine (L), alanine (A), and threonine (T). Initially, the beads are divided into 3 different pools, one pool for conjugation to each of the amino acids using standard solid-phase synthesis. Pool 1 is coupled to L, pool 2 to A, and pool 3 to T. Then, the beads from all pools are combined and randomly split into 3 new pools before a second round of amino acid conjugation. As before, pool 1 beads are coupled to L, pool 2 beads to A, and pool 3 beads to T. Finally, the pools are mixed and randomly sorted again for another round of amino acid conjugation. This results in a library of bead-bound peptides comprised of every combination of the 3 amino acids, totaling 27 different peptide sequences (3^3).

by Lam et al. in 1991.[66] Libraries containing α-amino acids are both easy to synthesize using standard solid-phase peptide chemistry and easy to sequence using an automated protein sequencer employing Edman degradation.[38] However, Edman degradation requires a free N-terminus, so libraries with more complex peptide structures, such as cyclic or branched peptides or peptides containing β- or γ-amino acids, necessitate including a chemical tag into the bead structure.[38] These chemical tags can be incorporated into the interior of the bead so as to not interfere with binding of the library peptides to targets of interest and then subsequently sequenced using either Edman microsequencing or mass spectrometry.[38] Lam and coworkers recently described two novel methods for generating beads with interior tags, termed bilayer beads.[67, 68] OBOC libraries have also been used to select multimeric ligands; Denmeade and co-workers synthesized OBOC dimer libraries for the selection of dimeric peptides.[69, 70]

1.4.3.2 *Advantages and Disadvantages of OBOC Libraries*

Similar to phage display, synthetic chemistry OBOC libraries are relatively inexpensive, easy to generate, and can display up to 10^8 different peptides, although most OBOC libraries are smaller in size (Table 1-1).[38] However, unlike phage display, OBOC libraries are not constrained to natural amino acids and can include both unnatural and D-amino acids, in addition to secondary structures not tolerated by the phage.[38] As both unnatural and D-amino acids are less susceptible to proteases and peptidases than natural L-amino acids, OBOC libraries have the potential to rapidly identify stable peptide sequences. The design of OBOC libraries also makes them ideal for use in optimization

of known ligands. Peptides previously isolated by phage display or other methods can be used as lead compounds for OBOC library construction, allowing for rapid generation of optimized peptides with higher affinity or specificity.[38] Despite these advantages, OBOC libraries are not as widely used as phage libraries, primarily due to the lack of commercially available libraries. Additionally, although the recent advances in creating bilayer beads has made it easier to identify the peptides displayed by the beads, the required techniques are more involved than the DNA sequencing used to identify phage peptide sequences. Importantly, OBOC libraries cannot be used to select specifically for peptides that internalize into cells *in vitro* or for *in vivo* screening due to the large size of the beads.

1.4.4 *Positional Scanning Synthetic Peptide Combinatorial Libraries (PS-SPCLs)*

1.4.4.1 *Synthesis of PS-SPCLs*

PS-SPCLs are made by synthesizing individual synthetic peptide combinatorial libraries with one amino acid held constant while the remaining amino acids are varied.[71-73] The peptide sequence is then scanned by creating additional unique combinatorial libraries that each hold a different amino acid constant. For a tetrapeptide positional scanning library, this results in four distinct library subsets such that each library mixture holds one of the four amino acid positions constant.[72] These library mixtures are represented by the designations O_1XXX, XO_2XX, XXO_3X, and $XXXO_4$.[72] For each library the O denotes the position that is held constant with one of the 20 amino acids while the X represents any amino acid. In practice this looks like Figure 1-4.[74] Mixture 1 consists of all peptides with a first amino acid "A" while Mixture 2 is all peptides with a

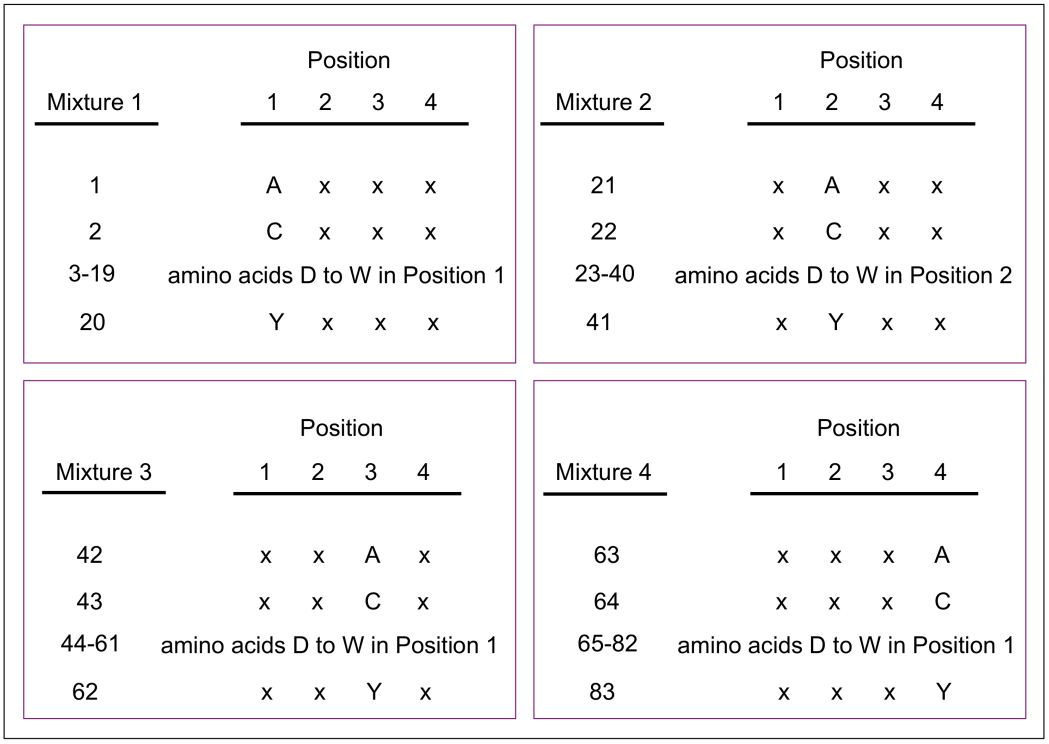

Figure 1-4. Design of a PS-SPCL library.

first amino acid of "C". Mixtures 3-20 each display one of the remaining 19 amino acids in the first amino acid position. The next library mixture, numbers 21-41, contains one of the 20 amino acids held constant in the second library position. This scanning is continued until each of the tetrapeptide positions has it's own pool of libraries.

1.4.4.2 *Advantages and Disadvantages of PS-SPCLs*

Advantages and disadvantages of PS-SPCLs are also listed in Table 1-1. As the PS-SPCLs can be used in solution, they are adaptable to almost any selection technique.[72] They can be incubated with cells or receptors, typically in a high throughput fashion such

as a 96 well plate or a microarray, and numerous readouts for binding exist. For example, screens can be made for binding compared to competitor fluorescently tagged natural ligands (looking for loss of fluorescence)[75, 76] or using biotinylated peptide and streptavidin-HRP as a detection reagent. PS-SPCLs are also relatively easy and inexpensive to synthesize in large numbers.[77] However, these libraries are not commercially available. Importantly, this approach depends upon the idea that each amino acid contributes individually to binding to the target of interest which may make it difficult to determine ideal peptide sequences when multiple peptide motifs exist for the given target.[77] Additionally, PS-SPCL selections typically require multiple rounds of peptide generation and testing for binding. After the ideal amino acids at each position are determined, all possible combinations of peptides using these ideal amino acids must be generated and further tested for binding.

1.5 Cancer Cell Targeting Peptides Isolated from Peptide Libraries

Cancer targeting peptides isolated from peptide libraries can be broken down into two main categories: cancer cell (or tumor cell) specific peptides and vasculature cell specific peptides. In addition to the tumor cells, the vasculature that feeds the tumor is an important target as it also contributes to tumor growth and viability; both tumor cells and tumor-vasculature cells have been used extensively as peptide selection targets. Additionally, peptides have been selected against other components of the tumor microenvironment such as tumor lymphatics and tumor macrophages.

1.5.1 *Cancer Targeting Peptides Isolated from Phage Display Libraries*

Peptide phage libraries were initially used to isolate ligands against known target proteins.[37, 40, 42] This *in vitro* approach met with great success and allowed selection of peptide ligands for receptors without known naturally occurring ligands.[78] Significantly, two papers published in 1996 expanded the field of phage display to include unbiased selection methods. For the first time, phage libraries were used to isolate peptides specific for given cell types without any prior knowledge of cellular receptors. In one paper, Pasqualini and Rhouslahti pioneered *in vivo* phage display by intravenously injecting phage libraries into mice.[79] After isolating organs of interest and recovering bound phage, they obtained peptides specific for the vasculature of the organs. In the second paper, Johnston and co-workers pioneered *in vitro* phage display against whole cells, by using cultured cells as their phage library target and specifically selecting for peptides that could bind and internalize into the cells.[80] The ligands isolated in both studies preferentially bound their target cell types over other non-target cells. Importantly, these studies demonstrated the feasibility of selecting peptides against receptors present in their native cellular conformations. Since these seminal papers, both *in vitro* selection against known target proteins and *in vivo* unbiased selection against cells or tissues have been extensively used to isolate cancer cell targeting peptides.

1.5.1.1 *Panning Phage Libraries Against Known Targets*

During the peptide selection process, commonly known as biopanning (panning), random peptide phage libraries are incubated with a target protein of interest to select for phage displaying peptides that specifically bind the protein (Figure 1-5a). Typically the

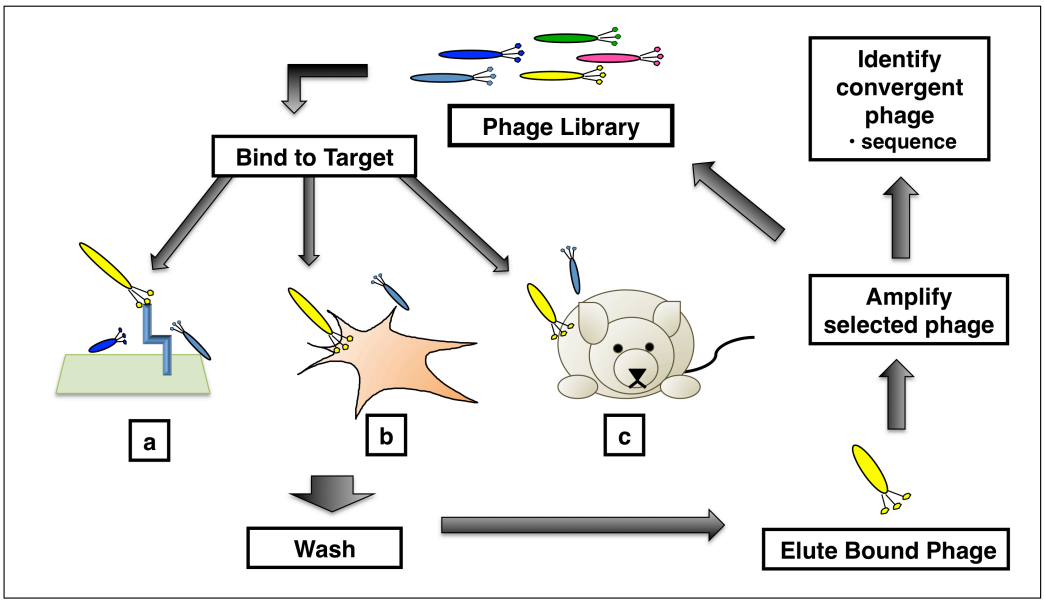

Figure 1-5. Phage library selection against: (a) a target protein, (b) cells *in vitro* or *ex vivo*, or (c) *in vivo*.

target receptor is immobilized on a solid support before addition of the phage library.[40] Alternatively, the target protein is overexpressed in a cell line and the receptor-overexpressing cells are used for the selection process. After the receptor binds and captures specific phage, the unbound phage are washed away and discarded before elution of the bound phage.[40] The resultant phage population is enriched for binding phage and is amplified by infection in *E. coli*.[40] Subsequent panning rounds are then repeated approximately 2-3 times, until specific phage clones emerge.[40] After the final round of selection, the DNA of the resulting phage clones is sequenced to determine their peptide sequence and reveal the candidate receptor specific peptides.[40] If desired, the panning process can also include negative selections in which the phage library is incubated with a control protein or with cells that do no overexpress the receptor of

interest. Performing this selection prior to the selection against the target protein allows for narrowing of the phage library to exclude peptides that bind nonspecifically to other, non-target proteins.

1.5.1.2 *Cancer Targeting Peptides Isolated from Panning Against Known Targets*

Table 1-2 lists the seminal cancer-targeting peptides identified by *in vitro* panning against purified proteins in addition to those isolated in the past 5 years. Only those peptides that have subsequently been shown to bind their target receptor in the context of cells are included. Peptides have been selected against 19 different target proteins. Isolated peptides range in size from 6-20 amino acids, are both linear and cyclic, and have very little sequence similarity. Significantly, 12 of the peptides have been shown to target tumors *in vivo* (Table 1-2).

1.5.1.3 *Unbiased Phage Library Panning Against Cells or Tissues In Vitro or Ex Vivo*

Unbiased panning of phage display peptide libraries can be performed *in vitro* against specific cells, *ex vivo* against cells isolated from animal models or human patients, or *in vivo* against animal or human tissues. Johnston and co-workers first described phage display for the isolation of peptides binding to whole cells *in vitro*.[80] Although whole cells are very heterogeneous targets, isolated peptides typically have high cellular specificity, binding selectively to the cells they were isolated against and not to other related cell types.[78] To help ensure cell specificity, negative selections against related cell types or against other normal cells can be used to exclude peptides that bind to all cell surfaces non-specifically.[78] However, such selections are often unnecessary as

selection against the target cell type alone is generally sufficient to yield highly specific ligands.[78]

In vitro or *ex vivo* panning against cells of interest involves a similar protocol to that used for *in vitro* panning against known target proteins. Random peptide phage libraries are incubated with the cell type of interest for a defined period of time before washing the cells to remove both extracellular and weakly bound phage (Figure 1-5b).[78] At this point, either surface-bound or internalized phages can be chosen for further characterization. If the goal is to isolate surface-bound phage, these phage are eluted and allowed to infect *E. coli* for phage amplification for further rounds of panning. If the goal is to isolate internalized phage, the cells are lysed and all associated phage used to infect *E. coli*. This panning process is then repeated approximately 4-6 times, until the ratio of input phage (total amount of phage originally incubated with the cells) to output phage (amount of bound or internalized phage) stagnates. As phage do not have tropism for mammalian cells and the only modified portion of the phage library is the unique peptide motif, the isolated phage should be specific for the cell type of interest.

There are several advantages to unbiased phage panning on whole cells as opposed to panning on target proteins alone.[78] First, cell receptors remain in their native membrane states – at their normal expression level, in their normal location, and with their normal membrane neighbors. It is impossible to recreate these same conditions for purified receptors. Second, selection can be tailored to isolate either membrane bound or internalized peptides. Selection against purified proteins only allows isolation of peptides that bind to the protein. Third, the selection is completely unbiased and can be performed without prior knowledge of cellular receptors, making it ideal for cells about which little

is known. By contrast, panning on isolated proteins obviously requires prior knowledge of which receptors make good targets. Finally, due to the unbiased nature of the cell panning approach, peptide identification and subsequent receptor identification can lead to the discovery of important cellular targets that were previously unknown.[81, 82]

The use of cells isolated from either animal models or human tissue for *ex vivo* unbiased panning has the additional advantage of allowing for isolation of peptides specific for cells as close to their native context as is possible outside the body. Cultured cells may acquire changes over time that subsequently affect the ligands they bind. Importantly, *ex vivo* panning on patient tissue allows isolation of peptides specific to human tissue and not to mouse or rat tissue, surmounting an obstacle encountered for many peptides isolated by *in vivo* panning in animal models.

1.5.1.4 *Cancer Cell Targeting Peptides Isolated by Unbiased Panning Against Cells or Tissues In Vitro or Ex Vivo*

Numerous tumor targeting peptides have been isolated using *in vitro* panning against cultured cells, as listed in Table 1-3. This list focuses on the seminal cancer-targeting peptides identified by *in vitro* cell panning in addition to those isolated in the past 5 years. All selections were continued for multiple panning rounds until emergence of convergent peptide sequences, resulting in the isolation of a few dominant peptide sequences per panning. Isolated peptides range in size from 7-20 amino acids and are both linear and cyclic. The variety of libraries and protocols used for panning and the diversity of cell lines used as targets has resulted in a diverse group of peptides with very

little sequence similarity. Although these peptides are isolated *in vitro*, many have already been shown to target tumors *in vivo* (Table 1-3).

Table 1-4 lists peptides identified by *ex vivo* panning on either isolated tumor cells or whole tumors. Significantly, laser capture microdissection (LCM) has recently been used to isolate cancer cells for *ex vivo* panning. LCM allows separation of cancer cells from other cell types residing in the tumor to ensure that the peptides isolated are binding the cancer cells. Kubo et al. used LCM to isolate colon cancer cells from patients for panning.[83] Two of the four isolated peptides have been shown to target tumors *in vivo* (Table 1-4).

Not included in Table 1-3 and Table 1-4 are studies that selected for peptide motifs instead of convergent target sequences. Instead of panning against a single cell line and selecting for the best binding sequences, these studies focused on generating consensus peptide motifs that bind to a panel of cell lines. In one such study, Arap and Pasqualini and co-workers used the NCI-60, a panel of human cancer cells encompassing different histological types and grades, for peptide selection.[84] This panel includes cell lines from kidney cancer, breast cancer, colon cancer, lung cancer, prostate cancer, ovarian cancer, tumors of the nervous system, melanoma, leukemia, and lymphoma. It is a particularly interesting group of cells to study because protein expression across the cell lines has been extensively examined. A group of 38 tripeptide motifs were identified that bound broadly across the panel of cells and clustered with cell lines known to express the same receptors. Similarly, Shukla and Krag used *ex vivo* panning on whole breast tumors from patients and examined motifs present among the isolated phage clones.[85] Panning for peptide motifs is more likely to help profile cell surfaces and expand knowledge about

similarities and differences between cancer cells and less likely to generate high affinity peptides.

1.5.1.5 *Unbiased Phage Library Panning In Vivo*

In vivo phage display was first described by Pasqualini and Rhouslahti as a means to select vasculature specific peptides.[79] Typically, a random peptide phage library is injected into the tail vein of mice or rats and allowed a brief (5-15 minute) circulation time (Figure 1-5c).[78] Phage recovery must occur relatively quickly after injection into the animals in order to maintain phage infectivity. The animals are then sacrificed and the desired tissues collected and homogenized. Phage isolated from these homogenates are then infected into *E. coli* for library amplification so that the panning process can be repeated. Typically, 3-5 pannings are sufficient to isolate target specific peptides.[78] As vasculature targets are more readily accessible and do not require tissue penetration, the majority of peptides selected in this manner target tumor vasculature and not the tumor itself. While a longer phage incubation time *in vivo* aids in tissue penetration, phage infectivity also decreases during circulation. However, despite these challenges, a variety of tumor specific phages have been isolated from *in vivo* panning (Table 1-5). Several groups also circumvented the problem by first performing *in vitro* panning to narrow the phage library followed by subsequent *in vivo* panning (Table 1-5). Other groups performed *in vivo* panning by injection of the phages at sites closer to the tumor (Table 1-5).

There are several advantages to *in vivo* phage panning. Just as with *in vitro* panning on cells, the approach keeps receptors in their native context, is entirely

unbiased, requires no prior knowledge of a cellular receptor, and has the potential to identify new cellular targets. However, unlike any of the other selection methods, phage isolated by *in vivo* panning are inherently able to reach their target *in vivo*. They come with the assurance that the receptor they target is both accessible from the bloodstream and able to bind its ligand in sufficient quantity for detection. While any peptides isolated still have to be synthesized off the scaffold of the phage and tested for serum stability and ability to target *in vivo*, it is helpful to know that an optimized peptide should be able to reach its target *in vivo*. Conversely, peptides isolated from whole cells do not come with this type of assurance and the receptor they target may not be as readily accessible from the bloodstream or may have a different cellular localization *in vivo* than *in vitro.*

However, one disadvantage of *in vivo* panning in mice or rats is that any peptides identified as homing to tumor vasculature are binding to mouse or rat tissue and not human tissue. Thus, they may not bind human tumor vasculature. The receptors they target may not even be available in human tissue. In order to translate these peptides to clinically relevant ligands, the target receptors will have to be examined in human tissue and the peptide sequences may have to be further optimized to bind their human counterparts. In order to bypass these problems, a few groups have turned to panning in humans. Arap and Pasqualinin were the first to perform *in vivo* phage display in human patients.[86] A patient with the B-cell cancer Waldenström macroglobulinemia was injected intravenously with phage and tissue collected from five areas of the body – bone marrow, fat, skeletal muscle, prostate, and skin – for identification of specific tripeptide motifs. One extended peptide motif was validated as evidence of the specific nature of these motifs. A phage bearing the peptide CGRRAGGSC was isolated from the prostate and

shown to recognize the vasculature of human prostate tissue specimens. The CGRRAGGSC peptide binds to IL-11Rα,[86, 87] which increases in expression during the progression of cancer.[88] This peptide is currently in phase 1 clinical studies for patients with prostate cancer.[89] Recently, the Krag lab performed a phase I study in which patients with different types of stage IV cancer were intravenously injected with phage libraries for panning followed by biopsy and then reinfusion of the library for further panning and biopsy steps.[90] One peptide phage clone isolated from a patient with stage IV melanoma subsequently bound *ex vivo* to tumor cells from the same patient, but not to tumor cells from other patients. Additionally, this peptide phage clone did not bind to human melanoctyes and bound only slightly to 1 of 6 melanoma cell lines tested. Thus, the peptide appears to be specific for the tumor from which it was isolated.

1.5.1.6 *Cancer Cell Targeting Peptides Isolated by Panning In Vivo*

Table 1-5 lists peptides identified by *in vivo* panning in animals. The majority of peptides isolated by *in vivo* panning in animals bind to the tumor vasculature and not the tumor cells, although a variety of peptides bind selectively to tumor cells or to both the vasculature and tumor cells. Tumor vasculature specific peptides are identified in the table with a **V**; tumor cell specific peptides, with a **T**; and peptides that bind both vasculature and tumor cells, with a **T/V**. Based upon the variety of peptides isolated from different tumor models, tumor vasculature appears to be shaped by the specific tumor type. Isolated peptides can even distinguish between drug or radiation treated tumor vasculature and their untreated tumor counterparts. Peptides have been isolated that can distinguish between the vasculature of untreated tumors compared to tumors treated with

the monoclonal antibody VEGF inhibitor bevacizumab[91] or tumors responding to treatment with the small molecule receptor tyrosine kinase inhibitor sunitinib.[92] Hallahan and colleagues also recently identified a peptide that binds specifically to the tumor vasculature of tumors treated with both radiation and the VEGF receptor tyrosine kinase inhibitor SU11248.[93]

One problem with the use of *in vivo* panning in animals is that the vasculature specific peptides that are isolated are binding to mouse or rat, and not human vasculature. Additional testing is required to determine whether or not they also bind human vasculature. One study bypassed the problem of selecting peptides against mouse vasculature by using mice injected with human endothelium for their *in vivo* panning. Mice were injected with tumor endothelial cells derived from human renal carcinomas mixed with Matrigel so that they formed human tumor vessels that grew into the murine vessels. *In vivo* panning in these mice thus resulted in peptides that could target human endothelium and not mouse endothelium.[94]

Selections can also be biased to identify peptides binding to other, nonvasculature, components of the tumor. Using *in vitro* or *ex vivo* phage display in combination with *in vivo* panning can help this process. Rhouslahti's group recently used sequential *ex vivo* and *in vivo* panning on a mouse xenograft MDA-MB-435[95-98] breast cancer model to identify peptides specific for both tumor lymphatics and tumor cells.[99-102] The peptide was isolated by using *ex vivo* panning on cell suspensions of MDA-MB-435 tumors that were depleted of endothelial cells, biasing towards non-vasculature targeting peptides.[99] Subsequent *in vivo* panning with this phage population led to selection of the cyclic 9-mer peptide, LyP-1.[99] LyP-1 has been shown to translocate to the nucleus upon

binding and to home to tumor lymphatic vessels in melanoma, breast, prostate, skin, and osteosarcoma tumors while not binding either tumor vasculature or normal tissue.[99, 101, 102] Other lymphatic homing peptides have been identified, as delineated in Table 1-5. This is significant as tumor lymphatic vessels serve as drainage systems and some evidence suggests that they are the route through which tumor cells escape to form metastases.

1.5.2 *Cancer Targeting Peptides Isolated from Bacterial Display Libraries*

1.5.2.1 *Using Bacterial Display Libraries for Unbiased Selection Against Cells or Tissues In Vitro or Ex Vivo*

All of the cancer targeting peptides identified by bacterial display have been isolated using unbiased peptide selection against cellular targets. Targets include both cells in culture used for *in vitro* selection and isolated murine or human cells used for *ex vivo* selection. There are two methods of bacterial display: panning,[60] similar to the method used with phage libraries, and a quantitative method employing fluorescence-activated cell sorting (FACS).[103] Bacterial library panning involves incubating the cells with the bacterial library followed by extensive washing to remove unbound bacteria. Bound bacteria are then recovered by vortexing or centrifugation and amplified for repeated panning rounds. After the final round of selection, the DNA of the resulting bacterial clones is sequenced to determine their peptide content and reveal the candidate receptor specific peptides. FACS screening for peptide selection is performed by first expressing the bacterial peptide libraries in *E. coli* that also expresses a GFP variant.[103] After incubating the fluorescent bacterial library with target cells and extensively washing to remove unbound bacteria, the cells are sorted by FACS looking for GFP

fluorescence. Cells with bacteria bound to them should carry a GFP signal that specifically allows for their isolation. As FACS quantifies that fluorescent signal, bacterial clones can be separated on the basis of the number of target cells they bind. The specific peptides displayed by the isolated bacterial clones are then determined using DNA sequencing.

1.5.2.2 *Cancer Cell Targeting Peptides Isolated from Bacterial Display Libraries by Unbiased Selection Against Cells or Tissues In Vitro or Ex Vivo*

Table 1-6 lists cancer specific peptides identified from screening bacterial libraries against cellular targets. Peptides have been selected against 7 cell lines *in vitro* and against 1 cell line *ex vivo*. These peptides range in size from 5-18 amino acids and the majority of the peptides are disulfide-constrained and cyclic. Three of the peptides target tumors *in vivo*.

1.5.3 *Cancer Targeting Peptides Isolated from OBOC Libraries*

Much like phage libraries, OBOC libraries have been used to select for peptides against both known targets and against unbiased cellular targets. OBOC libraries were originally used to select ligands against target proteins.[66] Then, in 1996, the same year that Pasqualini and Rhouslahti first described *in vivo* phage display[79] and that Johnston and co-workers pioneered unbiased *in vitro* phage display against cultured cells,[80] Pennington, Lam, and Cress first described the use of OBOC libraries for unbiased screening against live cells.[104]

1.5.3.1 *Using OBOC Libraries to Select Against Known Targets*

Soluble target proteins can be screened for binding to OBOC libraries using an enzyme-linked colorimetric assay.[65, 66, 105] This selection is relatively simple and involves the reaction of a secondary antibody labeled with alkaline phosphatase with the colorimetric substrate bromo-chloro-indolyl-phosphate (BCIP); any OBOC beads that are bound to the secondary antibody will turn turquoise upon addition of BCIP.[106] The first step of the selection is a negative selection to remove peptides that nonspecifically bind the secondary antibody. The OBOC library is incubated with the secondary antibody and the colorimetric BCIP substrate added. Any OBOC beads that turn turquoise are nonspecific binders that are excluded from further rounds of screening. For the actual screen, the OBOC library is incubated with the target protein of interest followed by thorough washing before the addition of the secondary antibody. Subsequent addition of BCIP causes all of the OBOC beads that bound the target protein to turn turquoise. The peptide content of isolated positive beads is then determined using Edman's sequencing or mass spectrometry.

1.5.3.2 *Cancer Targeting Peptides Isolated from OBOC Selection Against Known Targets*

Table 1-7 lists peptides identified by *in vitro* selection using OBOC libraries against purified proteins. Two receptors, the idiotypes IgMκ from both WEHI-231 and WEHI-279 B-cell lymphoma cells, were incubated with OBOC libraries for isolation of receptor specific peptides.[106] Four peptides selected against WEHI-231 IgMκ were able to bind the receptor in the context of the cells, and two peptides selected against WEHI-

279 cells were able to bind in the context of the cells. Tetramerization of the wGeyidvk peptide by biotinylation and subsequent incubation with avidin was also able to increase total cellular tyrosine phosphorylation levels.

1.5.3.3 *Using OBOC Libraries for Unbiased Selection Against Cells or Tissues In Vitro or Ex Vivo*

Screening of OBOC libraries against cells in culture or against cells isolated for *ex vivo* screening is relatively straightforward.[38] Prior to selection the library beads are washed thoroughly and the cells harvested and washed. The beads and cells are then gently mixed together and incubated under the appropriate conditions for the selection cell line. Positive "hits" are visualized by microscopy as beads covered in cells. These positive beads can then be selected and removed using a micropipette. As with phage display, negative selections can also be used to identify peptides that bind the cells nonspecifically. Lam and co-workers have employed two different negative screening methods to exclude cells that bind to the beads non-specifically.[38] The first negative screening method involves a normal screen against the cell type of interest followed by guanidinium chloride treatment to remove any bound cells so that the beads can be reused for incubation with a normal, control cell type. Beads binding both the target and control cell types are then discarded. In the second negative screening method, the target cells are fluorescently labeled and then mixed together with both control cells and the bead library. Any beads bound to both fluorescent target cells and unlabeled control cells are then discarded and beads that are only bound to the fluorescent target cells are considered "hits".

There are several advantages to screening OBOC libraries against live cells. Just as with *in vitro* phage panning on cells, the approach keeps receptors in their native context, is entirely unbiased, requires no prior knowledge of a cellular receptor, and has the potential to identify new cellular targets. However, unlike phage libraries, OBOC libraries cannot select for internalizing peptides due to the large size of the beads.

1.5.3.4 *Cancer Cell Targeting Peptides Isolated from OBOC Libraries by Unbiased Selection Against Cells or Tissues In Vitro or Ex Vivo*

Table 1-8 lists peptides identified by *in vitro* selection from OBOC libraries against cultured cells. Significantly, all of the peptides isolated from OBOC libraries for which receptors have been identified bind integrin receptors. Much of this is likely due to library synthesis as many of the libraries are designed with a bias towards sequences that are known to bind integrins. The vast majority of peptides selected using OBOC libraries contain either D-amino acids, other unnatural amino acids, or both. As unnatural amino acids are more resistant to peptidase cleavage, these amino acids may have better stability *in vivo*. To date, 6 of the OBOC selected peptides have been shown to target tumors *in vivo*.

1.5.4 *Cancer Targeting Peptides Isolated from PS-SPCLs*

1.5.4.1 *Using PS-SPCLs for Selection Against Target Proteins or Unbiased Selection Against Cells In Vitro*

PS-SPCLs have also been used to select for peptides against both known targets and against unbiased cellular targets. As the PS-SPCLs can be used in solution, they are

adaptable to almost any selection technique. They are typically incubated with cells or receptors in a high throughput fashion, such as using a 96 well plate or a microarray, and the readout for binding is very diverse. Screens can be made for binding verses competitor natural ligands that are fluorescently tagged, looking for loss of fluorescence,[75, 76] or can use biotinylated peptide and streptavidin-HRP as a detection reagent.[107] Other screens have used specific cellular effects as the readout (Table 1-9). Once all of the scanning library subsets are screened using the assay of choice to identity the "best" amino acid at each position, additional peptides are synthesized using all possible combinations of the "best" amino acids. These peptides are then used in the same selection process as the original library to identify which amino acid sequences best target the protein or cell type of interest. Although this screening process requires multiple rounds of peptide synthesis and testing, the best binding peptides are immediately discovered and no additional rounds of DNA sequencing or peptide sequencing are needed to determine the peptide composition.

1.5.4.2 *Cancer Cell Targeting Peptides Isolated from PS-SPCLs by Selection Against Target Proteins or Cells In Vitro*

Table 1-9 lists cancer specific peptides isolated from PS-SPCLs. Only one of the peptides isolated from PS-SPCLs has been shown to target tumors *in* vivo. PS-SPCLs are ideal for assays screening for cellular effects induced by peptides. Kang and co-workers used integrin microarrays to select peptides that inhibit angiogenesis. They first used an $\alpha_v\beta_3$ microarray and a PS-SPCL to screen for peptides that interfered with the $\alpha_v\beta_3$-vitronectin interaction.[75] Fluorescently labeled vitronectin

was mixed with the peptide library before addition to the microarray. Library peptides that inhibited the receptor-vitronectin interaction were thus visible by a reduced fluorescent signal. This resulted in the selection of two peptides HGDVHK and HSDVHK that were able to inhibit bFGF-induced HUVECs migration *in vitro* as well as inhibit new bFGF-induced blood vessel formation in a CAM assay. They later used an $\alpha_5\beta_1$ microarray and a PS-SPCL to screen for peptides that inhibit $\alpha_5\beta_1$-fibronectin interactions.[76] Fibronectin was labeled with the fluorescent dye Cy5 and mixed in increasing concentrations with the peptide library before addition to the microarray. Library peptides that inhibited the receptor-fibronectin interaction were thus visible by a reduced fluorescent signal. One isolated peptide, VILVLF, subsequently inhibited proliferation of HUVECs and inhibited angiogenesis in a bFGF-induced CAM angiogenesis assay. As $\alpha_5\beta_1$ is expressed at high levels in both angiogenic endothelial cells and several cancer types, this peptide may have future utility for antiangiogenic therapy.

1.5.5 *Summary of Cancer Targeting Peptides*

Phage display libraries, bacterial libraries, OBOC libraries, and PS-SPCLs have all been used to select a variety of cancer targeting peptides, although the vast majority of peptides have been selected from phage display libraries. A variety of peptides specific for a diverse range of receptors and cell types have been isolated from phage display libraries. Conversely, almost all of the peptides selected from OBOC libraries, and all of those with known receptors, target the same class of receptors – the integrins; this is primarily a result of library design with a bias towards sequences that are known to bind

integrins and with use of shorter peptide lengths. Additionally, only 8 cell lines have been used to select peptides from bacterial display libraries and only 6 peptides have been selected from PS-SPCLs. While all of the libraries can be used to select peptides from cell lines *in vitro* or *ex vivo*, only phage display libraries are amenable to *in vivo* selections.

Despite the large number of peptides selected using phage display libraries, only a small fraction of available human cancer cells have been used for peptide selections. For example, although there exist more than 200 lung cancer cell lines,[108] only 5 have been used for peptide selection. Additionally, it is unclear whether most of the isolated peptides bind broadly across the variety of available lung cancer cell lines or whether they are specific for the cell lines from which they were isolated. There would be great utility in isolating a panel of peptides that could bind the majority of lung cancer lines and thus be used to treat a majority of cases appearing in the clinic.

1.6 Drug Delivery Using Cancer Targeting Peptides

Cancer specific peptides are ideal ligands for tumor targeting therapies. Peptides are commonly used for three types of targeting applications: drug delivery, oligonucleotide delivery, or delivery of imaging agents. Both drug delivery and oligonucleotide delivery seek to inhibit tumor growth and improve survival while the delivery of imaging agents serves to image and detect tumors and cancerous cells. A variety of peptides selected from peptide libraries have been used for all 3 types of applications and are labeled in Table 1-2 to Table 1-9 according to their use. This discussion focuses on the use of peptides for drug delivery.

Peptides selected from phage-display libraries are particularly amendable for downstream targeting applications. While a few peptides selected from OBOC libraries, bacterial display, and PS-SPCLs have been used for imaging applications in animals (Table 1-6 to Table 1-9), only one peptide isolated from any of these library types, the HYD-1 peptide selected from an OBOC library, has been used for *in vivo* therapy in animals.[109] Peptides selected from phage display libraries, on the other hand, have been used extensively for *in vivo* therapy (Table 1-2 to Table 1-5). While some cancer specific peptides are inherently toxic and able to inhibit tumor growth by themselves, most peptides require attachment to a drug to exhibit anti-cancer activity. Peptides are attached to drugs in one of two ways: they are either directly conjugated to the drugs or are conjugated to a drug carrier. Drug carriers, as their name suggests, are structures that carry drug molecules and include polymer scaffolds, micelles, liposomes, and other nanoparticles. These nano-scale carriers each come with distinct advantages and disadvantages, as outlined in Table 1-10.

1.6.1 *Peptide-Drug Direct Conjugates*

The majority of library selected peptides used for targeted drug delivery have been direct peptide-drug conjugates. These conjugates can be broken down into three different categories: peptide-small molecule conjugates, peptide-peptide conjugates, and peptide-protein conjugates.

Peptides can be conjugated to a variety of chemotherapeutic drugs for specific delivery to tumors. These peptide-small molecule conjugates require chemical groups on both the peptide and the drug that are compatible for conjugation.[78] Additionally, the drug

is generally inactive while conjugated to the peptide, meaning that the covalent bond between the peptide and drug must break and release the drug for any therapeutic effects.[78] Ideally, the peptide-drug linkage remains stable under normal bodily conditions, breaking only once the conjugate has reached the tumor. Often acid labile linkers are employed; these linkers are intact at a pH of 7 but hydrolyze and release under acidic conditions, such as those of the lysosome.[78] Other types of drug linkers can also be used, such as esters or carbamates;[110, 111] these linkers are also stable under normal conditions and release after exposure to the high levels of esterases within cells.[78] Several different chemotherapeutic drugs have been directly conjugated to cancer specific peptides, including doxorubicin,[112-117] paclitaxel,[112, 118] and a vitamin E analog.[119] While most of these conjugates have only been used for *in vitro* toxicity studies, several have also been shown to inhibit tumor growth *in vivo*. The peptide LTVSPWY, isolated from panning a phage-display library against cultured SKBR3 breast cancer cells, inhibited breast tumor growth in transgenic mice when conjugated to the proapoptotic vitamin E analog, α-tocopheryl succinate.[119] Additionally, three different peptides conjugated to doxorubicin have been used to inhibit tumor growth in mice. The NGR and RGD-4C peptides, both isolated from *in vivo* phage panning in mice bearing MDA-MB-435[95-98] breast xenografts, also both inhibited MDA-MB-435 tumor growth when conjugated to doxorubicin.[115] Of note, both of these peptides target the tumor vasculature and not the tumor cells. However, a peptide specific for tumor cells has also proven effective for drug targeting *in vivo*. The tumor cell targeting A54 peptide, isolated from *in vivo* panning in mice bearing BEL-7402 hepatocellular carcinoma xenografts, also inhibited tumor growth when conjugated to doxorubicin.[117]

Cancer targeting peptides can also be conjugated to other peptides with known cell toxicity. The proapoptotic peptide $(KLAKLAK)_2$ is the most commonly used toxic peptide. Although inactive outside cells, the $(KLAKLAK)_2$ peptide exerts intracellular toxicity by disrupting the mitochondria, leading to subsequent cell death. This peptide is often synthesized using protease resistant D-amino acids, increasing its chances of reaching a tumor as an intact active peptide. Numerous cancer targeting peptides have been fused to the proapoptotic peptide for either *in vitro* killing of cancer cells[88, 120-124] or *in vivo* inhibition of tumor growth in rodents.[120, 124]

Other peptide-drug conjugates include peptide-protein fusion proteins. Unlike the chemical conjugation used to make peptide-small molecule and peptide-peptide conjugates, most of these conjugates are created genetically. The peptide is genetically expressed as a fusion protein with a protein toxic to the target cell type. Peptides selected from phage-displayed libraries have been fused to a variety of proteins, including toxic shock syndrome toxin 1,[125] vascular endothelial cell growth inhibitor,[126] the kringle 5 fragment of human plasminogen,[127] a fragment of tumstatin (tum-5),[128] interferon α (INFα2a),[129, 130] and interleukin-2 (IL-2).[131] Additionally, 3 peptides have been conjugated to either tumor necrosis factor-α (TNF-α) or a mutant version of the same protein.[132-137] Significantly, all of these peptide-protein fusions have been used for *in vivo* therapeutic experiments in rodents, leading to either inhibition of tumor growth or increased survival. Of particular interest is one of the TNF-α conjugates. A shortened version of the NGR peptide, CNGRCG, expressed as a fusion protein with TNF-α is currently in clinical trials.[138] Phase I and II trials for this peptide-protein conjugate went

so well that it was granted “Orphan Drug” status in both the European Union and the United States for the treatment of malignant pleural mesothelioma (MPM).[138] Phase III trials for NGR- TNF in MPM patients are ongoing.[138]

Both the primary advantages and disadvantages of peptide-drug conjugates lie in their small size. While this small size allows the conjugates better escape from the tumor vasculature and penetration through the tumor,[139] it also increases their blood clearance rate. Particles below a molecular weight of 40 kilodaltons (kDa) tend to experience rapid renal filtration and excretion from the body.[140] As most peptide-drug conjugates fall below this molecular weight cutoff, they are only therapeutically beneficial if they accumulate in the tumor at effective levels relatively quickly, before the majority of the conjugate is cleared from the body. However, reaching therapeutic levels is possible due to the high specificity and affinity of direct conjugates. Such conjugates tend to have low background uptake and high affinity for their targets.

1.6.2 *Peptides Conjugated to Drug Carriers*

Most drug carriers fall into one of 3 categories - polymer scaffolds, micelles, or liposomes – although a variety of other nanoparticles have been created. Liposomes are the most widely used drug carrier for peptide-targeted therapy and the vast majority of peptides isolated from phage display libraries that have been conjugated to nanoparticles for drug delivery have been conjugated to liposomes.

1.6.2.1 *Liposomes*

Liposomes are spherical nanoparticles formed by lipids self-assembling into a bilayer.[141] As liposomes are formed from phospholipids and cholesterol that are already a normal component of the human body, they are naturally biodegradable.[141] The inner compartment of a liposome is an aqueous phase that can encapsulate hydrophilic agents.[141] Therefore, these nanoparticles work well for delivery of hydrophilic drugs. However, hydrophobic drugs can also incorporate into the hydrophobic portions of the lipid membrane.[142] Early liposome formulations suffered from rapid blood clearance rates due to engulfment by the cells of the reticuloendothelial system, and in particular from Kupffer cells in the liver.[142] The reticuloendothelial system is the primary means by which foreign macromolecules are eliminated from the body and consists mostly of macrophages in the liver, spleen, and lymph nodes.[142] However, coating the outer lipid membrane with polyethylene glycol (PEG) increases circulation time of the liposomes by reducing interaction of the liposomes with serum proteins and thus delaying clearance by the reticuloendoethial system.[143]

One major advantage to using liposomes is that several liposome formulations are already clinically approved. The first liposome to gain clinical approval was liposomal amphotericin B, or Ambisome®, which was initially approved in 1990.[141, 144] Significantly, a pegylated form of liposomal doxorubicin (Stealth® liposomal doxorubicin) was the first nanoparticle drug approved for cancer treatment. Pegylated liposomal doxorubicin is marketed as DOXIL® in the United States and as Caelyx® in other countries and is currently approved in the United States for the treatment of ovarian cancer,[145] multiple myeloma,[146] and Kaposi's sarcoma.[147] It is also approved for use in

breast cancer patients in Europe.[148] Numerous clinical trials involving the drug are ongoing, including trials in patients with NSCLC.[149] DOXIL® is approximately 100 nm in size and contains the anthracycline chemotherapeutic doxorubicin,[141] which destroys cells by preventing DNA replication through at least two mechanisms: intercalation in and covalent binding to the DNA[150] and by inhibition of topoisomerase II.[151] DOXIL® inhibits tumor growth by passively accumulating in tumors based on the enhanced permeability and retention effect (described in more detail at the end of this section). After accumulating in tumors, DOXIL® remains in the extracellular space; it does not cross the cell membrane and enter into tumor cells.[152] Over time the liposome membrane slowly breaks down and free doxorubicin is released. As free doxorubicin easily crosses cell membranes, the released drug is able to reach its site of action in the nucleus.

Due to the success of DOXIL®, most peptides conjugated to liposomes for targeted drug delivery have been conjugated to liposomal forms of doxorubicin. Seventeen different peptides isolated from phage-display libraries have been conjugated to liposomal doxorubicin for either *in vitro* inhibition of cancer cell growth[153-157] or for *in vivo* inhibition of tumor growth in rodents.[154, 158-166] All of the targeted peptide-liposomal doxorubicin nanoparticles save one inhibited tumor growth better than liposomes without the targeting peptides. The liposomal studies involving one peptide are particularly worth noting. A peptide derivative of the tumor vasculature targeting NGR peptide,[115] the peptide GNGRG, was conjugated to liposomal doxorubicin. This is a derivative of the same NGR peptide that is in clinical trials in its TNF conjugated form. NGR-liposomal doxorubicin inhibited the growth of orthotopic neuroblastoma xenografts in mice, leading to tumor eradication in mice compared to mice treated with control peptide-liposomal

doxorubicin, which did not alter tumor growth compared to control mice.[165] This therapeutic result was the result of greater accumulation of the peptide-targeted liposomes in the tumor.[165] NGR-liposomes have been primed for potential future clinical trials by preparation using Good Manufacturing Practices (GMP)[167] and these liposomes have been shown to increase survival in orthotopic mouse lung, ovarian, and neuroblastoma xenografts.[166]

Liposomal formulations are advantageous for a variety of reasons (Table 1-10). The large hydrophilic interior of the liposome allows for the encapsulation of thousands of drug molecules, lending a peptide-targeted liposome a much higher drug:peptide ratio than peptide-drug direct conjugates with only a 1:1 peptide:drug ratio. Additionally, hydrophilic drugs can be loaded into liposomes in their natural state and do not require chemical modification for conjugation to the peptide and there is the potential for the encapsulation of multiple drugs within the same liposome. The long *in vivo* circulation time enjoyed by pegylated liposomes also means that the peptides will have longer to deliver their drug cargo to the tumor than will peptides directly conjugated to a therapeutic. However, liposomes also suffer from several disadvantages. In particular, the larger size (80-200nm) of liposomes prevents them from penetrating tumor tissue as well as smaller conjugates and can make it more difficult for them to escape from the tumor vasculature.[168]

1.6.2.2 *Polymer Scaffolds, Micelles, and other Nanoparticles*

Although liposomes are the most extensively used drug carriers for peptide-targeted delivery, polymer scaffolds and micelles are other important drug carriers.

Polymer scaffolds are created by attachment of water-soluble polymers to the drug.[169] Much like peptide-drug direct conjugates, these drug-polymer scaffolds also require chemically reactive groups and should remain intact until cell internalization, at which point the bond between the polymer and drug breaks for allowing the drug to release and exert its effects.[169] However, unlike peptide-drug direct conjugates, drug-polymer scaffolds have longer *in vivo* circulation times due to the polymer coating of the drug increasing the scaffold size. Additionally, polymer-drug conjugates' size can be tailored to reduce renal clearance. A major disadvantage to these conjugates is that it can be difficult to control both the length of the polymers and the amount of drug conjugated to the scaffold. However, polymer scaffolds have progressed extensively through the drug pipeline, with polymers conjugated to paclitaxel, camptothecin, doxorubicin, carboplatin, and 1,2-diaminocyclohexane (DACH)-platinate all in clinical trials.[169] Despite these successes, very few phage display selected peptides have been conjugated to polymer scaffolds.

Micelles are a class of polymer nanoparticles formed by amphiphilic copolymers, which have both a hydrophilic component and a hydrophobic component.[170] Upon exposure to an aqueous solution, the insoluble hydrophobic portions of the polymer aggregate into a core structure, with the hydrophilic polymers forming a shell that surrounds the core. These self-forming nanoparticles are typically 50 – 100 nm in size.[171] Micelles have many of the same advantages of liposomes, as they are able to incorporate unmodified drugs and can encapsulate multiple agents at once at a fairly high concentration of drug per micelle. Much like pegylation of liposomes for longer *in vivo* circulation times, micelles are often formed used polyethylene glycol (PEG) to give them

longer clearance rates.[171] As micelles tend to be smaller than liposomes, they cannot incorporate as many drug molecules as the larger nanoparticles and have intermediate circulation times. Their smaller size may also allow for better escape from the vasculature and better tumor penetration. Significantly, several micelle formulations are currently in clinical trials.[172]

The hydrophobic core of micelles allows them encapsulate hydrophobic drugs, but not hydrophilic drugs. Many traditional small molecule cancer drugs are hydrophobic, making them perfect candidates for micelle entrapment. However, micelles cannot be used for hydrophilic drug delivery applications. Micelles are also less stable than liposomes. In order to remain intact as nanoparticles, micelles must maintain a critical micelle concentration (CMC).[171] The CMC is the concentration of individual amphiphilic copolymers required for the micelle structure to form. Below the CMC, micelles fall apart into the individual copolymers, releasing the entrapped drug. However, micelles can often be designed to remain intact *in vivo* long enough to reach their target.[171]

Despite the many advantages of micelles, very few peptides selected from phage display libraries have been conjugated to this class of nanoparticles. Both peptide-targeted paclitaxel micelles and peptide-targeted doxorubicin/superparamagnetic iron oxide (SPIO) micelles[173] have been used to selectively kill cancer cells *in vitro* but neither platform has yet met success *in vivo*. However, the success of other micelle formulations suggests that peptide-targeted micelles should be further explored.

Although less commonly used, a variety of other nanoparticles have been used for peptide-targeted drug delivery. These include nanoworms,[174, 175] particles created from

a phage coat protein,[176] nab-paclitaxel,[177-180] microbubbles,[181] and polyester based particles.[182] In particular, nab-paclitaxel, a nanoparticle formed by albumin-coated paclitaxel, has been conjugated to several peptides for tumor inhibition in rodents.[177-180] As an untargeted form of nab-paclitaxel, Abraxane®, is approved for clinical use, these nanoparticles are an attractive drug targeting candidate.

1.6.2.3 *Role of the Enhanced Permeability and Retention Effect for the Delivery of Drug Carriers to Tumors*

One important factor to consider when using drug carriers for drug delivery is the passive accumulation of nano-sized particles in the tumor through the enhanced permeability and retention (EPR) effect.[183] Unlike the vasculature of normal tissue, tumor vasculature is very irregular and disordered. Nano-sized particles can escape through this leaky vasculature into the tumor tissue and are subsequently retained by the tumor due to the poor lymphatic drainage systems of tumors. The EPR effect is thought to affect particles between 50 and 400 nm,[184] meaning that all of the drug carriers described above are inherently subject to passive tumor accumulation. Thus tumor accumulation of peptide targeted drug carriers will depend not only on the specific targeting peptide but also on EPR-driven effects. Interestingly, studies with targeted liposomes have demonstrated two types of tumor drug accumulation, both of which lead to desirable therapeutic outcomes. Some peptide-targeted liposomes, in particular those targeting the tumor vasculature, deliver more doxorubicin to the tumors than non-targeted liposomes,[159, 165] suggesting that the targeted liposomes are accumulating in the tumor based on both the peptide targeting abilities and the EPR effect. Other antibody-targeted

liposome formulations accumulated in the tumor at levels similar to non-targeted liposomes, however unlike the non-targeted liposomes, these targeted liposomes internalized into tumor cells and were better distributed throughout the tumor tissue.[185, 186] While the targeting ligand did not override the EPR effect driving tumor accumulation of these liposomal formulations, the altered location of the drug in the tumors still increased efficacy.

1.7 Aims of this Study

Tumor targeting therapies that specifically deliver drugs to the tumor, reducing accumulation and toxicity in non-target tissues, are a promising niche of cancer therapeutics. This study aims to use peptide ligands to develop new targeting therapeutics for the treatment of NSCLC, a notoriously deadly disease.

Previous work in our lab utilized phage display peptide libraries to isolate a suite of 11 different peptides specific for NSCLC (Chapter 2). The peptides exhibit many features that should facilitate their use in downstream applications, including high affinity, specificity for cancer cells as compared to normal cells, and easy translation from phage displayed peptides to chemical synthesis. One of these peptides, the H2009.1 peptide, targets the restrictively expressed integrin $\alpha_v\beta_6$ (Chapter 3). As $\alpha_v\beta_6$ is not expressed in normal tissue but is overexpressed in numerous cancers of the epithelium, it is an attractive tumor target. More than half of NSCLC patient tumors express $\alpha_v\beta_6$, warranting the development of $\alpha_v\beta_6$-targeting therapies.

To develop therapies specific for $\alpha_v\beta_6$-positive NSCLC, I sought to translate the H2009.1 peptide from a phage display selected peptide to a viable tumor targeting ligand.

Initial studies evaluate the ability of the H2009.1 peptide to target tumors *in vivo* (Chapter 2). Subsequent studies focus on the development of two different types of H2009.1-targeted therapeutics: liposomal drugs and direct peptide-drug conjugates. *In vitro* studies optimize the ideal construct for H2009.1 peptide targeting of liposomal doxorubicin, comparing the effects of peptide affinity, valency, and concentration on nanoparticle targeting to $\alpha_v\beta_6$-positive NSCLC cells (Chapter 4). The *in vivo* efficacy of these various H2009.1 peptide-targeted liposomal doxorubicin formulations is explored in a NSCLC tumor model (Chapter 5). Additionally, two different H2009.1 peptide drug conjugates are examined for both *in vitro* and *in vivo* $\alpha_v\beta_6$-specific targeting and efficacy (Chapter 6).

This work contributes to the development of targeted therapies for the treatment of $\alpha_v\beta_6$-positive NSCLC and is expected to promote and direct the design of future therapies targeting $\alpha_v\beta_6$. As $\alpha_v\beta_6$ is expressed by numerous other cancers of the epithelium, these results are expected to translate to the treatment of other tumor types.

Table 1-2. Peptides Selected from Phage Library Panning *In Vitro* Against Target Proteins

Protein used for selection	Peptide sequence[a,b,c,d]	*In vitro* therapy[e]	*In vivo* homing validated	*In vivo* delivery[e]
HER2/neu/ ErbB2	WTGW**C**LNPEESTWGF**C**TGSF[187] (pIII, **T**)			
	KCCYSL[188] (pIII, **T**)		Yes[189-191]	microSPECT/CT of ^{111}In-DOTA-peptide in tumors in mice[190, 191] **(Imaging)** microPET/CT of ^{64}Cu-DOTA, NOTA, & CB-TE2A-peptide conjugates in tumors in mice[189] **(Imaging)**
EGFR	YHWYGYTPQNVI (GE11)[192] (pIII, **T**)	Conjugated to PEI for delivery of luciferase gene[192] **(Oligo)** Conjugated to doxorubicin-loaded liposomes to kill cells[155] **(Drug)** Peptide-lytic peptide chimera kills cells[120] **(Drug)** LPEI-PEG-Peptide polyplexed with NIS gene specifically transfected cells & allowed ^{125}I uptake[193] **(Oligo)** Peptide-Au nanoparticles with phthalocyanine killed cells after irradiation[174] **(Drug)**	Yes[155, 192, 193]	Cy5.5-labeled peptide & Cy5.5-labeled peptide-liposomes imaged in tumor-bearing mice[155] **(Imaging)** Conjugated to PEI for delivery of luciferase gene to tumors in mice[192] **(Oligo)** Peptide-lytic peptide chimera inhibits tumor growth in mice[120] **(Drug)** LPEI-PEG-Peptide polyplexed with NIS gene homed to tumors in mice, allowing imaging with ^{123}I and inhibition of tumor growth with ^{131}I[193] **(Imaging, Drug)**
Hepsin (PC3 cells over-expressing Hepsin)	IPLVVPL[194] (pIII, **T**)		Yes	Peptide conjugated to fluorescent nanoparticle, cross-linked iron oxide (CLIO) for fluorescence-mediated tomography of tumors in mice **(Imaging)**

Protein used for selection (cont.)	**Peptide sequence[a,b,c,d] (cont.)**	***In vitro* therapy[e] (cont)**	***In vivo* homing validated (cont)**	***In vivo* delivery[e] (cont)**
Tie2 (SMMC772 cells over-expressing Tie2)	NSLSNASEFRAPY[195] (GA5) (pIII, **V**)	Conjugated to PEI for delivery of luciferase gene **(Oligo)**	Yes	Conjugated to PEI for delivery of WT p53 gene by intratumoral injection in mice **(Oligo)**
Tie2	TMGFTAPRFPHY[196] (PH1) (pIII, **V**)	Conjugated to cisplatin loaded liposomes for specific cell killing **(Drug)**		
IL-6 receptor (gp80)	LSLITRL[197] (pIII, **T/V**)	Peptide itself had anti-angiogenic properties **(Peptide)**		Peptide itself injected i.p. into tumor-bearing mouse inhibited tumor growth **(Peptide)**
$\alpha_5\beta_1$	GA**C**RGD**C**LGA[198] (pIII, **T/V**)			
$\alpha_6\beta_1$	VSWFSRHRYSPFAVS[199] (pIII, **T/V**)			
	HRWMPHVFAVRQGAS[199] (pIII, **T/V**)			
	FGRIPSPLAYTYSFR[199] (pIII, **T/V**)			
EphA2	YSAYPDSVPMMS (YSA)[200] (pIII, **T/V**)	Peptide functionalized nanogels loaded with EGFR siRNA knocked down EGFR[201] **(Oligo)** Peptide modified adenovirus with luciferase gene delivers gene to cells[202] **(Oligo)**		Peptide conjugated to rhodamine-tagged magnetic nanoparticles bound to ovarian cancer cells injected into peritoneum & visualized the cells after magnet placed above mouse[203] **(Imaging)**

Protein used for selection (cont.)	Peptide sequence[a,b,c,d] (cont.)	*In vitro* therapy[e] (cont)	*In vivo* homing validated (cont)	*In vivo* delivery[e] (cont)
MMP-9	**C**TTHWGFTL**C**[204] (CTT) (pIII, **T/V**)	Peptide itself inhibits cell migration[204] and invasion[205] **(Peptide)** Peptide-doxorubicin liposomes increased cell death[206] **(Drug)**	Yes[164, 207-210]	Gamma imaging of tumor-bearing mice given ^{99m}Tc-CTT liposomes encapsulated with ^{125}I-albumin[208] & microPET imaging of tumor-bearing mice given ^{64}Cu-DOTA-CTT[209] **(Imaging)** Peptide itself when injected into mice adjacent to the tumor or i.p. injected inhibited tumor growth & improved survival[204] **(Peptide)** a hydrophilic peptide derivative injected via tail vein inhibited tumor growth & improved survival[205] **(Peptide)** Hydrophilic derivative peptide-doxorubicin liposomes increased survival in tumor-bearing mice[164] **(Drug)** Chimeric Vascular endothelial growth inhibitor (VEGI)-peptide inhibited tumor growth in mice when injected i.p.[126] **(Drug)** Fusion of peptide with kringle 5 fragment of human plasminogen inhibited tumor growth and increased survival in tumor-bearing mice after i.p. injection[127] **(Drug)**
TAG-72	FRER**C**DKHPQK**C**TKFL[211] (pVIII hybrid, **T**)		Yes	SPECT/CT of tumors in mice with ^{99m}Tc-labeled peptide **(Imaging)**
	DPRH**C**QKRVLP**C**PAWL[211] (pVIII hybrid, **T**)		Yes	SPECT/CT of tumors in mice with ^{99m}Tc-labeled peptide **(Imaging)**
	NPGT**C**KDKWIE**C**LLNG[212] (pVIII hybrid, **T**)		Yes	
	GGVS**C**MQTSPV**C**ENNL[213] (A2-6) (pVIII hybrid, **T**)			

Protein used for selection (cont.)	**Peptide sequence[a,b,c,d] (cont.)**	***In vitro* therapy[e] (cont)**	***In vivo* homing validated (cont)**	***In vivo* delivery[e] (cont)**
E-cadherin (& N-cadherin)	SWELYYPLRANL[214] (pIII, **T/V**)			
Human N-cadherin	H-SWTLYTPSGQSK-NH_2[215] (pIII, **T/V**)	Peptide inhibited adhesion and tube formation of HUVECs **(Peptide)**		
Human carbonic anhydrase IX (CAIX)	YNTNHVPLSPKY (CaIX-P1)[216] (pIII, **T**)		Yes	
Galectin-3	ANTP**C**GPYTHD**C**PVKR[217] (G3-C12) (pVIII hybrid, **T**)		Yes[218, 219]	SPECT/CT[218] & microSPETC/CT[219] imaging of tumors in mice injected with ^{111}In-DOTA-peptide **(Imaging)**
	PQNSKIPGPTFLDPH[217] (G3-A9) (pVIII hybrid, **T**)			
Phophatidyl serine	**C**LSYYPSY**C**[220] (pIII, **T/V**)		Yes	Fluorescein-labeled peptide imaged in mice with or without anti-cancer drug camptothecin treatment to induce cellular apoptosis **(Imaging, Drug)**
Met (NIH 3T3 cells transfected with HGF/SF and Met and SK-LMS-1/HGF cells which express Met)	YLFSVHWPPLKA[221] (pIII, **T/V**)		Yes	Radionuclear imaging of tumor-bearing mice injected with ^{125}I-peptide **(Imaging)**
Prostate-specific membrane antigen (PSMA)	WQPDTAHHWATL[222] (pIII, **T/V**)			
VEGFR-3	**C**SDSWHYW**C**[223] (pIII, **V**)			

a – Cysteine residues that form disulfide bonds are indicated in bold.

b - Common peptide names that have been used in the literature are indicated in parenthesis next to the peptide sequence.

c – The phage display library type is also indicated in parenthesis. All phage are filamentous unless noted as T7 phage.

d – **T** indicates tumor cell targeting and **V** indicates tumor vasculature targeting.

e – The type of agent used for targeting is designated in parenthesis. **Peptide** indicates an unconjugated peptide; **drug**, peptide conjugation to a drug; **imaging**, peptide conjugation to an imaging agent; and **oligo**, peptide conjugation to a oligonucleotide or other gene delivery vehicles.

Table 1-3. Peptides Selected From Panning Phage Libraries Against Cultured Cells

Cancer Type	Cell Line used for Selection[a]	Peptide Sequence[b,c,d,e]	Receptor Identified	*In vitro* therapy[g]	*In vivo* Homing Validated	*In vivo* delivery[g]
Hepatocellular carcinoma	BEL-7402	TACHQHVRMVRP[224] (pIII)				
	SMMC-7721	KSLSRHDHIHHH[125] (pIII)		Peptide itself inhibits cell migration **(Peptide)** Peptide-toxic shock syndrome toxin 1 (TSST-1) fusion protein killed cells **(Drug)**		Peptide-toxic shock syndrome toxin 1 (TSST-1) fusion protein inhibited tumor growth in mice **(Drug)**
	Mahlavu	SFSIIHTPILPL[162] (pIII)		Virus-like particles modified with peptide and loaded with doxorubicin, cisplatin, and 5-fluorouracil, or an siRNA cocktail against cyclins, or ricin toxin A-chain selectively kill cells[176] **(Drug, Oligo)**	Phage homing inhibited by peptide	Pepitde-liposomal doxorubicin inhibited tumor growth in mice **(Drug)**
Melanoma	Me6652/4	**C**TVALPGGYVRV**C**[118] (phagemid displaying different peptides on pVII and pIX)	GRP78	Peptide-taxol[118] and peptide-prodrug doxorubicin or taxol[112] killed cells **(Drug)**		
	B16-F10 (murine)	TRTKLPRLHLQS[225] **(f)** (pIII)				
	B16-F10-Nex2 (murine)	**C**SSRTMHH**C**[226] (pIII)	cadherins	Peptide itself reduced cell viability and inhibited cell invasion **(Peptide)**		Peptide itself decreased metastatic nodules after i.p. injection in mice and delayed tumor growth and improved survival for xenografts in mice **(Peptide)**
	B16 cells cocultured with B-1 lymphocytes (murine malignant melanoma model)	**C**LFMRLAW**C**[227] (pIII)	MUC18			
Prostate	Capan-2 (irradiated)	SHGFSRHSMTLI[228] (pIII)			Yes	
	LNCaP	DPRATPGS[229] (pVIII landscape)				
	DU-145	FRPNRAQDYNTN[230] (DUP-1) (pIII)		Both peptide and A10 RNA aptamer-doxorubicin conjugated through streptavidin or conjugated to TCL-SPION selectively killed cells[113] **(Drug)**	Yes[230, 231]	
	PC3	DTPYDLTG[232] (pVIII landscape)				
		DTDSHVNL[232] (pVIII landscape)		Landscape phage pVIII coat protein displaying peptide inserted into Doxil® for specific cell killing[157] **(Drug)**		

Cancer Type (cont.)	Cell Line used for Selection[a] (cont.)	Peptide Sequence[b,c,d,e] (cont.)	Receptor Identified (cont.)	*In vitro* therapy[g] (cont.)	*In vivo* Homing Validated (cont.)	*In vivo* delivery[g] (cont.)
Prostate (cont.)		DVVYALSDD[232] (pVIII landscape)		Landscape phage pVIII coat protein displaying peptide incorporated into Doxil® for specific cell killing[157] **(Drug)**		
	PC-1	GGKRPAR[233] (T7 phage) (specifically looking for phage that bound NRP-1)	Neuropilin-1 (NRP-1)			
		RIGRPLR[233] (T7 phage) (specifically looking for phage that bound NRP-1)	Neuropilin-1 (NRP-1)			
Gastric	XGC9811-L4	GRRTRSRRLRRS[234] (pIII)		Peptide itself decreased cell invasion and migration and adherence to Type IV collagen **(Peptide)**		
	GC9811-P	SMSIASPYIALE[235] (pIII)		Peptide itself decreased invasion and adhesion of cells **(Peptide)**		Mice with peritoneal dissemination models of gastric cancer treated i.p. with peptide had fewer metastases to the peritoneum and significantly longer survival **(Peptide)**
Gastric Cancer Vasculature	HUVECs and SGC7901 coculture (looking for binding to HUVECs)	**C**TKNSYLM**C**[236] (GEBP11) (pIII)				
Colon	HT29	**C**PIEDRPM**C**[121] (RPMC) (pIII)	$\alpha_5\beta_1$[237]	Peptide-$_D$(KLAKLAK)$_2$ selectively killed cells **(Drug)**	Yes[237]	Gamma imaging of ^{111}In-DOTA-RPMC in tumor-bearing mice[237] **(Imaging)** Fluorescence endoscopy of colon cancer in mouse with peptide-FITC[237] **(Imaging)**
	WiDr	HEWSYLAPYPWF[238] (HEW) (pIII)		Peptide-lacZ adenoviruses selectively infected cells[239] **(Oligo)**	Did not home[239]	
		QIDRWFDAVQWL[238] (pIII)				
	SW480	VHLGYAT[240] (pIII)				
	T84	**C**QARGDLGKIR**C**[241] (pIII)				
Head and Neck	MDA167Tu	TSPLNIHNGQKL[242] (HN-1) (pIII)		Peptide conjugated to the PKCε peptide inhibited cell motility, invasion, and proliferation[243] **(Drug)**	Yes[242, 243]	Peptide conjugated to the PKCε peptide injected i.p. inhibited tumor growth in mice[243] **(Drug)**
	HNO223	SPRGDLAVLGHKY[244] (HBP-1) (pIII)	$\alpha_v\beta_6$ (suggested)		Yes	
	NPC-TW 04	RLLDTNRPLLPY[161] (pIII)			Phage homing inhibited by peptide	Peptide-liposomal doxorubicin inhibited tumor growth in mice **(Drug)**
	Hep-2	**C**RLTGGKGVG**C**[245] (phagemid pVIII hybrid)				

Cancer Type (cont.)	Cell Line used for Selection[a] (cont.)	Peptide Sequence[b,c,d,e] (cont.)	Receptor Identified (cont.)	*In vitro* therapy[g] (cont.)	*In vivo* Homing Validated (cont.)	*In vivo* delivery[g] (cont.)
Breast	MDA-MB-231	YQATPARFYTNT[238] (pIII)				
		CGWMGLEL**C**[238] (pIII)				
	SKBR3	LTVSPWY[246] (pIII)	ErbB2[119]	Peptide-antisense oligonucleotide against ErbB2 inhibited ErbB2 gene expression in cells **(Oligo)** Peptide-proapoptotic α-tocopheryl succinate (α-TOS) selectively killed cells[119] **(Drug)**	Yes[247]	Peptide-proapoptotic α-tocopheryl succinate (α-TOS) injected i.p. into transgenic mice bearing breast carcinomas reduced initial tumor volume[119] **(Drug)** Tetrameric far-red fluorescent protein (KatushkaS158A) used as a scaffold to create an octavalent peptide fluorescent nanoparticle allowed far-red fluorescent imaging of tumors in mice[247] **(Imaging)**
		WNLPWYYSVSPT[246] (pIII)				
	MCF-7	DMPGTVLP[248, 249] (pVIII landscape)		Landscape phage pVIII coat protein displaying peptide incorporated into liposomes loaded with *PRDM14* siRNA knocked down PRDM14 protein expression[248, 249] **(Oligo)** Landscape phage pVIII coat protein displaying peptide incorporated into Doxil® for specific cell killing[248] **(Drug)**		
Neuro-blastoma	WAC 2	HLQIQPWYPQIS[250] (pIII)				
		VPWMEPAYQRFL[250] (p160) (pIII)		Peptide-micelles loaded with paclitaxel killed cells[251] **(Drug)**	Yes[252, 253]	
Glioma	RG2 (rat)	VGLPEHTQ[254] (pVIII landscape)				
		ELRGDSLP[254] (pVIII landscape)				
		DSTKSGNM[254] (pVIII landscape)				
		DYDMTKNT[254] (pVIII landscape)				
		DLTKSTAP[254] (pVIII landscape)				
		ESRGDSYA[254] (pVIII landscape)				
	U87-MG	M**C**PKHPLG**C**[255] (pIII)				
		VTWTPQAWFQWV (VTW)[256] (pIII)	GP130 (suggested)			
	Gli36	LLADTTHHRPWT[257] (pIII)				
	Mixture of dGli36, SF767, U87MG, U251MG, & U373MG	LWATFPPRPPWL[258] (pIII)		Peptide-(K_{16}) complexed with luciferase DNA transfected SF767 glioma cells **(Oligo)**		
Cervical	SiHa	**C**RLTGGKGVG**C**[259] (phagemid pVIII hybrid)				
		CADPNSVRAM**C**[259] (phagemid pVIII hybrid)				

Cancer Type (cont.)	Cell Line used for Selection[a] (cont.)	Peptide Sequence[b,c,d,e] (cont.)	Receptor Identified (cont.)	*In vitro* therapy[g] (cont.)	*In vivo* Homing Validated (cont.)	*In vivo* delivery[g] (cont.)
Cervical (cont.)	SiHa (cont.)	**C**AAHYRVGPW**C**[259] (phagemid pVIII hybrid)				
	HeLa	**C**SSGKPLV**C**[260] (pIII)		Peptide increased transfection of luciferase DNA polyplex **(Oligo)**		
		CNISRTGT**C**[260] (pIII)		Peptide increased transfection of luciferase DNA polyplex **(Oligo)**		
		CNSTELSG**C**[260] (pIII)		Peptide increased transfection of luciferase DNA polyplex **(Oligo)**		
Thyroid Cancer	TT	**C**HTFEPVG**C**[261] (pIII)		Peptide linked to adenovirus vector expressing GFP infected cells **(Oligo)**		
	FRO82-2	EDYELMDLLAYL[262] (FROP-1) (pIII)			Yes	
Rhabdo-myosarcoma	RD	**C**QQSNRGDRKR**C**[263] (T7 phage)	$\alpha_V\beta_3$			
		CMGNKRSAKRP**C**[263] (T7 phage, **T/V**)			Yes	
Lymphoma	A20 (murine)	SAKTAVSQRVWLPSHRGGEP (A20.1)[264] (pIII)				
		KSREHVNNSACPSKRITAAL (A20.2)[264] (pIII)		"		
		WLSEAGPVVTVRALRGTGSW (PCM.1)[264] (pIII)		"		
	Molt-4	**C**AYHRLRR**C**[122] (pIII)		Peptide-proapoptotic peptide $_D$(KLAKLAK)$_2$ killed cells **(Drug)**		
		CGFYWLRS**C**[123] (pIII)	Neuropilin-1 (NRP-1)	Peptide-proapoptotic peptide $_D$(KLAKLAK)$_2$ killed cells **(Drug)**		
Leukemia	Kasumi-1	**C**PLDIDFY**C**[265] (pIII)	$\alpha_4\beta_1$			
Lung Cancer	H1299 (large cell)	VSQTMRQTAVPLLWFWTGSL (H1299.1)[266] (pIII)		Peptide-doxorubicin conjugate selectively killed cells[114] **(Drug)**		
		YAAWPASGAWTGTAPCSAGT (H1299.2)[267] (pIII)				
		EHMALTYPFRPP (ZS-1)[268] (pIII)				
		QQMHLMSYAPGP (ZT-1)[269] (PhD NE Bio)				
	H2009 (adeno-carcinoma)	RGDLATLRQLAQEDGVVGVR (H2009.1)[266] (pIII)	$\alpha_V\beta_6$[81]	Peptide-doxorubicin conjugate[114] and peptide-polyglutamic acid polymer-doxorubicin conjugate[270] selectively killed cells **(Drug)** peptide conjugated to micelles loaded with doxorubicin and SPIO selectively killed cells[173] **(Drug)**	Yes[271]	

Cancer Type (cont.)	Cell Line used for Selection[a] (cont.)	Peptide Sequence[b,c,d,e] (cont.)	Receptor Identified (cont.)	*In vitro* therapy[g] (cont.)	*In vivo* Homing Validated (cont.)	*In vivo* delivery[g] (cont.)
Lung Cancer (cont.)	A549 (adeno-carcinoma)	MTVCNASQRQAHAQATAVSL (A549.1)[266] (pIII)				
	CL1-5	TDSILRSYDWTY[159] (pIII)			Yes	Peptide-liposomal doxorubicin and liposomal vinorelbine inhibited tumor growth in mice **(Drug)**
Ovarian Cancer	SK-OV-3	SVSVGMKPSPRP[272] (pIII)				
Barrett's Esophagus	OE33	SNFYMPL[273] (pIII)				
Osteosarcoma	143B	ASGALSPSRLDT (OSP-1)[274] (pIII)	HSPG		Yes	microPET imaging with ^{18}F-peptide in tumor-bearing mice **(Imaging)**
B cell lymphoma	Raji	**C**TLPHLKM**C**[275] (pIII)	variable region of human immune-globulin heavy chain (suggested)			

a – All cell lines are of human origin unless otherwise indicated.
b – Cysteine residues that form disulfide bonds are indicated in bold.
c – Common peptide names that have been used in the literature are indicated in parenthesis next to the peptide sequence.
d – The phage display library type is also indicated in parenthesis. All phage are filamentous unless noted as T7 phage.
e – All peptides bind to tumor cells unless otherwise indicated. **V** indicates tumor vasculature targeting.
f – Two round of *in vivo* display before final selection on cultured cells.
g – The type of agent used for targeting is designated in parenthesis. **Peptide** indicates an unconjugated peptide; **drug**, peptide conjugation to a drug; **imaging**, peptide conjugation to an imaging agent; and **oligo**, peptide conjugation to a oligonucleotide or other gene delivery vehicles.

Table 1-4. Peptides Selected From Panning Phage Libraries Against Cells *Ex Vivo*

Cancer Type[a]	Cells or Tumor used for Selection[a]	Peptide Sequence[b,c,d]	Receptor Identified	*In vitro therapy*[e]	*In vivo* Homing Validated	*In vivo* delivery[e]
Colon	Human colonic adenomas	VRPMPLQ[276] (pIII)				Topical administration of peptide-fluorescein for imaging colonic adenomas in humans **(Imaging)**
	Resected human colon tumors	SPTKSNS[83] (pIII)				
Bladder	Cells from HT-1376 xenograft	**C**SNRDARR**C**[277] (pIII)			Yes	
Pancreatic	Pancreatic ductual carcinomas arising from Kras/p52$^{L/L}$ mice	KTLLPTP[278] (pIII)	Plectin-1		Yes[82, 278]	Conjugated to crosslinked iron oxide-Cy5.5 nanoparticles for intravital confocal microscopy in tumor-bearing mice[278] **(Imaging)** ^{111}In labeled peptide used for SPECT/CT imaging in tumor-bearing mice[82] **(Imaging)**

a – All cell lines are of human origin unless otherwise indicated.
b – Cysteine residues that form disulfide bonds are indicated in bold.
c – Common peptide names that have been used in the literature are indicated in parenthesis next to the peptide sequence.
d – The phage display library type is also indicated in parenthesis. All phage are filamentous unless noted as T7 phage.
e – The type of agent used for targeting is designated in parenthesis. **Imaging** indicates peptide conjugation to an imaging agent.

Table 1-5. Peptides Selected From Panning Phage Libraries *In Vivo*

Tumor Type[a]	Peptide Sequence[b,c,d,e,f]	Receptor Identified	*In vitro* therapy[k]	*In vivo* Homing Validated with Free Peptide	*In vivo* delivery[k]
Gastric (AZ-P7a)	SWKLPPS[153] **(g)** (pIII, **T**)	$\alpha_3\beta_1$ (suggested)	Peptide-liposomal doxorubicin selectively killed cells **(Drug)**	Yes	
Human gastric adenocarcinoma (freshly injected into mice)	**C**GNSNPKS**C**[279] (GX1) (pIII, **V**)		Peptide itself and peptide-recombinant human tumor necrosis factor alpha (rmhTNFα) induce HUVEC apoptosis[132] **(Peptide, Drug)**	Yes[132, 280-283]	SPECT imaging of $^{99}Tc^{m}$-peptide and $^{99}Tc^{m}$-peptide-rmhTNFα in SGC7901 tumor-bearing mice[132] **(Imaging)** Peptide-rmhTNFα inhibits SGC7901 tumor growth in mice[132] **(Drug)** Near infrared fluorescence imaging of Cy5.5-peptide in U87MG tumor-bearing mice[282] **(Imaging)** microPET imaging of ^{64}Cu-DOTA-peptide in U87MG tumor-bearing mice[283] **(Imaging)**
Lung (irradiated and SU11248 treated murine Lewis lung carcinoma) & Glioblastoma (GL261, murine)	HVGGSSV[93] **(h)** (T7 phage, **V**)	TIP-1[177]		Yes[93, 163, 177, 284, 285]	Near infrared fluorescence imaging of Cy7-peptide in various types of tumor-bearing mice treated with irradiation or TKI (tyrosine kinase inhibitors) or both[93] **(Imaging)** Peptide-nab-paclitaxel inhibited Lewis lung carcinoma and H460 tumor growth in mice in conjunction with irradiation and when labeled with Alexa Fluor 750 was used for near infrared fluorescence imaging of irradiated Lewis lung carcinoma tumors[177] **(Drug, Imaging)** Near infrared fluorescence imaging of irradiated Lewis lung carcinoma tumors with Alexa Fluor 750-peptide[284] **(Imaging)** Near infrared fluorescence imaging of irradiated H460 tumors with Alexa Fluor 750-labeled peptide-FePt nanoparticles[285] **(Imaging)** Near infrared fluorescence imaging of irradiated Lewis lung carcinoma tumors with Alexa Fluor 750 peptide liposomes[163] **(Imaging)** Lewis lung carcinoma and H460 tumor growth inhibition with both iirradiation and peptide liposomal doxorubicin[163] **(Drug)**
Lung (CL1-5)	SVSVGMKPSPRP[160] (pIII, **V**)			Pepitde blocked phage homing	Peptide liposomal doxorubicin inhibited CL1-5 tumor growth and increased survival in mice **(Drug)**

Tumor Type[a] (cont.)	**Peptide Sequence[b,c,d,e,f] (cont.)**	**Receptor Identified (cont.)**	***In vitro* therapy[k] (cont.)**	***In vivo* Homing Validated with Free Peptide (cont.)**	***In vivo* delivery[k] (cont.)**
Lung (H460)	R**C**PLSHSLI**C**Y[286] (pIII, **T**)			Yes	
Oral (SAS)	SVSVGMKPSPRP[160] (pIII, **V**)				Peptide liposomal doxorubicin inhibited SAS tumor growth and increased survival in mice **(Drug)**
	SNPFSKPYGLTV[158] (pIII, **V**)			Yes	Peptide liposomal doxorubicin inhibited tumor growth and increased survival in mice for various tumor types **(Drug)**
	YPHYSLPGSSTL[158] (pIII, **V**)			Yes	Peptide liposomal doxorubicin inhibited tumor growth and increased survival in mice for various tumor types **(Drug)**
Nasopharyngeal Carcinoma (CNE-1)	EDIKPKTSLAFR[287] (pIII, **ND**)			Yes	
Prostate (PC-3)	IAGLATPGWSHWLAL[288] (G1) (pIII, **T**)		Peptide itself killed cells[289] **(Peptide)**	Yes[289]	^{111}In-DOTA-peptide used for SPECT/CT imaging of PC-3 tumors in mice[289] **(Imaging)**
	LKGD**C**TQRYVY**C**MKSK[289] (H5) (pVIII hybrid, **T**)		Peptide itself killed cells **(Peptide)**	Yes	^{111}In-DOTA-peptide used for SPECT/CT imaging of PC-3 tumors in mice **(Imaging)**
	CRGDKGPD**C**[178] (iRGD) (T7 phage, **T/V**)	$\alpha_v\beta_3$, $\alpha_v\beta_5$ then cleaved to CRGDK and binds NRP-1	Peptide-abraxane killed cells **(Drug)**	Yes[178, 179]	Near infrared imaging of tumors in mice with novo pancreatic ductal adenocarcinoma using peptide-Cy7 **(Imaging)** MRI of 22Rv1 orthotopic xenografts in mice using peptide-linked SPIO nanoworms **(Imaging)** Peptide-abraxane inhibited 22Rv1 and BT474 orthotopic tumor growth in mice **(Drug)** Co-injection of peptide with Nab-paclitaxel or injection of peptide conjugated to Nab-paclitaxel inhibited BT474 or 22Rv1 orthotopic tumor growth in mice[179] **(Drug)** Co-injection of peptide with doxorubicin inhibited 22Rv1 and 4T1 orthotopic tumor growth in mice[179] **(Drug)** Co-injection of peptide with liposomal doxorubicin inhibited 22Rv1 orthotopic tumor growth in mice[179] **(Drug)** Co-injection of peptide with trastuzumab eradicated BT474 orthotopic tumors in mice[175] **(Drug)** CGKRK-$_D$[KLAKLAK]$_2$-iron oxide nanoworms systemically injected into mice with 005 tumors prolonged survival when co-injected with the peptide[290] **(Drug)**
Prostate Tumors from TRAMP mice	**C**REAGRKA**C**[101] (REA) **(i)** (T7 phage, **L**)			Yes	Peptide-$_D$(KLAKLAK)$_2$ conjugate reduced PPC1 orthotopic tumor lymphatic vessels in mice **(Drug)**

Tumor Type[a] (cont.)	**Peptide Sequence[b,c,d,e,f] (cont.)**	**Receptor Identified (cont.)**	***In vitro* therapy[k] (cont.)**	***In vivo* Homing Validated with Free Peptide (cont.)**	***In vivo* delivery[k] (cont.)**
Prostate (DU145)	YR**C**TLNSPFFWEDMTHE**C**HA[124] (pIII, **T**)	CRKL	Peptide-proapoptotic peptide $_D$(KLAKLAK)$_2$ killed cells **(Drug)**		Peptide-proapoptotic peptide $_D$(KLAKLAK)$_2$ inhibited DU145 tumor growth in mice **(Drug)**
Prostate (PPC-1)	RPARPAR[291] **(i)** (T7 phage, **T**)	Neuropilin-1 (NRP-1)[291, 292]		Yes (but in normal mice accumulated in first met vascular beds)	
Breast (MDA-MB-435[95-98])	**C**NGR**C**VSG**C**AGR**C**[115] (NGR) **(j)** (pIII, **V**)	Amino-peptidase N (CD13)[293]		Peptide blocked phage homing[115]	Peptide-doxorubicin conjugate inhibited MDA-MB-435 tumor growth & prolonged survival in mice[115] **(Drug)** Tum-5-peptide (tumstatin gene fragment) inhibited S180 tumor growth in mice[128] **(Drug)** Peptide-TNF (tumor necrosis factor α) inhibited tumor growth[133] and synergistically increased the effects of various chemotherapy drugs on tumor inhibition in mice (for various tumor types)[134-136] **(Drug)** Human interferon alpha (hIFN-α2a)-peptide[129] and recombinant hIFN-α2a-peptide[130] inhibited tumor growth in mice when injected i.p. in various tumor models (immunogenicity of rhIFN-α2a-peptide also tested in rats and rhesus monkeys) **(Drug)** Peptide-liposomal doxorubicin inhibited growth of orthoptoic neuroblastoma xenografts in mice[165] & increased survival in mouse lung, ovarian, and neuroblastoma xenografts[166] **(Drug)**

Tumor Type[a] (cont.)	**Peptide Sequence[b,c,d,e,f] (cont.)**	**Receptor Identified (cont.)**	***In vitro* therapy[k] (cont.)**	***In vivo* Homing Validated with Free Peptide (cont.)**	***In vivo* delivery[k] (cont.)**
Breast (MDA-MB-435) (cont.)	**C**DC**R**GD**CFC** (RGD-4C)[115] **(j)** (pIII, **T**/**V**)	$\alpha_v\beta_3$, $\alpha_v\beta_5$ $\alpha_5\beta_1$	Peptide-adeno-associated virus phage vector (AAVP) transfected cells with β-galactosidase or GFP[294, 295] **(Oligo)** Peptide-Delta-24 adenovirus (an adenovirus with anticancer activity) killed a variety of cancer cell lines[295] **(Drug)**	Yes[296]	Peptide-doxorubicin conjugate inhibited MDA-MB-435 tumor growth & prolonged survival in mice[115] and inhibited MH134 orthotopic tumor growth in mice[116] **(Drug)** Scintigraphic imaging of DU145 tumors in mice using $^{99m}Tc(CO_3)$-peptide and $^{99m}Tc(CO_3)$-HPMA polymer-peptide ; the polymer was also imaged in PC-3 tumors[298] **(Imaging)** Peptide-adeno-associated virus phage vector (AAVP) delivered GFP to KS1767 xenografts in mice & delivered luciferase to DU145 xenografts as evidenced by bioluminescent imaging[294] **(Imaging)** Peptide-adeno-associated virus phage vector (AAVP) delivered the *HSVtk* gene to DU145 xenografts as evidenced by PET imaging with [^{18}F]FEAU[294] **(imaging)** Peptide-adeno-associated virus phage vector (AAVP)-*HSVtk* gene and treatment with gancilovir, inhibited growth of DU145, KS1767, and UC3 xenografts in mice and inhibited growth of EF43-FGF4 mouse mammary tumors[294] **(Oligo, Drug)** MicroPET imaging of ^{64}Cu-DOTA-Peptide-tumor necrosis factor-α (TNF) in mice bearing U87MG and MDA-MG-435 tumors[137] **(Imaging)** Peptide-tumor necrosis factor-α (TNF) inhibited of MDA-MB-435 orthotopic tumor growth[137] **(Drug)** Intratumoral injection of peptide-Delta-24 adenovirus (an adenovirus with anticancer activity) into orthotopic U-87 MG tumors in mice increased survival[295] **(Drug)**

Tumor Type[a] (cont.)	**Peptide Sequence[b,c,d,e,f] (cont.)**	**Receptor Identified (cont.)**	***In vitro* therapy[k] (cont.)**	***In vivo* Homing Validated with Free Peptide (cont.)**	***In vivo* delivery[k] (cont.)**
Breast (MDA-MB-435) (cont.)	**C**GNKRTRG**C** (LyP-1)[99] **(i)** (T7 phage, **T/L/M**)	p32/ gC1qR[297]	Peptide itself induced cell death[100] **(Peptide)** Baculovirus displaying peptide-VSVG protein fusions and carrying luciferase gene specifically transduced cells[298, 299] **(Oligo)** Peptide coupled to microbubbles containing paclitaxel killed cells when treated in combination with ultrasound[181] **(Drug)** Peptide-doxorubicin liposomes killed MDA-MB-435 cells with or without heat treatment[154] **(Drug)**	Yes[99, 100]	Peptide itself inhibited MDA-MB-435 tumor growth in mice[100] **(Peptide)** Dye-labeled –peptide-abraxane inhibited tumor growth in mice[180] **(Drug)** Peptide doxorubicin liposomes did not change tumor growth compared to non-targeted liposomes[300] **(Drug)** Near-infrared fluorescence imaging and *ex vivo* imaging of lymphanogenesis using Cy5.5-peptide injected via middle phalanges of both upper extremities in 4T1 tumor bearing mice[301] **(Imaging)** Peptide-doxorubicin liposomes injected after gold nanorod-mediated heating of tumors caused tumor regression in mice with MDA-MB-435 tumors[154] **(Drug)**
Breast (MDA-MB-231 and MCF-7 in mice treated with sunitinib and responding to therapy)	EGEVGLG[92] **(h)** (T7 phage, **V** after sunitinib treatment)			Yes	Peptide-Alexa Fluor 750 used for near-infrared imaging of sunitinib treated MDA-MB-435 and MCF7 tumors in mice **(Imaging)**
Medullary Thyroid Carcinoma (murine RET-C634R transgenic model)	**C**SRESPHP**C**[302] **(i)** (pIII, **T**)			Peptide blocked phage homing	Peptide linked to adenovirus expressing the oncogene inhibitor RETΔTK inhibited MTC tumor growth in mice and tumor growth for transgenic RET mice[303] **(Oligo, Drug)** Peptide linked to adenovirus expressing luciferase imaged in MTC and RET tumors[303] **(Oligo, Imaging)**
Medullary Thyroid Carcinoma (TT)	**C**HTFEPVG**C**[261] (pIII, **T**)		Peptide linked to adenovirus vector expressing GFP infected cells **(Oligo)**		
Basal cell squamous carcinoma from K14-HPV16 mice	CGKRK[304] **(i)** (T7 phage, **V**)		Recombinant silk protein-polylysine-luciferase plasmid DNA-monomeric or dimeric peptide complexes transfected cells[305] **(Oligo)** Baculovirus displaying peptide-VSVG protein fusions and carrying luciferase gene specifically transduced cells[298] **(Oligo)** Peptide-$_D$[KLAKLAK]$_2$-iron oxide nanoworms killed cells and inhibited tube formation of HUVECs[175] **(Drug)**	Yes[175, 304, 306]	Peptide-$_D$[KLAKLAK]$_2$-iron oxide nanoworms decreased the number of blood vessels in bFGF-Matrigel plugs in mice[175] **(Drug)** Peptide-$_D$[KLAKLAK]$_2$-iron oxide nanoworms systemically injected into mice bearing lentiviral (H-RasV12-shp53) induced brain tumors cured most mice[175] **(Drug)** Peptide-$_D$[KLAKLAK]$_2$-iron oxide nanoworms co-injected with the iRGD peptide into mice with 005 tumors prolonged survival[175] **(Drug)**

Tumor Type[a] (cont.)	**Peptide Sequence[b,c,d,e,f] (cont.)**	**Receptor Identified (cont.)**	***In vitro* therapy[k] (cont.)**	***In vivo* Homing Validated with Free Peptide (cont.)**	***In vivo* delivery[k] (cont.)**
Basal cell squamous carcinoma from K14-HPV16 mice (cont.)	CDTRL[304] **(i)** (T7 phage, **V**)			Yes	
Melanoma (C8161)	**C**LSDGKRK**C**[101] (LSD) **(i)** (T7 phage, **L**)			Yes	Peptide-$_D$(KLAKLAK)$_2$ conjugate reduced C8161 orthotopic tumor lymphatic vessels in mice (**Drug)**
Melanoma (murine B16-F10)	TRTKLPRLHLQS (WDC-2)[225] **(g, i)** (pIII, **T**)				Phage inhibited B16-F10 tumor growth when injected adjacent to tumor **(Peptide)**
RIP1-Tag2 mice Pancreatic islets	CRGRRST (RGR)[307] **(i)** (T7 phage, **V**)	PDGFRβ		Yes	Combination treatment with peptide-anti-CD40 antibody and murine IL-2-peptide fusion protein increased survival in RIP1-Tag5 mice and 80% of mice treated with the combination treatment plus adoptive transfers of anti-Tag CD4$^+$ and CD8$^+$ T cells survived long-term[131] **(Drug)**
	CRSRKG (RSR)[307] (T7 phage, **V**)			Yes	
	CKAAKNK (KAA)[307] (T7 phage, **V**)			Yes	
	CKGAKAR (KAR)[307] (T7 phage, **T**)				
	FRVGVADV (VGVA)[307] (T7 phage, **T**)				
Human patient with Waldenström macroglobulinemia B cell malignancy (isolated from pancreas)	**C**GRRAGGS**C**[86] (pIII, **T**)	IL-11Rα[86, 87]	Peptide-proapoptotic peptide $_D$(KLAKLAK)$_2$ killed cells[88] **(Drug)**		^{111}In-DTPA-IR dye-peptide construct used for both SPECT/CT and near-infrared imaging in a mouse bearing a MDA-MB-231 tumor[308] **(imaging)**
Dysplatic Colon Mucosa/colon adenomas from *CPC*;*Apc* mice	QPIHPNNM[309] (T7 phage, **T**)			Yes[309, 310]	FITC-peptide bound adenomas in *CPC*;*Apc* mice as viewed by endoscopy[309] and microendoscopy[310] (peptide solution introduced into the colon prior to washing) **(Imaging)**
Colorectal (Bevacizumab-treated LS174T)	LLADTTHHRPWT[91] (BRP) **(h)** (pIII, bevacizumab-treated **V**)			Yes	Peptide-IRDye800 used for near-infrared imaging of bevacizumab-treated LS174T tumors in mice **(Imaging)** PET imaging with ^{18}F-FP-Peptide in mice bearing LS174T tumors treated with bevacizumab **(Imaging)**
Gliomas (irradiated murine GL261)	GIRLRG[182] **(h)** (T7 phage, irradiated **V**)	GRP78		Yes	Peptide-Alexa Fluor 750 used for near-infrared imaging in mice with irradiated Gl261 tumors **(Imaging)** Peptide conjugated to nanoparticle encapsulating paclitaxel inhibits MDA-MB-231 tumor growth in irradiated mice **(Drug)**
Hepatocarcinoma (BEL-7402)	AGKGTPSLETTP[117] (A54) (pIII, **T**)		Peptide-doxorubicin conjugate selectively killed cells **(Drug)**		Peptide-doxorubicin conjugate inhibited tumor growth and increased survival in mice with BEL-7402 tumors **(Drug)**

Tumor Type[a] (cont.)	**Peptide Sequence[b,c,d,e,f] (cont.)**	**Receptor Identified (cont.)**	***In vitro* therapy[k] (cont.)**	***In vivo* Homing Validated with Free Peptide (cont.)**	***In vivo* delivery[k] (cont.)**
Human Renal Carcinoma Tumor Endothelial Cells	**C**VGNDNSS**C**[94] (pIII, **V**)			Yes	Biotinylated peptide conjugated to saporin induced apoptosis in the tumor endothelial cells subcutaneously injected into mice **(Drug)**
	CQSHKLPS**C**[94] (pIII, **V**)				
	CTTLQSAQ**C**[94] (pIII, **V**)				

a – All tumors are human xenografts unless otherwise indicated.
b – Cysteine residues that form disulfide bonds are indicated in bold.
c – Common peptide names that have been used in the literature are indicated in parenthesis next to the peptide sequence.
d – The phage display library type is also indicated in parenthesis. All phage are filamentous unless noted as T7 phage.
e – T indicates tumor cell targeting, **V** indicates tumor vasculature targeting, **L** indicates tumor lymphatics homing, and **M** indicates tumor associate macrophage homing. **ND** means it is unclear whether the peptide binds the tumor cells or tumor vasculature.
f – Intravenous injections used for selection unless otherwise indicated.
g – Selection used intraperitoneal injections instead of intravenous injections.
h – Selection used intracardiac injections instead of intravenous injections.
i – Combination of *ex vivo*/*in vivo* panning employed.
j – This peptide has been used in numerous other studies not listed.
k – The type of agent used for targeting is designated in parenthesis. **Peptide** indicates an unconjugated peptide; **drug**, peptide conjugation to a drug; **imaging**, peptide conjugation to an imaging agent; and **oligo**, peptide conjugation to a oligonucleotide or other gene delivery vehicles.

Table 1-6. Peptides Isolated from Bacterial Display Libraries

Cancer Type	Cell Line used for Selection[a]	Peptide Sequence[b,c,d]	Receptor Identified	*In vitro therapy*	*In vivo* Homing Validated	*In vivo* delivery[e]
Prostate Cancer	PC-3M-1E8	NVVRQ (TMTP1)[311] (FliTrx library)			Yes	FITC-peptide for whole-body mouse imaging in MKN-45sci metastatic tumor-bearing mice **(Imaging)**
	PC-3	**C**PGDRGQRRLFSKIEGP**C** (MM-2)[312] (FliTrx library)			Yes	
Breast Cancer	ZR-75-1	G**C**LQILPTLSE**C**FGR[103] (OmpA library)				
		LKV**C**GRYPGI**C**DGIR[103] (OmpA library)				
		T**C**VLHRQR**C**LMFTLR[103] (OmpA library)				
		I**C**VNIKKSLWA**C**EIR[103] (OmpA library)				
		WARVLLIEGRLIVCE[103] (OmpA library)				
		WWDMVSDRYIWKPVK[103] (OmpA library)				
		VP**C**QKRPGWV**C**LW[103] (CPX library)				
		KW**C**VIWSKEG**C**LF[103] (CPX library)				
		SSW**C**MRGQYNKI**C**MW[103] (CPX library)				
		VE**C**YLIRDNL**C**IY[103] (CPX library)				
		WW**C**LGERVVR**C**AH[103] (CPX library)				
		FY**C**VIERLGV**C**LY[103] (CPX library)				
		RV**C**FLWQDGR**C**VF[103] (CPX library)				
	MDA-MB-231	MS**C**LMNSNSF**C**SI[313] (CPX library)				
		WA**C**LMNMYSF**C**SS[313] (CPX library)				
		LR**C**LTTLDNF**C**TI[313] (CPX library)				
		LI**C**LHRIDRF**C**SV[313] (CPX library)				
		ME**C**LKSMFTY**C**DI[313] (CPX library)				
		LS**C**LYSMYSY**C**DV[313] (CPX library)				
		LW**C**LTDLMGW**C**TV[313] (CPX library)				
		LG**C**LLDVQSW**C**IV[313] (CPX library)				
		LW**C**LLDLMSW**C**EI[313] (CPX library)				
		LD**C**FRNIYGF**C**NI[313] (CPX library)				
		LK**C**LWEMRGF**C**EI[313] (CPX library)				
		VD**C**LFHTDRF**C**YI[313] (CPX library)				
		WR**C**LMSLETW**C**MV[313] (CPX library)				
		LA**C**LMSLEQW**C**AV[313] (CPX library)				
		WS**C**LWDLSQF**C**NF[313] (CPX library)				
		PS**C**LFNLDSF**C**EF[313] (CPX library)				
	MCF-7	VE**C**DPVRNNF**C**WW[313] (CPX library)				
		RV**C**TWNWSWI**C**KE[313] (CPX library)				
		LE**C**HRLRTNM**C**FL[313] (CPX library)				
		EW**C**GIVRVGY**C**LG[313] (CPX library)				

Cancer Type (cont.)	Cell Line used for Selection[a] (cont.)	Peptide Sequence[b,c,d] (cont.)	Receptor Identified (cont.)	*In vitro* therapy (cont.)	*In vivo* Homing Validated (cont.)	*In vivo* delivery[e] (cont.)
Breast Cancer		DA**C**GIIHVGY**C**KV[313] (CPX library)				
		RM**C**TWNLEWV**C**DL[313] (CPX library)				
		RL**C**VWDWEWL**C**RD[313] (CPX library)				
		RV**C**TWRMVWV**C**DY[313] (CPX library)				
		NL**C**RGDLEKL**C**MK[313] (CPX library)				
		YA**C**RGDAYYL**C**AT[313] (CPX library)				
		HS**C**RGDMALL**C**WL[313] (CPX library)				
		FA**C**RGDRWVL**C**NS[313] (CPX library)				
		GL**C**VADGRPR**C**LE[313] (CPX library)				
		GW**C**FRDGRPM**C**SY[313] (CPX library)				
	T47D	FW**C**MGDGRPR**C**TG[313] (CPX library)				
		VW**C**YLWKYGY**C**VY[313] (CPX library)				
		PI**C**RGDRDWR**C**RD[313] (CPX library)				
		GQIWKGEWVKLWRDV[313] (CPX library)				
Hepatoma (Liver)	HepG2	IAVAPGWLWEEE[314] (FliTrx library)				
		KELCELDSLLRI[314] (FliTrx library)				
		TRGRPRDVANGH [314] (FliTrx library)				
		IRELYSYDDDFG[314] (FliTrx library)				
		ESLSVDFMGERA[314] (FliTrx library)				
		QELAPYSWSEKD[314] (FliTrx library)				
		ARRILKGGGVHT[314] (FliTrx library)				
Murine Squamous Carcinoma	SCC VII **(f)**	**C**GGRKLGG**C**[315] (FliTrx library)				
		CGGRRLGG**C**[315] (FliTrx library)			Yes	Peptide-ultrasound-contrast-microbubbles gave enhanced ultrasound contrast of tumors in mice[316] **(Imaging)**

a – All cell lines are of human origin unless otherwise noted.
b – Cysteine residues that form disulfide bonds are indicated in bold.
c – Common peptide names that have been used in the literature are indicated in parenthesis next to the peptide sequence.
d – Library type
e – The type of agent used for targeting is designated in parenthesis. **Imaging** indicates peptide conjugation to an imaging agent.
f – This was an *ex vivo* panning.

Table 1-7. Peptides Isolated From OBOC Libraries and Selected Against Target Proteins

Protein Used for Selection	Peptide Sequence[a]	*In vitro* therapy	*In vivo* Homing Validated with Free Peptide	*In vivo* delivery
IgMκ secreted by WEHI-231 cells	wGeyidvk[106]			
	wGeyvmvnG[106]			
	TGWYVPKSIDN[106]			
	NWFQDEWYIPD[106]			
IgMκ secreted by WEHI-279 cells	LRWFERETNV[106]			
	nItaGmtkG[106]			

a – Lowercase indicates D-amino acids.

Table 1-8. Peptides Isolated From OBOC Libraries and Selected Against Cultured Cells

Cancer Type	Cell Line used for Selection[a]	Peptide Sequence[b,c,d,e]	Receptor Identified	*In vitro* therapy[f]	*In vivo* Homing Validated with Free Peptide	*In vivo* delivery[f]
Breast Cancer	MDA-MB-231	**c**dGLGBN**c**[317] (LXY1)	$\alpha_3\beta_1$		Yes[318]	Peptide-biotin-streptavidin-Cy5.5 used for near infrared imaging of U-87MG tumor in mouse[318] **(Imaging)**
		cdGTyr(3-NO_2)GBN**c**[317]	$\alpha_3\beta_1$		Yes	Peptide-biotin-streptavidin-Cy5.5 used for near infrared imaging of orthotopic MDA-MB-231 tumors in mice **(Imaging)**
	$\alpha_v\beta_3$ integrin-transfected K562 leukemia cells	**c**GRGDdv**c**[319]	$\alpha_v\beta_3$		Yes	Peptide-biotin-streptavidin-Cy5.5 used for near infrared imaging of U-87MG and A375M tumors **(Imaging)**
	Jurkat	LTGpLDI[320]	$\alpha_4\beta_1$			
B-cell Lymphoma	Raji	**c**LDYWD**c**[38]	$\alpha_4\beta_1$			
		cWDLDHH**c**[38]	$\alpha_4\beta_1$			
		sppLDIn[38]	$\alpha_4\beta_1$			
		eapLDId[38]	$\alpha_4\beta_1$			
		fypLDFf[38]	$\alpha_4\beta_1$			
		FSIpLDI[38]	$\alpha_4\beta_1$			
		QSYpLDF[38]	$\alpha_4\beta_1$			
Ovarian Cancer	CaOV-3, SKOV-3, OVCAR-3, & ES-2	**c**LDWDL**c**[321]				
		cDGLGDD**c**[321]	α_3			
		cDGWGPN**c**[321]	α_3			
	ES-2	**c**dGHCitGPQ**c**[322] (OA02)	α_3		Yes	Peptide-biotin-streptavidin-Cy5.5 and peptide-Cy5.5 used for near infrared imaging of ES-2 tumors in mice **(Imaging)** [^{64}Cu] DOTA-Peptide used for MicroPET imaging of ES-2 tumor and SKOV3 metastatic lesion in mice[38] **(Imaging)**
		c-Nle-DWEE**c**[38]	$\alpha_4\beta_1$			
		c-Nle-DVDE**c**[38]	$\alpha_4\beta_1$			
		c-Nle-D-Chg-YM**c**[38]	$\alpha_4\beta_1$			
		cSD-Nle-D-Chg-**c**[38]	$\alpha_4\beta_1$			
		yminp-Nle-Dldnhh[38]	$\alpha_4\beta_1$			
		vswamp-Nle-Dlgspd[38]	$\alpha_4\beta_1$			
		vqgp-Nle-Dlafvl[38]	$\alpha_4\beta_1$			
		vgnvp-Nle-Dlgqea[38]	$\alpha_4\beta_1$			
		wdinp-Nle-Dlgsfn[38]	$\alpha_4\beta_1$			
		wsrip-Nle-Dlqeps[38]	$\alpha_4\beta_1$			
	SKOV-3	**c**dG-Cha-G-HCit-Q**c**[38]				
		cdG-Chg-G-Hyp-N**c**[38]				
		cdG-HCit-GPQ**c**[38]				
		cdGIGPQ**c**[38]				
		cdGLGQ-Bta-**c**[38]				
		cdG-Phe-GP-Cha-**c**[38]				
		cdG-Tyr-Gl-Pra-**c**[38]				
		cLDl-Chg-Hyp-Y**c**[38]	$\alpha_4\beta_1$			
		c-Nle-D-Chg-NDF**c**[38]	$\alpha_4\beta_1$			

Cancer Type (cont.)	Cell Line used for Selection[a] (cont.)	Peptide Sequence[b,c,d,e] (cont.)	Receptor Identified (cont.)	*In vitro* therapy[f] (cont.)	*In vivo* Homing Validated with Free Peptide (cont.)	*In vivo* delivery[f] (cont.)
		c-Nle-D-Nle-PhgD**c**[38]	$\alpha_4\beta_1$			
		cDEL-Nle-EW**c**[38]	$\alpha_4\beta_1$			
Lung Cancer	A549	**c**NGQGEQ**c**[323] (pA)	$\alpha_3\beta_1$			
	H1650	**c**NleDNleTHypg**c** (pM2)[324]	$\alpha_4\beta_1$			
Prostate	DU145	LNIVSVNGRHX (RU-1)[104]				
		DNRIRLQAKXX (RX-1)[104]				
		kmviywkag (RZ-3)[325]	$\alpha_3\beta_1$[326]			
		kikmviswkg (HYD-1)[325]	$\alpha_6\beta_1$, $\alpha_3\beta_1$[326]	Peptide itself induced cell death in the multiple myeloma cell lines[109] **(Peptide)**		Peptide itself inhibited H929 tumor growth in SCID-hu mice when injected i.p.[109] **(Peptide)**
	LNCaP	QMARIPKRLARH[69]				
Glioblastoma	U-87MG	**c**dGLGBN**c**[318] (LXY1)			Yes	Peptide-biotin-streptavidin-Cy5.5 used for near infrared imaging of U-87MG tumor in mouse **(Imaging)**
Bladder Cancer	5637	**c**QDGRMGF**c**[327] (PLZ4)			Yes	Near-infrared imaging of fresh human baldder tumor-bearing mice with peptide-biotin-SA-Cy5.5 conjugate **(Imaging)**

a – All cell lines are of human origin.
b – Cysteine residues that form disulfide bonds are indicated in bold.
c – Lowercase indicates D-amino acids.
d – Abbreviations for unnatural amino acids are as follows: B = hydroxyproline, Cha = cyclohexylalanine, Chg = α-cyclohexylgycine, HCit = homocitrulline, Hyo = hydroxyproline, Bta = benzothioenylalanine, Phe = 4-methylphenylalanine, Pra = propargylglycine, Tyr = 3-nitrotyrosine, and Nle = norleucine.
e – Common peptide names that have been used in the literature are indicated in parenthesis next to the peptide sequence.
f – The type of agent used for targeting is designated in parenthesis. **Peptide** indicates an unconjugated peptide and **imaging**, peptide conjugation to an imaging agent.

Table 1-9. Peptides Isolated from PS-SPCLs

Protein or Cell Line used for Selection[a]	**Peptide Sequence**[b]	**Receptor Identified**	***In vitro* therapy**[c]	***In vivo* Homing Validated**	***In vivo* delivery**[c]
NR6M [NR6 cells transfected to overexpress EGFRvIII (mutation variant III)]	H-FALGEA-NH_2 [107]	EGFRvIII			4-[^{18}F]fluorobenzoyl-peptide used for microPET imaging of NR6M cells in mice[328] **(Imaging)**
	H-FALIEA-NH_2 [107]	EGFRvIII			
$\alpha_5\beta_1$ (looking for ability to compete with fibronectin for binding)	VILVLF[76] (A5-1)	$\alpha_5\beta_1$	Peptide itself inhibited proliferation, bFGF-induced migration, bFGF-induced tubular network formation of HUVEC cells and bFGF-induced neovascularization in a chorioallantoic membrane angiogenesis assay **(Peptide)**		
$\alpha_v\beta_3$ (looking for ability to compete with vitronectin for binding)	HGDVHK-NH_2[75]	$\alpha_v\beta_3$	Peptide itself inhibited bFGF-induced HUVEC cell migration and bFGF-induced neovascularization in a chorioallantoic membrane angiogenesis assay **(Peptide)**		
	HSDVHK-NH_2[75]	$\alpha_v\beta_3$[75, 329]	Peptide itself inhibited bFGF-induced HUVEC cell migration and bFGF-induced neovascularization in a chorioallantoic membrane angiogenesis assay **(Peptide)** Peptide itself inhibited HUVEC proliferation[330] **(Peptide)**		

Protein or Cell Line used for Selection[a] (cont.)	Peptide Sequence[b] (cont.)	Receptor Identified (cont.)	*In vitro* therapy[c] (cont.)	*In vivo* Homing Validated (cont.)	*In vivo* delivery[c] (cont.)
U266 B myeloma cells (looking for stimulation of inositol phosphates)	WKYMVM-NH_2 [331]	Formyl peptide receptor-like 1 (FPRL1)[332, 333] & N-formyl peptide receptor-like 2 (FPRL2) [332]			

a – All cell lines are of human origin.
b – Common peptide names that have been used in the literature are indicated in parenthesis next to the peptide sequence.
c – The type of agent used for targeting is designated in parenthesis. **Peptide** indicates an unconjugated peptide and **imaging**, peptide conjugation to an imaging agent.

Table 1-10. Comparison of Different Therapeutic Platforms Used for Targeted Delivery[a]

	Advantages	Disadvantages
Direct Conjugate < 2 nm 	• Better escape from the vasculature • Better diffusion through the interstitial space of tumor • Able to control peptide-drug ratio • Less non-specific uptake in non target cells	• Drug release is necessary • Lower drug load • Rapid clearance rate
Liposomes 80 – 200 nm 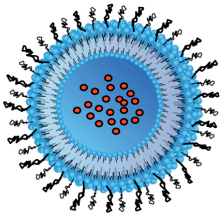	• Higher drug load • Drug molecule is unmodified • Single coupling chemistry for different drugs • Can incorpoarte multiple therapeutic reagents in a single nanoparticle • Takes advantage of the EPR effect • Longer circulation time • Can conjugate multiple peptides to liposome surface	• Less efficient escape from the vasculature • Large size reduces diffusion through the tumor • Higher background uptake in non-targeted cells
Micelles 50 – 100 nm 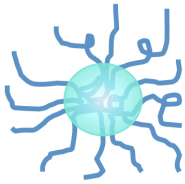	• Moderate drug load • Drug molecule is unmodified • Single coupling chemistry for different drugs • Can incorporate multiple therapeutic reagents in a single nanoparticle • Reduced renal circulation • Moderate circulation time • Takes advantage of EPR effect • Can conjugate multiple peptides to liposome surface	• Less stable than liposomes • Concentration must remain above CMC • Currently limited to the encapsulation of hydrophobic drugs • Increased background uptake due to polymer
Polymer Scaffolds < 10 nm 	• Increased drug load • Takes advantage of EPR effect • Reduced renal clearance • Longer circulation time	• Difficult to control polymer chain length • Difficult to control drug load • Requires direct conjugation of the drug

a – This table is a modified version of a table from reference [78].

CHAPTER TWO

IDENTIFICATION AND CHARACTERIZATION OF A SUITE OF TUMOR TARGETING PEPTIDES SPECFIC FOR NON-SMALL CELL LUNG CANCER

2.1 Introduction

Lung cancer kills more men and women each year than any other cancer, accounting for more than half of all cancer deaths in the United States.[3] Significantly, only 16% of lung cancer patients live to 5 years after diagnosis.[3] Lung cancer is a complex and diverse disease that encompasses very different tumor types arising from the lung. Over 85% of lung cancers are categorized as non-small cell lung cancer (NSCLC), and NSCLC is further subdivided into squamous cell carcinoma, adenocarcinoma, or large-cell carcinoma.[6] One of the challenges of lung cancer treatment arises from the large heterogeneity of lung tumors. Approximately half of all tumors comprise more than one of these histopathological types,[8] making it difficult to classify tumors for later therapy decisions.

An emerging paradigm for cancer treatment is the idea of personalized medicine. Based on the concept of the "magic bullet" drug introduced by Paul Ehrlich in the 20th century,[27] an ideal targeting therapy demonstrates high affinity for and toxicity against the tumor while reducing harmful side effects. A personalized therapy, therefore, should be specific for some feature of the tumor that is distinctive compared to the rest of the body. One method for developing such magic bullet targeted therapies is to use tumor targeting ligands that are specific for unique molecular components of a tumor. Such ligands can first be used to categorize those tumors that express a clinically relevant cell

surface biomarker which may help with the decision of which treatment to pursue. Additionally, the tumor targeting ligand can be attached to a drug for specific delivery to the biomarker-expressing tumors; this approach is expected to increase the specificity and efficacy of the given drug. Subsequent conjugation of the same tumor targeting ligand to a molecular imaging agent allows for tumor imaging and the ability to monitor the expression of the biomarker throughout the course of treatment.

Antibodies have traditionally been the gold standard of targeting reagents. There are currently 12 monoclonal antibodies approved for clinical use for cancer patients in different countries around world.[29, 30] Despite these clinical successes, antibodies suffer from several disadvantages. It is difficult to chemically modify antibodies and is particularly difficult to manufacture antibody conjugates.[29] The size of immunoconjugates also inhibits their tumor penetration, making it difficult for the conjugates to reach the entirety of the tumor.[31, 32] Additionally, nonspecific clearance of antibodies by the reticuloendothelial system can lead to accumulation of any conjugated drugs or toxins in unwanted sites such as the liver and bone, damaging these organs.[33, 34] Significantly, the 12 clinically approved antibodies only target 8 different biomarkers. This small number of biomarkers fails to reflect the diversity of tumors, highlighting the need for additional tumor targeting ligands.

Peptides are an attractive alternative to antibody targeting therapies. Unlike antibodies, peptides are easy to synthesize in large quantities[35] and their smaller size improves tissue penetration while preventing nonspecific uptake by the reticuloendothelial system. Additionally, peptides can be chemically modified to alter affinity, charge, hydrophobicity, stability, and solubility and can be optimized for *in vivo*

use through reiterative modifications. Importantly, peptides can display antibody-like affinities for their receptors. Several naturally occurring peptides, such as Luteinzing-hormone-releasing hormone (LHRH), somatostatin and their derivatives are useful for tumor targeting, due to overexpression of their receptors on many cancer cells.[36] However, these peptides only bind a minute fraction of the receptors overexpressed on neoplastic cells. Therefore, peptide libraries are often used to select additional cancer targeting peptides.

Phage display can be used for unbiased selection of peptides that bind cells in culture, and a number of peptides specific for a variety of cancer cell lines have been identified from phage displayed peptide libraries [38, 78] Despite the large number of peptides selected using phage display libraries, only a small fraction of available human cancer cells have been used for peptide selections. Additionally, there have not been any attempts to generate a panel of peptides specific for a given cancer subtype. Although there exist more than 200 lung cancer cell lines,[108] only 4 had been used for peptide selection prior to this study.[159, 160, 268, 269, 323, 324] It is also unclear whether these isolated peptides bind broadly across the variety of available lung cancer cell lines or whether they are specific for the cell lines from which they were isolated.

We sought to generate the first panel of peptides specific for a cancer subtype, focusing on NSCLC. By biopanning multiple phage displayed peptide libraries against 8 different NSCLC cell lines, we isolated 11 different peptides that bind to 85% of the NSCLC lines tested. These peptides are not patient or subclass specific but bind to cell lines from different patients and to all of the major NSCLC subclasses. Synthesis of the peptides as multimeric tetramers results in ligands with antibody-like affinities in the

picomolar to low nanomolar range. Significantly, 5 of the tetrameric peptides home to tumors in mice.

2.2 Materials and Methods

2.2.1 *Materials*

All Fmoc amino acids, the NovaPEG Rink Amide resin and 2-(1*H*-benzotriazole-1-yl)-1,1,3,3-tetramethyluronium hexafluorophosphate (HBTU) were purchased from Novabiochem® (EMD Millipore, Billerica, MA). The Fmoc-β-Ala-CLEAR™ Acid Resin was purchased from Peptides International (Osaka, Japan), β-maleimidopropionic acid from Tokoyo Chemical Industry Co. Ltd. (Portland, OR), and Fmoc-NH-$(PEG)_{11}$-COOH ($C_{42}H_{65}NO_{16}$) from Polypure (Oslo, Norway). *N*-Methylmorpholine (NMM) was purchased from ACROS Organics (Geel, Belgium). Anhydrous hydroxybenzotriazole (HOBt) was purchased from SynBioSci (Livermore, CA). Piperidine was purchased from Sigma-Aldrich Inc. (Livermore, CA). The IRDye 800CW Maleimide dye was purchased from LI-COR® (Lincoln, NE). For cell culture, fetal bovine serum (FBS) was purchased from Gemini Bio-Products (West Sacramento, CA) and both RPMI 1640 and Trypsin EDTA, 1x from Mediatech, Inc. (Fisher Scientific, Pittsburgh, PA).

2.2.2 *Cell Lines*

All human NSCLC cell lines were provided by the UT Southwestern Medical Center Hamon Center for Therapeutic Oncology Research and maintained according to published protocols.[334] The H2009, H1299, and H460 cell lines were all grown at 37°C and 5% CO_2 in RPMI 1640 supplemented with 5% FBS.

2.2.3 *Peptide Synthesis and Purification*

Monomeric peptides were synthesized on a Symphony Synthesizer (Rainin Instruments, Protein Technologies, Inc., Woburn, MA) by standard Fmoc solid-phase peptide synthesis on a Rink Amide AM resin (substitution level 0.71 mmol/g). All amino acids were Fmoc-protected, and the Fmoc was removed to allow for amino acid coupling using 20% Piperidine in DMF. The amino acids were subsequently coupled at a 5-fold excess using HBTU, HOBt, and NMM coupling for 45 minutes. The PEG group added to each amino acid was purchased as Fmoc-NH-$(PEG)_{11}$-COOH and was coupled in the same manner as the amino acids, except that it was coupled at a 2.5-fold excess. For preparation of N-terminal acetylated peptides, after coupling of the N-terminal amino acid, a solution of 90% DMF, 5% 0.4 M NMM, and 5% acetic anhydride was added to the reaction vessel and mixed for 40 minutes. The synthesized peptides were removed from the resin by shaking in a mixture of 94%:2.5%:1.0%:2.5%: of triofluoroacetic acid (TFA):triisopropylsilane:H_2O:ethanediothiol (EDT) for 2-4 hours. The majority of the TFA solution was then removed by N_2 pressure before precipitation in diethyl ether at -80°C for a minimum of 2 hours. Precipitated peptide was dried under vacuum for a minimum of 12 hours.

The tetrameric cores were also synthesized on the Symphony Synthesizer using the Fmoc-β-Ala-CLEAR™ Acid Resin (substitution level 0.40 mmol/g) under the same coupling conditions as the monomeric peptides. Fmoc-Cys(Acm)-OH was first coupled to the resin followed by Fmoc-Lys(Fmoc)-OH, $[Fmoc\text{-}Lys(Fmoc)\text{-}OH]_2$, and finally $(\beta\text{-maleimidopropionic acid})_4$. The cores were removed from the resin in the same manner as the monomeric peptides.

The crude monomeric peptides and tetrameric cores were purified by reverse phase high-performance liquid chromatography (HPLC) using a SPIRIT™ Spirit Peptide C18 5 μm, 25 x 2.12 (AAPPTec®, Louisville, KY) on a Breeze™ HPLC (Waters Corporation, Milford, MA). H_2O/0.1% TFA (eluent A) and acetonitrile/0.1% TFA (eluent B) were used for purification as follows: 0-1 minute, 90% A, 10% B at 10mL/minute; from 1-100 minutes, eluent B was increased from 10% to 60% at a flow rate of 10 mL/minute. The peptides were detected by ultraviolet (UV) absorbance at 220nm. Matrix-assisted laser desorption/ionization time of flight mass spectrometry was used to confirm peptide mass (Voyager-DE™ PRO, Applied Biosystems, Inc., Foster City, CA). The mass of the monomeric peptides and tetrameric cores were determined in reflective mode using α-cyano-4-hydroxycinnamic acid as a matrix.

The tetrameric peptides were synthesized by coupling purified monomeric peptide to purified tetrameric core (8:1 monomeric peptide to tetrameric core) for 2 hours at room temperature in phosphate buffered saline, pH 7.4, containing 10 mM EDTA. Afterwards, excess monomeric peptide was removed by reverse phase HPLC using the same elution method that was used for purification of the monomeric peptides and tetrameric core. The mass of the tetrameric peptides were also determined using matrix-assisted laser desorption/ionization time of flight mass spectrometry using linear mode and sinapinic acid as a matrix.

2.2.4 *Labeling the Peptides with a Near-Infrared Dye*

Before the tetrameric peptides could react with a maleimide-activated dye, the unique cysteine placed before the branch point of the tetramers had to be deprotected to

remove the acetamidomethyl (Acm) group protecting the thiol of the cysteine. The tetrameric peptides were deprotected by reaction of the peptide (0.35 μmol) with AgOAc (0.168 M AgOAc in 99:1 TFA:anisole to a total volume of 350 μL) for 2 hours at 4°C. The majority of the TFA solution was then removed under a slow stream of nitrogen and the peptide precipitated in diethyl ether at -80°C for a minimum of 30 minutes. After removing the ether from the precipitated peptide, the peptide was reacted with 150 μL of a 0.2 M dithiothreitol (DTT) solution (DTT dissolved in 1 M acetic acid) for a minimum of 5 hours shaking. The resulting solution was centrifuged and the supernatant taken for HPLC purification of the deprotected peptide. Additional tetrameric peptide was recovered from the pellet by shaking in 8 M guanidine HCl for an additional 5 hours. The supernatant resulting from centrifugation of this mixture was also taken for HPLC purification. The deprotected tetramers were purified using the same HPLC conditions as used for the other peptides and the deprotection was verified by mass spectrometry, using the same method used for the protected tetramers.

Purified deprotected tetramers were labeled with the near-infrared IRDye 800CW Maleimide dye using cysteine-maleimide chemistry. Each peptide (168 nmol) was reacted for 2 hours at room temperature with dye (84 nmol, 01.mg) in 1.5 mL phosphate buffered saline, pH 7.4, containing 10mM EDTA. The dye-labeled peptides were purified by HPLC employing the same HPLC conditions used for the other peptides and the dye-labeling was verified by mass spectrometry, using the same method as used for the protected tetrameric peptides.

2.2.5 *Effects of the Peptides on Cell Growth*

All assays were carried out using Corning® Costar® 96-well, black, clear bottom cell culture plates (Fisher Scientific, Pittsburg, PA). H2009 cells were plated at 2,000 cells/well and both H1299 and H460 cells were plated at 1,000 cells/well in a volume of 50 μL media per well. The cells were allowed 24 hours to incubate before the addition of peptides. Each peptide was then added to the cells in a volume of 50 μL on top of the media. The peptides were added at total concentrations of 0.1, 1, and 10 μM, with 8 replicates per concentration. After the cells were incubated with the peptides for 72 hours, the number of viable cells were determined using the CellTiter-Glo® Luminescent Cell Viability Assay (Promega Corporation, Madison, WI), following the instructions indicated by the manufacturer. Luminescence was measured on a SpectraMax M5 plate reader (Molecular Devices, LLC, Sunnyvale, CA).

2.2.6 *In Vivo Targeting Experiments*

Animal protocols were approved by the Institutional Animal Care and Use Committee at UT Southwestern Medical Center. Male or female NOD/SCID mice (from the UT Southwestern Medical Center Mouse Breeding Core Facility) were injected with either 1 million H2009 or H1299 cells in the right flank and 10 days later were injected with 1 million H460 cells in the left flank. All cells were injected in phosphate buffered saline, pH 7.4, and were prepared for injection by incubating the cells with 0.05% Trypsin-EDTA (Gibco®, Life Technologies™, Grand Island, NY) for 10 minutes, quenching the trypsin with media, and washing the cells with phosphate buffered saline

before final suspension in the phosphate buffered saline at a concentration of 10 million cells per mL. After tumor cell injection and 3.5 – 4 weeks for the tumors to grow, each mouse bore either dual H2009 and H460 xenografts or dual H1299 and H460 xenografts. Mice were then injected via tail vein with 30-53 μg of near-infrared dye labeled tetrameric peptide in phosphate buffered saline, pH 7.4. The H2009.1 peptide was injected into mice bearing dual H2009 and H460 tumors while the H460.1, HCC15.1, acetylated HCC15.2, and acetylated H1299.2 peptides were injected into mice bearing dual H1299 and H460 tumors. At 24 hours after peptide injection, the mice were imaged for dye fluorescence using a Pearl® Impulse Small Animal Imaging System (LI-COR®, Lincoln, NE). Immediately afterwards, the mice were sacrificed for *ex vivo* imaging of organs. For each mouse, the heart, liver, spleen, kidneys, lung, and tumors were imaged for dye fluorescence.

2.3 Previous Work

2.3.1 *Isolation of a Panel of NSCLC-Binding Peptides*

Previous work in our lab focused on an unbiased selection of peptides specific for NSCLC using phage displaying peptide libraries for the selection and intact NSCLC cells as the bait (Figure 2-1). Using this method, we selected peptides specific for NSCLC cells without prior knowledge of the cell surface landscape of these cells, such as which cellular receptors are overexpressed or prominent. Such an unbiased approach is particularly useful for isolating cell targeting ligands as it allows the cells themselves to choose which peptides to bind. Additionally, selection against whole cells keeps cellular

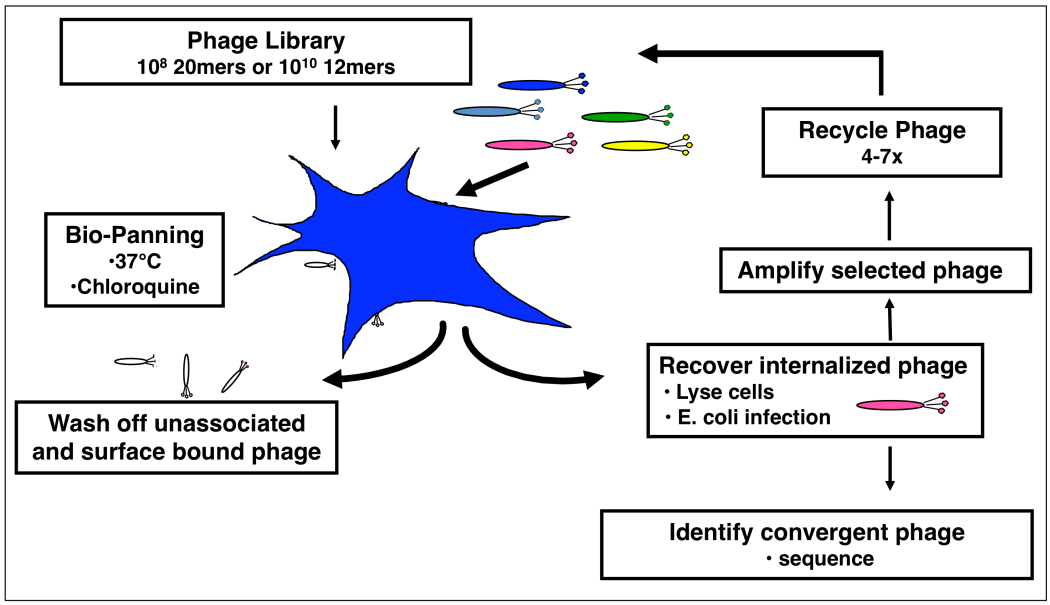

Figure 2-1. Biopanning on NSCLC cells using phage displaying peptide libraries.

receptors in their native context, meaning that isolated peptides will bind not just a specific receptor but to that receptor within its cellular context. Selection against cells can also be biased towards ligands that internalize into the cells, by employing an acid wash or a protease treatment to strip off or digest any cellular membrane-associated phage. As cellular internalization may be important for later applications of the peptides, such as targeted delivery of drugs to their site of action within cells, we chose to only select for internalizing peptides.

We isolated a panel of 11 NSCLC specific peptides by biopanning (panning) against 8 different NSCLC cell lines (Table 2-1). Three different phage libraries were used for panning to increase our chances of isolating different peptides: two 20-mer peptide libraries and one commercially available 12-mer library. Most selections were

Table 2-1. NSCLC Binding Peptides

Peptide Name	Cell Line Used for Selection	Peptide Sequence	Selectivity[a]	Specificity[b]
H1299.1	H1299 (LC)	VSQTMRQTAVPLLWFWTGSL	190	45
H1299.2	H1299 (LC)	YAAWPASGAWTGTAPCSAGT	83	29
H2009.1	H2009 (AD)	RGDLATLRQLAQEDGVVGVR	300	140
H460.1	H460 (LC)	EAMNSAEQSAAVVQWEKRRI	120	400
A549.1	A549 (AD)	MTVCNASQRQAHAQATAVSL	21	7.8
HCC15.1	HCC15 (SQ)	ATEPRKQYATPRVFWTDAPG	44	34
HCC15.2	HCC15 (SQ)	FHAVPQSFYTAP	220	73
HCC95.1	HCC95 (SQ)	MRGQTGKLPTEHFTDTGVAF	20	69
H1155.1	H1155 (LC)	MTGKAAAPHQEDRHANGLEQ	55	39
H1155.2	H1155 (LC)	MEKLPLSKTGRTVSEGVSPP	61	25
H661.1	H661 (LC)	TNSCRGDWLCDAVPEKARV	26	90

a - Selectivity is defined as the output phage/input phage normalized to a control phage.
b - Specificity is the ratio of the selectivity value for the cancer cell line and a normal bronchial epithelial control cell line, BEAS-2B.

carried out until a single peptide sequence emerged, which typically took 4-6 rounds of panning, with the exception of the selection against H1155 cells. This selection yielded 2 prominent peptides, the H1155.1 and H1155.2 peptides. Each peptide was named for the cell line on which it was selected with the addition of a decimal and number that signifies the order in which the peptides were isolated. All of the peptides are selective for their target cell line, binding 20-300 fold better than a control phage and binding the target cells 8-400 fold better than they bind a control immortalized human bronchial epithelial cell line, BEAS-2B. Significantly, this panel of 11 peptides includes peptides specific for every major subtype of NSCLC: large-cell (LC), adenocarcinoma (AD), and squamous carcinoma (SQ).

2.3.2 *Peptide Binding Profiles Across 40 NSCLC Cell Lines*

Due to the large heterogeneity of NSCLC cells, we were not sure whether the NSCLC targeting peptides would only bind to the cell line from which they were isolated or would also bind to other NSCLC cells. Therefore, the peptides were tested for binding to 40 different lung cancer cell lines (Figure 2-2a). Many of the peptides bind to a large number of cell lines. Interestingly, the peptides distinguish cellular features that are not detected by normal histopathological subtyping; the peptides are not specific for one particular NSCLC subtype, binding to large-cell, adenocarcinoma, and squamous cell lines. The peptides also bind to cell lines isolated from different patients, indicating that they bind receptors common to NSCLC cells as opposed to patient-specific receptors. The H2009.1 and HCC15.2 peptides bind to the broadest ranges of cells, and cells that bind the H2009.1 peptide tend to bind that peptide almost exclusively, with the exception of the H1993, H2073, H358, and H322 cells which also bind several other peptides. The H1299.1 and H1299.2 peptides also target fairly broadly and exhibit almost identical binding profiles, indicating that they may share a receptor or bind receptors with co-regulated expression. The panel included one set of cells originating from a patient's primary tumor and its corresponding metastasis, the H2073 and H1993 cells, respectively. As these cell lines also exhibit almost identical peptide binding profiles, it may be possible to use the same peptide to both image and treat a primary tumor and its metastases. Significantly, the 11 peptides bind to 85% of the NSCLC cell lines tested, suggesting that a relatively small number of peptides may be used to recognize features general to NSCLC.

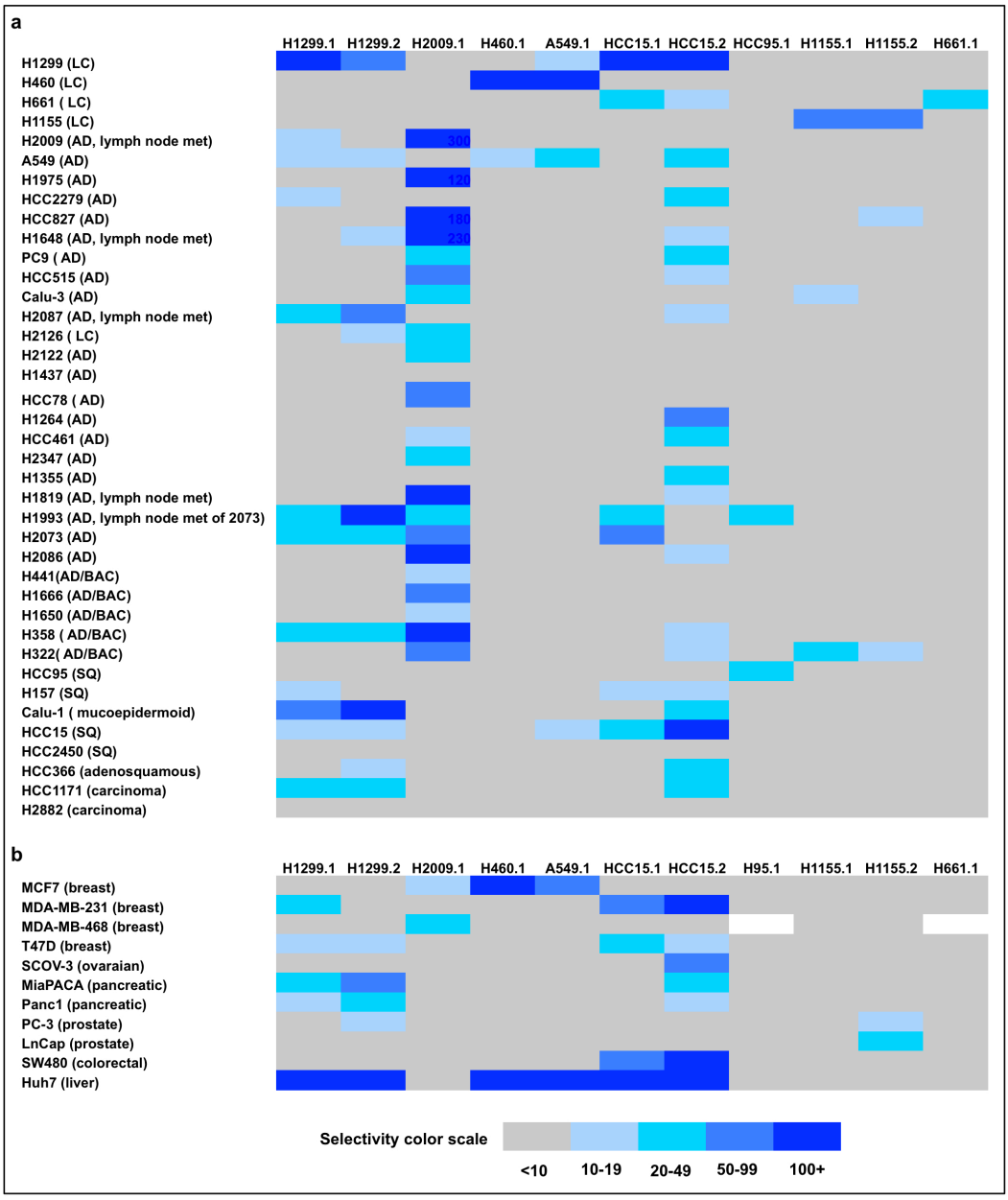

Figure 2-2. Binding profile of targeting peptides across 40 NSCLC cell lines (a) and 11 cancerous cell lines from other organs (b).

2.3.3 *NSCLC-Binding Peptides Bind Human Cancer Cells from Other Organs*

We also sought to determine whether the isolated peptides were specific for NSCLC or whether they would also bind to cancer cells derived from organs other than the lung. Eight of the peptides bind to cancerous cell lines originating in other organs, suggesting that these peptides may also be useful in targeting cancer types other than NSCLC (Figure 2-2b). Similar to their restrictive binding among the different NSCLC cell lines, the H95.1, H1155.1, and H661.1 peptides failed to bind cell lines from other organs sites. The HCC15.2 peptide, on the other hand, exhibited the broadest binding, with selectivity for 5 of the 11 cell lines tested. All 11 of the cancer cells from other organs bound to at least one of the peptides, save the prostate cancer PC-3 cells. The liver cancer Huh 7 cells reach selectivity values over 100 for six of the peptides. Thus, liver carcinomas may have a similar cell membrane profile as NSCLC cells.

2.3.4 *Tetramerization of the Peptides Yields Antibody-Like Affinities*

While the NSCLC specific peptides bind and target a variety of cancerous cells, all of the previous assays used phage displaying the peptide sequences. As phage are not amenable to most clinical applications, the peptides must be chemically synthesized for further downstream utility. Therefore, it is important to determine whether the chemically synthesized peptides maintain the same cellular affinity and specificity as the peptides displayed on the phages. However, chemical synthesis of monomeric peptides isolated by phage display often results in ligands with significantly lower affinity than the corresponding phage. This loss of affinity has significantly limited the clinical utility of peptides isolated from phage-displayed libraries.

The widely used M13 phage libraries present peptides at the N-terminus of the phage pIII coat protein, which is displayed at one end of the phage in 3-5 copies. Thus, target specific binding of the phage is likely driven by both the peptide sequence and the multimeric presentation of peptides. Therefore, we hypothesized that synthesizing multivalent peptides that mimicked the presentation of the peptide by the phage would allow for multivalent binding and increase cellular affinity. Employing a trilysine dedrimeric core, we can synthesize peptides that display four peptide copies in the same valency and orientation as the phage (Scheme 2-1). We previously demonstrated that tetrameric peptide presentation works as a general construct for peptides selected by phage display against a variety of cell types, allowing the peptides to maintain their cell specificity while increasing affinity relative to the monovalent peptides.[264, 266, 267, 335, 336] The tetrameric core can also accommodate modifications before the lysine branches, in a space that should not interfere with the peptide binding sequences. Thus, different chemical moieties tailored to the desired use of the peptide can be easily included in the tetrameric construct. For example, Scheme 2-1 shows a unique cysteine before the branch point of the tetrameric core. This cysteine can then be used for later conjugation to maleimide-activated dyes or drugs. Alternatively, a biotinylated glutamic acid can be inserted instead of the cysteine, for later use with streptavidin labeled reagents. Using cysteine-maleimide chemistry, we can make the tetrameric peptides with high yield and purity.[271] First, the monomeric peptides are synthesized with C-terminal polyethylene glycol (PEG) groups to both increase solubility and provide space between the peptide sequence responsible for binding and the point of attachment to the tetrameric core. A C-terminal cysteine is included after the PEG groups to allow conjugation of the monomeric

peptide to a separately synthesized tetrameric core bearing four maleimide groups for conjugation to monomeric peptides. The tetrameric peptides are then synthesized by reacting purified monomeric peptide and purified tetrameric core in solution at room temperature for 2 hours.

We synthesized the 6 most promising NSCLC targeting peptides - H1299.1, H1299.2, H2009.1, H460.1, HCC15.1, and HCC15.2 - as both monomeric and tetrameric peptides. Together, these peptides bind 75% of the NSCLC cells and 90% of the other cancer cells tested. To compare the targeting abilities of these peptides, we determined their half-maximal binding affinities for the cell lines from which they were isolated (Table 2-2). The half-maximal binding affinity refers to the concentration of peptide needed to block 50% of the binding of its cognate phage. As anticipated, tetramerization dramatically increased peptide affinity for the majority of the peptides. With the exception of the HCC15.2 peptide, all of tetrameric peptides displayed >45-fold affinity compared to their corresponding monomer. These non-additive increases in affinity are likely the result of the multivalent binding from the four monomers displayed by each tetrameric peptide. The much smaller 3-fold boost in binding for the HCC15.2 peptide tetramer verses monomer indicates that this peptide likely does not bind its receptor in a multivalent fashion. Significantly, the peptides exhibit low picomolar to low nanomolar affinities, the same type of affinities typically demonstrated by antibodies. To our surprise, even high concentrations (10 μM) of the H460.1 monomer and tetramer peptides were unable to block binding of the H460 phage. Thus, the H460.1 peptide may not function outside the context of the phage or may bind but fail to saturate binding.

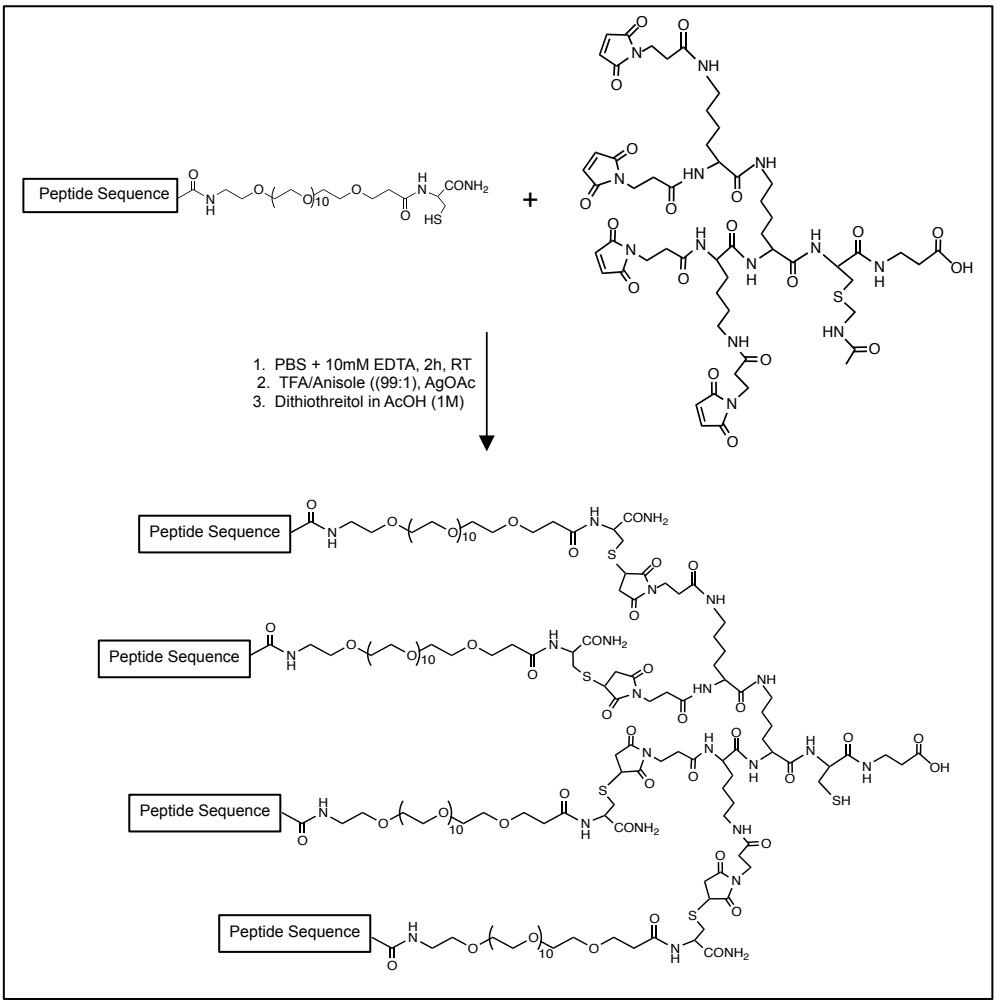

Scheme 2-1. Synthesis of tetrameric peptides.

Table 2-2. Binding Affinities of NSCLC Binding Peptides

Peptide	Sequence	Half maximal binding (nM)	
		Monomer	Tetramer
H2009.1	RGDLATLRQLAQEDGVVGVR	22	0.34
H1299.1	VSQTMRQTAVPLLWFWTGSL	1900	42
H1299.2	YAAWPASGAWTGTAPCSAGT	21	0.12
HCC15.1	ATEPRKQYATPRVFWTDAPG	400	0.0071
HCC15.2	FHAVPQSFYTAP	44	16

2.3.5 *The NSCLC Targeting Peptides Mediate Cellular Uptake*

To determine where the peptides localized after binding to NSCLC cells, the H2009.1, H1299.1, H1299.2, HCC15.1, and HCC15.2 peptides were synthesized as tetramers with a biotin group prior to the branch of the tetrameric core. These biotinylated peptides were then incubated with streptavidin coated fluorescent Qdots (SAQdot605) to allow for fluorescent microscopy examination of their cellular localization. After a 10 minute incubation with either H2009 or H1299 cells, each peptide delivered Qdots into the cell line for which it displays specificity (Figure 2-3). Thus, the H2009.1 peptide-Qdots internalized into H2009 cells but did not accumulate in non-target H1299 cells. Similarly, the H1299.1, H1299.2, HCC15.1, and HCC15.2 peptides carried Qdots into the binding H1299 cells but not into the non-binding H2009 cells. Each peptide delivered Qdots homogenously across their target cell line population, and all

peptides but the H1299.1 peptide demonstrated a punctate perinuclear staining. The H1299.1 peptide-Qdots instead localized diffusely to the cytoplasm.

The H460.1 peptide was also synthesized as a biotinylated tetramer for conjugation to streptavidin Qdots. While this peptide was unable to block binding of the H460.1 phage to H460 cells, it was still able to bind MC7 target cells (Figure 2-3b). Fluorescent microscopy demonstrated specific binding of the H460.1 peptide-Qdots to MCF7 cells. Strikingly, these peptide-Qdots displayed a very different cellular localization than the other peptide-Qdots, accumulating at distinct areas on or near the cell membrane. H460.1 phage displayed similar localization in MCF7 cells (Figure 2-3c). As the phage were detected for microscopy using anti-phage antibodies without permeabilizing the cells, they are all located to the outside of the cell on the cell membrane. Therefore, the H460.1 peptide likely binds the cell surface but does not internalize into the cells, which may also explain why the H460.1 peptide was unable to block phage binding. An extracellular target is a surprising result as both the peptide selection procedure and the microscopy studies included two pH2.2 acid washes, which were anticipated to remove any phage or peptides binding to the outer cell membrane. Therefore, the target of the H460.1 peptide is an outer membrane receptor and their interaction is stable even at low pH. This receptor may also be secreted or shed by the MC7 cells, as the H460.1 peptide-Qdots also accumulate in the extracellular space between cells, a phenomenon not observed when the H460.1-Qdots were incubated with non-target cells.

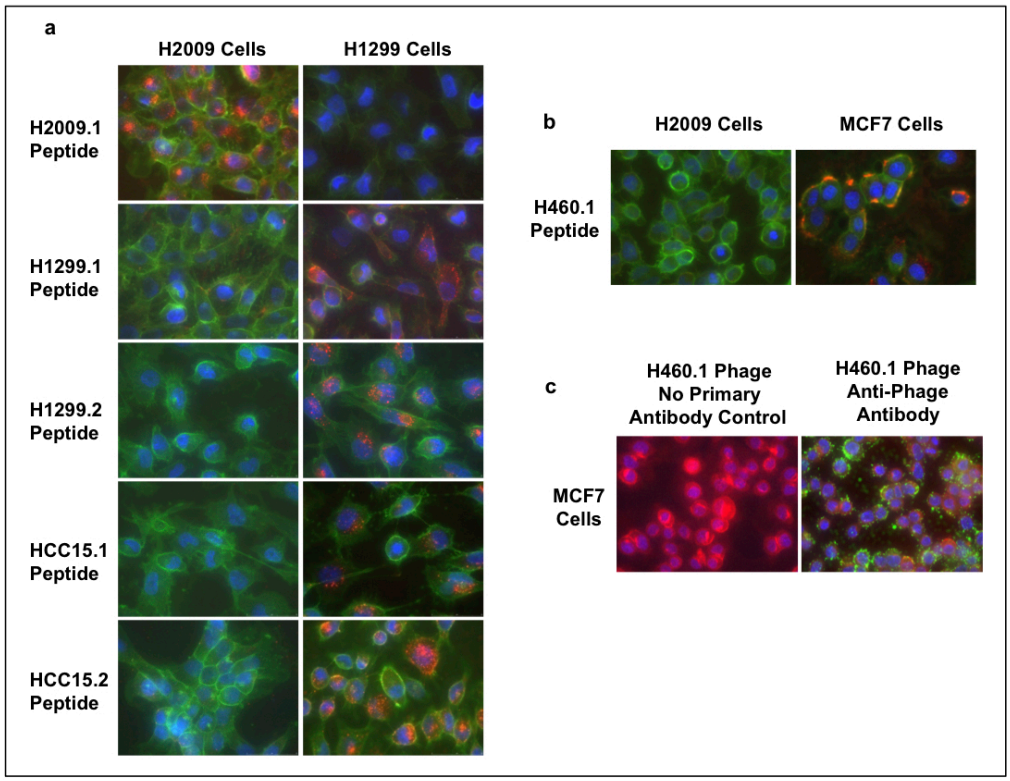

Figure 2-3. NSCLC binding peptides internalize into cells *in vitro*. (a-b) Microscopy images of tetrameric peptide-Qdots (SAQdot605) in cells. The peptide-Qdots are shown in red, the cell membranes in green and DAPI nuclei stain in blue. (c) Microscopy images of H460.1 phage in MCF7 cells. The anti-phage antibody stain is shown in green, the cell membrane stain in red, and the DAPI nuclei stain in blue.

Table 2-3. Truncation of the H2009.1 Peptide Maintains Binding Affinity

Peptide	Sequence	Valency	Half maximal binding (nM)
H2009.1 20-mer	RGDLATLRQLAQEDGVVGVR	monomer	22
H2009.1 20-mer	RGDLATLRQLAQEDGVVGVR	tetramer	0.34
H2009.1 10-mer	RGDLATLRQL	monomer	9.2
H2009.1 10-mer	RGDLATLRQL	tetramer	0.011
H2009.1 7-mer	RGDLATL	monomer	5.2
H2009.1 7-mer	RGDLATL	tetramer	0.018

2.3.6 *Truncated H2009.1 and H1299.2 Peptides Maintain Binding Affinity of the Parental Peptides*

While the peptides demonstrate high affinity as 20-mers, we sought to further optimize them for later applications. As shorter peptides are easier and less expensive to synthesize, shortening the peptide length could be beneficial as long as peptide binding affinity remains unaltered. Alanine scanning is an easy mechanism for determining the necessary amino acids for peptide binding. In this method, peptides are chemically synthesized with some of the amino acids replaced with alanine residues. By creating a series of peptides with different amino acids changed to alanine, those amino acids that contribute to binding can be identified. If a particular amino acid or series of amino acids are important for binding, substituting alanine in their place will reduce or abrogate peptide affinity.

Systematic alanine scanning of the H2009.1 peptide determined that the N-terminal amino acids are crucial for binding while some of the C-terminal amino acids are dispensable. Changing the last 10 amino acids of the original 20-mer H2009.1 peptide

to alanine did not alter binding affinity of the peptide and changing the last 13 amino acids to alanine also had minimal effects on binding. Subsequent chemical synthesis of the 10-mer H2009.1 monomeric and tetrameric peptides demonstrated that these peptides actually display increased affinity compared to the parental 20-mer peptides (Table 2-3). Thus, the last 10 amino acids of the original peptide may have actually interfered with peptide binding. Shortening the H2009.1 peptide to a 7-mer also resulted in peptides with high affinity, although not quite as high as the 10-mer peptides. Therefore, for all future applications we employed the highest affinity 10-mer peptides.

Alanine scanning was also employed for optimization of the H1299.2 peptide. We were particularly interested in shortening this peptide due to the cysteine residue located towards the C-terminus of the peptide. As cysteine residues can easily form disulfide bonds with other cysteine residues, the only way to prevent intra- or inter-molecular binding among different branches of the H1299.2 peptide is to chemically protect the cysteine of the peptide. Therefore, if the cysteine is not required for peptide binding, its removal could simplify the peptide synthesis for downstream studies. Accordingly, alanine scanning of the H1299.2 peptide revealed that the last 5 amino acids are not required for binding. Thus the peptide can be truncated immediately before the problematic cysteine residue. Synthesis of the H1299.2 15-mer monomeric and tetrameric peptides resulted in peptides with identical affinity as the parental peptides. Therefore all further downstream applications for this peptide utilized the 15-mer peptides.

2.4 Results

2.4.1 *The NSCLC Targeting Peptides Do Not Affect Cell Growth or Viability*

While peptides selected by phage display are often treated as inert targeting ligands, it is important to consider that they are likely binding cellular receptors and could, therefore, initiate a variety of receptor-mediated signaling events. For utility in future downstream targeting applications, it is particularly important to determine whether the peptides either increase or inhibit cell growth. While cell growth inhibition could be of benefit for therapeutic applications, peptides that increase cellular growth would work against any drug delivery applications. To address these concerns, I tested the effects of the 5 broadest binding peptides, the H2009.1, H1299.2, HCC15.1, HCC15.2, and H460.1 tetrameric peptides, on the growth of H2009, H1299, and H460 cells (Figure 2-4). Each cell line was incubated with 0.1 – 10 μM of the various peptides for 3 days before measuring the number of viable cells. However, none of the peptides affected cell growth, even at peptide concentrations of 10 μM. Thus the peptides neither stimulate cell growth nor inhibit cell viability, suggesting that they could be good candidates for *in vivo* targeting applications.

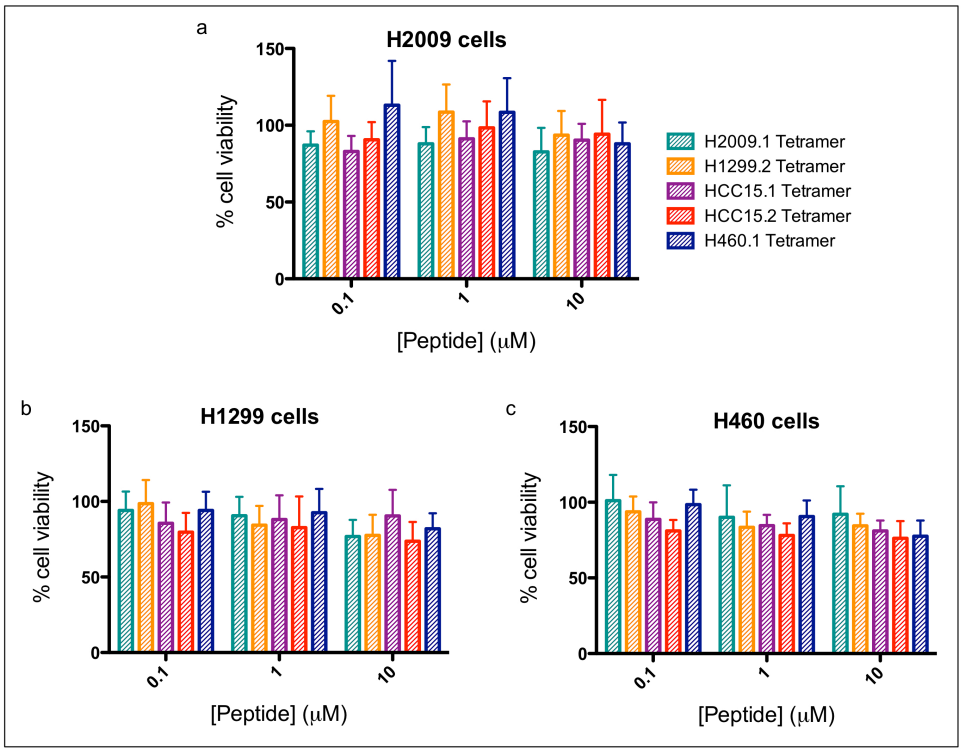

Figure 2-4. NSCLC binding peptides do not affect cell viability. Peptides were incubated with cells for 3 days, at which point viability was determined and normalized to non-treated cells.

2.4.2 *The Peptides Home to NSCLC Xenograft Tumors In Vivo*

While the peptides target cells *in vitro*, further applications of these peptides requires the ability to target tumors *in vivo*. To examine the ability of the peptides to home to tumors in mice, the H2009.1, H1299.2, HCC15.1, HCC15.2, and H460.1 tetrameric peptides were synthesized with unique cysteine residues (Scheme 2-1) for conjugation to a maleimide-activated near-infrared dye. The H1299.1 peptide was not tested for *in vivo* targeting because it binds the same cells as the H1299.2 peptide but has lower affinity and poorer solubility. The dye-labeled peptides were injected intravenously into mice bearing different tumors on either flank – one tumor which should bind the peptide and another control non-binding tumor.

The H2009.1 peptide was injected into 5 mice bearing dual H2009 and H460 tumors. As expected based on peptide specificity *in vitro*, whole mouse fluorescent imaging revealed that the H2009.1 peptide accumulated specifically in its target H2009 tumor, but not in the non-target H460 tumor, demonstrating a 120-fold preference for the H2009 tumor (Figure 2-5a). The organs and tumor tissue were also imaged *ex vivo* to verify this specificity and to examine peptide accumulation in other organs. The *ex vivo* imaging closely mirrors the whole mouse imaging, as peptide accumulation is only observed in the H2009, and not the H460 tumor. Importantly, this imaging reveals a 110-fold preference of the peptide for the H2009 tumor compared to the lung of the mouse, an important distinction for a lung-cancer targeting peptide. The peptide also appears to clear primarily through the kidneys, and to a much lesser extent, through the liver. Accordingly, removing the kidney from the fluorescent field of view increases the visible signal in both the H2009 tumor and the liver, due to saturation of the signal when the

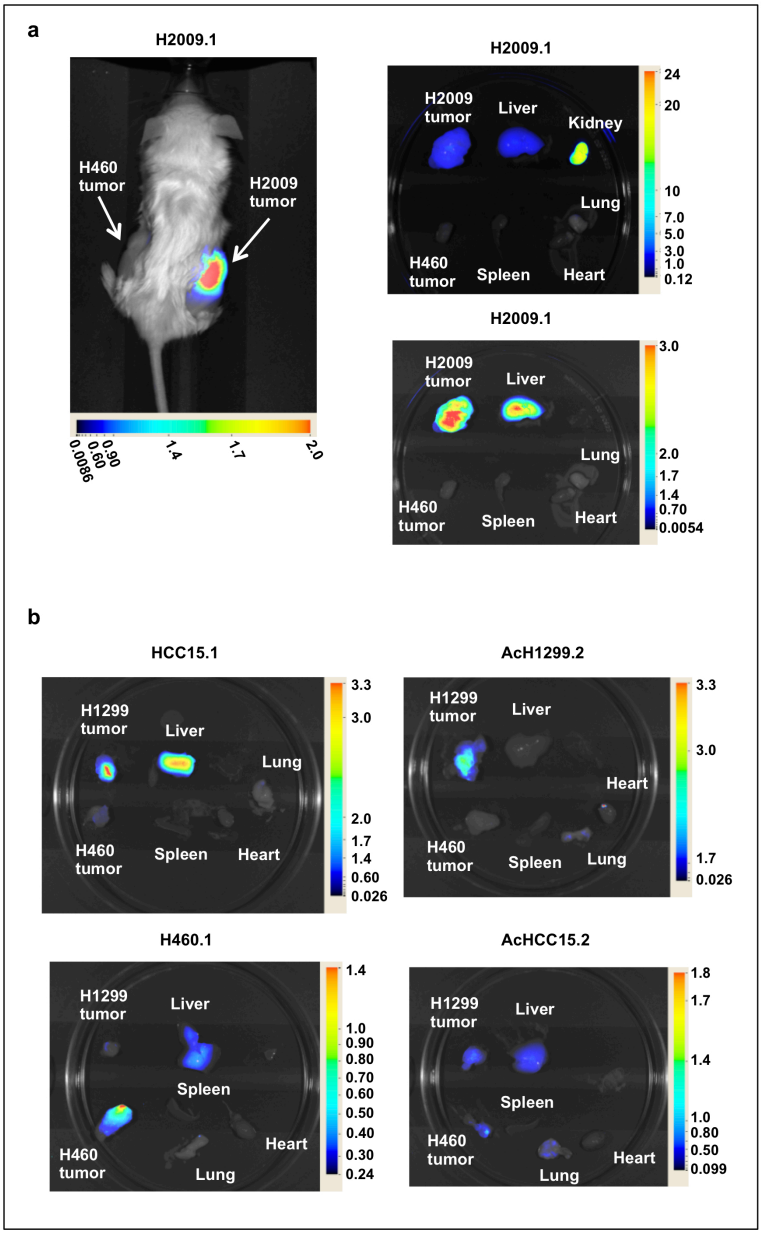

Figure 2-5. The 5 best binding tetrameric NSCLC peptides home to tumors *in vivo*. Mice bearing either dual H2009 and H460 tumors or dual H1299 and H460 tumors were injected via tail vein with near infrared dye-labeled peptides and imaged 24 hours later. Organs were then removed for *ex vivo* imaging. (a) Mouse bearing dual H2009 and H460 tumors injected with dye-labeled H2009.1 tetrameric peptide. (b) Mice bearing dual H1299 and H460 tumors injected with dye-labeled HCC15.1, AcH1299.2, H460.1, or AcHCC15.2 tetrameric peptides.

kidney is included in the image. The heart and spleen, meanwhile, only accumulate very low levels of the H2009.1 peptide. The levels of H2009.1 peptide that accumulated in the tumor and organs were also quantified for the other 4 injected mice (Table 2-4). While there was some variation from one mouse to another, the H2009.1 peptide always maintained its tumor specificity, targeting the H2009 tumor at least 20-fold better than the H460 tumor in every case. Additionally, the H2009.1 peptide always distinguished between the H2009 tumor and the lung.

The HCC15.1 and H460.1 peptides also specifically homed to their target tumors *in vivo* (Figure 2-5b). Both peptides were injected into mice bearing dual H1299 and H460 tumors. The HCC15.1 peptide specifically accumulated in its target H1299 tumor over the non-target H460 tumor, demonstrating a 5-fold preference for the H1299 tumor. This peptide also bound to the H1299 tumor 6-fold better than to the mouse lung. A total of 3 mice were injected with this peptide, and as before, while mouse-to-mouse variation was observed, the peptide always distinguished the H1299 tumor from the other tissues (Table 2-5). The H460.1 peptide specifically accumulated in the H460 tumor, demonstrating a 8-fold preference for the H460 tumor compared to the H1299 tumor and a 15-fold preference for the H460 tumor compared to the lung. Two additional mice displayed the same H460 tumor affinity and specificity for the H460.1 peptide and that data is quantified in Table 2-6. As with the H2009.1 peptide, both the H1299.2 and H460.1 peptides also cleared through the liver and kidney.

Table 2-4. Quantification of H2009.1 Peptide Accumulation in Mice Bearing Dual H2009 and H460 Xenografts

Mouse	Signal									
	peptide amount	H2009 tumor	H460 tumor	liver	lung	spleen	H2009 tumor/ H460 tumor	H2009 tumor/ liver	H2009 tumor/ lung	H2009 tumor/ spleen
1	30 μg	1810	37	7800	75	50	50	0.23	24	36
2	30 μg	17000	430	11000	2300	below detection	40	1.6	7.6	>17000
3	30 μg	9300	430	7600	48	26	22	1.2	190	360
4	30 μg	8000	380	5600	180	2.1	21	1.4	45	3700
5	30 μg	14000	110	9300	130	18	120	1.5	110	740

Table 2-5. Quantification of HCC15.1 Peptide Accumulation in Mice Bearing Dual H1299 and H460 Xenografts

Mouse	Signal									
	peptide amount	H1299 tumor	H460 tumor	liver	lung	spleen	H1299 tumor/ H460 tumor	H1299 tumor/ liver	H1299 tumor/ lung	H1299 tumor/ spleen
1	43 μg	2400	500	6600	430	13	4.8	0.40	5.6	190
2	43 μg	2000	570	4000	270	below detection	3.6	0.50	7.5	>2000
3	63 μg	1000	690	2400	740	68	1.5	0.40	1.4	15

Table 2-6. Quantification of H460.1 Peptide Accumulation in Mice Bearing Dual H460 and H1299 Xenografts

Mouse	Signal									
	peptide amount	H1299 tumor	H460 tumor	liver	lung	spleen	H1299 tumor/ H460 tumor	H1299 tumor/ liver	H1299 tumor/ lung	H1299 tumor/ spleen
1	44 μg	170	1400	1500	94	16	8.4	1.0	15	89
2	44 μg	no tumor	1600	1200	96	65	-	1.3	17	25
3	89 μg	100	4900	3400	1900	64	46	1.4	2.5	76

Table 2-7. Quantification of AcH1299.2 Peptide Accumulation in Mice Bearing Dual H1299 and H460 Xenografts

Mouse	Signal									
	peptide amount	H1299 tumor	H460 tumor	liver	lung	spleen	H1299 tumor/ H460 tumor	H1299 tumor/ liver	H1299 tumor/ lung	H1299 tumor/ spleen
1	53 μg	8200	4200	41	3100	below detection	2.0	200	2.7	>8200
2	53 μg	2400	620	310	4700	85	3.8	7.6	0.50	28
3	53 μg	9700	2100	650	1500	150	4.7	15	6.6	67

Table 2-8. Quantification of AcHCC15.2 Peptide Accumulation in Mouse Bearing Dual H1299 and H460 Xenografts

Mouse	Signal									
	peptide amount	H1299 tumor	H460 tumor	liver	lung	spleen	H1299 tumor/ H460 tumor	H1299 tumor/ liver	H1299 tumor/ lung	H1299 tumor/ spleen
1	33 μg	1000	670	2400	740	68	1.5	0.40	1.4	15

The dye-labeled H1299.2 and HCC15.2 peptides did not originally target tumors *in vivo*. However, *in vivo* targeting was rescued by acetylating the amino-termini of both peptides, implicating that the amino-termini are required for binding but are rapidly cleaved after *in vivo* injection. As both the H1299.2 and HCC15.2 peptides target H1299 tumors but not H460 tumors, mice bearing both of these tumors were injected with either peptide. Acetylated H1299.2 (AcH1299.2) peptide demonstrated the expected specificity for the H1299 tumor, targeting this tumor 5-fold better than the H460 tumor and 7-fold better than the lung (Figure 2-5b). Peptide accumulation in the tumors and organs are quantified in Table 2-7. Interestingly, the H1299.2 peptide demonstrated much lower

levels of liver accumulation than the other peptides, suggesting that this peptide clears mainly through the kidneys or clears on a faster time scale than the other peptides.

The acetylated HCC15.2 (AcHCC15.2) peptide did not maintain its *in vitro* specificity *in vivo*, accumulating to similar levels in both the H1299 and H460 tumors, with only a 1.5-fold preference for the H1299 tumor (Figure 2-5b, Table 2-8). This peptide also accumulated to a similar extent in the lung. Although it is not clear why this peptide displayed less specificity *in vivo*, the peptide may be unstable *in vivo* in a manner not altered by the amino-terminus acetylation or the acetylation itself may have altered the specificity of the peptide. Additionally, the peptide affinity may not be high enough to achieve tumor specific peptide accumulation. It is also impossible to exclude the possibility that the HCC15.2 receptor is ubiquitously expressed *in vivo*. However, as only one mouse was imaged for this peptide, this mouse may have been an anomaly. Additional mice should be investigated to verify the *in vivo* specificity of the AcHCC15.2 peptide.

2.5 Discussion

Previous work in our lab identified the first panel of peptides specific for one particular disease type. A suite of 11 different peptides specific for NSCLC were isolated from phage display library screenings against cultured NSCLC cells. The peptides exhibit many features that should facilitate their use in downstream applications, including high affinity, specificity for cancer cells as compared to normal cells, and easy translation from phage displayed peptides to chemical synthesis. Using a stringent cutoff of selectivity ≥20 as a measure of positive binding, these 11 peptides bound to 85% of the

NSCLC cell lines tested. Additionally, 35% of the NSCLC cells bound to two or more of the peptides. All of the peptides bound to cell lines other than the cell line from which they were selected save the H661.1 peptide, which bound restrictively to the H661 cell line. The H2009.1 peptide demonstrated the broadest NSCLC binding, targeting 45% of the cells. The HCC15.2 peptide also bound broadly, targeting almost a third of the NSCLC cells. These high percentages suggest that our peptides could have great utility for targeting NSCLC as a whole; the well-known breast cancer target HER-2 is only expressed in 25% of breast cancers.[337]

Chemical synthesis of peptides isolated from phage display libraries often results in ligands with lower affinities and reduced activity, limiting the use of the peptides for further applications. However, we surmounted this difficulty by synthesizing tetrameric peptides that mimic the multimeric peptide display by the phage. By conjugating four copies of the monomeric peptide to a trilysine core, we generated tetrameric peptides with affinities in the picomolar to nanomolar range. Most of the peptides received a more than additive increase in affinity in going from the monomeric platform to the tetrameric platform, likely due to multimeric binding. Importantly, these peptides have antibody-like affinities but are a tenth the size of antibodies. Additional microscopy studies revealed that the 5 broadest binding peptides, the H2009.1, H1299.1, H1299.2, HCC15.1, and HCC15.2 tetrameric peptides, internalize into their target cell types *in vitro*. Another peptide, the H460.1 peptide, targets specifically but remains cell-surface bound.

In an effort to examine the utility of these NSCLC specific peptides for downstream applications, I examined both the effects of the peptides on cell viability and the ability of the peptides to home to tumors *in vivo*. The H2009.1, H1299.2, HCC15.1,

HCC15.2, and H460.1 tetrameric peptides that demonstrated specific binding for their target cell types were tested in these assays. The H1299.1 peptide was not tested because it binds the same cells as the H1299.2 peptide but has lower affinity and poorer solubility. Significantly, none of the peptides either stimulated cell growth or inhibited cell viability, suggesting that they could be good candidates for *in vivo* targeting applications. While cell growth inhibition could be of benefit for therapeutic applications, peptides that increase cellular growth would work against any drug delivery applications.

The H2009.1, H1299.2, HCC15.1, HCC15.2, and H460.1 peptides all homed to tumors *in vivo*. Significantly, all of the peptides except the HCC15.2 peptide maintained their *in vitro* tumor specificity *in vivo*. While both the H1299.2 and HCC15.2 peptides failed to target tumors in their original state, N-terminal acetylation restored targeting. These modifications highlight the ease of chemically altering peptides to improve half-life due to proteolysis. Although all of the peptides demonstrated large levels of renal clearance, additional chemical modifications have been shown to reduce glomerular filtration, and conjugating the peptides to a larger particle, such as a nanoparticle, is expected to reduce uptake.[338-341]

Due to their high antibody-like affinities, cancer cell specificities, and ability to target tumors *in vivo*, these NSCLC peptides have great clinical potential. Additionally, the tetrameric peptide platform is versatile, allowing for easy incorporation of the peptides into a variety of drug delivery or imaging agents. It is anticipated that use of these peptides will improve drug delivery to and imaging of their target cell types and expand the number of targeting therapies available for patients with NSCLC.

2.6 Acknowledgements

The previous work from our lab described in Section 2.3 was a concerted effort by a large group of people from the lab. The work was done by the following people (in order of contribution): Dr. Michael J. McGuire, Dr. Shunzi Li, Lei Wu, Shaghayegh Rezaie, Ying-Horng Liu, Naveen Pattisapu, James Issac, and Dr. Tsukasa Oyama. Additionally, our collaborators Michael Peyton, Dr. Xian-Jin Xie, and Dr. John D. Minna contributed to the work. The work in the results section, Secton 2.4, was also a collaboration among several people in the lab. Dr. Shunzi Li synthesized and purified all of the peptides and Dr. Michael J. McGuire and I worked together on the animal experiments.

CHAPTER THREE

THE CASE FOR H2009.1 PEPTIDE TARGETING THERAPIES SPECIFIC FOR $\alpha_v\beta_6$

3.1 Introduction

The restrictively expressed integrin $\alpha_v\beta_6$ is emerging as a viable target for many epithelial-derived cancers.[342-352] $\alpha_v\beta_6$ belongs to the class of heterodimeric cell adhesion receptors known as integrins; these receptors mediate both cell-extracellular matrix adhesion and cell-cell adhesion and are heavily involved in cell signaling.[353] Each integrin is composed of both an α and a β subunit.[353] There exist 18 different α subunits and 8 different β subunits which heterodimerize in a variety of combinations to create a total of 24 different integrins.[353] While α_v can dimerize with a variety of different β subunits, the β_6 subunit exclusively dimerizes with the α_v subunit.[353] The $\alpha_v\beta_6$ heterodimer was originally identified in human pancreatic cancer cells[354] and subsequently discovered to be epithelial specific. While $\alpha_v\beta_6$ is not expressed or expressed only at very low levels in normal adult cells, it is known to up-regulate during times of tissue remodeling such as inflammation and wound healing.[346, 355] Additionally, $\alpha_v\beta_6$ is expressed in a variety of eptithelial-derived tumor types, including ovarian,[342] breast,[343] colon,[344, 356] cervical,[348] uterine,[349] oral,[350-352] and gastric[347] cancers.

The role of $\alpha_v\beta_6$ in epithelial cancers is still being elucidated. Several studies have linked $\alpha_v\beta_6$ with poor patient prognosis[344, 345] and others suggest that $\alpha_v\beta_6$ promotes metastasis by increasing cell invasion and migration.[349, 352, 356, 357] The studies in colon cancer provide a good example. Analysis of a panel of 488 patient colorectal tumor

sections revealed that 18% expressed $\alpha_v\beta_6$.[344] The patients with $\alpha_v\beta_6$-positive tumors had a significantly worse prognosis, with a median survival of 5 years compared to a median of 16.5 years for patients with $\alpha_v\beta_6$-negative (or low expression) tumors. Additionally, $\alpha_v\beta_6$ was an independent prognostic variable predictive of poor outcome for patients with early-stage colorectal cancer. Another study determined $\alpha_v\beta_6$ levels in primary patient colon tumors and examined the incidence of liver metastasis 3 years later.[356] Patients with $\alpha_v\beta_6$-positive tumors were 6 times more likely to develop metastases. Together these studies demonstrate that $\alpha_v\beta_6$ expression in colon tumors correlates with increased tumor metastasis and a decrease in patient survival.

It is clear that patients with $\alpha_v\beta_6$-positive tumors need new treatment options. Additionally, the aggressiveness of $\alpha_v\beta_6$-positive tumors highlights the need for a method to detect these tumors so that treatment can begin as early as possible, before metastases arise. One method to address these needs is the development of targeted therapies and imaging agents specific for $\alpha_v\beta_6$. Such agents would consist of an $\alpha_v\beta_6$-specific ligand conjugated to a drug or imaging agent. Julie Sutcliffe and colleagues have developed $\alpha_v\beta_6$-targeted positron emission tomography (PET) imaging agents using the A20FMDV2 peptide, an $\alpha_v\beta_6$-specific 20-amino acid peptide derived from an envelope protein of the foot-and-mouth disease virus.[358, 359] A pegylated ^{18}F-labeled version of A20FMDV2 targets $\alpha_v\beta_6$-expressing pancreatic xenografts in mice, allowing for PET imaging of the tumors.[359] This study demonstrates the utility of developing $\alpha_v\beta_6$-targeting agents.

As described in Chapter 2, our lab previously generated a suite of NSCLC targeting peptides. These peptides were selected by panning several different phage display peptide libraries against a variety of NSCLC cell lines. While our panel of NSCLC targeting peptides includes at least 4 peptides that selectively target tumors *in vivo*, the H2009.1 peptide is particularly attractive for future studies due to its broad binding across NSCLC cell lines; it binds to 45% of the cell lines tested (Chapter 2). Additionally, as described in this chapter, our lab identified the cellular receptor for this peptide as the restrictively expressed integrin $\alpha_v\beta_6$.

Our discovery that the H2009.1 peptide binds to $\alpha_v\beta_6$ on the membrane of NSCLC cells was the first description of $\alpha_v\beta_6$ expression in NSCLC. Therefore, we probed $\alpha_v\beta_6$ expression in NSCLC patient tumor samples and correlated expression of the integrin with known patient outcomes. Our results demonstrate that $\alpha_v\beta_6$ is highly expressed in NSCLC patient tumor samples and is predictive of poor patient outcome. Based on the prevalence of $\alpha_v\beta_6$ in NSCLC and other types of cancers as well as the ability of the H2009.1 $\alpha_v\beta_6$-targeting peptide to home to tumors in mice (Chapter 2), we believe that the of development H2009.1-targeted therapeutics is warranted. This chapter explains our previous studies with the H2009.1 peptide and our studies of the role of $\alpha_v\beta_6$ in NSCLC, with the purpose of building a case for the development of $\alpha_v\beta_6$ targeting therapies using the H2009.1 peptide.

3.2 Previous Work

3.2.1 *The Receptor for the H2009.1 Peptide is the Restrictively Expressed Integrin $\alpha_v\beta_6$*

Previous work in our lab identified the receptor of the H2009.1 peptide as the integrin $\alpha_v\beta_6$ using a combination of bioinformatics and molecular biology. The first 3 amino acids of the H2009.1 peptide are RGD, a well-known integrin-binding motif.[360] A BLAST search in the SwissProt database with the H2009.1 peptide sequence revealed that the first 8 amino acids of the peptide are identical to part of the SAT-1 type foot-and-mouth disease virus (FMDV, accession number 15420033). In the virus, the RGD motif is found within the GH loop of the coat protein VP1 and functions by initiating both binding and invasion into epithelial host cells. As various integrins, including $\alpha_v\beta_1$, $\alpha_v\beta_3$, $\alpha_v\beta_6$, and $\alpha_5\beta_1$ had been proposed as the receptors for the virus,[361-365] we sought to test whether one of these integrins might be the receptor for the H2009.1 peptide. As shown in Figure 3-1, only the $\alpha_v\beta_6$ function blocking antibody inhibited binding of the H2009.1 phage to H2009 cells. Additionally, the binding of the H2009.1 peptide to cells was shown to correlate to the levels of $\alpha_v\beta_6$ expressed by the cells, and transfecting β_6 into SW480 cells that do not normally express the integrin converted these cells from H2009.1 peptide non-binding to binding.

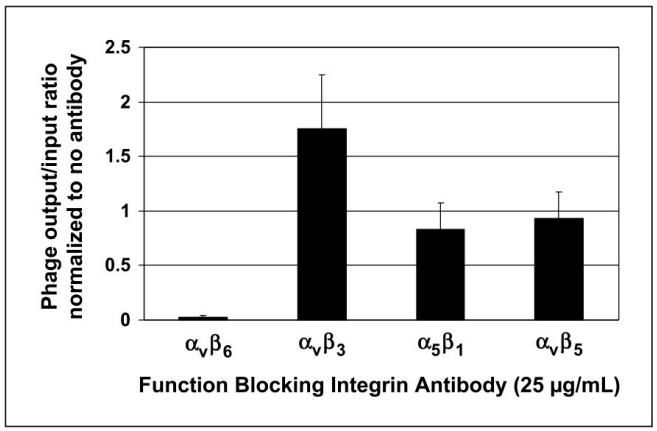

Figure 3-1. The receptor for the H2009.1 peptide is the restrictively expressed integrin $\alpha_v\beta_6$. Blocking of phage uptake is observed when the binding assay is done in the presence of anti-$\alpha_v\beta_6$ antibody. All values are normalized to phage uptake in the absence of antibody. Figure from reference 81.

3.2.2 *The Integrin $\alpha_v\beta_6$ is Expressed in Human Lung Tumors and Correlates with Poor Patient Survival*

While $\alpha_v\beta_6$ is not expressed by normal adult cells, it is known to up-regulate during wound healing.[346, 355] Additionally, $\alpha_v\beta_6$ is expressed by a variety of epithelial-derived cancers, including ovarian,[342] breast,[343] colon,[344] cervical,[348] uterine,[349] oral,[350-352] and gastric[347] cancers. However, our discovery that the H2009.1 peptide binds to $\alpha_v\beta_6$ in NSCLC cells was the first report of the integrin's expression in lung cancer. To examine whether $\alpha_v\beta_6$ is expressed in patient lung tumors, we used immunohistochemistry to determine expression of the integrin in 31 different human tumor samples including surrounding normal bronchial or bronchiolar tissue. As visualized by brown staining in Figure 3-2, $\alpha_v\beta_6$ expression is high in the tumors and only barely detectable in the normal tissue ($p < 0.0001$).

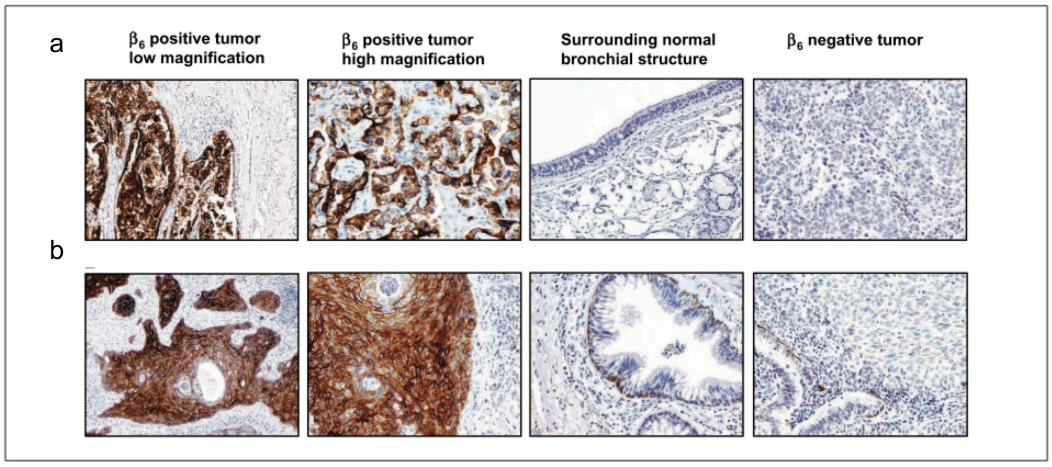

Figure 3-2. The integrin $\alpha_v\beta_6$ is expressed preferentially in lung tumors compared with surrounding normal tissue. Tumor samples were probed for $\alpha_v\beta_6$ expression, shown in brown, using an $\alpha_v\beta_6$-specific antibody. (a) Examples of both $\alpha_v\beta_6$-positive and $\alpha_v\beta_6$-negative adenocarcinoma tumors and surrounding normal bronchial tissue. (b) Examples of both $\alpha_v\beta_6$-positive and $\alpha_v\beta_6$-negative squamous tumors and surrounding normal bronchial tissue. Figure from reference 81.

To further probe the role of $\alpha_v\beta_6$ in lung cancer, we examined an array of patient NSCLC tumor samples for β_6 expression using immunohistochemistry. The panel included 271 NSCLC tumors, including 164 adenocarcinomas, 98 squamous cell carcinomas, 6 adenosquamous carcinomas, and 3 bronchioloalveolar cancers. Significantly, 56% of these NSCLC tumors stained positive for β_6. This β_6 expression was independent of the tumor subtype; all of the major subtypes tested displayed similar expression levels of the integrin ($p = 0.90$, Fisher exact test). It is important to note that the panel of tumors did not include any large cell lung carcinomas, which are one of the major subtypes of NSCLC. Therefore, the expression of β_6 within this NSCLC subclass is unknown. There was also no difference in expression of β_6 among different stages of

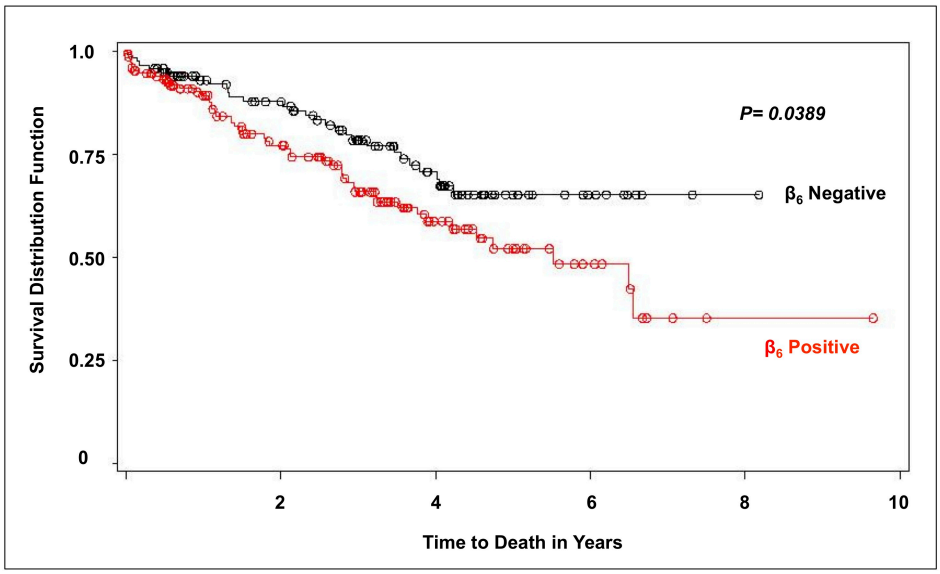

Figure 3-3. Kaplan-Meier survival analysis indicates that β6 expression correlates with reduced survival times. Patients were grouped by β6 expression status and survival analyzed using a log-ranked test. The survival times for all patients were longer than the standard lung cancer patient due to the high percentage of early-stage patients in this study. Figure from reference 81.

NSCLC ($p = 0.63$, Fisher exact test). β_6 expression did, however, correlate with smoking status. Tumor samples from patients who were current or former smokers expressed lower levels of β_6 than the samples from non-smokers ($p = 0.033$, χ^2 test). Therefore, β_6 expression occurs in more than half of all NSCLCs, regardless of tumor subtype or stage, and to correlate with patients with no history of smoking.

As the clinical outcomes were known for all of the patient tumor samples, we were also able to probe the relationship between β_6 expression and patient survival. As demonstrated in Figure 3-3, patients with β_6-negative tumors lived significantly longer than patients with β_6-positive tumors ($p = 0.039$, log-ranked test). β_6 expression also predicts a poor patient outcome; the hazard ratio for patients with β_6-positive tumors is

1.9, meaning that patients whose tumors express β_6 are almost twice as likely to die as those whose tumors are β_6-negative.

3.2.3 *The Integrin $\alpha_v\beta_6$ Increases During the Sequential Pathogenesis of Squamous Cell Carcinoma of the Lung*

Our collaborators at The University of Texas MD Anderson Cancer Center also examined the expression of $\alpha_v\beta_6$ during the progression of NSCLC squamous cell carcinoma. 73 samples of normal bronchial epithelial tissue and 44 samples of pre-cancerous squamous metaplastic or dysplastic bronchial epithelial tissue were obtained from areas adjacent to squamous cell lung tumors in patients. Comparison of the $\alpha_v\beta_6$ levels in these epithelial tissues relative to levels in 106 primary squamous cell tumor samples revealed that $\alpha_v\beta_6$ increases in a stepwise manner as tumor progression occurs (Figure 3-4). While $\alpha_v\beta_6$ is only minimally expressed in normal tissue, it is expressed at easily visible levels in pre-cancerous tissue and expressed at very high levels in cancerous tissue. These results suggest that $\alpha_v\beta_6$ could be a good target for the early detection and treatment of NSCLC.

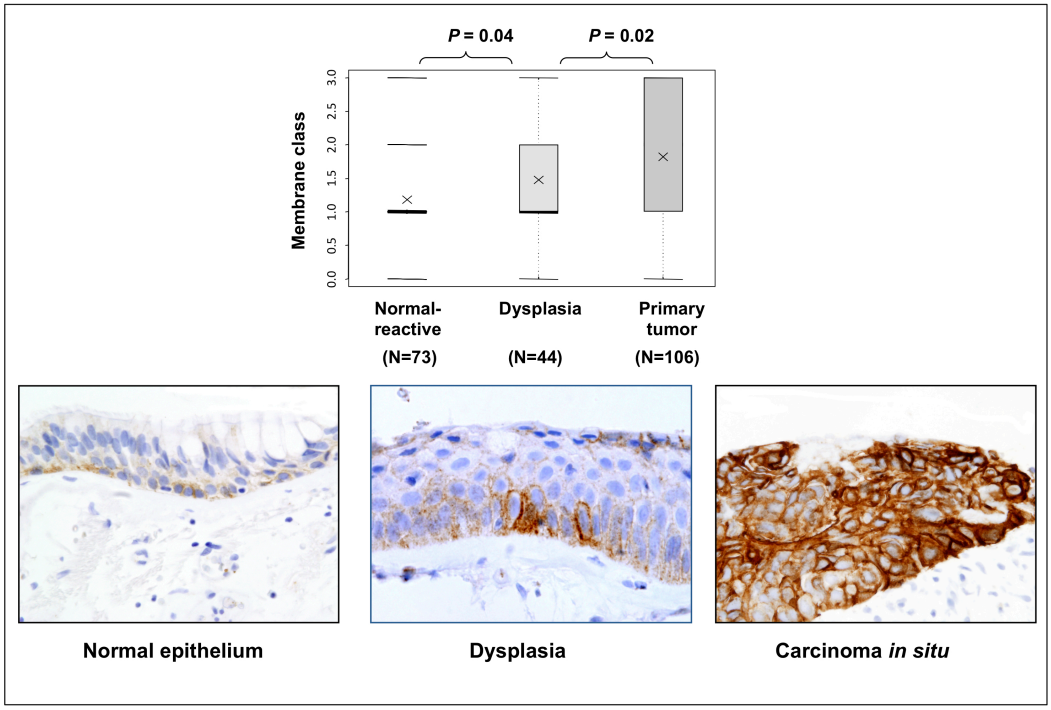

Figure 3-4. The integrin $\alpha_v\beta_6$ increases during progression of squamous cell carcinoma in the lung. Immunohistochemical expression of $\alpha_v\beta_6$ (brown staining) was scored in normal and reactive bronchial epithelium, squamous dysplasias and carcinoma *in situ*, and primary squamous cell carcinoma. The number of samples for each tissue type is indicated. Example microphotographs representative of each tissue category are also shown. Figure from reference 366.

3.3 Discussion

The integrin $\alpha_v\beta_6$ is not expressed in normal adult tissue, but upregulates during times of tissue remodeling such as inflammation and wound healing.[346, 355] Additionally, numerous cancers of epithelial origin, including ovarian,[342] breast,[343] colon,[344, 356] cervical,[348] uterine,[349] oral,[350-352] and gastric[347] cancers express $\alpha_v\beta_6$. Of note, several studies in various cancer types have linked $\alpha_v\beta_6$ with poor patient prognosis.[344, 345] Our discovery that the H2009.1 peptide binds to $\alpha_v\beta_6$ on the membrane of NSCLC cells was the first description of $\alpha_v\beta_6$ expression in NSCLC. Therefore, we sought to examine the prevalence of $\alpha_v\beta_6$ among patient NSCLC tumors and to evaluate the outcomes of patients bearing either $\alpha_v\beta_6$-positive or $\alpha_v\beta_6$-negative tumors. Our results demonstrate that $\alpha_v\beta_6$ is expressed in 56% of NSCLC patient tumor samples and only rarely expressed in normal tissue. Expression of this integrin is predictive of poor patient survival and $\alpha_v\beta_6$ is "turned on" early in the disease progression of NSCLC indicating that it may be a good biomarker for early cancer detection and treatment of NSCLC.

The H2009.1 peptide binds to $\alpha_v\beta_6$ with high affinity and specificity. An optimized tetrameric version of the peptide binds $\alpha_v\beta_6$-epxressing cells with a half-maximal binding affinity of 11 pM, putting this peptide in the range of antibody targeting reagents. Additionally, the H2009.1 peptide internalizes into $\alpha_v\beta_6$-positive cells *in vitro* and homes to $\alpha_v\beta_6$-positive, and not $\alpha_v\beta_6$-negative, NSCLC tumors *in vivo* (Chapter 2). Based on these features, the H2009.1 peptide is an attractive candidate for the development of $\alpha_v\beta_6$-targeting therapeutics for the treatment of NSCLC. The remainder of this dissertation will focus on the development of several unique H2009.1 targeted

therapies on a variety of different drug platforms. H2009.1-targeted therapies are expected to selectively target and destroy $\alpha_v\beta_6$-expressing NSCLC cells and to translate to a variety of other $\alpha_v\beta_6$-expressing cancers.

3.4 Acknowledgements

All of the work in this chapter is previous work from our lab and from our collaborators. The work in Sections 3.2.1 and 3.2.2 was done by the following people (in order of contribution): Anissa N. Elayadi, Kausar N. Samli, Ludmila Prudkin, Ying-Horng Liu, and Dr. Michael J. McGuire. Additionally, our collaborators Aihua Bian, Dr. Xian-Jin Xie, Dr. Ignacio I. Wistuba, and Dr. Jack A. Roth contributed to the work. The work in Secton 3.2.3 was performed by our collaborators at The University of Texas MD Anderson Cancer Center. The following people contributed to that work: Ludmila Prudkin, Diane D. Liu, Natalie C. Ozburn, Dr. Menghong Sun, Dr. Carmen Behrens, Dr. Ximing Tang, Dr. Kathlynn C. Brown, Dr. B. Nebiyou Bekele, Dr. Cesar Moran, and Dr. Ignacio I. Wistuba.

CHAPTER FOUR

FROM PHAGE DISPLAY TO NANOPARTICLE DISPLAY: FUNCTIONALIZING LIPOSOMES WITH MULTIVALENT PEPTIDES IMPROVES TARGETING TO THE $\alpha_v\beta_6$ CANCER BIOMARKER

4.1 Introduction

Targeting ligands that specifically recognize certain cell types or biological structures are emerging as important tools for cell-specific delivery of therapeutics and imaging agents. While antibodies have traditionally been the gold standard for cell-targeting,[29, 367] peptides are an attractive alternative. Unlike antibodies, peptides are easy to synthesize in large quantities[35] and their smaller size improves tissue penetration while preventing nonspecific uptake by the reticuloendoethial system. Additionally, peptides can be chemically modified to alter affinity, charge, hydrophobicity, stability, and solubility. In this manner, peptides can be optimized for *in vivo* use through reiterative modifications.

Phage display[37, 40, 42] is a powerful method for screening large peptide libraries for specific binding to a desired target,[38, 78] including proteins,[40] whole cells[80] and tissues.[79] However, chemical synthesis of peptides identified by phage display often results in ligands with significantly lower affinity than the corresponding phage, likely due to a loss of multivalency. The widely used and commercially available M13 phage libraries present peptides at the N-terminus of the phage pIII coat protein, which is displayed at one end of the filamentous phage in 3-5 copies. Thus, target-specific binding

of the phage is likely driven by both the peptide sequence and the multimeric presentation of peptides.

Many naturally occurring ligands bind via multivalent interactions,[368] and multivalency is a proven synthetic approach to improving affinity of moderate binders.[368, 369] We previously demonstrated that peptide affinity is increased by mimicking the multimeric presentation of the phage (Chapter 2).[266] Employing a trilysine dendrimeric core, we synthesized tetrameric peptides that display four peptide copies in the same valency and orientation as the phage. In a similar fashion, dendrimeric wedges displaying 2-5 peptide copies have also been used to emulate phage displayed peptides for increased affinity.[370, 371] Our tetrameric peptide presentation works as a general construct for peptides selected by phage display against a variety of cell types, allowing the peptides to maintain their cell specificity while increasing affinity relative to the monovalent peptides.[264, 266, 267, 335, 336] Importantly, tetramerization increases affinity of the peptides for their target cells by >45-fold compared to the corresponding monomeric peptides. The non-additive increase in affinity likely results from multivalent binding. While dimer and trimer peptides displaying either two or three peptide copies also increase affinity compared to the corresponding monomer, the tetrameric peptide construct displays the highest affinity.[271] Importantly, the tetrameric peptides rival the affinity of antibodies.[271] We recently developed a convergent method for the synthesis of tetrameric peptides with high yield and purity, expanding the utility of these tetrameric peptides.[271]

One of the downstream applications of phage display isolated peptides is incorporation into drug delivery or molecular imaging systems. As nanoparticles are able to encapsulate a variety of imaging agents or therapeutics, they are particularly attractive

for ligand-guided delivery to cells or organs. It has been assumed that conjugation of multiple copies of a ligand to the surface of a nanoparticle will impart multivalent binding and improve affinity of the ligand for its target.[368] An assortment of monomeric peptides selected from phage display libraries have been attached to nanoparticle platforms for imaging or therapy applications in animals.[154, 163, 372] However, it is unclear whether these platforms display the peptides in an ideal multimeric conformation. Additionally, increasing the copy number of the ligand on the nanoparticle to improve the effects of multivalent binding can result in increased non-specific binding. Nanoparticle display of higher affinity, multimeric peptides may further increase targeting, resulting in optimized therapeutic or imaging outcomes.

Multivalent sugar ligands have been used for targeting of liposomes[373-376] and the dendritic display of mannose, a known multivalent ligand, on the surface of nanoparticles has been shown to increase affinity for a Concanavalin A target protein.[377] However, there are no reports of multimeric peptide ligands conjugated to nanoparticles. It is unknown whether the multivalency of the nanoparticle is sufficient to provide selective targeting or whether a multivalent phage-mimicking peptide could further enhance nanoparticle targeting. The goal of this chapter is to examine the effects of peptide concentration, affinity, and valency on nanoparticle delivery.

For this study, I chose the H2009.1 peptide as a model ligand for studying the effects of peptide affinity and valency with the goal of translating phage display selected peptides to nanoparticle-targeting peptides. The H2009.1 peptide was originally selected by biopanning a phage display library against the non-small cell lung cancer (NSCLC) cell line H2009.[266] The peptide was subsequently discovered to bind the restrictively

expressed integrin $\alpha_v\beta_6$ on the cell surface (Chapter 3).[81] $\alpha_v\beta_6$ is emerging as a viable target for many epithelial-derived cancers,[342-352] including NSCLC; it is expressed in 56% of NSCLC patient tumor samples and only rarely expressed in normal tissue.[366] Importantly, $\alpha_v\beta_6$ is "turned on" early in the disease progression of NSCLC indicating that it may be a good biomarker for early cancer detection and treatment.[366] While a monomeric version of the H2009.1 peptide binds $\alpha_v\beta_6$-expressing H2009 cells with a half-maximal binding affinity of 9.2 nM, displaying the peptide on a tetrameric scaffold increases affinity three orders of magnitude, down to 11 pM. The H2009.1 peptide specifically binds and internalizes into $\alpha_v\beta_6$-expressing cells and targets $\alpha_v\beta_6$-positive tumors in mice, making this peptide a good model ligand with clinical relevance (Chapter 2). In this study, we conjugated either monomeric or tetrameric H2009.1 peptides to liposomal doxorubicin for a systematic comparison of the effects of peptide concentration, affinity, and valency in targeting $\alpha_v\beta_6$-positive NSCLC cells (Figure 4-1), with the goal of translating peptides isolated from phage displayed libraries to nanoparticle display.

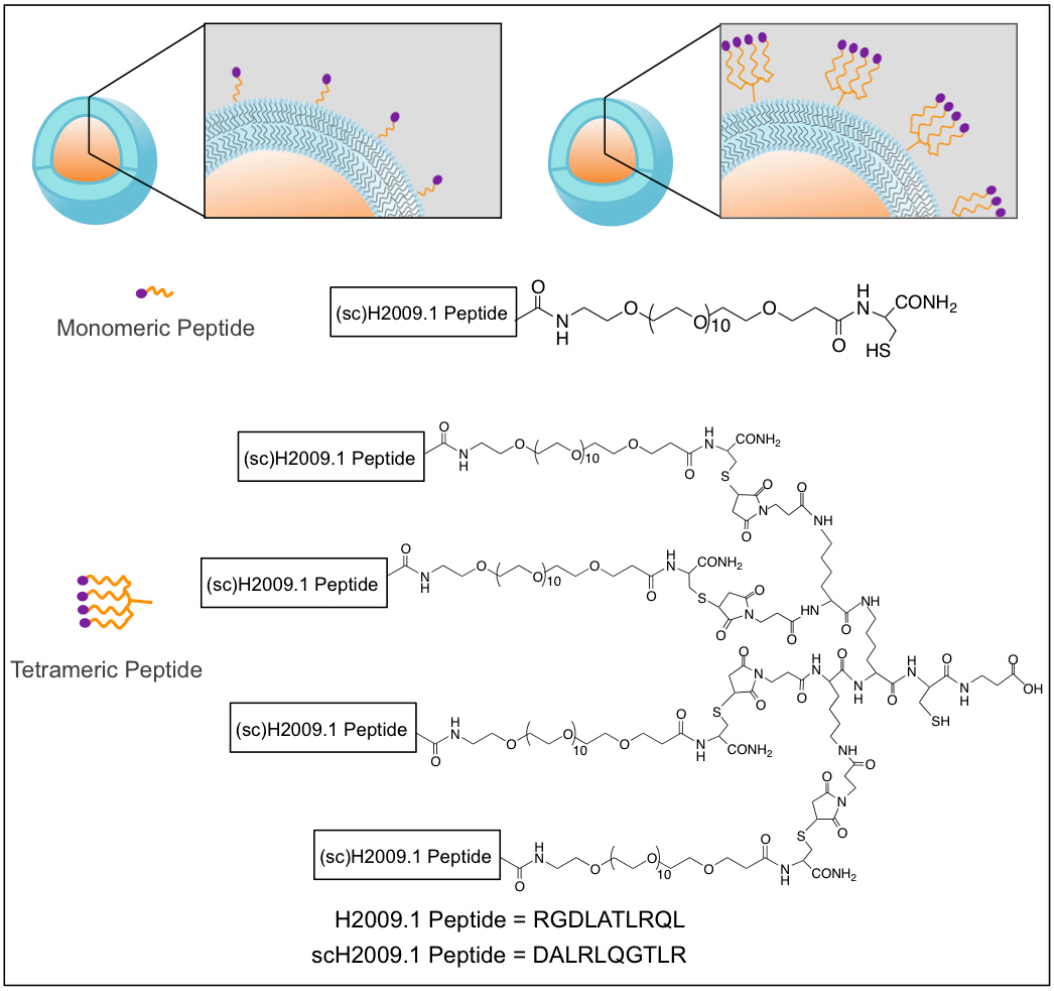

Figure 4-1. Liposomes displaying either monomeric or tetrameric H2009.1, or scH2009.1 peptides. The peptides are conjugated to the liposome via reaction of DSPE-PEG_{2000}-maleimide with a unique thiol on the peptide.

4.2 Materials and Methods

4.2.1 *Materials*

All Fmoc amino acids, the NovaPEG Rink Amide resin and 2-(1*H*-benzotriazole-1-yl)-1,1,3,3-tetramethyluronium hexafluorophosphate (HBTU) were purchased from Novabiochem® (EMD Millipore, Billerica, MA). The Fmoc-β-Ala-CLEAR™ Acid Resin was purchased from Peptides International (Osaka, Japan), β-maleimidopropionic acid from Tokoyo Chemical Industry Co. Ltd. (Portland, OR) and Fmoc-NH-$(PEG)_{11}$-COOH ($C_{42}H_{65}NO_{16}$) from Polypure (Oslo, Norway). *N*-Methylmorpholine (NMM) was purchased from ACROS Organics (Geel, Belgium). Anhydrous hydroxybenzotriazole (HOBt) was purchased from SynBioSci (Livermore, CA). Piperidine, Sepharose CL-4B and Sephadex G-50 were purchased from Sigma-Aldrich Inc. (Livermore, CA). Lipids were purchased from Avanti® Polar Lipids, Inc. (Alabaster, AL) and doxorubicin HCl for injection, from Bedford Laboratories™ (Bedford, OH). For cell culture, fetal bovine serum (FBS) was purchased from Gemini Bio-Products (West Sacramento, CA) and both RPMI 1640 and Trypsin EDTA, 1x from Mediatech, Inc. (Fisher Scientific, Pittsburgh, PA).

4.2.2 *Cell Lines*

All human NSCLC cell lines were provided by the UT Southwestern Medical Center Hamon Center for Therapeutic Oncology Research and maintained according to published protocols.[334] The H2009, H1975, and H460 cell lines were all grown at 37°C and 5% CO_2 in RPMI 1640 supplemented with 5% FBS.

4.2.3 *Peptide Synthesis and Purification*

Monomeric peptides were synthesized on a Symphony Synthesizer (Rainin Instruments, Protein Technologies, Inc., Woburn, MA) by standard Fmoc solid-phase peptide synthesis on a Rink Amide AM resin (substitution level 0.71 mmol/g). All amino acids were Fmoc-protected, and the Fmoc was removed to allow for amino acid coupling using 20% Piperidine in DMF. The amino acids were subsequently coupled at a 5-fold excess using HBTU, HOBt, and NMM coupling for 45 minutes. The PEG group added to each amino acid was purchased as Fmoc-NH-$(PEG)_{11}$-COOH and was coupled in the same manner as the amino acids, except that it was coupled at a 2.5-fold excess. The synthesized peptides were removed from the resin by shaking in a mixture of 94%:2.5%:1.0%:2.5%: of triofluoroacetic acid (TFA):triisopropylsilane:H_2O:ethanediothiol (EDT) for 2-4 hours. The majority of the TFA solution was then removed under N_2 pressure before precipitation in diethyl ether at -80°C for a minimum of 2 hours. Precipitated peptide was dried under vacuum for a minimum of 12 hours.

The tetrameric cores were also synthesized on the Symphony Synthesizer using the Fmoc-β-Ala-CLEAR™ Acid Resin (substitution level 0.40 mmol/g) under the same coupling conditions as the monomeric peptides. Fmoc-Cys(Acm)-OH was first coupled to the resin followed by Fmoc-Lys(Fmoc)-OH, $[Fmoc\text{-}Lys(Fmoc)\text{-}OH]_2$, and finally $(\beta\text{-maleimidopropionic acid})_4$. The cores were removed from the resin in the same manner as the monomeric peptides.

The crude monomeric peptides and tetrameric cores were purified by reverse phase high-performance liquid chromatography (HPLC) using a SPIRIT™ Spirit Peptide

C18 5 μm, 25 x 2.12 (AAPPTec®, Louisville, KY) on a Breeze™ HPLC (Waters Corporation, Milford, MA). H_2O/0.1% TFA (eluent A) and acetonitrile/0.1% TFA (eluent B) were used for purification as follows: 0-1 minute, 90% A, 10% B at 10mL/minute; from 1-100 minutes, eluent B was increased from 10% to 60% at a flow rate of 10 mL/minute. The peptides were detected by ultraviolet (UV) absorbance at 220nm. Matrix-assisted laser desorption/ionization time of flight mass spectrometry was used to confirm peptide mass (Voyager-DE™ PRO, Applied Biosystems, Inc., Foster City, CA). The mass of the monomeric peptides (average mass calculated/MH+: 1843.02/1844.18) and tetrameric core (average mass calculated/MNa+: 1251.49/1274.27) were determined in reflective mode using α-cyano-4-hydroxycinnamic acid as a matrix.

The tetrameric peptides were synthesized by coupling purified monomeric peptide to purified, deprotected tetrameric core (8:1 monomeric peptide to tetrameric core) for 2 hours at room temperature in phosphate buffered saline, pH 7.4, containing 10 mM EDTA. Afterwards, excess monomeric peptide was removed by reverse phase HPLC using the same elution method that was used for purification of the monomeric peptides and tetrameric core. The mass of the tetrameric peptides (average mass calculated/MH+: 8629.01/8626.77) were also determined using matrix-assisted laser desorption/ionization time of flight mass spectrometry using linear mode and sinapinic acid as a matrix.

Before the tetrameric peptides could react with the maleimide-activated lipid on the liposome surface, the unique cysteine placed before the branch point of the tetramers had to be deprotected to remove the acetamidomethyl (Acm) group protecting the thiol of the cysteine. The tetrameric peptides were deprotected by reaction of the peptide (0.35 μmol) with AgOAc (0.168 M AgOAc in 99:1 TFA:anisole to a total volume of 350 μL)

for 2 hours at 4°C. The majority of the TFA solution was then removed under a slow stream of nitrogen and the peptide precipitated in diethyl ether at -80°C for a minimum of 30 minutes. After removing the ether from the precipitated peptide, the peptide was reacted with 150 μL of a 0.2 M dithiothreitol (DTT) solution (DTT dissolved in 1 M acetic acid) for a minimum of 5 hours shaking. The resulting solution was centrifuged and the supernatant taken for HPLC purification of the deprotected peptide. Additional tetrameric peptide was recovered from the pellet by shaking in 8 M guanidine HCl for an additional 5 hours. The supernatant resulting from centrifugation of this mixture was also taken for HPLC purification. The deprotected tetramers were purified using the same HPLC conditions as used for the other peptides and the deprotection was verified by mass spectrometry, using the same method used for the protected tetramers (average mass calculated/MH+: 8557.94/8558.38).

4.2.4 *Preparation of Liposomal Doxorubicin*

Liposomes were prepared from solutions of the lipids hydrogenated soy L-α-phophatidylcholine (HSPC), cholesterol, 1,2-distearoyl-*sn*-glycero-3-phosphoethanolamine-N-[carbonyl-methoxy(polyethylene glycol)-2000] (DSPE-PEG_{20000}), and 1,2-distearoyl-*sn*-glycero-3-phosphoethanolamine-N-[maleimide(polyethylene glycol)-2000] (DSPE-PEG_{2000}-maelimide) in 2:1 chloroform:methanol (Table 4-1). The 0.64% liposomes were prepared from mixtures of 100 mg (131 μmol) of HSPC, 25.4 mg (65.6 μmol) of cholesterol, 14.7 mg (5.20 μmol) of DSPE-PEG_{20000} and 3.85 mg (1.31 μmol) of DSPE-PEG_{2000}-maleimide. The 1.3%

liposomes were prepared from mixtures of 100 mg (131 μmol) of HSPC, 25.4 mg (65.6 μmol) of cholesterol, 10.9 mg (3.87 μmol) of DSPE-PEG_{20000} and 7.92 mg (2.69 μmol) of DSPE-PEG_{2000}-maelimide. The 2.0% liposomes were prepared from mixtures of 100mg (131 μmol) of HSPC, 25.4 mg (65.6 μmol) of cholesterol, 6.99 mg (2.49 μmol) of DSPE-PEG_{20000} and 12.0 mg (4.10 μmol) of DSPE-PEG_{2000}-maelimide.Solvent was removed under a slow stream of nitrogen at 45ºC, and the lipid film was left under vacuum overnight. The dried lipid film was hydrated with 155 mM $(NH_4)_2SO_4$ buffer, pH 5.5, by intermittently heating at 65ºC and vortexing. Liposomes were subsequently extruded 20 times through double-stacked 100nm membranes, and PD-10 desalting columns (GE Healthcare, Waukesha, WI**)** were used to change the outer liposomal buffer to 123 mM NaCitrate, pH 5.5. At this point a small portion of the liposomes were set aside to remain doxorubicin-free. As doxorubicin interferes with the assay used to determine the amount of peptide coupling to the liposome surface (described in Section 5.2.6), a small subset of liposomes were saved for characterization of peptide coupling to the entire batch of liposomes. These liposomes were desalted into HEPES buffered saline using a PD-10 desalting column. Doxorubicin was loaded remotely (post-liposome formation) into the remainder of the liposomes by incubation of liposomes and doxorubicin at 65ºC for 1 hour. Free doxorubicin was removed using a Sephadex G-50 column equilibrated with HEPES buffered saline. Peptides were conjugated to liposomes by reaction for 24 hours

Table 4-1. Liposome Formulations

	Formulation (molar percentages)		
Lipid	**0.64%**	**1.3%**	**2.0%**
HSPC[a]	65%	65%	65%
Cholesterol	32%	32%	32%
DSPE-PEG$_{2000}$[b]	2.5%	1.9%	1.2%
DSPE-PEG$_{2000}$-Maleimide[c]	0.64%	1.3%	2.0%

a Hydrogenated soy phosphatidylcholine.
b 1,2-distearoyl-*sn*-glycero-3-phosphoethanolamine-N-[carbonyl-methoxy(polyethyelene glycol)-2000].
c 1,2-distearoyl-*sn*-glycero-3-phosphoethanolamine-N-[maleimide(polyethylene glycol)-2000].

at a ratio of 2:1 peptide: DSPE-PEG$_{2000}$-maelimide in a solution of HEPES buffered saline, and excess peptide was removed using Sepharose CL-4B columns. Each peptide conjugated to the liposomes was coupled to two forms of the liposomes: liposomes without doxorubicin and doxorubicin-loaded liposomes. The liposomes without doxorubicin were used to determine peptide coupling to the liposomes and the doxorubicin-loaded liposomes were used for all other experiments.

4.2.5 *Liposome Characterization*

Liposome size was determined using a Malvern Zetasizer (Worcestershire, UK), and phospholipid content was determined using the Modified Bartlett Procedure.[378] Doxorubicin concentration was determined by absorbance at 480 nm after the addition of 1% Triton X-100 and heating at 95ºC as detailed elsewhere.[379] The amounts of peptide

conjugated to the liposomes were determined using the CBQCA Protein Quantitation Kit (Life Technologies™, Grand Island, NY) according to the manufacturer's instructions, with standard curves generated by peptides containing tyrosine residues. Peptide number/liposome was calculated by assuming 80,000 phospholipid molecules/liposome for a liposome size of 100 nm.[380]

4.2.6 *Doxorubicin Fluorescence in Cells*

H2009 cells were plated in 12 well plates and 48 hours later, once the cells reached 90% confluency, incubated with doxorubicin liposomes for 1 hour. After washing the cells twice with PBS, PBS + 5% Triton was added and the plates were shaken for 15 minutes to lyse the cells. Doxorubicin concentration was determined by absorbance at 590 nm compared to doxorubicin standards in untreated cells using a F-7000 Fluorescence Spectrophotometer (Hitachi, Tokyo, Japan).

4.2.7 *Liposome Accumulation in Cells as Monitored by Flow Cytometry*

H2009 or H1299 cells were plated in 12 well plates and 48 hours later, once the cells reached 90% confluency, incubated with 8-20μM (based on doxorubicin concentration) doxorubicin liposomes for 1 hour. All wells were then washed (with gentle shaking) with 4 x 1mL of PBS + 0.1% BSA and cells were removed from the plates after incubation on ice for 30 min. in 1mL/well of Enzyme-free Cell Dissociation Buffer (Life Technologies). A Cell Lab Quanta™ SC flow cytometer (Beckman Coulter) was used to measure doxorubicin fluorescence for 10,000 cells per treatment group in channel 2 (excitation 488nm, emission 550-600nm). No significant fluorescence

quenching by the membranes of the intact cells and liposomes was observed in these assays.

4.2.8 *Cell Viability*

H2009 or H1299 cells were plated in Corning® Costar® 96-well, black, clear bottom cell culture plates (Fisher Scientific, Pittsburg, PA). The cells were seeded at 2,000 cells/well in a volume of 50 μL R5 media per well. After 24h, cells were treated with doxorubicin liposomes in 50 μL R5 at varying concentrations (10-10240 nM based on total doxorubicin concentration) to produce a final volume of 100 μL. Untreated cells were incubated with R5 media alone. Each treatment was performed in sets of 8 replicates. After incubation with the liposomes for 1 hour, all wells were washed twice with 100 μL of R5 before the addition of 100 μL of fresh R5. The cells were maintained at 37°C and 5% CO_2 for an additional 96 hours, with one media change at 72 hours. At 120 hours, cell viability was determined using the ATP-based CellTiter-Glo® Luminescent Cell Viability Assay (Promega Corporation, Fitchburg, WI). Luminescence was detected using a SpectraMax M5 Multi-Mode Microplate Reader (Molecular Devices, Sunnyvale, CA).

4.2.9 *Confocal Microscopy*

H2009 cells were plated at 1,000 cells/plate in poly-d-lysine coated glass bottom culture dishes (MatTek Corporation, Ashland, MA). Once the cells had adhered to the plates, ~24 hours later, they were incubated with 4μM (based on total doxorubicin

concentration) of either free doxorubicin or 1.3% H2009.1 tetrameric liposomes. After 1 hour, the cells were washed twice with R5 before the addition of fresh R5. The cells were then examined using a Nikon TE2000-E microscope (Melville, NY), observing doxorubicin fluorescence (excitation 485 nm , emission 595 nm).

4.3 Results

4.3.1 *Preparation of Liposomes Functionalized with either Monomeric or Tetrameric H2009.1 Peptides*

Pegylated liposomal doxorubicin was chosen as a model nanoparticle system due to its widespread clinical use. As liposomes are small vesicles formed from lipid bilayers, their aqueous interior allows encapsulation of a variety of hydrophilic or amphipathic drugs or imaging agents. Additionally, the ~100nm size of pegylated liposomal doxorubicin is ideal for tumor targeting, falling within the desired range for extravasation from the blood vessels into the tumor.[379] Polyethylene glycol (PEG) lipids prolong liposome *in vivo* circulation times by reducing interaction of the liposomes with serum proteins and delaying clearance of the nanoparticles by the reticuloendoethial system.[143] While there are a growing number of nanomedicine platforms which I could explore, using a well characterized nanoparticle drug delivery system for this study will speed advances from chemical optimization to clinical use.

Liposomes were prepared by mixing hydrogenated soy phosphatidylcholine (HSPC), cholesterol, DSPE-PEG_{20000} (1,2-distearoyl-*sn*-glycero-3-phosphoethanolamine-N-[carbonyl-methoxypolyethyelene glycol-2000]), and DSPE-PEG_{2000}-maelimide (1,2-distearoyl-*sn*-glycero-3-phosphoethanolamine-N-[maleimide(polyethylene glycol)-2000])

at a molar ratio of 2:1:0.08:0.02, resulting in liposomes with 0.64% of the total lipid displaying maleimide groups. This formulation has been used for antibody conjugation to liposomes and serves as a reasonable starting point. The maleimide-activated lipid allows for conjugation of cysteine containing peptides to the liposome, displaying the peptides outside the PEG brush layer coating the liposome. To examine the effect of peptide density on liposome targeting ability, additional liposome formulations were prepared with increasing amounts of maleimide-activated lipid, keeping the total amount of pegylated lipid constant. All the liposome formulations are named according to the percentage of lipid bearing maleimide functionality – 0.64%, 1.3%, or 2.0% liposomes (Table 4-1). Replacing all the pegylated lipid with maleimide-pegylated lipid, to make 3.2% maleimide liposomes, resulted in liposomes with high nonspecific cellular binding (data not shown).

To investigate whether peptide valency affects liposomal targeting, I synthesized four different peptides for conjugation to the doxorubicin liposomes – the targeting H2009.1 monomeric and tetrameric peptides and sequence scrambled control versions of these peptides, denoted as scH2009.1 peptides (Figure 4-1). The scH2009.1 peptides serve as important controls as they contain the same amino acids as the H2009.1 peptides but display the amino acids in a scrambled order that renders the peptides unable to bind $\alpha_v\beta_6$. Carboxy-terminal PEG groups were included in the monomeric peptides to increase solubility and to provide space between the peptide sequence responsible for binding and the point of attachment to either the nanoparticle or tetrameric core. The tetrameric peptides were synthesized from the monomeric peptides and a maleimide-activated tetrameric core using a convergent synthesis previously described.[271] All monomeric and

tetrameric peptides display a unique C-terminal cysteine for reaction with the maleimide-activated lipid on the liposome surface.

Peptide functionalized liposomes were synthesized using thiol-maleimide chemistry from the reaction of cysteine-bearing peptides with maleimide-bearing liposomes. β-Mercaptoethanol was used to quench any unreacted maleimide groups. The peptide functionalized liposomes ranged in size from 100-130nm and reached optimal doxorubicin loading levels of 166-186 μgrams doxorubicin/μmoles phospholipid. As shown in Table 4-2, peptide coupling efficiency to the liposomes was typically >90% and correlated with the amount of maleimide-activated lipid. Based on a liposome size of 100nm, the peptide density ranges from approximately 740 peptides/liposome for the 0.64% liposomes to approximately 2,400 peptides/liposome for the 2.0% liposomes. Due to anticipated lipid partitioning between the exterior and interior lipid layers, it was expected that only half of the maleimide-lipid would be available for coupling. Accordingly, peptide coupling efficiency was predicted to be 50% based on the total amount of DSPE-PEG_{2000}-maleimide. However, > 90% peptide coupling is consistently observed, indicative of maleimide-lipid partitioning to the outer lipid layer. Protein quantification is performed on intact liposomes; it is unlikely that the CBCQA assay used to quantify peptide coupling would detect peptides in the internal compartment of the liposome, further suggesting that the maleimide-lipid-peptide conjugate is partitioning to the outside face of the liposome. To ensure that the peptides were not inserting into the lipid bilayer, I added cysteine-bearing peptides to liposomes in which the maleimide groups had already been quenched with β-mercaptoethanol. After following my normal 24 hour reaction time period and removing excess peptide, I was unable to detect any

Table 4-2. Characterization of Peptide Coupling to Liposomes

liposome maleimide percentage	peptide	nmole peptide/μmole phospholipid	peptides/liposome[a]
0.64	H2009.1 tetramer	9.1	720
	scH2009.1 tetramer	9.4	760
1.3	H2009.1 monomer	15	1200
	H2009.1 tetramer	18	1400
	scH2009.1 tetramer	19	1500
2.0	H2009.1 monomer	30	2400
	H2009.1 tetramer	30	2400
	scH2009.1 tetramer	32	2600

a – Peptide number/liposome was calculated by assuming 80,000 phospholipid molecules/liposome for a liposome size of 100 nm (reference [380])

peptide associated with the liposomes. This result indicates that the peptide is not directly inserting into the lipid bilayer. It is also highly unlikely that the peptide would traverse the membrane to become entrapped in the core of the liposome. Thus, my peptide coupling values appear to reflect the actual numbers of peptides displayed on the exterior of the liposomes due to partitioning of maleimide-lipid to the outer lipid layer. However, I cannot rule out the possibility that some of the peptide bound to maleimide-lipid resides in the interior of the liposome due to lipid flipping.

4.3.2 *Effects of H2009.1 Peptide Valency and Concentration on Liposome Targeting to $\alpha_v\beta_6$-Expressing Cells*

The ability of the monomeric and tetrameric peptide bearing liposomes to bind and target their receptor, $\alpha_v\beta_6$, was examined by measuring the amount of liposomal doxorubicin internalized into $\alpha_v\beta_6$-expressing cells. After incubating liposomes with cells and subsequently washing to remove any unbound nanoparticles, both the cells and

liposomes were lysed with detergent and the amount of cell-associated doxorubicin quantified by measuring total doxorubicin fluorescence. Based on a standard curve of free doxorubicin, this assay was able to detect doxorubicin amounts above ~0.4 pmole. Cells were counted prior to fluorescence measurements so that the doxorubicin concentration could be normalized on a per cell basis. My results are calculated as picomoles of doxorubicin per 10,000 cells. As a note of reference, delivery of a single 100 nm liposome with a loading of 180 μgrams of doxorubicin/μmoles phospholipid should deliver ~2.6 x 10^4 molecules (4.3 x 10^{-8} pmoles) of doxorubicin.

To determine whether peptide valency plays a role in targeting $\alpha_v\beta_6$, $\alpha_v\beta_6$-positive H2009 cells were incubated with either 2.0% H2009.1 monomeric or 0.64% H2009.1 tetrameric liposomes, which bear similar numbers of individual peptide units. Cell associated doxorubicin was not measurable for the 2.0% monomeric liposomes until the two highest drug treatment concentrations. However, all treatment concentrations of the 0.64% H2009.1 tetrameric liposomes resulted in detectable cellular doxorubicin levels. Significantly, the 0.64% H2009.1 tetrameric liposomes demonstrated 5-10 fold more drug uptake than the 2.0% H2009.1 monomeric liposomes (Figure 4-2a). Thus, although the 0.64% H2009.1 tetrameric and 2.0% H2009.1 monomeric liposomes display similar numbers of monomeric H2009.1 peptide units, the liposomes displaying tetrameric peptides receive a synergistic boost in targeting $\alpha_v\beta_6$-positive H2009 cells. The multivalency inherently given to the monomeric peptides by conjugation to the liposome surface is not as effective for targeting as the multimeric tetrameric peptides displayed in a multivalent fashion on the liposomal surface. This is the first demonstration that a multimeric peptide functions better than a monomeric peptide on a nanoparticle platform.

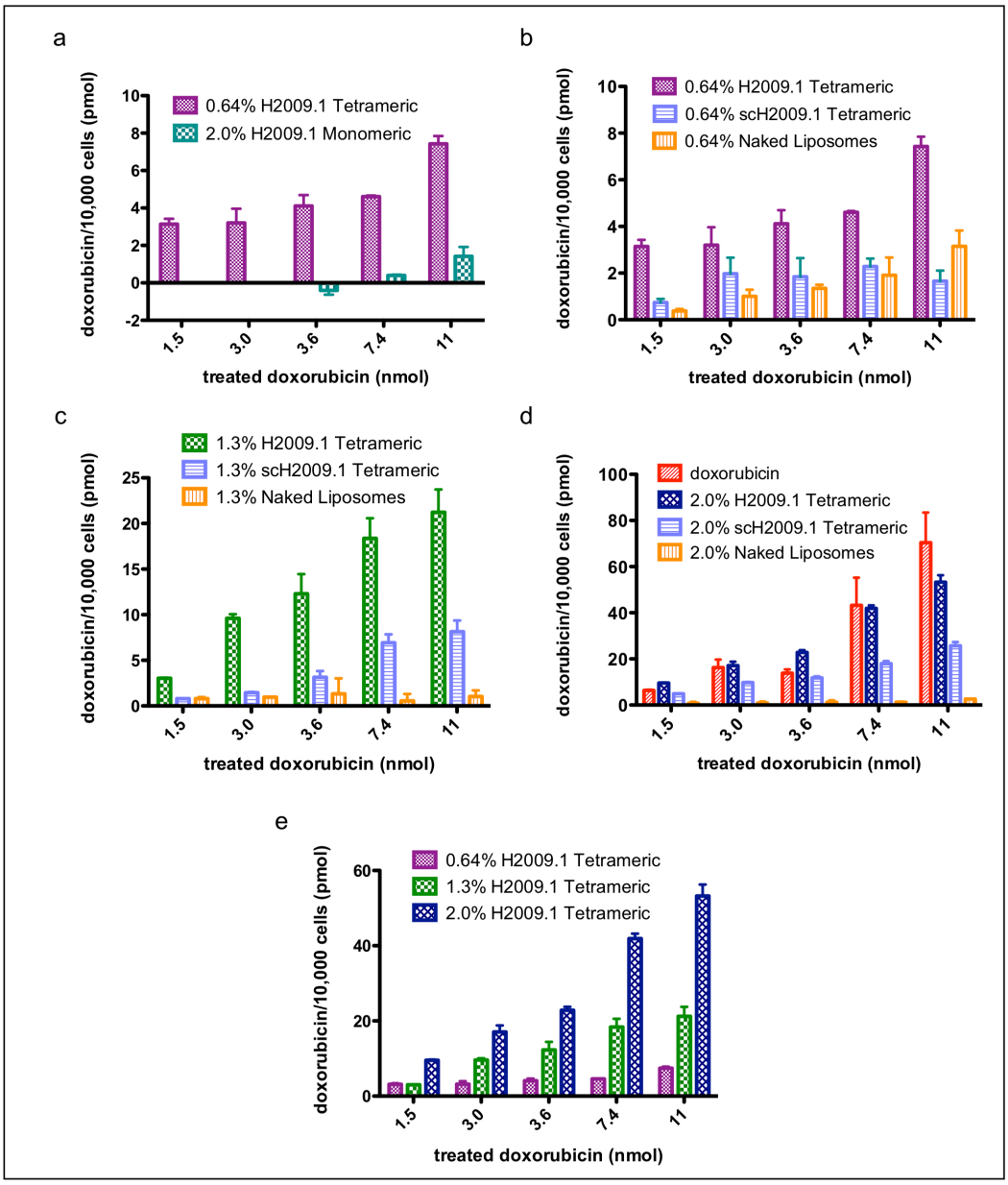

Figure 4-2. H2009.1 tetrameric liposomes target $\alpha_v\beta_6$-expressing cells better than monomeric liposomes and targeting increases with increasing peptide density. $\alpha_v\beta_6$-expressing H2009 cells were incubated with increasing concentrations of different liposome formulations. Cellular doxorubicin concentrations were determined as pmol doxorubicin/10,000 cells.

To determine the effect of peptide density on liposomal targeting, I compared the amount of doxorubicin internalized into cells incubated with the 0.64%, 1.3%, and 2.0% H2009.1 tetrameric liposomes. Increasing liposomal peptide density increased targeting to $\alpha_v\beta_6$-expressing H2009 cells (Figure 4-2c). While the 1.3% H2009.1 tetrameric liposomes display twice as much peptide as the 0.64% H2009.1 liposomes, they target H2009 cells 3-4 fold better at all concentrations except for the lowest treatment concentration. The discrepancy at the lower concentration is most likely due to the sensitivity of the assay. Similarly, the 2.0% H2009.1 tetrameric liposomes display 1.5 times more peptide than the 1.3% H2009.1 tetrameric liposomes yet target H2009 cells 2-3-fold better than the 1.3% liposomes. The nonlinear increase in targeting with increasing peptide density indicates that the peptide amount alone is not sufficient for the improved specificity of the 1.3% and 2.0% liposomes. The extra layer of multivalency provided by the liposomes also plays a role in targeting.

To ensure that the H2009.1 tetrameric peptide mediates $\alpha_v\beta_6$-receptor binding, control scH2009.1 tetrameric liposomes and control "naked", no peptide, liposomes were synthesized and tested for binding to H2009 cells. At all treatment concentrations, the 0.64% H2009.1 tetrameric liposomes delivered 2-4 fold more doxorubicin than the scH2009.1 tetrameric liposomes and 2-8 fold more doxorubicin than the naked liposomes (Figure 4-2b). Similar trends emerged for the 1.3% and 2.0% liposomes functionalized with higher concentrations of peptide (Figure 4-2c-d). Thus, the specific sequence of the H2009.1 tetrameric peptide, and not just the presence of a peptide, mediates receptor specific binding, resulting in enhanced delivery of doxorubicin to H2009 cells.

One concern with increasing liposomal peptide number is that higher peptide concentrations could lead to higher nonspecific uptake merely due to charge effects. Positively charged lipids are commonly used to courier cargo across the negatively charged cell membrane. The H2009.1 monomeric peptide has a +2 charge at neutral pH and the tetrameric peptide has a +8 charge. Thus, the 2.0% liposomes, with approximately 2400 tetrameric peptides per liposome, bear a +19E3 charge. As the scH2009.1 peptide bears the same charge as the H2009.1 peptide without $\alpha_v\beta_6$ specificity, any affinity of the scH2009.1 peptide modified liposomes for $\alpha_v\beta_6$-expressing cells is the result of nonspecific accumulation. Accordingly, the scH2009.1 functionalized liposomes exhibit an increased cell binding at the 2.0% density. While the 0.64% and 1.3% scH2009.1 tetrameric liposomes generally accumulate in H2009 cells at similar levels, as expected for liposomes displaying a control peptide, the 2.0% scH2009.1 tetrameric liposomes consistently target the H2009 cells 3-7 fold better than the other scH2009.1 peptide liposome formulations (Figure 4-2b-d). Binding of the 2.0% scH2009.1 tetramer liposomes is driven entirely by the presence of the peptide; the naked, no peptide, 2.0% liposomes accumulate in cells to the same extent as the 0.64% and 1.3% naked liposomes. Thus, the increased affinity of the 2.0% scH2009.1 tetrameric liposomes is likely due to charge effects. Despite nonspecific cellular accumulation, the 2.0% liposomes functionalized with the H2009.1 tetrameric peptide still target $\alpha_v\beta_6$ 2-fold better than 2.0% liposomes functionalized with the scH2009.1 tetrameric peptide (Figure 4-2d). Thus, a combination of receptor-specific binding and nonspecific cellular interactions contribute to cellular binding when the peptide density is increased to 2.0%.

Targeting of the H2009.1 tetrameric liposomes was verified using flow cytometry to determine the relative amount of cell associated doxorubicin. Although this assay cannot provide absolute quantification of doxorubicin uptake, flow cytometry can provide relative ratios between liposomal formulations and is expected to be more sensitive at lower doxorubicin concentrations. Additionally, it can determine if uptake is homogeneous throughout the cell population or if a subset of non-binding cells exists. Consistent with the previous data, the 0.64%, 1.3%, and 2.0% H2009.1 tetrameric liposomes exhibit increased binding to H2009 cells compared to corresponding scH2009.1 tetrameric and naked liposomes (Figure 4-3a-c). In three independent flow assays, I determined the doxorubicin uptake for either the H2009.1 tetrameric or scH2009.1 tetrameric liposomes as compared to the corresponding naked liposomes. Modification of liposomes with the H2009.1 tetrameric peptide dramatically improved targeting compared to the naked liposomes, with values ranging from a 47% increase for the 0.64% liposomes to a 170% increase for the 2.0% liposomes (Figure 4-3d). Additionally, the uniform shift in the fluorescence channel suggests that the bulk of the cell population is binding the H2009.1 liposomes (Figure 4-3).

As previously observed, increasing H2009.1 peptide density on the liposome surface also increases targeting, with the highest peptide concentration 2.0% liposomes targeting 4-fold better than the lowest peptide concentration 0.64% liposomes (Figure 4-3d). Additionally, while each H2009.1 tetramer liposome targets better than its corresponding scH2009.1 tetramer liposome, this targeting differential decreases as the

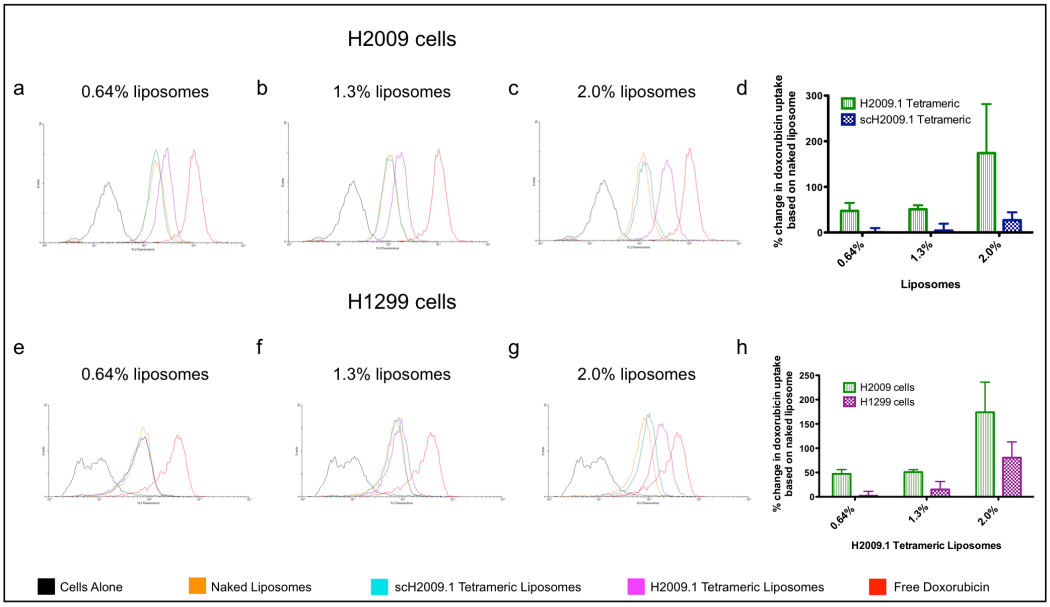

Figure 4-3. H2009.1 tetrameric peptide liposomes display specificity for $\alpha_v\beta_6$-expressing H2009 cells compared to $\alpha_v\beta_6$-low-expressing H1299 cells. Cells were incubated with different liposome formulations and liposome accumulation in cells measured using flow cytometry. Representative flow cytometry analyses for H2009 cells are shown in panels a-d and for H1299 cells are shown in panels e-h. Panels d & h show the averages from 3 independent flow assays in which the mean fluorescence intensities of the H2009.1 tetrameric and scH2009.1 tetrameric liposomes were normalized to the mean fluorescence intensity of the naked liposomes.

amount of peptide increases. The lowest peptide concentration 0.64% H2009.1 tetrameric liposomes bind 190-fold better than the corresponding scH2009.1 tetrameric liposomes, while the highest peptide concentration 2.0% H2009.1 tetrameric liposomes only bind 6-fold better than the corresponding scH2009.1 tetrameric liposomes. Despite this decrease in the targeting difference between the H2009.1 tetrameric liposomes and the scH2009.1 tetrameric liposomes, it is still clear that the specific sequence of the H2009.1 tetrameric peptide, and not just the presence of a peptide, directs liposome targeting.

These results demonstrate that multimeric display of a phage-selected peptide on a nanoparticle increases cell binding compared to monomeric presentation, even at high densities of the monomeric peptide. While the liposome itself is inherently a multivalent platform, functionalizing the nanoparticle with multiple copies of the monomeric peptide is not as effective as attaching multiple copies of the phage-mimicking tetrameric peptide. Yet increasing the number of multimeric peptides on the liposome also increases cell binding, suggesting the liposome platform provides a second level of multivalent binding. Thus, both the multivalent peptide and the multivalent liposome scaffold work together to increase targeting to $\alpha_v\beta_6$-expressing cells.

4.3.3 *Specificity of H2009.1 Tetrameric Peptide Liposomes for $\alpha_v\beta_6$*

To further verify the specificity of H2009.1 peptide liposomes for $\alpha_v\beta_6$, I compared liposomal targeting to $\alpha_v\beta_6$-positive verses $\alpha_v\beta_6$-negative cells. Flow cytometry was used to follow binding of the peptide-modified liposomes to an $\alpha_v\beta_6$-expressing cell line (H2009) verses an $\alpha_v\beta_6$-negative NSCLC cell line (H1299). The 0.64%, 1.3%, and 2.0% H2009.1 tetrameric liposomes exhibit increased cellular association to the H2009 cells compared to corresponding scH2009.1 tetrameric and naked liposomes (Figure 4-3a-d). However, these same 0.64% and 1.3% H2009.1 tetrameric liposomes display no specific binding to H1299 cells, accumulating to the same extent as the scH2009.1 tetrameric and naked liposomes in the non-targeted cells (Figure 4-3e,f, & h). At higher peptide concentrations, the $\alpha_v\beta_6$-specificity is dampened; the 2.0% H2009.1 tetrameric liposomes display a 2-fold preference for H1299 cells over

the control scH2009.1 liposomes (Figure 4-3h). While I observed some nonspecific uptake of the 2.0% liposomes into H2009 cells, peptide charge is unlikely the only driving force behind the accumulation of 2.0% H2009.1 tetrameric liposomes into H1299 cells. If the effect were exclusively charge dependent, the 2.0% scH2009.1 tetrameric liposomes would bind to the same extent as the 2.0% H2009.1 tetrameric liposomes, since the H2009.1 and scH2009.1 peptides contain the same amino acids and same charge. Therefore, while some of the cellular association of the 2.0% H2009.1 tetrameric liposomes with H1299 cells may be the result of nonspecific binding, the H2009.1 tetrameric peptide liposomes may also be binding to low levels of $\alpha_v\beta_6$ on the H1299 cells that are detected as the affinity of the liposomes increases. Consistent with this observation, the H2009.1 peptide exhibits a low level of binding to H1299 cells, albeit at levels at least 60-fold lower than the H2009 cells, and low levels of $\alpha_v\beta_6$ have been detected in H1299 cells.[81] This highlights a challenge in cell-specific targeting, especially in regards to targeting tumor cells. It is unlikely that a cell is completely devoid of a cellular receptor; instead, there is differential receptor expression between the cancer cell and its normal counterpart. As the affinity of a cell-targeting ligand increases, so does the likelihood of its binding the low levels of its receptor found on normal cells. However, the 2.0% H2009.1 tetrameric liposomes still demonstrated 2-fold greater affinity for the $\alpha_v\beta_6$-positive H2009 cells over the $\alpha_v\beta_6$-negative H1299 cells (Figure 4-3h). In summary, the higher density of the tetrameric peptide on the liposome results in increased cellular targeting yet this increase comes at the cost of higher nonspecific binding and decreased cell specificity.

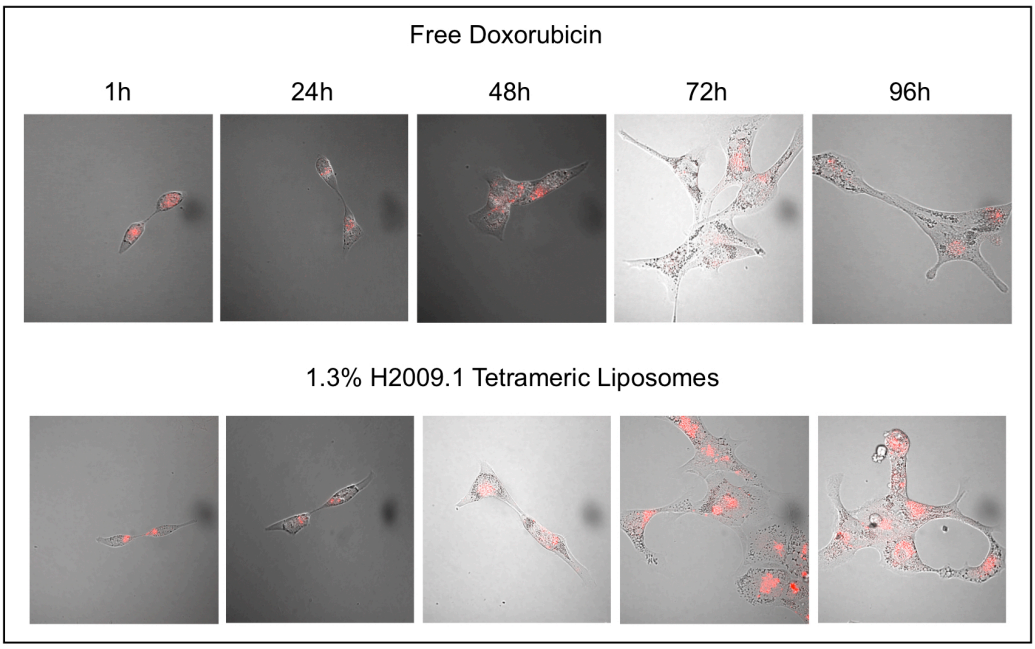

Figure 4-4. Time course for release of doxorubicin from 1.3% H2009.1 Tetrameric Liposomes. Cells were treated with either free doxorubicin or 1.3% H2009.1 tetrameric liposomal doxorubicin for 1 hour before the drug was removed. Doxorubicin fluorescence was observed by confocal microscopy at the indicated time after initial treatment.

4.3.4 *Drug Release*

Doxorubicin must enter the cell nucleus in order to exert its effects. To visualize the subcellular localization and entry of H2009.1 liposomes into the nucleus, H2009 cells were incubated with either free doxorubicin or the 1.3% H2009.1 tetrameric liposomes and doxorubicin fluorescence was examined by confocal microscopy (Figure 4-4). Free doxorubicin was visible in the cell nucleus as early as 1 hour after incubation and began to visibly affect cell structure 48 hours after treatment. By 72 hours, cells treated with free doxorubicin began to bleb, indicative of apoptosis. In contrast, the 1.3% H2009.1 tetrameric liposomes initially appeared perinuclear and doxorubicin did not localize to

the nucleus until 48 hours after treatment. By 72 hours, the liposome-treated cells were bloated and abnormal and at 96 hours they began to bleb. Thus, it requires approximately 48 hours for the internalized liposomes to release their cargo allowing for observable nuclear accumulation of doxorubicin. While liposomal drug release is delayed, alterations in cellular structure occur only 24 hours later than the free drug. These results demonstrate that the H2009.1 tetrameric peptide does not prevent liposomal drug release. Additionally, the H2009.1 tetrameric liposomes remain intact extracellularly, releasing doxorubicin only after internalization into cells. Importantly, even though the liposomes are initially trapped within a perinuclear compartment, they degrade and release free doxorubicin to its site of action in the nucleus.

4.3.5 *Cytotoxicity of H2009.1 Monomeric and Tetrameric Peptide Liposomes*

In order to serve as viable treatment options, the H2009.1 peptide liposomes must not only accumulate in $\alpha_v\beta_6$-positive cells, but also exert specific cytotoxic effects to these cells. I anticipated that increased cellular binding would improve the cytotoxicity of liposomal doxorubicin. To examine the ability of the H2009.1 liposomes to induce cell death, I compared the cytotoxic effects of the various peptide liposome constructs. As expected from the ability of the H2009.1 peptide to specifically direct liposomes to these cells, all of the H2009.1 tetrameric liposomes were more cytotoxic than the corresponding scH2009.1 tetrameric and naked liposomes. The IC_{50} values were determined for each liposome formulation and are detailed in Table 4-3. The IC_{50} for

Table 4-3. IC_{50} Values of Different Liposome Formulations on $\alpha_v\beta_6$-Positive H2009 Cells[a]

Drug Formulation	IC50 on H2009 cells (nM)
0.64% H2009.1 Tetrameric	1500 ± 200
0.64% scH2009.1 Tetrameric	2400 ± 120
0.64% Naked	7400 ± 1400
1.3% H2009.1 Monomeric	5700 ± 120
1.3% H2009.1 Tetrameric	970 ± 130
1.3% scH2009.1 Tetrameric	2000 ± 330
1.3% Naked	Not reached[b]
2.0% H2009.1 Tetrameric	360 ± 35
2.0% scH2009.1 Tetrameric	610 ± 90
2.0% Naked	6900 ± 960
Free Doxorubicin	430 ± 75

a – Cells were incubated with liposomes for 1 hour followed by a 120 hour receovery in media.
b – Not reached at the highest treatment concentration of 10.2 μM.

each H2009.1 peptide liposome was approximately 2-fold lower than the corresponding scH2009.1 peptide liposome. Additionally, the IC_{50} decreased with increasing peptide concentration. Importantly, the IC_{50} values correlate with the amount of internalized doxorubicin measured in Figure 4-2. Significantly, the 2.0% H2009.1 tetrameric liposomes (360 ± 35 nM) gave an IC_{50} value similar to that of free, non-liposome encapsulated, doxorubicin (430 ± 75 nM) as expected from their similar levels of accumulation quantified by the doxorubicin uptake studies. Due to its ability to easily cross the cell membrane, free doxorubicin accumulates quickly in the cell nucleus and often demonstrates better *in vitro* cytotoxicity than liposome-encapsulated doxorubicin.

While the 2.0% H2009.1 tetrameric liposomes gave the lowest IC_{50} value (360 ± 35 nM), the 1.3% H2009.1 tetrameric liposomes (970 ± 130 nM) have the best $\alpha_v\beta_6$-specific cytotoxicity based on their differential cytotoxicity compared to both the

Table 4-4. IC_{50} Values of Different Liposome Formulations on $\alpha_v\beta_6$-Negative H1299 Cells[a]

Drug Formulation	IC50 on H1299 cells (nM)
1.3% H2009.1 Tetrameric	3700 ± 130
1.3% scH2009.1 Tetrameric	3500 ± 400
1.3% Naked	Not reached[b]
Free Doxorubicin	1400 ± 58

a – Cells were incubated with liposomes for 1 hour followed by a 120 hour receovery in media.
b – Not reached at the highest treatment concentration of 10.2 μM.

scH2009.1 and naked liposomes. The IC_{50} value of the 1.3% scH2009.1 tetrameric liposomes (2000 ± 330 nM) is 2-fold lower than the value for the 1.3% H2009.1 tetrameric liposomes, and the 1.3% naked liposomes have the highest IC_{50} value of the liposomes tested (IC_{50} not reached in our assays); thus, the 1.3% liposomes inherently have low background uptake into the H2009 cells. The 1.3% H2009.1 tetrameric liposomes also demonstrate $\alpha_v\beta_6$-specific cytotoxicity, selectively killing H2009 cells, and not the H1299 cells when compared to the control scH2009.1 tetrameric liposomes (Table 4-4). The 2.0% scH2009.1 tetrameric liposomes display increased cytotoxicity compared to the other scH2009.1 liposome formulations, consistent with the doxorubicin uptake data demonstrating increased nonspecific accumulation of these liposome in cells. While the 0.64% scH2009.1 tetrameric (2400 ± 115 nM) and 1.3% scH2009.1 tetrameric liposomes (2030 ± 328 nM) have similar IC_{50} values, the 2.0% scH2009.1 tetrameric liposomes have a much lower IC_{50} value (608 ± 89.7 nM). Therefore, although the higher peptide density displayed on the 2.0% liposomes increases cell cytotoxicity, it reduces $\alpha_v\beta_6$-specificity. Thus, the 1.3% liposomes represent the best specific targeting

formulation. The efficacy and specificity of peptide-targeted liposomes ride a fine balance and the liposome with the lowest IC_{50} may not be the best for targeted therapy.

I also examined the effects of peptide valency on the cytotoxicity of the ideal 1.3% liposome platform, comparing liposomes functionalized with H2009.1 monomeric or tetrameric peptides. Consistent with the liposomal targeting data that demonstrated more than additive targeting for the tetrameric verses monomeric liposomes, the monomeric liposomes (5700 ± 120) were 6-fold less cytotoxic than the tetrameric liposomes (970 ± 130). These data further support the benefit of the layered valency of multivalent tetrameric peptides displayed in a multivalent fashion on the liposomal surface.

4.4 Discussion

Phage display is a powerful method for screening a library of peptides for specific binding to a desired cell type. Peptides with specificity for a particular cell type can be identified after 3-5 rounds of screening. However, removal of peptides from the phage context through chemical synthesis often results in ligands with significantly lower affinity, likely due to loss of multivalency. As the phage displays 3-5 copies of a given peptide, multivalent interactions are expected to contribute to phage peptide binding. Additionally, when whole cells serve as the bait for the selection, peptides that bind clustered cellular receptors are likely to dominate because of the multivalent presentation of the peptide ligand on the phage. The synthesis of only one peptide copy, therefore, fails to reconstitute this ideal structure. To address the loss in peptide affinity upon synthesis, we developed a higher affinity tetrameric peptide construct that mimics the

original peptide presentation of the phage[266] and demonstrated the utility of this construct for peptides selected against a variety of cell types.[264, 266, 267, 335, 336]

One of the primary uses of peptides selected by phage display is conjugation of the peptides to therapeutics or imaging agents for specific delivery to target cell types. The peptides can either be linked directly to the desired cargo or to a cargo-carrier such as a nanoparticle. Nanoparticles are receiving considerable attention for targeted delivery applications due to their ability to encapsulate a variety of imaging agents or therapeutics. With the goal of optimizing the path from peptides selected by phage display to presentation of these peptides on a nanoparticle surface for targeted delivery, I set out to examine the effects of peptide concentration, affinity, and valency on nanoparticle delivery and therapeutic efficacy. As a nanoparticle is considered a multivalent platform for ligand display, I was particularly interested in the effects of multivalent peptide presentation on the multivalent nanoparticle.

Here I report the first demonstration that a multivalent peptide functions better than a monomeric peptide on a nanoparticle platform, using the H2009.1 peptide as a model. The $\alpha_v\beta_6$-specific H2009.1 peptide was originally selected from a pIII phage displayed peptide library using the NSCLC cell line H2009 as bait. The H2009.1 peptide retains its binding specificity when displayed on a liposome, delivering liposomes to $\alpha_v\beta_6$-expressing cells. Significantly, liposomes displaying the higher affinity multivalent H2009.1 tetrameric peptide demonstrate higher specificity and greater toxicity towards $\alpha_v\beta_6$-expressing cells than liposomes displaying the lower affinity monomeric H2009.1 peptide. Additionally, I demonstrate that tetrameric peptide concentration plays a role in liposomal targeting. Liposomes displaying approximately 1400 tetrameric peptides per

liposome (1.3% formulation) target better than liposomes displaying approximately 700 tetrameric peptides per liposome (0.64% formulation) and have less nonspecific toxicity than liposomes displaying higher concentrations of peptide (2.0% formulation). My results suggest that the layered valency effect given by the multivalent liposomal presentation of the already multivalent H2009.1 tetrameric peptide renders more efficient cell targeting.

The enhancement in binding and targeting imparted by liposomal display of the tetrameric verses monomeric H2009.1 peptide is likely due to differences in their ability to engage in multivalent binding with $\alpha_v\beta_6$ on the surface of the cell. Even when the total number of individual peptide units are the same, the tetrameric H2009.1 liposome binds to H2009 cells 5-10 fold better than the monomeric peptide formulation. The tetrameric peptide has been optimized for optimal multivalent binding outside the context of the liposome. However, the monomeric peptide is dependent on the liposome to provide the multivalent scaffolding. For a 1.3% liposome with a diameter of 100 nm, there is approximately 1 peptide per 22 nm^2 on the liposome surface and increasing the density of peptides to 2.0% provides 1 peptide for every 13 nm^2. Accordingly, the monomeric peptides may be less likely to either achieve cooperative binding or to influence the binding of other monomeric peptides. I cannot rule out the possibility that there is some multivalent binding involved with the monomeric peptides, however, my results clearly demonstrate that tetrameric display of the peptide improves liposome binding and drug delivery.

In contrast to the monomeric peptides, the tetrameric peptide scaffold places the peptide branches in close proximity, leaving them primed for multivalent interactions

with $\alpha_v\beta_6$. However, increasing the density of multimeric peptides on the liposome also increases cell binding indicating that the liposome platform does provide a second level of multivalent binding. Thus, both the multivalent peptide and the multivalent liposome scaffold work together to increase targeting to $\alpha_v\beta_6$-expressing cells. This multi-layered approach to developing high affinity targeted nanoparticles may improve the utility of moderate affinity peptides.

It is also important to note that the curvature of the liposome limits the initial contact interface between the cell and liposome. The surface area of contact is dependent on the radius of the liposomal sphere as well as the extended length of the PEG linker. As a rough estimate, a 100 nm liposome with 1400 peptides will only display ~200 of these peptides to the cell surface upon initial interaction with the cell.[381] Thus, while liposomes displaying monomeric peptides will only present 200 peptide units to the cell, liposomes displaying tetrameric peptides will present 800 peptide units, increasing the local concentration of ligand. Clearly this is an oversimplification and cell wrapping around the nanoparticle during endocytosis will increase ligand-receptor interactions. However, the tetrameric display will present a greater number of ligands in the correct orientation for receptor binding.

There exist several different models for multivalent ligand binding that are applicable in this context.[369] In the "chelate effect," multimeric ligands bind to clustered receptors. In a second model, after one arm of a multivalent ligand binds to its receptor, other receptors are recruited to the first receptor and subsequently bind additional arms of the multivalent ligand. A third model suggests that the higher local concentration of peptide units displayed by a multimeric ligand lends higher affinity for binding to a single

receptor. Although I speculate that in my system receptor clustering leads to a chelate effect, each of these models requires a multimeric ligand with appropriate spacing and conformation. The distance between monomeric peptides on the liposome surface in conjunction with the curvature of the liposome membrane likely keeps the individual monomeric chains too far apart for simultaneous binding to clustered receptors or for achieving a high local concentration of peptide. By contrast, the tetrameric presentation of peptides keeps the local concentration of monomeric chains high while displaying each chain in an orientation suitable for binding to multiple receptors.

Creating different types of nanoparticles that display the monomeric peptides in closer contact may also recapitulate multimeric binding. However, my studies suggest that high concentrations of peptide on the liposomal surface increase nonspecific binding and this observation is likely to hold true for other nanoparticle platforms. In order to achieve the same absolute number of peptide branches as the ideal 1.3% tetrameric liposome, a 100 nm nanoparticle would have to bear 5600 monomeric peptides. This would require an increase of DSPE-PEG-Maleimide to 5.2% of the total lipid content and may destabilize the liposome. Additionally, the coupling efficiency is likely to decrease as the ratio of DSPE-PEG-maleimide increases. Finally, I have observed that an increase of the DSPE-PEG-Maleimide past 3.0% increases nonspecific binding even in the absence of peptide. Smaller sized nanoparticles could display monomeric peptides in closer proximity for multivalent interactions, but care must to taken to ensure that the nanoparticle size is large enough for any desired *in vivo* applications. Additionally, peptides displayed on smaller sized nanoparticles will suffer more from curvature effects

of the nanoparticle; even though the peptides may display in closer proximity, the curvature of the nanoparticle surface may prevent ideal multimeric interactions.

These studies were performed using whole cells instead of a target receptor immobilized on a solid surface. As receptor number, orientation, and localization could greatly affect ligand binding, it is important to study receptor-ligand interactions in their native context. Meijer et al. previously demonstrated that the binding of multivalent peptide dendrimers is affected by receptor density.[371] By using cells that express $\alpha_v\beta_6$ as my target, I maintain a more relevant receptor display and optimize the liposome system within a biological context. While the tetrameric peptide delivers nanoparticles more effectively to these physiologically relevant cells *in vitro*, it remains to be seen whether this will hold true *in vivo*. Biodistribution for tumor targeting *in vivo* depends on many aspects not present in the *in vitro* context such as nanoparticle half-life, tumor vasculature leakiness and size, and receptor levels and availability. Nevertheless, our *in vitro* studies are promising and the tetrameric H2009.1 peptide liposomes merit further *in vivo* evaluation.

Peptides selected using whole cells as the phage library target are especially likely to benefit from tetrameric nanoparticle display as the receptor is in its native, multimeric-peptide binding context; the receptor may reside in clusters or diffuse through the cell membrane to bind different arms of the multivalent phage peptide. Of particular advantage, high affinity peptide-targeted nanoparticles can be designed without knowledge of the amount of receptor, arrangement of the receptor on the cell surface, or even the identity of the receptor. Biopanning pIII phage displayed peptide libraries on whole cells does not require a priori knowledge of the receptor and the selection process

identifies peptides that bind to cell surface receptors in their native context. Assuming the peptides can transition from the phage particle to the trilysine core without loss of affinity or specificity, it is likely that the tetrameric peptide will be functional on the liposome. This alleviates the need for rational design to achieve a targeted liposome with the optimized ligand spacing. The same cannot be said for the monomeric peptide as the liposome scaffold does not recapitulate the peptide display found on the phage.

Peptide tetramerization for nanoparticle delivery is expected to apply to the majority of peptides selected by phage display. We have tested an assortment of peptides selected from different phage libraries against a variety of targets; typically a synergetic increase of >10–fold in affinity is observed upon tetramerization. Preliminary experiments in our lab with another cancer cell-targeting peptide isolated by phage display suggest that a tetrameric version of this peptide can also be used for effective liposomal delivery to cells (data not shown). Thus, the tetrameric scaffold may act as a general method for taking peptides from phage display to nanoparticle display.

4.5 Acknowledgements

I want to thank Dr. Shunzi Li for the synthesis of the monomeric peptides and tetrameric core used in this study.

CHAPTER FIVE

IN VIVO EFFICACY OF H2009.1 PEPTIDE TARGETED LIPOSOMES

5.1 Introduction

Over 85% of lung cancers are classified as NSCLC,[6] and there is a dire need for new treatments for this deadly disease. One new paradigm for cancer treatment is the development of targeting therapies that use tumor-specific ligands to selectively deliver drugs to cancer cells. Nanoparticle drugs are particularly attractive for use with tumor-specific ligands due to the encapsulation of the drug within a nanoparticle, which prevents drug activity until its release from the nanoparticle, increases blood circulation time, and benefits from passive accumulation of the nanoparticle in the tumor due to the EPR effect.

Liposomes, in particular pegylated liposomal doxorubicin (DOXIL®), are commonly used for targeting drug delivery. DOXIL® was the first nanoparticle clinically approved for cancer treatment and is currently used in the United States for the treatment of ovarian cancer,[145] multiple myeloma,[146] and Kaposi's sarcoma.[147] It is also approved for use in breast cancer patients in Europe.[148] Numerous clinical trials involving the drug are ongoing, including trials in patients with NSCLC.[149] DOXIL® is approximately 100 nm in size and contains the anthracycline chemotherapeutic doxorubicin,[141] which destroys cells by preventing DNA replication through at least two mechanisms: intercalation in and covalent binding to DNA[150] and by inhibition of topoisomerase II.[151]

Due to the success of DOXIL®, most targeting ligands conjugated to nanoparticles for targeted drug delivery have been conjugated to liposomal forms of doxorubicin. Both antibody and peptide targeting ligands have been used to increase the efficacy and decrease the toxicity of liposomal doxorubicin by actively targeting tumor and tumor vasculature cells.[154, 158-166, 382-384] Of particular interest, anti-HER2 liposomal doxorubicin formulations are being scaled up for clinical trials,[385] and anti-EGFR liposomal doxorubicin formulations were well tolerated in a phase I clinical trial.[386] Liposomal doxorubicin conjugated to a peptide derivative of the tumor vasculature targeting NGR peptide,[115] the peptide GNGRG, has been primed for potential future clinical trials by preparation using Good Manufacturing Practices (GMP).[167] NGR-liposomal doxorubicin inhibited the growth of orthotopic neuroblastoma xenografts in mice, leading to tumor eradication, while treatment with control peptide-liposomal doxorubicin did not alter tumor growth compared to control mice.[165] NGR targeted liposomes have also been shown to increase survival in orthotopic mouse lung, ovarian, and neuroblastoma xenografts.[166]

Included among the many advantages of using liposomal doxorubicin for targeting therapies is the high drug to targeting ligand ratio due to the thousands of doxorubicin molecules trapped inside each liposome. Additionally, pegylated liposomal doxorubicin enjoys long *in vivo* circulation times, extending the time targeting ligands have to deliver their cargo to the tumor. Another important factor contributing to liposomal drug efficacy is the passive accumulation of nano-sized particles in the tumor through the EPR effect.[183] Unlike the vasculature of normal tissue, tumor vasculature is irregular and disordered. Nano-sized particles can escape through this leaky vasculature

into the surrounding tumor tissue and are subsequently retained within the tumor due to the poor lymphatic drainage systems of tumors. Thus tumor accumulation of ligand-targeted liposomes depends not only on the specific targeting ligand but also on EPR-driven effects. Interestingly, studies with targeted liposomes have demonstrated two mechanisms for improved tumor drug accumulation, both of which lead to desirable therapeutic outcomes. Some peptide-targeted liposomes, in particular those targeting the tumor vasculature, including the NGR-liposomes, deliver more doxorubicin to the tumors than non-targeted liposomes,[159, 165] suggesting that the targeted liposomes are accumulating in the tumor based on both the peptide targeting abilities and the EPR effect. Other antibody-targeted liposome formulations, including anti-HER2 and anti-EGFR liposomes, accumulate in the tumor at levels similar to non-targeted liposomes. However unlike the non-targeted liposomes, these targeted liposomes internalize into tumor cells and exhibit better distribution throughout the tumor tissue.[185, 186] While the targeting ligand does not override the EPR effect driving tumor accumulation of these liposomal formulations, the altered location of the drug in the tumors increases efficacy.

As described in Chapter 2, we isolated a peptide, termed the H2009.1 peptide, from panning a phage-displayed peptide library against the NSCLC cell line H2009. The H2009.1 peptide is specific for the restrictively expressed integrin $\alpha_v\beta_6$, which is emerging as a viable target for many epithelial-derived cancers,[342-352] including NSCLC. It is expressed in 56% of NSCLC patient tumor samples and rarely expressed in normal tissue (Chapter 3). Importantly, $\alpha_v\beta_6$ is "turned on" early in the disease progression of NSCLC indicating that it may be a good biomarker for early cancer detection and treatment.

I previously demonstrated that the H2009.1 tetrameric peptide targets tumors *in vivo* (Chapter 2). Additionally, with the goal of translating peptides isolated from phage display libraries into effective therapeutic delivery agents, I examined the best platform for displaying the peptides on liposomal doxorubicin for drug delivery *in vitro* (Chapter 4). Liposomes displaying the higher affinity multivalent H2009.1 tetrameric peptide demonstrate higher specificity and greater toxicity towards $\alpha_v\beta_6$-expressing cells than liposomes displaying the lower affinity monomeric H2009.1 peptide. Additionally, the concentration of peptide displayed on the liposome plays a role in targeting. Liposomes displaying approximately 1400 tetrameric peptides per liposome, a 1.3% liposome formulation, target better than 0.64% liposomes displaying approximately 700 tetrameric peptides per liposome. While it is encouraging that these liposomes work well *in vitro*, the true goal of our studies is to develop clinically relevant therapy agents. Therefore, it is important to determine the *in vivo* efficacy of the liposomes. This chapter examines the *in vivo* therapeutic efficacy of H2009.1 peptide targeted liposomal doxorubicin, beginning with the optimal 1.3% H2009.1 tetrameric formulation and moving to test the effects of peptide density and valency on therapeutic results *in vivo*.

Despite the targeting differences between the different liposome formulations *in vitro*, all of the H2009.1 liposome platforms exhibit identical efficacy *in vivo*. Additionally, there is no efficacy difference between the H2009.1 liposomes and control no-peptide liposomes. Subsequent experiments demonstrate that this result is due to identical EPR-based liposome tumor accumulation and failure of the liposomes to penetrate the tumor tissue past areas immediately adjacent to the tumor vasculature.

5.2 Materials and Methods

5.2.1 *Materials*

All Fmoc amino acids, the NovaPEG Rink Amide resin and 2-(1*H*-benzotriazole-1-yl)-1,1,3,3-tetramethyluronium hexafluorophosphate (HBTU) were purchased from Novabiochem® (EMD Millipore, Billerica, MA). The Fmoc-β-Ala-CLEAR™ Acid Resin was purchased from Peptides International (Osaka, Japan), β-maleimidopropionic acid from Tokoyo Chemical Industry Co. Ltd. (Portland, OR) and Fmoc-NH-$(PEG)_{11}$-COOH ($C_{42}H_{65}NO_{16}$) from Polypure (Oslo, Norway). *N*-Methylmorpholine (NMM) was purchased from ACROS Organics (Geel, Belgium). Anhydrous hydroxybenzotriazole (HOBt) was purchased from SynBioSci (Livermore, CA). Piperidine, Sepharose CL-4B and Sephadex G-50 were purchased from Sigma-Aldrich Inc. (Livermore, CA). Lipids were purchased from Avanti® Polar Lipids, Inc. (Alabaster, AL) and doxorubicin HCl for injection from Bedford Laboratories™ (Bedford, OH). The Molecular Probes® dyes DiI [DiI$(C)_{18}$(3), 1,1'-dioctadecyl-3,3,3',3'-tetramethylindocarbocyanine perchlorate] and DiR [$DiOC_{18}$(7), 1,1'-dioctadecyl-3,3,3',3'-tetramethylindotricarbocyanine iodide], were purchased from Life Technologies™ (Grand Island, NY). For cell culture, fetal bovine serum (FBS) was purchased from Gemini Bio-Products (West Sacramento, CA) and both RPMI 1640 and Trypsin EDTA, 1x from Mediatech, Inc. (Fisher Scientific, Pittsburgh, PA).

5.2.2 *Cell Lines*

All human NSCLC cell lines were provided by the UT Southwestern Medical Center Hamon Center for Therapeutic Oncology Research and maintained according to published protocols.[334] The H2009, H1975, and H460 cell lines were all grown at 37°C and 5% CO_2 in RPMI 1640 supplemented with 5% FBS.

5.2.3 *Peptide Synthesis and Purification*

Monomeric peptides were synthesized on a Symphony Synthesizer (Rainin Instruments, Protein Technologies, Inc., Woburn, MA) by standard Fmoc solid-phase peptide synthesis on a Rink Amide AM resin (substitution level 0.71 mmol/g). All amino acids were Fmoc-protected, and the Fmoc was removed to allow for amino acid coupling using 20% Piperidine in DMF. The amino acids were subsequently coupled at a 5-fold excess using HBTU, HOBt, and NMM coupling for 45 minutes. The PEG group added to each amino acid was purchased as Fmoc-NH-$(PEG)_{11}$-COOH and was coupled in the same manner as the amino acids, except that it was coupled at a 2.5-fold excess. For preparation of N-terminal acetylated peptide, after coupling of the N-terminal amino acid, a solution of 90% DMF, 5% 0.4 M NMM, and 5% acetic anhydride was added to the reaction vessel and mixed for 40 minutes. The synthesized peptides were removed from the resin by shaking in a mixture of 94%:2.5%:1.0%:2.5%: of triofluoroacetic acid (TFA):triisopropylsilane:H_2O:ethanediothiol (EDT) for 2-4 hours. The majority of the TFA solution was then removed under N_2 pressure before precipitation in diethyl ether at -80°C for a minimum of 2 hours. Precipitated peptide was dried under vacuum for a minimum of 12 hours.

The tetrameric cores were also synthesized on the Symphony Synthesizer using the Fmoc-β-Ala-CLEAR™ Acid Resin (substitution level 0.40 mmol/g) under the same coupling conditions as the monomeric peptides. Fmoc-Cys(Acm)-OH was first coupled to the resin followed by Fmoc-Lys(Fmoc)-OH, $[\text{Fmoc-Lys(Fmoc)-OH}]_2$, and finally $(\beta\text{-maleimidopropionic acid})_4$. The cores were removed from the resin in the same manner as the monomeric peptides.

The crude monomeric peptides and tetrameric cores were purified by reverse phase high-performance liquid chromatography (HPLC) using a SPIRIT™ Spirit Peptide C18 5 μm, 25 x 2.12 (AAPPTec®, Louisville, KY) on a Breeze™ HPLC (Waters Corporation, Milford, MA). H_2O/0.1% TFA (eluent A) and acetonitrile/0.1% TFA (eluent B) were used for purification as follows: 0-1 minute, 90% A, 10% B at 10mL/minute; from 1-100 minutes, eluent B was increased from 10% to 60% at a flow rate of 10 mL/minute. The peptides were detected by ultraviolet (UV) absorbance at 220nm. Matrix-assisted laser desorption/ionization time of flight mass spectrometry was used to confirm peptide mass (Voyager-DE™ PRO, Applied Biosystems, Inc., Foster City, CA). The mass of the monomeric peptides (average mass calculated/MH+: 1843.02/1844.18) and tetrameric core (average mass calculated/MNa+: 1251.49/1274.27) were determined in reflective mode using α-cyano-4-hydroxycinnamic acid as a matrix.

The tetrameric peptides were synthesized by coupling purified monomeric peptide to purified, deprotected tetrameric core (8:1 monomeric peptide to tetrameric core) for 2 hours at room temperature in phosphate buffered saline, pH 7.4, containing 10 mM EDTA. Afterwards, excess monomeric peptide was removed by reverse phase HPLC

using the same elution method that was used for purification of the monomeric peptides and tetrameric core. The mass of the tetrameric peptides (average mass calculated/MH+: 8629.01/8626.77) were also determined using matrix-assisted laser desorption/ionization time of flight mass spectrometry using linear mode and sinapinic acid as a matrix.

Before the tetrameric peptides could react with the maleimide-activated lipid on the liposome surface, the unique cysteine placed before the branch point of the tetramers had to be deprotected to remove the acetamidomethyl (Acm) group protecting the thiol of the cysteine. The tetrameric peptides were deprotected by reaction of the peptide (0.35 μmol) with AgOAc (0.168 M AgOAc in 99:1 TFA:anisole to a total volume of 350 μL) for 2 hours at 4°C. The majority of the TFA solution was then removed under a slow stream of nitrogen and the peptide precipitated in diethyl ether at -80°C for a minimum of 30 minutes. After removing the ether from the precipitated peptide, the peptide was reacted with 150 μL of a 0.2 M dithiothreitol (DTT) solution (DTT dissolved in 1 M acetic acid) for a minimum of 5 hours shaking. The resulting solution was centrifuged and the supernatant taken for HPLC purification of the deprotected peptide. Additional tetrameric peptide was recovered from the pellet by shaking in 8 M guanidine HCl for an additional 5 hours. The supernatant resulting from centrifugation of this mixture was also taken for HPLC purification. The deprotected tetramers were purified using the same HPLC conditions as used for the other peptides and the deprotection was verified by mass spectrometry, using the same method used for the protected tetramers (average mass calculated/MH+: 8557.94/8558.38).

5.2.4 *Preparation of Liposomal Doxorubicin*

Liposomes were prepared from solutions of the lipids hydrogenated soy L-α-phophatidylcholine (HSPC), cholesterol, 1,2-distearoyl-*sn*-glycero-3-phosphoethanolamine-N-[carbonyl-methoxy(polyethylene glycol)-2000] (DSPE-PEG_{20000}), and 1,2-distearoyl-*sn*-glycero-3-phosphoethanolamine-N-[maleimide(polyethylene glycol)-2000] (DSPE-PEG_{2000}-maelimide) in 2:1 chloroform:methanol. The 0.64% liposomes were prepared from mixtures of 100 mg (131 μmol) of HSPC, 25.4 mg (65.6 μmol) of cholesterol, 14.7 mg (5.20 μmol) of DSPE-PEG_{20000} and 3.85 mg (1.31 μmol) of DSPE-PEG_{2000}-maelimide. The 1.3% liposomes were prepared from mixtures of 100 mg (131 μmol) of HSPC, 25.4 mg (65.6 μmol) of cholesterol, 10.9 mg (3.87 μmol) of DSPE-PEG_{20000} and 7.92 mg (2.69 μmol) of DSPE-PEG_{2000}-maelimide. Solvent was removed under a slow stream of nitrogen at 45ºC, and the lipid film was left under vacuum overnight. The dried lipid film was hydrated with 155 mM $(NH_4)_2SO_4$ buffer, pH 5.5, by intermittently heating at 65ºC and vortexing. Liposomes were subsequently extruded 20 times through double-stacked 100nm membranes, and PD-10 desalting columns (GE Healthcare, Waukesha, WI**)** were used to change the outer liposomal buffer to 123 mM NaCitrate, pH 5.5. At this point a small portion of the liposomes were set aside to remain doxorubicin-free. As doxorubicin interferes with the assay used to determine the amount of peptide coupling to the liposome surface (described in Section 5.2.6), a small subset of liposomes were saved for characterization of peptide coupling to the entire batch of liposomes. These liposomes were desalted into HEPES buffered saline using a PD-10 desalting column. Doxorubicin

was loaded remotely (post-liposome formation) into the remainder of the liposomes by incubation of liposomes and doxorubicin at 65ºC for 1 hour. Free doxorubicin was removed using a Sephadex G-50 column equilibrated with HEPES buffered saline. Peptides were conjugated to liposomes by reaction for 24 hours at a ratio of 2:1 peptide: DSPE-PEG_{2000}-maelimide in a solution of HEPES buffered saline, and excess peptide was removed using Sepharose CL-4B columns. Each peptide conjugated to the liposomes was coupled to two forms of the liposomes: liposomes without doxorubicin and doxorubicin-loaded liposomes. The liposomes without doxorubicin were used to determine peptide coupling to the liposomes and the doxorubicin-loaded liposomes were used for all other experiments.

5.2.5 *Preparation of DiI or DiR-Labeled Liposomes*

DiI or DiR dye labeled liposomes were prepared exactly as the doxorubicin-loaded liposomes except that they were not loaded with doxorubicin but instead were labeled with the lipophilic dye of interest. The 1.3% liposome formulation was prepared exactly as described in Section 5.2.4 with the addition of the DiI or DiR dye into the mixture of lipids in 2:1 chloroform:methanol. The DiI or DiR dyes were dissolved in ethanol at a concentration of 2.5 mg/mL and were added to lipid mixture at a ratio of 3.75 μg dye/0.5 mg lipid. Solvent was removed under a slow stream of nitrogen at 45ºC, and the lipid film was left under vacuum overnight. The dried lipid film was hydrated with 155 mM $(NH_4)_2SO_4$ buffer, pH 5.5, by intermittently heating at 65ºC and vortexing. Liposomes were subsequently extruded 20 times through double-stacked 100 nm membranes, and PD-10 desalting columns (GE Healthcare, Waukesha, WI) were used to

change the outer liposomal buffer to HEPES buffered saline. Peptides were conjugated to liposomes by reaction for 24 hours at a ratio of 2:1 peptide: DSPE-PEG_{2000}-maelimide in a solution of HEPES buffered saline and excess peptide was removed using Sepharose CL-4B columns.

5.2.6 *Liposome Characterization*

Liposome size was determined using a Malvern Zetasizer (Worcestershire, UK), and phospholipid content was determined using the Modified Bartlett Procedure.[378] Doxorubicin concentration was determined by absorbance at 480 nm after the addition of 1% Triton X-100 and heating at 95ºC as detailed elsewhere.[379] The amounts of peptide conjugated to the liposomes were determined using the CBQCA Protein Quantitation Kit (Life Technologies™, Grand Island, NY) according to the manufacturer's instructions, with standard curves generated by peptides containing tyrosine residues. Peptide number/liposome was calculated by assuming 80,000 phospholipid molecules/liposome for a liposome size of 100 nm.[380]

5.2.7 *Establishment of Mouse Tumor Models*

Animal protocols were approved by the Institutional Animal Care and Use Committee at UT Southwestern Medical Center. Female NOD/SCID mice (from the UT Southwestern Medical Center Mouse Breeding Core Facility) were injected with 1 million H2009, H1975, or H460 cells in the right flank. All cells were injected in phosphate buffered saline, pH 7.4, and were prepared for injection by incubating the cells with 0.05% Trypsin-EDTA (Gibco®, Life Technologies™, Grand Island, NY) for 10

minutes, quenching the trypsin with media, and washing the cells with phosphate buffered saline before final suspension in the phosphate buffered saline at a concentration of 10 million cells per mL.

5.2.8 In Vivo *Therapeutic Experiments*

Subcutaneous H2009 tumors were established in the flank of NOD/SCID mice. Once palpable tumors had formed, 18 days after tumor cell implantation, the mice were treated with HBS (control) or different liposome formulations, based on the total concentration of doxorubicin. The different liposome formulations and treatment doses are described in detail in Section 5.3. For all experiments, mice were treated once weekly for 3 weeks, on days 18, 25, and 32, via tail vein injection. Tumors were measured by an independent scientist, and tumor volumes were calculated from the formula $V = (l \times w^2)/2$.

5.2.9 *Statistical Methods*

The statistical significance of tumor size differences between drug treated groups and the control group were calculated using one way ANOVA with Dunnett's multiple comparison test and between different drug treated groups, using one way ANOVA with Tukey's multiple comparison test. The statistical significance of differences between survival curves were calculated from Kaplan-Meier curves with log-rank tests. All calculations were determined using GraphPad Prism.

5.2.10 In Vivo *and* Ex Vivo *Near Infrared Imaging*

Mice bearing subcutaneous H2009, H1975, or H460 tumors in the right flank were injected via tail vein with DiR-labeled liposomes at a concentration of 22.22 μmol phospholipid/kg. This phospholipid/kg concentration correlates to the same amount of phospholipid (and therefore the same number of liposomes) as present in a treatment of 4 mg/kg liposomal doxorubicin. H2009 and H460 tumor-bearing mice were injected with DiR-labeled versions of the 1.3% H2009.1 tetrameric, AcH2009.1 tetrameric, scH2009.1 tetrameric, or naked liposomes with 3 mice per liposome group. Mice bearing H1975 tumors were injected with DiR-labeled versions of the 1.3% H2009.1 tetrameric, scH2009.1 tetrameric, or naked liposomes with 3 mice per liposome group. For each mouse, Nair® was used to remove all hair from the lower half of the body. At 24, 48, and 72 hours post-liposome injection, the mice were imaged for DiR dye fluorescence using an IVIS® Lumina (Caliper Life Sciences, Hopkinton, MA). After whole mouse imaging at 72 hours, all mice were sacrificed and organs removed for *ex vivo* fluorescent imaging.

5.2.11 *Microscopy of DiI Liposomes in Tumor Sections*

Mice bearing subcutaneous H2009, H1975, or H460 tumors were injected via tail vein with DiI-labeled liposomes at a concentration of 22.22 μmol phospholipid/kg. For each tumor type, mice were injected with DiI-labeled versions of the 1.3% H2009.1 tetrameric, scH2009.1 tetrameric, or naked liposomes, with 3 mice per liposome group. One mouse from each treatment group was sacrificed at 24 hours, a second mouse at 48 hours, and the third mouse at 72 hours. Upon sacrifice, the tumors were removed and

snap frozen inside cryomolds using Tissue-Tek® O.C.T. Compound mounting medium (Fisher Scientific, Pittsburgh, PA).

For microscopy, the tumors were sectioned at 10 μm using a Leica CM3050S cryostat (Leica Microsystems Inc., Buffalo Grove, IL). Sections were obtained from the top, middle, and bottom of each tumor. All slides were prepared for microscopy and stained for vasculature using the following protocol: 1 – warm to room temperature for 30 minutes, 2 – acetone fix for 10 minutes, 3 – wash 3 times in phosphate buffered saline (PBS) for 5 minutes per wash, 4 – block for 1 hour in PBS blocking solution (PBS with 1% goat serum and 1% bovine serum albumin), 5 – incubate overnight at 4°C with primary antibody in PBS blocking solution, 6 - wash 3 times in PBS for 5 minutes per wash, 7 – incubate with secondary antibody in PBS blocking solution for 1 hour at room temperature, 8 - wash 3 times in PBS for 5 minutes per wash, and 9 – mount with Dapi Fluoromount-G (SouthernBiotech, Birmingham, AL). For the vasculature stain, a CD31 primary antibody (Rat AntiMouse CD31, catalog # 550274, BD Biosciences, San Jose, CA) was diluted 1:50 in PBS blocking solution and a fluorescein goat anti-rat secondary antibody (catalog # A10528, Life Technologies™, Grand Island, NY) was diluted 1:100 in PBS blocking solution. Slides were imaged on a Leica CTR5500 microscope (Leica Microsystems Inc., Buffalo Grove, IL) and a DeltaVision *pDV* deconvolution microscope (Applied Precision, Inc., Issaquah, WA).

5.2.12 *β_6 Staining of Tumor Sections*

Tumor sections prepared from the tumors containing DiI-liposomes (Section 5.2.9) were stained for β_6 expression using the same staining protocol as the CD31 vasculature stain but substituting a β_6 primary antibody (catalog # MAB2076Z, EMD Millipore, Billerica, MA) for the CD31 antibody. The β_6 antibody was also diluted 1:50 in PBS blocking solution. Slides were imaged on a Leica CTR5500 microscope (Leica Microsystems Inc., Buffalo Grove, IL) and a DeltaVision *pDV* deconvolution microscope (Applied Precision, Inc., Issaquah, WA).

5.3 Results

5.3.1 In vivo *Efficacy of H2009.1 Tetrameric Peptide Liposomes Targeting $\alpha_v\beta_6$*

In order to examine whether the $\alpha_v\beta_6$-specific H2009.1 peptide can be used to increase the *in vivo* delivery and efficacy of liposomal doxorubicin towards $\alpha_v\beta_6$-expressing NSCLC tumors, I began by treating tumor-bearing mice with the 1.3% H2009.1 tetrameric peptide liposome formulation that gave the best *in vivo* efficacy with limited non-specific toxicity. $\alpha_v\beta_6$-expressing H2009 cells were injected into NOD/SCID mice to form subcutaneous H2009 xenografts. At day 18, once the mice had formed palpable tumors, they were treated with HEPES buffered saline (HBS) as a control; free, non-liposome encapsulated, doxorubicin; $\alpha_v\beta_6$-targeted 1.3% H2009.1 tetrameric liposomal doxorubicin; or control liposomal doxorubicin formulations. Two different liposome formulations were used as non-targeted controls: 1.3% “naked”, no peptide, liposomes and 1.3% scH2009.1 tetrameric liposomes. The 1.3% naked liposomes serve

as a normal, non-peptide targeted liposome control, which should only accumulate passively in tumors based on the EPR effect. The 1.3% scH2009.1 tetrameric liposomes display a sequence scrambled version of the H2009.1 peptide that does not target $\alpha_v\beta_6$; therefore, these liposomes serve as a control for the specificity of the H2009.1 peptide for $\alpha_v\beta_6$ verses a scrambled peptide with the same amino acids. The mice were treated via tail vein intravenous injections once weekly for 3 weeks with 4 mg/kg of each liposome formulation, based on total doxorubicin concentration, on days 18, 25, and 32 after tumor cell implantation.

As depicted in Figure 5-1a, all of the liposome formulations significantly inhibited tumor growth compared to the control HBS treated group, with p values less than 0.001. However, no difference was observed between any of the liposome formulations. The targeted 1.3% H2009.1 tetrameric liposomes did not inhibit tumor growth differently than either the control scH2009.1 tetrameric or naked liposomes. The liposome treated curves look virtually identical up to day 64, at which point the scH2009.1 tetrameric curve separates out slightly but is still within the margin of error of the H2009.1 tetrameric and naked liposome groups. Importantly, this effect is repeatable; the data in Figure 5-1 represent the combination of multiple separately conducted experiments: 4 experiments for the control group, 2 experiments for both the 1.3% H2009.1 tetrameric and naked liposomes, and 1 experiment for the scH2009.1 tetrameric liposomes.

Free, non-liposome encapsulated, doxorubicin proved toxic to the mice at this 4 mg/kg dosing regimen. The free doxorubicin treated mice all died on day 32, before

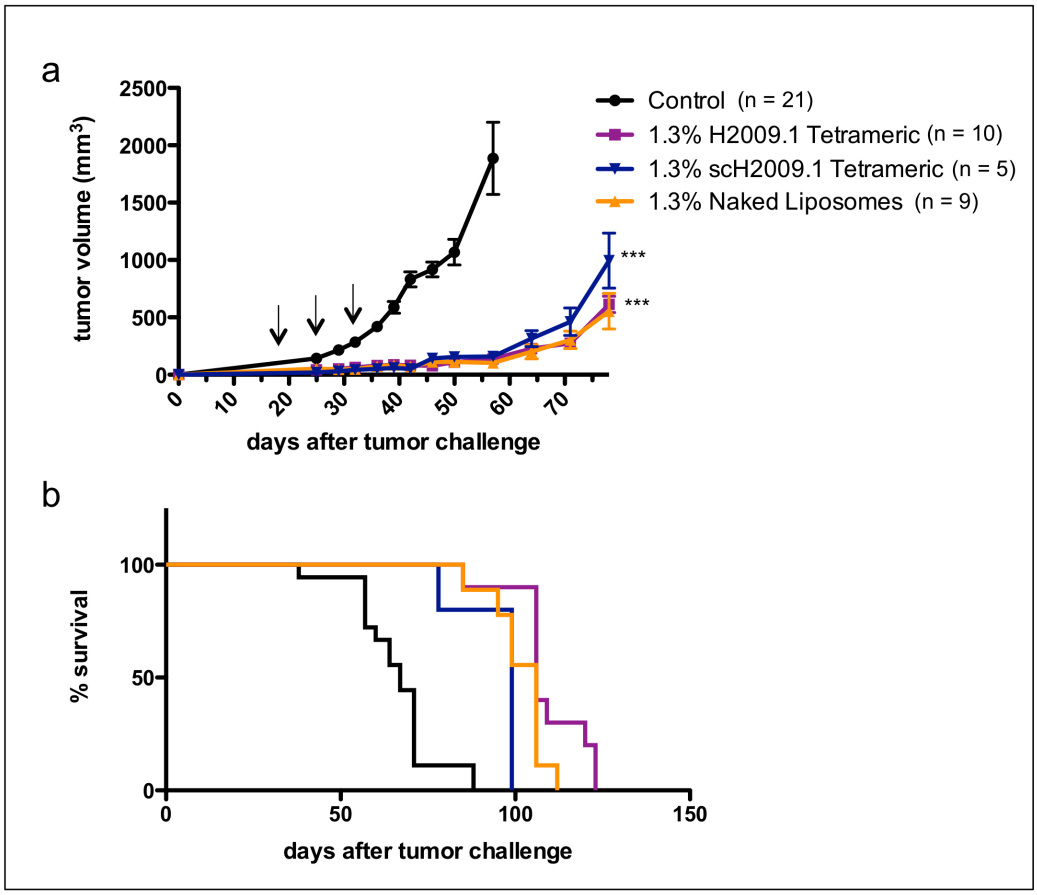

Figure 5-1. The 1.3% H2009.1 tetrameric, scH2009.1 tetrameric and naked liposomes display similar efficacy towards H2009 subcutaneous tumors at treatment doses of 4 mg/kg. Subcutaneous H2009 tumors were established in the flank of NOD/SCID mice. Once palpable tumors had formed, 18 days after tumor cell implantation, the mice were treated with HBS (control) or 4mg/kg of free doxorubicin, 1.3% H2009.1 tetrameric liposomes, 1.3% scH2009.1 tetrameric liposomes, or 1.3% naked liposomes, based on the total concentration of doxorubicin. Mice were treated once weekly for 3 weeks, on days 18, 25, and 32, as indicated by the arrows in (a). Tumors were measured by an independent scientist, and tumor volumes were calculated from the formula $V = (l \times w^2)/2$. (a) Tumor growth curves. (b) Kaplan-Meier survival curves. *** $p < 0.001$ verses control.

receiving the third and final dose of drug. Therefore, two injections of 4 mg/kg doxorubicin, for a total of 8 mg/kg doxorubicin, are sufficient for drug-induced toxicity. All of the other mice lived until they were sacrificed due to their tumors reaching a length of 2 cm (Figure 5-1b). As expected from the tumor growth curves, there was a significant survival difference between the control group and all of the liposome treatment groups ($p < 0.0001$ for the 1.3% H2009.1 tetrameric and naked liposomes and $p = 0.0007$ for the 1.3% scH2009.1 tetrameric liposomes). While three of the 1.3% H2009.1 tetrameric liposome treated mice lived longer than any of the 1.3% naked liposome treated mice, these differences were not statistically significant. However, there was a significant survival difference between mice treated with the 1.3% H2009.1 tetrameric and scH2009.1 tetrameric liposomes ($p = 0.0068$). Thus, although treatment with 1.3% H2009.1 tetrameric liposomes did not improve therapeutic efficacy at a 4 mg/kg dosing regimen compared to the non-targeted naked liposomes, these $\alpha_v\beta_6$-targeted liposomes increased survival compared to the control peptide scH2009.1 tetrameric liposomes.

As there was no increased benefit for 1.3% liposomes displaying the H2009.1 tetrameric peptide verses control naked liposomes, we reasoned that the $\alpha_v\beta_6$-specific targeting of the H2009.1 peptide liposomes might be masked by the efficacy of the naked liposomes at treatment concentrations of 4 mg/kg (12 mg/kg total). Therefore, we decreased the treatment concentrations by 2-fold to determine whether the 1.3% H2009.1 tetrameric liposomes could target and treat better than the naked liposomes at a lower concentration. As before, H2009 xenografts were established and treatment begun at day 18 with either HBS, free doxorubicin, 1.3% H2009.1 tetrameric liposomal doxorubicin,

1.3% scH2009.1 tetrameric liposomal doxorubicin, or 1.3% naked liposomal doxorubicin. This time, however, the mice were treated with 2 mg/kg instead of 4 mg/kg of drug at days 18, 25, and 32. Unfortunately, treatment at these lower drug concentrations did not increase the efficacy of the H2009.1 tetrameric liposomes compared to naked, non-targeted, liposomes. Once again, there was no tumor growth difference between the 1.3% H2009.1 tetrameric, scH2009.1 tetrameric, and naked liposomes (Figure 5-2a). All of the liposome formulations and free doxorubicin inhibited tumor growth compared to the control HBS-treated mice ($p < 0.05$ and $p < 0.01$, respectively), and all 3 liposome formulations inhibited tumor growth compared to free doxorubicin ($p < 0.001$), but the 3 liposome formulations themselves were indistinguishable. Similarly, while the H2009.1 targeted liposomes increased survival compared to control mice ($p = 0.0025$), there was no survival difference between mice treated with either free doxorubicin or the 3 liposome formulations (Figure 5-2b). Directly comparing the tumor sizes of mice treated with 2 mg/kg verses 4 mg/kg of 1.3% H2009.1 tetrameric liposomal doxorubicin (Figure 5-2c), demonstrated that the higher dose 4 mg/kg treatments were significantly more effective at inhibiting tumor growth than the lower dose 2 mg/kg treatments ($p < 0.001$) and also increased survival (Figure 5-2d, $p = 0.0005$). Studies with an even higher 6 mg/kg dosing regimen proved toxic to mice (data not shown). Therefore, although the 1.3% H2009.1 tetrameric liposomes inhibit H2009 tumor growth to the same extent as the non-targeted naked liposomes at both low and high drug treatment concentrations, the higher drug treatments lead to a better therapeutic outcome.

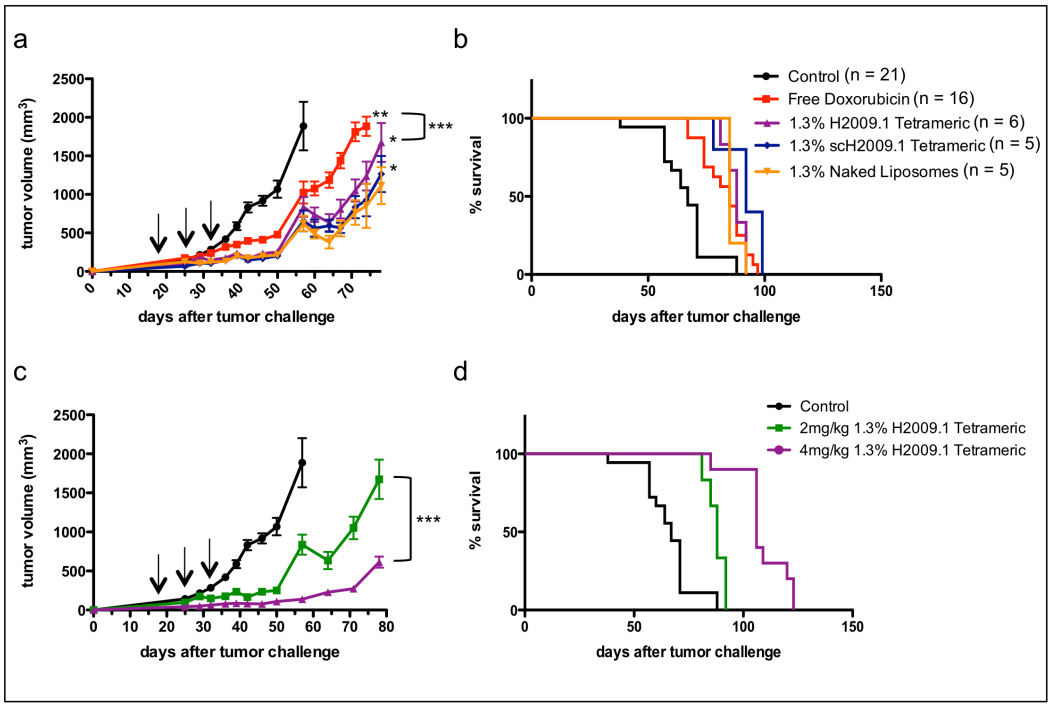

Figure 5-2. The 1.3% H2009.1 tetrameric, scH2009.1 tetrameric and naked liposomes display similar efficacy towards H2009 subcutaneous tumors at treatment doses of 2 mg/kg. Subcutaneous H2009 tumors were established in the flank of NOD/SCID mice. Tumor-bearing mice were treated with HBS (control) or 2 mg/kg of free doxorubicin, 1.3% H2009.1 tetrameric liposomes, 1.3% scH2009.1 tetrameric liposomes, or 1.3% naked liposomes, based on the total concentration of doxorubicin. Mice were treated once weekly for 3 weeks, on days 18, 25, and 32, as indicated by the arrows in (a & c). Tumors were measured by an independent scientist, and tumor volumes were calculated from the formula $V = (l \times w^2)/2$. (a & c) Tumor growth curves. (b & d) Kaplan-Meier survival curves. * $p < 0.05$ verses control, ** $p < 0.01$ verses control, *** $p < 0.001$ between bracketed groups.

5.3.2 *Effects of Peptide Concentration and Valency on* In vivo *Efficacy of H2009.1 Peptide Liposomes*

As demonstrated in Chapter 4, the concentration of tetrameric peptide displayed on the liposome surface contributes to the targeting specificity and toxicity of the liposomes. The 1.3% liposomes, which display approximately 1400 tetrameric peptides per liposome, led to better cell uptake and cell toxicity *in vitro* than 0.64% liposomes displaying only 700 peptides per liposome. However, it is unclear whether these same targeting differences hold true *in vivo*. Drug delivery *in vitro* is a relatively simple system involving only the cells, targeted liposomes, and growth media. Conversely, *in vivo* delivery involves the complex biological milieu and depends upon the half-life of the liposomes, the tumor vasculature leakiness and size, and the levels and availability of the $\alpha_v\beta_6$ receptors. As the expression levels and availability of $\alpha_v\beta_6$ may differ between cells *in vitro* and tumors *in vivo*, liposomes displaying lower concentrations of the H2009.1 tetrameric peptide may target better than liposomes displaying higher concentrations of the peptide *in vivo*. Therefore, I treated mice bearing subcutaneous H2009 tumors with the lower peptide concentration displaying 0.64% H2009.1 tetrameric liposomes and compared the efficacy of this formulation to the higher peptide concentration 1.3% H2009.1 tetrameric liposomes. These experiments were performed as before, treating once weekly for 3 weeks starting at day 18 using the 4 mg/kg dose that led to better efficacy. Unlike the *in vitro* experiments, which resulted in a 3-4 fold targeting increase

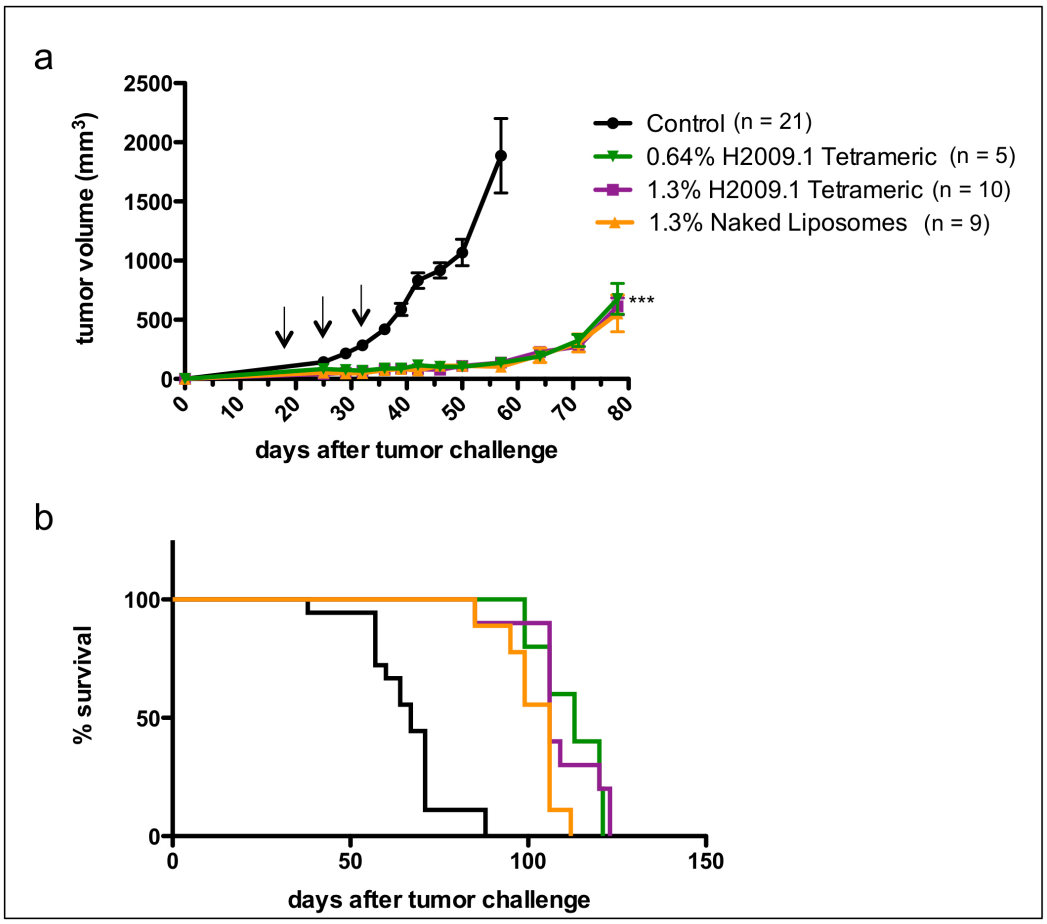

Figure 5-3. Liposomal peptide concentration does not alter *in vivo* efficacy. The 0.64% and 1.3% H2009.1 tetrameric liposomes display similar efficacy towards H2009 subcutaneous tumors. Subcutaneous H2009 tumors were established in the flank of NOD/SCID mice. Tumor-bearing mice were treated with HBS (control) or 4 mg/kg of 0.64% H2009.1 tetrameric liposomes, 1.3% H2009.1 tetrameric liposomes, or 1.3% naked liposomes. Mice were treated once weekly for 3 weeks, on days 18, 25, and 32, as indicated by the arrows in (a). Tumors were measured by an independent scientist, and tumor volumes were calculated from the formula $V = (l \times w^2)/2$. (a) Tumor growth curves. (b) Kaplan-Meier survival curves. *** $p < 0.001$ verses control.

and a 1.5-fold toxicity increase for the 1.3% H2009.1 tetrameric liposomes verses the 0.64% H2009.1 tetrameric liposomes, there was no efficacy difference between the two formulations against H2009 xenografts (Figure 5-3). Both the tumor growth curves and survival curves were similar for the liposomes displaying different amounts of peptide. Thus, while peptide concentration alters liposomal targeting *in vitro*, this does not hold true *in vivo*.

Peptide valency also altered liposomal targeting *in vitro*. As described in Chapter 4, liposomes displaying the higher affinity tetrameric H2009.1 peptide were 6-fold more toxic towards $\alpha_v\beta_6$-positive H2009 cells *in vitro* than liposomes displaying the lower affinity monomeric H2009.1 peptide. However, based on the failure of the H2009.1 tetrameric peptide liposomes to alter tumor size or survival compared to the non-peptide naked liposomes *in vivo*, we reasoned that a high affinity ligand might inhibit nanoparticle targeting *in vivo*. The high affinity tetrameric peptide might not penetrate the tumor as well as a lower affinity ligand due to its stronger affinity for $\alpha_v\beta_6$. This could result in the tetrameric peptide liposomes accumulating only in $\alpha_v\beta_6$-expressing tumor cells near the blood vessels through which they entered the tumor, without any penetration into other areas of the tumor. Alternatively, the lower affinity monomeric peptide liposomes might display better tumor distribution and better therapeutic effects by bypassing some of the $\alpha_v\beta_6$-expressing tumor cells near the blood vessels to enter $\alpha_v\beta_6$-expressing cells further into the tumor. To test this hypothesis, I treated H2009 xenograft-bearing mice with 1.3% H2009.1 monomeric liposomal doxorubicin and compared the efficacy of this formulation to that of the 1.3% H2009.1 tetrameric

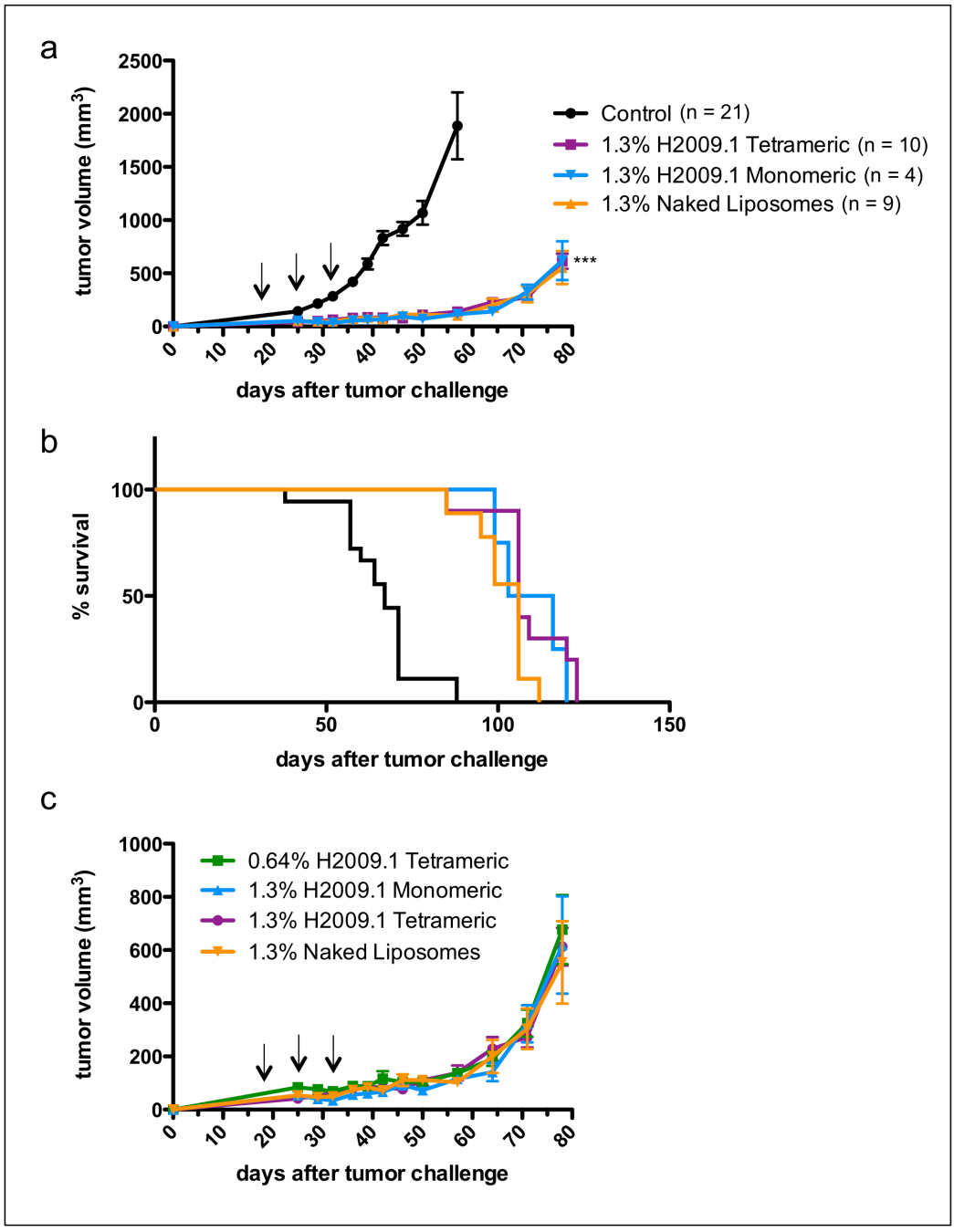

Figure 5-4. The valency of peptides displayed on liposomal doxorubicin does not alter *in vivo* efficacy. The 1.3% H2009.1 monomeric and tetrameric liposomes display similar efficacy towards H2009 subcutaneous tumors. Subcutaneous H2009 tumors were

established in the flank of NOD/SCID mice. Tumor-bearing mice were treated with HBS (control) or 4 mg/kg of 1.3% H2009.1 monomeric, H2009.1 tetrameric, or naked liposomes. Mice were treated once weekly for 3 weeks, on days 18, 25, and 32, as indicated by the arrows in (a). Tumors were measured by an independent scientist and tumor volumes were calculated from the formula $V = (l \times w^2)/2$. (a) Tumor growth curves. (b) Kaplan-Meier survival curves. *** $p < 0.001$ verses control.

liposomal doxorubicin. As demonstrated in Figure 5-4a-b, the valency of the H2009.1 peptide did not affect either the tumor size or the survival of the treated mice. The 1.3% H2009.1 monomeric liposomes inhibited tumor growth to the same extent as both the 1.3% H2009.1 tetrameric liposomes and the control 1.3% naked liposomes. Figure 5-4c shows the 0.64% H2009.1 tetrameric, 1.3% H2009.1 monomeric, 1.3% H2009.1 tetrameric, and 1.3% naked liposomes all graphed on the same axis. Unlike the *in vitro* studies, which revealed better targeting for all of the peptide liposomes compared to the naked liposomes, with the 1.3% H2009.1 tetrameric liposomes displaying the best efficacy, there was no therapeutic difference between any of the liposome formulations *in vivo*.

5.3.3 *Biodistribution and Tumor Accumulation of Different Liposome Formulations*

Based on the failure of the $\alpha_v\beta_6$-specific H2009.1 tetrameric liposomes to treat $\alpha_v\beta_6$-positive tumors more effectively *in vivo* than naked, no peptide, liposomes, I examined the biodistribution of the different liposome formulations and the total levels of liposome accumulation in the tumors. It is important to distinguish whether the H2009.1 tetrameric peptide drives higher liposome accumulation in the tumors for the peptide bearing liposomes or whether the liposome nanoparticle itself drives all tumor accumulation based on the EPR effect. If the EPR effect is driving liposome accumulation in tumors, we expect to see the same level of tumor accumulation for the H2009.1-peptide targeted liposomes as the naked liposomes. To visualize and quantify liposome biodistribution and tumor uptake, the liposomes were prepared as before except that they were not loaded with doxorubicin but instead were labeled with the lipophilic

near infrared dye DiR, which incorporates into the lipid membrane. As before, 1.3% liposomes bearing the H2009.1 tetrameric, scH2009.1 tetrameric, or no peptide were prepared. Additionally, liposomes were conjugated to an amino-terminus acetylated version of the H2009.1 tetrameric peptide, labeled as AcH2009.1 tetrameric. Although AcH2009.1 tetrameric liposomes were not tested in the tumor growth studies, I wanted to investigate whether an acetylated version of the H2009.1 tetrameric peptide could increase tumor uptake *in vivo*. As demonstrated in Chapter 2 for the H1299.2 and HCC15.2 peptides, acetylation of the amino-terminus of some peptides can increase *in vivo* tumor accumulation and specificity of peptides, most likely by inhibiting N-terminal peptide degradation by peptidases and proteases. Additionally, N-terminal acetylation may be of particular benefit for peptides attached to a long-circulating nanoparticle due to differences in half-life between the peptide and the nanoparticle. The half-life of liposomal doxorubicin is > 18 hours in mice and > 50 hours in humans,[141] while the half-life of the H2009.1 tetrameric peptide in human serum is 14 hours. Thus, the H2009.1 peptide may begin to degrade while still conjugated to a circulating liposome, reducing the ability of the peptide to specifically target liposomes at later time points. N-terminal acetylation could prevent this problem by increasing peptide half-life.

In order to fully examine H2009.1 peptide-driven liposome targeting to $\alpha_v\beta_6$, two different tumor models were examined for liposome accumulation: $\alpha_v\beta_6$-positive H2009 tumors and $\alpha_v\beta_6$-negative H460 tumors. Xenograft tumors were established in the right flank of NOD/SCID mice, and tumor bearing mice were injected via tail vein with the different DiR-labeled liposome formulations for imaging via whole mouse fluorescent

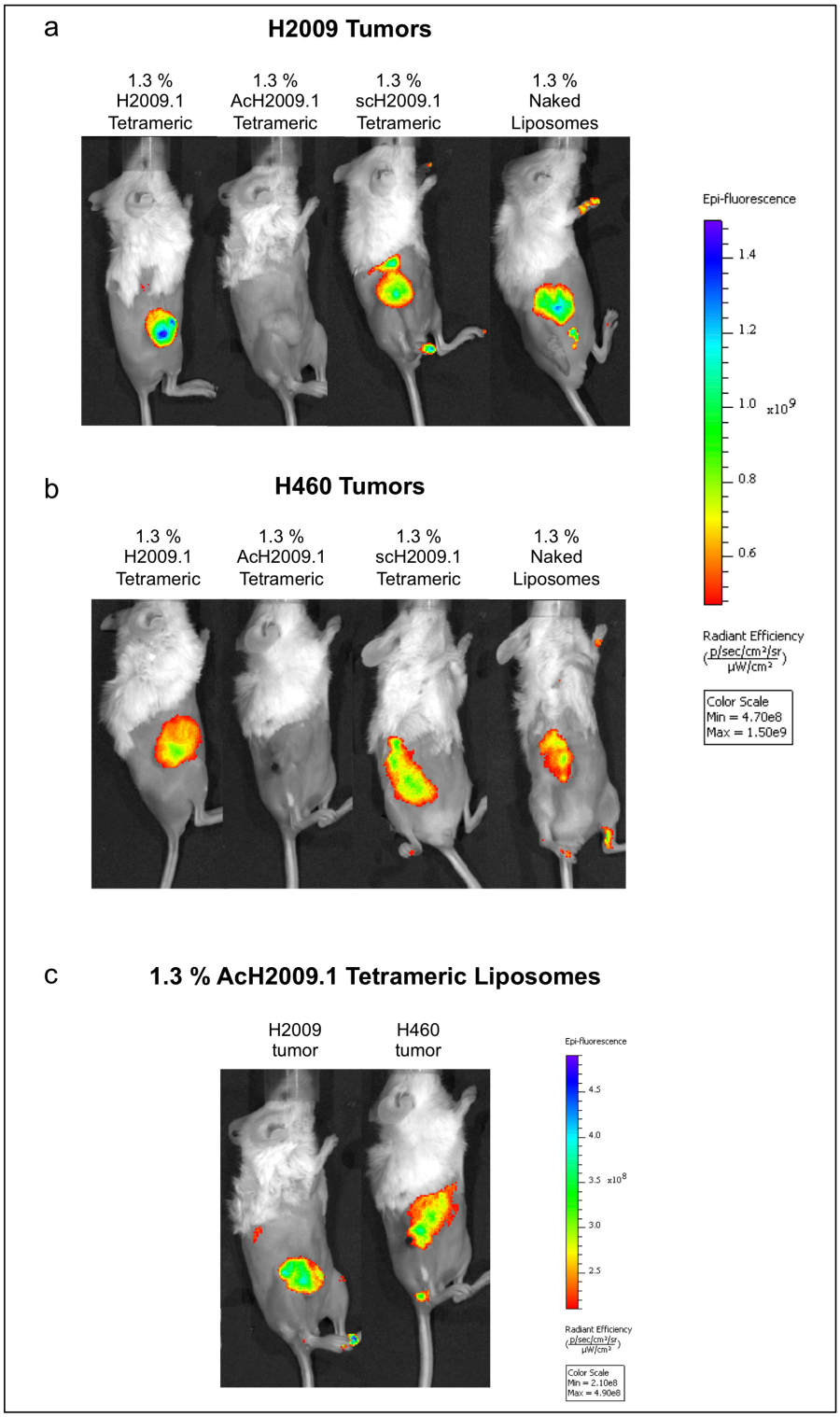
a
H2009 Tumors
1.3 % H2009.1 Tetrameric
1.3 % AcH2009.1 Tetrameric
1.3 % scH2009.1 Tetrameric
1.3 % Naked Liposomes
Epi-fluorescence
1.4
1.2
1.0 x10^9
0.8
0.6
Radiant Efficiency
(p/sec/cm²/sr / µW/cm²)
Color Scale
Min = 4.70e8
Max = 1.50e9
b
H460 Tumors
1.3 % H2009.1 Tetrameric
1.3 % AcH2009.1 Tetrameric
1.3 % scH2009.1 Tetrameric
1.3 % Naked Liposomes
c
1.3 % AcH2009.1 Tetrameric Liposomes
H2009 tumor
H460 tumor
Epi-fluorescence
4.5
4.0
3.5 x10^8
3.0
2.5
Radiant Efficiency
(p/sec/cm²/sr / µW/cm²)
Color Scale
Min = 2.10e8
Max = 4.90e8

Figure 5-5. The 1.3% H2009.1 tetrameric, scH2009.1 tetrameric, and naked liposomes accumulate in both $\alpha_v\beta_6$-positive H2009 and $\alpha_v\beta_6$-negative H460 tumors to the same extent. Subcutaneous H2009 or H460 tumors were established in the flank of NOD/SCID mice. Tumor bearing mice were then injected via tail vein with either 1.3% H2009.1 tetrameric, AcH2009.1 tetrameric, scH2009.1 tetrameric, or naked liposomes labeled with the near infrared dye DiR. Animals were imaged at 24, 48, and 72 hours post-liposome injection. Shown are representative images from the 72 hour time point. (a) Liposome accumulation in H2009 tumors. (b) Liposome accumulation in H460 tumors. (c) 1.3% AcH2009.1 tetrameric liposome accumulation in both H2009 and H460 tumors displayed on a different epi-fluorescence scale that allows for visualization of the tumor accumulation.

Table 5-1. Quantification of the tumor accumulation of 1.3% H2009.1 tetrameric, AcH2009.1 tetrameric, scH2009.1 tetrameric, and naked DiR-labeled liposomes in $\alpha_v\beta_6$-positive H2009 and H1975 tumors and $\alpha_v\beta_6$-negative H460 tumors determined by whole mouse fluorescent imaging.

	Liposome Formulation	Radiant Efficiency (x 10^9)		
		24hrs	48hrs	72hrs
H2009 tumors	H2009.1 Tetrameric	10.1 ± 0.0922	10.2 ± 0.601	12.2 ± 0.452
	AcH2009.1 Tetrameric	5.96 ± 1.86	5.36 ± 1.91	5.96 ± 1.59
	scH2009.1 Tetrameric	9.91 ± 1.37	12.1 ± 0.676	12.8 ± 1.03
	Naked	9.41 ± 1.65	11.3 ± 1.54	13.3 ± 2.32
H1975 tumors	H2009.1 Tetrameric	8.00 ± 0.810	9.50 ± 0.650	9.70 ± 1.39
	scH2009.1 Tetrameric	10.3 ± 1.61	10.9 ± 2.65	11.1 ± 1.98
	Naked	8.10 ± 2.32	9.30 ± 1.83	11.3 ± 1.64
H460 tumors	H2009.1 Tetrameric	12.4 ± 1.90	12.8 ± 1.80	12.6 ± 1.39
	AcH2009.1 Tetrameric	5.30 ± 0.529	4.95 ± 0.327	5.08 ± 0.373
	scH2009.1 Tetrameric	12.3 ± 3.01	14.1 ± 4.68	14.9 ± 3.77
	Naked	8.26 ± 1.20	11.3 ± 1.65	11.2 ± 0.840

imaging at 24, 48, and 72 hours post-injection. Table 5-1 lists quantified values of liposome accumulation in both H2009 and H460 tumors, and Figure 5-5 shows representative images for one mouse from each liposome formulation at 72 hours post-injection. As is evident in Figure 5-5a, there was no difference in liposome accumulation in H2009 tumors for the H2009.1 tetrameric, scH2009.1 tetrameric, or naked liposomes. While each liposome formulation continued to accumulate in the tumors up to 72 hours (Table 5-1), the H2009.1 tetrameric liposomes did not increase targeting to the $\alpha_v\beta_6$-expressing H2009 tumors. Interestingly, the AcH2009.1 tetrameric liposomes targeted the H2009 tumors 2-fold less than any of the other liposome formulations, suggesting that acetylation of the H2009.1 peptide actually inhibits nanoparticle tumor uptake. The tumor uptake of the AcH2009.1tetrameric liposomes was so much lower than the other liposome formulations that it was impossible to image all of the formulations using the same epi-fluroescence scale. AcH2009.1 tetrameric liposome tumor accumulation was not visible in the mice when using the scale that best demonstrated the tumor uptake of the H2009.1 tetrameric, scH2009.1 tetrameric, and naked liposomes (Figure 5-5a). However, increasing the radiant efficiency units allowed for visualization of the AcH2009.1 tetrameric liposome tumor accumulation (Figure 5-5c). Similar to the $\alpha_v\beta_6$-positive H2009 tumors, there was no difference in liposome accumulation in the $\alpha_v\beta_6$-negative H460 tumors (Figure 5-5b). Additionally, acetylation of the H2009.1 peptide inhibited tumor uptake into this tumor model, also decreasing uptake by 2-fold and making it difficult to image mice on the same scale (Figure 5-5b-c). These results are not surprising as H460 tumors do not express $\alpha_v\beta_6$ and therefore should not accumulate

higher levels of $\alpha_v\beta_6$-targeted H2009.1 tetrameric liposomes. However, the results with the $\alpha_v\beta_6$–positive H2009 tumors suggest that the tumor accumulation of the H2009.1 tetrameric, scH2009.1 tetrameric, and naked liposomes is entirely driven by the EPR effect. Regardless of the $\alpha_v\beta_6$ expression levels of the tumor or of the ability of the liposomes to specifically target $\alpha_v\beta_6$, all liposome formulations accumulate to the same extent in the H2009 and H460 tumors.

At 72 hours, the mice in each liposome group were sacrificed and their organs removed for *ex vivo* organ fluorescent imaging to look at the biodistribution of the liposomes in the different tumor-bearing mice. Figure 5-6 shows representative images of the organs from H2009.1 tetrameric, AcH2009.1 tetrameric, scH2009.1 tetrameric, and naked liposome treated mice bearing either H2009 or H460 tumors, and Table 5-2 lists the quantification of the liposome accumulation in the tumors imaged *ex vivo*. For each mouse, the organs were imaged on both sides, and the average of the radiant efficiency value for each organ side used as the actual value of the liposome accumulation in that tissue. As expected for a liposome nanoparticle, all of the liposome formulations appear to clear through the liver and spleen. Each liposome formulation was only observed in the tumor, liver, and spleen of any of the mice. Like the *in vivo* imaging, *ex vivo* imaging of organs and tumors from mice bearing H2009 tumors demonstrated no difference in tumor accumulation among the different liposome formulations with the exception of the AcH2009.1 tetrameric liposomes, which accumulated 2-fold less than the other liposome types (Figure 5-6a, Table 5-2). Conversely, *ex vivo* imaging of the H460 organs and tumors gave slightly different results than the *in vivo* tumor imaging. While the H2009.1 tetrameric and scH2009.1 tetrameric liposomes accumulated at equal levels, the naked

liposomes appeared to accumulate at levels 2-fold lower, similar to lower level of accumulation of the AcH2009.1 tetrameric liposomes. It is unclear why this discrepancy appeared between the *in vivo* and *ex vivo* imaging. As the H460 tumors do not express $\alpha_v\beta_6$, they should not specifically accumulate the $\alpha_v\beta_6$-targeting H2009.1 tetrameric liposomes. Additionally, dye-labeled H2009.1 tetrameric peptide homes to H2009 tumors and not H460 tumors (Chapter 2), further suggesting that this *ex vivo* result is an anomaly. However, nonspecific accumulation based on peptide charge may play a larger role in peptide targeted-liposome delivery to H460 tumors. Each peptide-bearing liposome has a +11,200 charge (+8 charge per peptide, with 1,400 peptides per liposome). As *ex vivo* imaging allows for imaging of the entire tumor, such nonspecific accumulation may be more evident in *ex vivo* as opposed to *in vivo* imaging.

While the H2009.1 tetrameric peptide does not alter liposome accumulation in the $\alpha_v\beta_6$-positive H2009 tumors, this could be an effect of the tumor vasculature structure of that particular tumor type. A different tumor model with its own unique tumor vasculature pattern might experience different levels of liposome accumulation based on the number or leakiness of blood vessels; this could allow the H2009.1 peptide to override the EPR effect and produce a greater degree of liposome extravasation into the tumor tissue. Therefore, I also examined the accumulation of different liposome formulations in mice bearing the $\alpha_v\beta_6$–positive H1975 tumors. As with the H2009 and H460 tumor models, this experiment was performed by injecting the liposomes in the tail vein of H1975 tumor-bearing mice and then imaging the mice at 24, 48, and 72 hours after liposome injection. Only the H2009.1 tetrameric, scH2009.1 tetrameric, and naked

Table 5-2. Quantification of the organ and tumor accumulation of 1.3% H2009.1 tetrameric, AcH2009.1 tetrameric, scH2009.1 tetrameric, and naked DiR-labeled liposomes in $\alpha_v\beta_6$-positive H2009 and H1975 tumors and $\alpha_v\beta_6$-negative H460 tumors as determined by *ex vivo* imaging.

	Liposome Formulation	Radiant Efficiency (x 10^9)
H2009 tumors	H2009.1 Tetrameric	5.25 ± 3.03
	AcH2009.1 Tetrameric	2.29 ± 1.32
	scH2009.1 Tetrameric	5.27 ± 3.04
	Naked	6.35 ± 3.67
H1975 tumors	H2009.1 Tetrameric	3.76 ± 0.920
	scH2009.1 Tetrameric	4.99 ± 1.57
	Naked	3.86 ± 1.24
H460 tumors	H2009.1 Tetrameric	7.14 ± 0.374
	AcH2009.1 Tetrameric	4.88 ± 3.20
	scH2009.1 Tetrameric	6.36 ± 0.935
	Naked	3.77 ± 0.404

liposomes were used for this experiment as the AcH2009.1 tetrameric liposomes did not appear to target well in the H2009 tumor model. Imaging the liposome-injected H1975 tumor-bearing mice gave results similar to those of the H2009 tumor-bearing mice (Figure 5-7a, Table 5-1). Once again, there was no difference between the tumor accumulation of the H2009.1 tetrameric, scH2009.1 tetrameric, and naked liposomes. These same results also held true for *ex vivo* imaging of the organs and tumors from the H1975 tumor-bearing mice (Figure 5-6b, Table 5-2). Therefore, changing to a different $\alpha_v\beta_6$-expressing tumor model did not alter the EPR-driven accumulation of all of the liposome formulations.

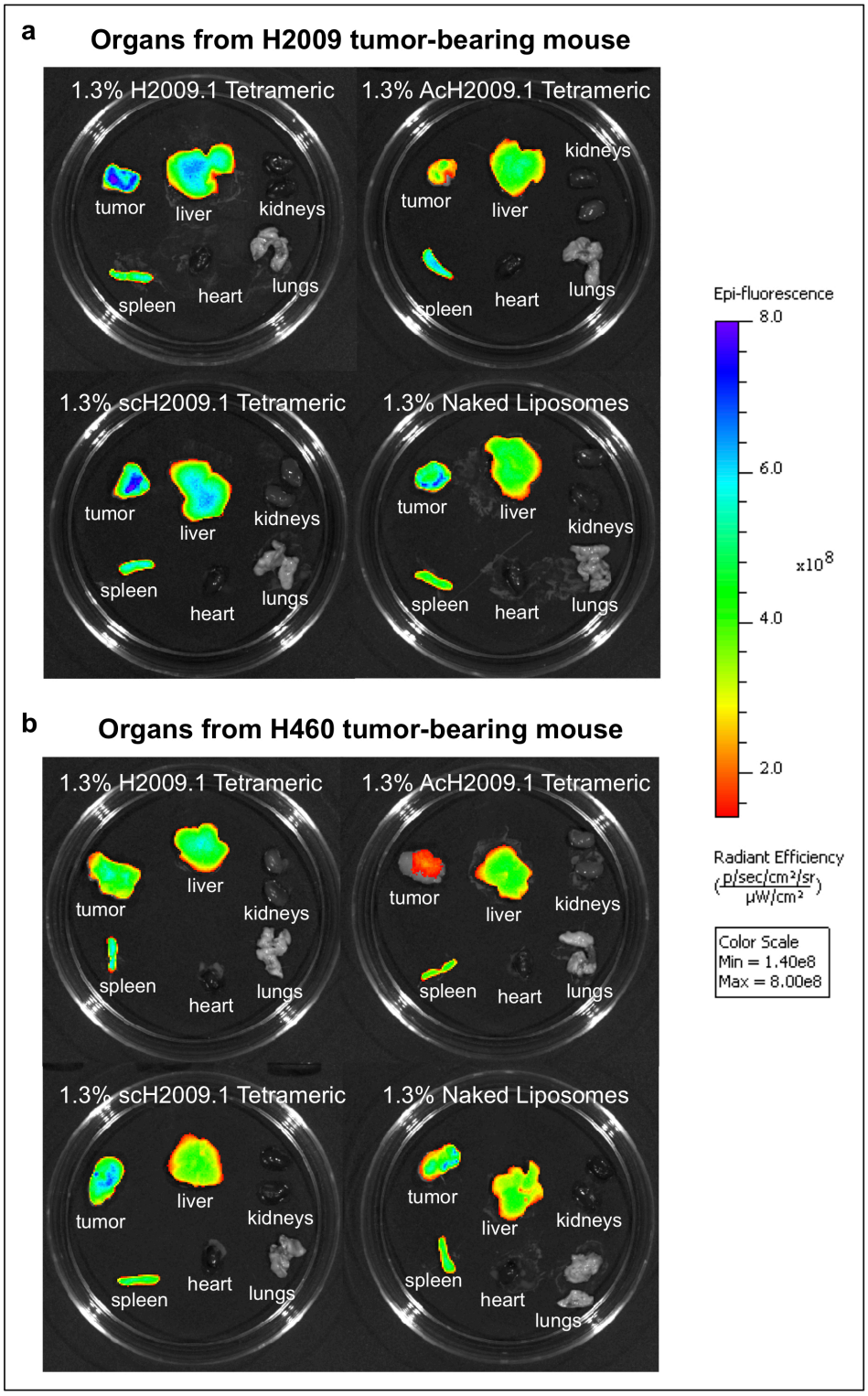
a
Organs from H2009 tumor-bearing mouse
1.3% H2009.1 Tetrameric
tumor
liver
kidneys
spleen
heart
lungs
1.3% AcH2009.1 Tetrameric
tumor
liver
kidneys
spleen
heart
lungs
1.3% scH2009.1 Tetrameric
tumor
liver
kidneys
spleen
heart
lungs
1.3% Naked Liposomes
tumor
liver
kidneys
spleen
heart
lungs
b
Organs from H460 tumor-bearing mouse
1.3% H2009.1 Tetrameric
tumor
liver
kidneys
spleen
heart
lungs
1.3% AcH2009.1 Tetrameric
tumor
liver
kidneys
spleen
heart
lungs
1.3% scH2009.1 Tetrameric
tumor
liver
kidneys
spleen
heart
lungs
1.3% Naked Liposomes
tumor
liver
kidneys
spleen
heart
lungs
Epi-fluorescence
8.0
6.0
4.0
2.0
x10^8
Radiant Efficiency
(p/sec/cm²/sr / µW/cm²)
Color Scale
Min = 1.40e8
Max = 8.00e8

Figure 5-6. *Ex vivo* imaging demonstrates that the 1.3% H2009.1 tetrameric, scH2009.1 tetrameric, and naked liposomes accumulate in both $\alpha_v\beta_6$-positive H2009 and $\alpha_v\beta_6$-negative H460 tumors to the same extent and all liposomes clear through the liver and spleen. Subcutaneous H2009 or H460 tumors were established in the flank of NOD/SCID mice. Tumor bearing mice were then injected via tail vein with either 1.3% H2009.1 tetrameric, AcH2009.1 tetrameric, scH2009.1 tetrameric, or naked liposomes labeled with the near infrared dye DiR. At 72 hours post-liposome injection, the mice were sacrificed and the organs removed for *ex vivo* fluorescent imaging. (a) Representative image of liposome accumulation in tumors and organs from a H2009 tumor-bearing mouse. (b) Representative image of liposome accumulation in tumors and organs from a H460 tumor-bearing mouse.

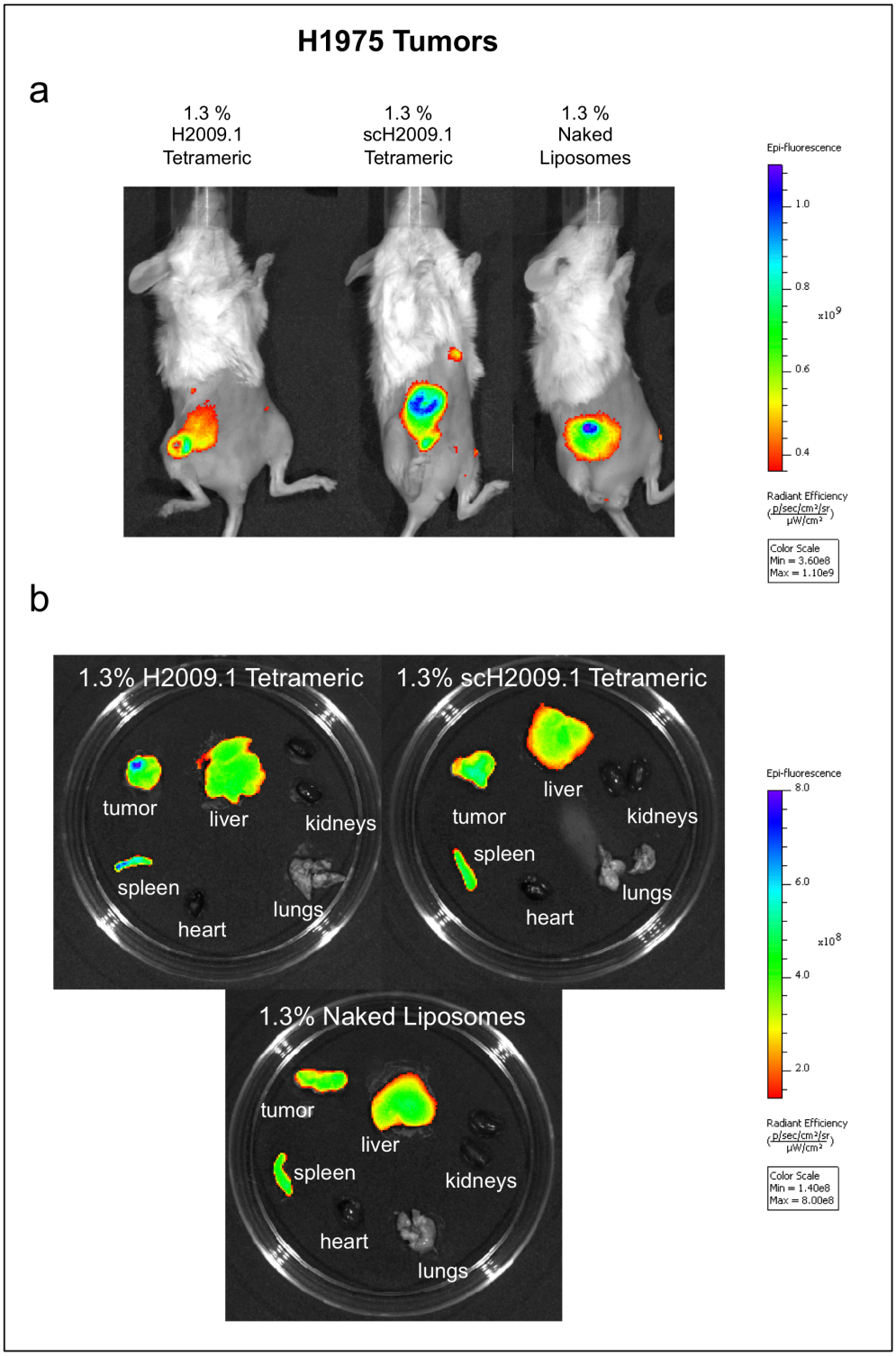
H1975 Tumors
a
1.3 % H2009.1 Tetrameric
1.3 % scH2009.1 Tetrameric
1.3 % Naked Liposomes
Epi-fluorescence
1.0
0.8
x10^9
0.6
0.4
Radiant Efficiency
Color Scale
Min = 3.60e8
Max = 1.10e9
b
1.3% H2009.1 Tetrameric
tumor
liver
kidneys
spleen
lungs
heart
1.3% scH2009.1 Tetrameric
liver
tumor
kidneys
spleen
lungs
heart
1.3% Naked Liposomes
tumor
liver
spleen
kidneys
heart
lungs
Epi-fluorescence
8.0
6.0
x10^8
4.0
2.0
Radiant Efficiency
Color Scale
Min = 1.40e8
Max = 8.00e8

Figure 5-7. Fluorescent imaging demonstrates that the 1.3% H2009.1 tetrameric, scH2009.1 tetrameric, and naked liposomes accumulate in $\alpha_v\beta_6$-positive H1975 tumors to the same extent and all liposomes clear through the liver and spleen. Subcutaneous H1975 tumors were established in the flank of NOD/SCID mice. Tumor bearing mice were then injected via tail vein with either 1.3% H2009.1 tetrameric, scH2009.1 tetrameric, or naked liposomes labeled with the near infrared dye DiR. (a) Animals were imaged at 24, 48, and 72 hours post-liposome injection. Shown are representative images from the 72 hour time point. (b) At 72 hours post-liposome injection, the mice were sacrificed and the organs removed for *ex vivo* fluorescent imaging. Shown are representative images of liposome accumulation in tumors and organs.

5.3.4 *Penetration of Liposomes in Tumors*

While the H2009.1 tetrameric, scH2009.1 tetrameric, and naked liposomes accumulate in tumors to the same extent, it is unclear whether they display a similar tissue distribution or whether they differ in terms of tissue penetration and location within the tumor tissue. In order to achieve effective $\alpha_v\beta_6$ targeting, the H2009.1 tetrameric liposomes must enter the tumor through blood vessels and then penetrate into the tumor tissue. To fully understand why the H2009.1 tetrameric liposomes do not increase therapeutic effects compared to the scH2009.1 tetrameric or naked liposomes, I investigated the tumor penetration and localization of the different liposome formulations. Liposomes were prepared with the fluorescent lipophilic dye DiI, which incorporates into the lipid membrane. These liposomes are similar to the liposomes prepared for the whole mouse imaging studies except that they include a lower wavelength dye that allows for visualization of the liposomes via microscopy of tumor sections.

Mice bearing either $\alpha_v\beta_6$-positive H2009 or H1975 or $\alpha_v\beta_6$-negative H460 xenografts were injected via tail vein with DiI-labeled 1.3% H2009.1 tetrameric, scH2009.1 tetrameric, or naked liposomes and sacrificed at 24, 48, or 72 hours post-liposome injection. At the time of sacrifice, the tumors were removed and frozen for sectioning and microscopy. The tumor sections were also stained for tumor blood vessels using an anti-CD31 antibody. Representative images of liposome accumulation in H2009 tumors are shown in Figure 5-8, in H1975 tumors in Figure 5-9, and in H460 tumors in

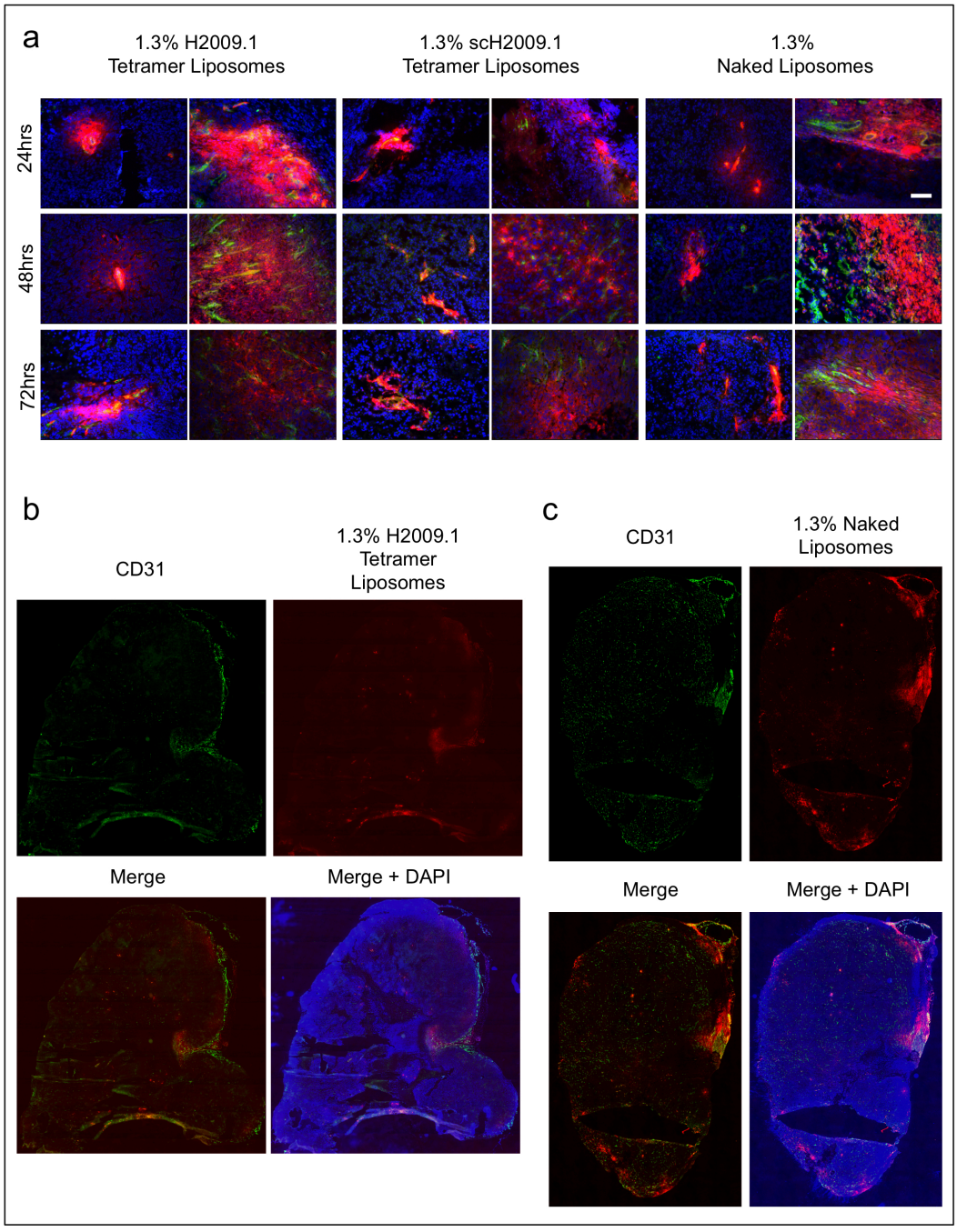

Figure 5-8. Fluorescent microscopy of H2009 tumor sections from mice injected with 1.3% H2009.1 tetrameric, scH2009.1 tetrameric, and naked liposomes demonstrates that each liposome formulation accumulates only in the area immediately adjacent to blood

vessels. Subcutaneous H2009 tumors were established in the flank of NOD/SCID mice. Tumor bearing mice were then injected via tail vein with either 1.3% H2009.1 tetrameric, scH2009.1 tetrameric, or naked liposomes labeled with the dye DiI. At 24, 48, or 72 hours post-liposome injection, the mice were sacrificed and the tumors removed for sectioning and fluorescent microscopy. blue – DAPI, red – DiI-labeled liposomes, and green – CD31 staining. (a) 10X images of liposome accumulation in tumors. The white scale bar indicates 100 μm. (b) Representative whole tumor image from a mouse injected with 1.3% H2009.1 tetrameric liposomes and sacrificed 48 hours after injection. (c) Representative whole tumor image from a mouse injected with 1.3% naked liposomes and sacrificed 48 hours after injection.

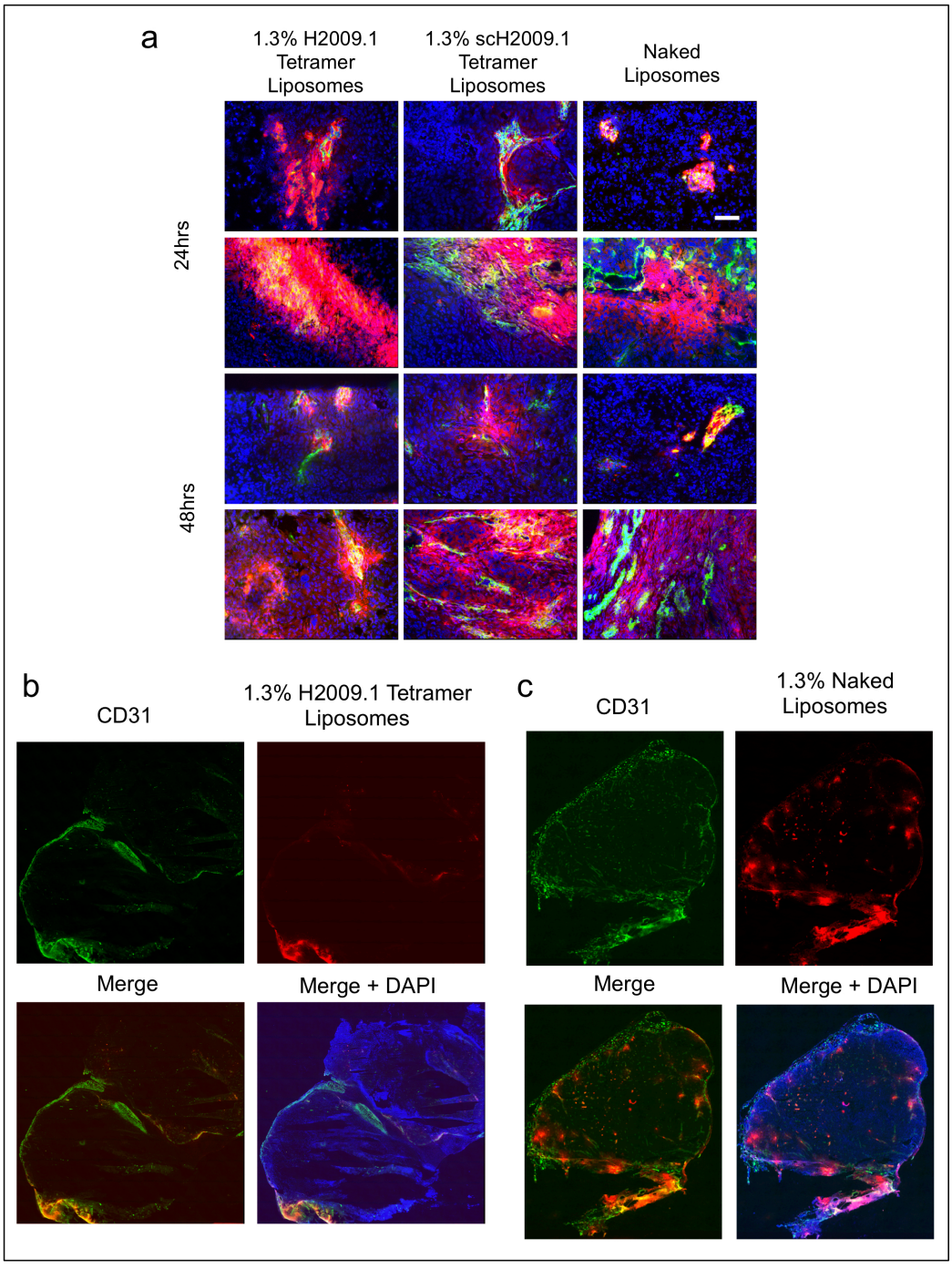

Figure 5-9. Fluorescent microscopy of H1975 tumor sections from mice injected with 1.3% H2009.1 tetrameric, scH2009.1 tetrameric and naked liposomes demonstrates that

each liposome formulation accumulates only in the area immediately adjacent to blood vessels. Subcutaneous H1975 tumors were established in the flank of NOD/SCID mice. Tumor bearing mice were then injected via tail vein with either 1.3% H2009.1 tetrameric, scH2009.1 tetrameric, or naked liposomes labeled with the dye diI. At 24 or 48 hours post-liposome injection, the mice were sacrificed and the tumors removed for sectioning and fluorescent microscopy. blue – DAPI, red – DiI-labeled liposomes, and green – CD31 staining. (a) 10X images of liposome accumulation in tumors. The white scale bar indicates 100 μm. (b) Representative whole tumor image from a mouse injected with 1.3% H2009.1 tetrameric liposomes and sacrificed 24 hours after injection. (c) Representative whole tumor image from a mouse injected with 1.3% naked liposomes and sacrificed 24 hours after injection.

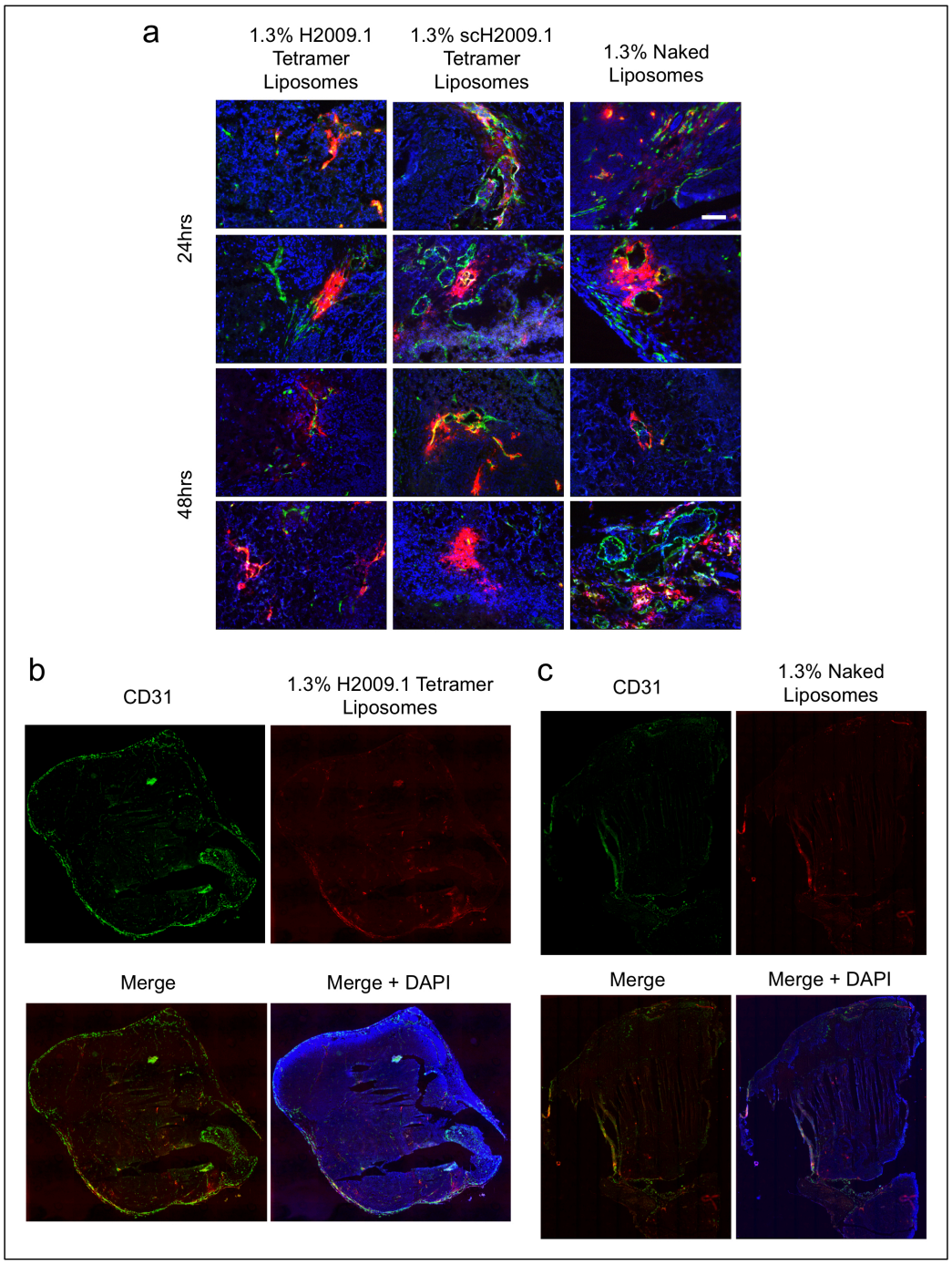

Figure 5-10. Fluorescent microscopy of H460 tumor sections from mice injected with 1.3% H2009.1 tetrameric, scH2009.1 tetrameric and naked liposomes demonstrates that each liposome formulation accumulates only in the area immediately adjacent to blood

vessels. Subcutaneous H460 tumors were established in the flank of NOD/SCID mice. Tumor bearing mice were then injected via tail vein with either 1.3% H2009.1 tetrameric, scH2009.1 tetrameric, or naked liposomes labeled with the dye DiI. At 24 or 48 hours post-liposome injection, the mice were sacrificed and the tumors removed for sectioning and fluorescent microscopy. blue – DAPI, red – DiI-labeled liposomes, and green – CD31 staining. (a) 10X images of liposome accumulation in tumors. The white scale bar indicates 100 μm. (b) Representative whole tumor image from a mouse injected with 1.3% H2009.1 tetrameric liposomes and sacrificed 48 hours after injection. (c) Representative whole tumor image from a mouse injected with 1.3% naked liposomes and sacrificed 48 hours after injection.

Figure 5-10. In each figure, part (a) shows 10X images of liposome accumulation in tumors, part (b) shows a whole image of a tumor from a representative mouse treated with 1.3% H2009.1 tetrameric liposomes, and part (c) shows a whole image of a tumor from a representative mouse treated with 1.3% naked liposomes. Both the $\alpha_v\beta_6$-positive H2009 and H1975 tumors and the $\alpha_v\beta_6$-negative H460 tumors exhibited similar patterns of liposome accumulation. All of the liposome formulations accumulated in the tumors in areas immediately adjacent to the tumor blood vessels, and none of the liposomes penetrated further into the tumor tissue. While there were some areas of high liposome accumulation, these were all found in highly vascularized regions of the tumors and the same pattern of high liposome accumulation was observed for the H2009.1 tetrameric, scH2009.1 tetrameric, and naked liposomes in each tumor type. Liposome accumulation was mostly observed in regions with prominent blood vessels near the tumor periphery. Other areas of the tumor with smaller blood vessels or more isolated blood vessels demonstrated little liposome accumulation. The ~100 nm liposome size may prevent extravasation through smaller blood vessels.

To verify that the receptor for the H2009.1 tetrameric peptide was still expressed in these tumors, the H2009, H1975, and H460 tumors were stained for $\alpha_v\beta_6$ expression using immunofluorescence with an anti- β_6 antibody. As expected, the H2009 and H1975 tumors exhibited high levels of β_6 while no β_6 was observed in the H460 tumors (Figure 5-11a). Additionally, β_6 was expressed widely throughout both the H2009 and H1975 tumors, as demonstrated by whole tumor imaging of a H2009 tumor (Figure 5-11b). Therefore, although the receptor for the H2009.1 tetrameric liposomes is expressed

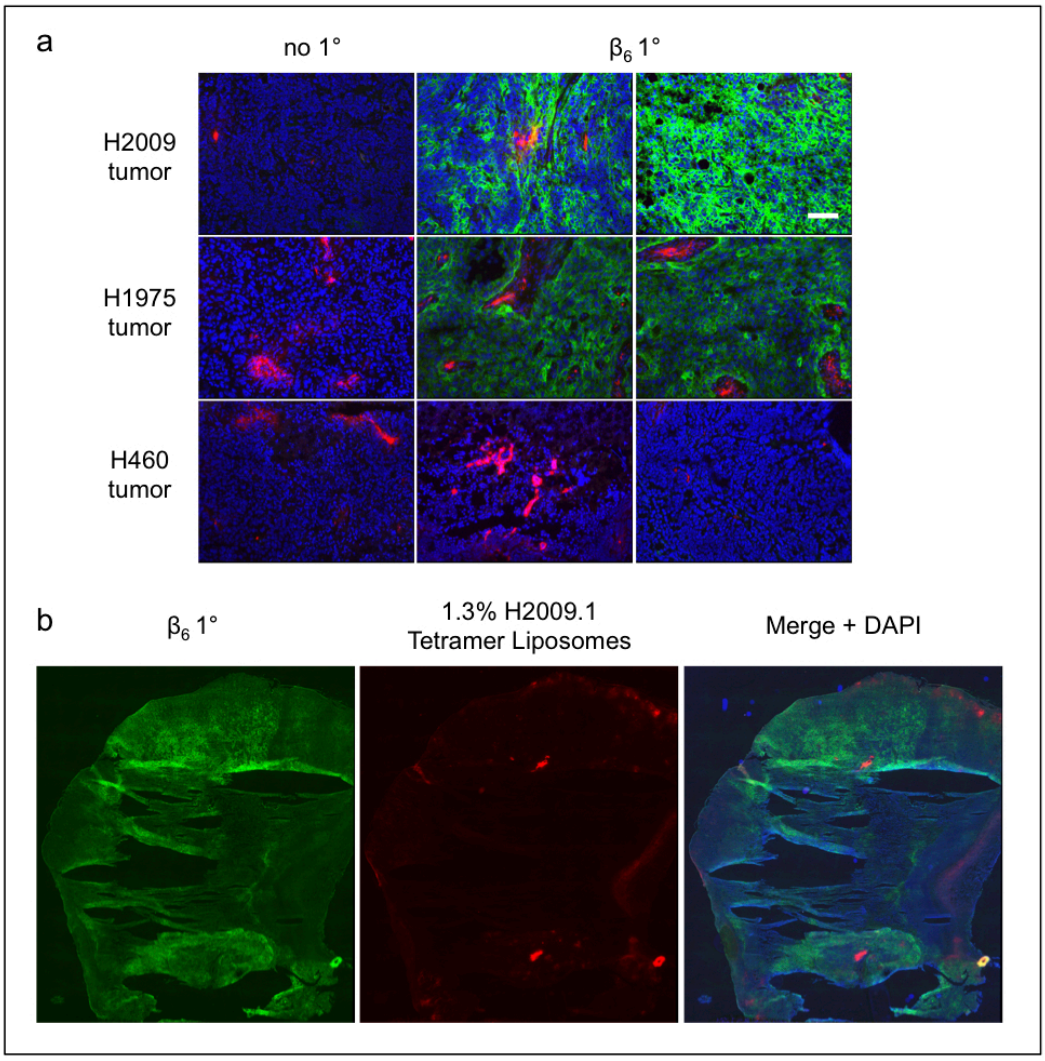

Figure 5-11. H2009 and H1975 tumors express $\alpha_v\beta_6$ while H460 tumors do not express the integrin. Subcutaneous H2009, H1975, or H460 tumors were established in the flank of NOD/SCID mice. Tumor bearing mice were then injected via tail vein with 1.3% H2009.1 tetrameric liposomes labeled with the dye DiI. At 24 hours post-liposome injection, the mice were sacrificed and the tumors removed for sectioning and fluorescent microscopy. blue – DAPI, red – DiI-labeled 1.3% H2009.1 tetrameric liposomes, and green – β_6 staining. (a) 10X images of tumors. (b) Representative whole tumor images of β_6-stained H2009 tumor section.

throughout the tumor, the targeted liposomes are unable to reach most of the $\alpha_v\beta_6$-expressing tumor cells due to a failure to penetrate through the tumor tissue. Thus, it appears that the lack of additional efficacy for the H2009.1 tetrameric liposomes compared to the naked liposomes is at least in part a result of the inability of the targeted liposomes to penetrate into the tumor tissue to enter $\alpha_v\beta_6$-expressing cells.

5.4 Discussion

The clinical success of pegylated liposomal doxorubicin, or DOXIL®, makes it an attractive nanoparticle platform for targeted drug delivery, and a variety of targeting ligands conjugated to liposomal forms of doxorubicin demonstrate increased efficacy compared to non-targeted liposomes, either by inhibiting tumor growth or by increasing survival of tumor-bearing rodents.[154, 158-166, 382-384] Several antibody-targeted forms of liposomal doxorubicin are either entering[385] or already in[386] clinical trials and at least one peptide-targeted form of liposomal doxorubicin is being manufactured using GMP to ease the transition to clinical trials.[167] These targeted forms of liposomal doxorubicin rely on both passive targeting from the EPR effect and on active targeting from the specificity of the targeting ligand for tumor or tumor vasculature cells.

Encouraged by the successes met with ligand-targeted forms of liposomal doxorubicin, I previously developed targeted liposomes specific for the integrin $\alpha_v\beta_6$ by conjugating the $\alpha_v\beta_6$-specific H2009.1 peptide to the surface of liposomal doxorubicin (Chapter 4). These studies demonstrated that liposomes displaying the tetrameric H2009.1 peptide at approximately 1400 peptides per liposome, a 1.3% H2009.1 tetrameric formulation, had the best $\alpha_v\beta_6$-specific cell targeting and toxicity.

Significantly, the ideal 1.3% H2009.1 tetrameric liposome formulation was 2-fold more toxic to cells than liposomes bearing the control scrambled scH2009.1 peptide and more than 10 times more toxic than naked, no peptide, liposomes. Based on these exciting *in vitro* results and with the goal of developing clinically relevant therapy agents, I chose to study the efficacy of H2009.1 peptide liposomes *in vivo*.

As the 1.3% H2009.1 tetrameric form of liposomal doxorubicin was the most effective *in vitro*, I began by examining the *in vivo* therapeutic efficacy of these liposomes compared to both control no peptide, naked liposomes and liposomes bearing the control scH2009.1 tetrameric peptide. While all 3 liposome formulations significantly inhibited tumor growth and increased survival compared to control buffer treated mice, there was no difference in efficacy between any of the liposome formulations. Unlike the *in vitro* results, the H2009.1 tetrameric, scH2009.1 tetrameric, and naked liposomes displayed similar toxicity. Additionally, in stark contrast to their lower efficacy *in vitro*, 0.64% H2009.1 tetrameric liposomes displaying lower numbers of peptides and 1.3% H2009.1 monomeric liposomes displaying the lower affinity monovalent peptide also inhibited tumor growth in a manner identical to that of the 1.3% H2009.1 tetrameric and naked liposomes. Thus, all of the liposome formulations tested, whether $\alpha_v\beta_6$-targeted or untargeted, and regardless of the number and valency of conjugated peptides, inhibited tumor growth to exactly the same extent. While peptide valency and concentration alter liposomal targeting *in vitro*, this does not hold true *in vivo*.

Due to the failure of the H2009.1 peptide liposomes to differentially inhibit tumor growth, I examined the levels of tumor uptake and the tumor distribution of the different liposome formulations. Significantly, the 1.3% H2009.1 tetrameric, scH2009.1

tetrameric, and naked liposomes accumulated in tumors to the same extent, regardless of tumor $\alpha_v\beta_6$ expression levels. This suggests that the EPR effect drives liposome accumulation in tumors and that any active targeting driven by the H2009.1 peptide would have to occur after entry into the tumor tissue. Several other targeted liposomes have shown increased efficacy compared to non-targeted liposomes despite identical EPR-driven levels of tumor accumulation, including the antibody-targeted liposome formulations anti-HER2 and anti-EGFR liposomal doxorubicin.[185, 186] The increased efficacy of these formulations has been attributed to internalization of the targeted liposomes into tumor cells while the non-targeted liposomes remained in the extracellular space. As doxorubicin must enter the nuclei of cells to exert its effects, ligand-directed cellular internalization of the drug could easily drive beneficial therapeutic effects.

The similar levels of tumor accumulation for my various liposomal formulations coupled with their identical antitumor effects suggested that the tissue distribution of these liposomes did not allow for efficient $\alpha_v\beta_6$ targeting. Therefore, I examined the tissue distribution of the 1.3% H2009.1 tetrameric, scH2009.1 tetrameric, and naked liposomes in both $\alpha_v\beta_6$-positive and $\alpha_v\beta_6$-negative tumors. All liposomes remained clustered around the tumor blood vessels with little penetration past blood vessel rich areas of the tissue, and there was very little difference in liposome accumulation and penetration in $\alpha_v\beta_6$-positive verses $\alpha_v\beta_6$-negative tumors. Thus, we believe that the H2009.1 tetrameric peptide was unable to effectively target $\alpha_v\beta_6$ and carry liposomes into the majority of tumor cells due to an inability of the liposomes to penetrate the tumor tissue and access most of the $\alpha_v\beta_6$-expressing cells. The H2009.1 peptide is unlikely to

increase tumor inhibition compared to non-targeted liposomes if it is not able to alter liposomal tumor distribution.

This study highlights the challenges of *in vivo* drug targeting. Targeted therapies that work well *in vitro* do not always maintain specific efficacy *in vivo*, even when the targeting ligand itself homes to tumors. Tumor targeting *in vivo* depends on many aspects not present in the *in vitro* context including nanoparticle half-life, tumor vasculature leakiness and size, particle penetration through the tumor tissue, and receptor levels and availability. These variables will change depending on the tumor type, nanoparticle type, tumor target, and targeting ligand. Accordingly, it is difficult to predict how well a targeting therapy will translate from the *in vitro* to *in vivo* context. While our original prediction that H2009.1 peptide targeting of liposomal doxorubicin would increase drug efficacy *in vivo* did not hold true, several of our findings are not without precedent. These include the similar levels of tumor accumulation for the different liposome formulations and the poor tumor penetration of the liposomes.

Mathematical modeling of the relationship between molecular size and tumor uptake predicts that all particles above 50 nm in size, whether targeted or untargeted, will accumulate in tumors to the same extent based on the EPR effect.[387] In practice, similar tumor uptake has been observed for several different ligand-targeted forms of liposomal doxorubicin.[185, 186] Therefore, it is not surprising that both H2009.1 peptide-targeted and untargeted liposomes accumulated in tumors at similar levels. Additionally, other studies have demonstrated poor tumor penetration for ~100 nm nanoparticles. A detailed comparison of the tumor accumulation and penetration of pegylated gold nanoparticles ranging in size from 20 – 100 nm demonstrated poor tumor penetration for the 100 nm

particles, with the larger nanoparticles localizing only to the area immediately adjacent to the vasculature.[388] Interestingly, there was an inverse relationship between particle size and tumor accumulation. While the 100 nm nanoparticles had the highest levels of tumor accumulation, tumor accumulation of the 20 nm particles was almost 40 times lower. However, the smaller 20 nm particles exhibited the best tumor penetration and distribution.

The affinity of targeting ligands is also known to affect tumor delivery. Most studies examining affinity have been performed using antibodies but are expected to hold true for other targeting ligands. Both mathematical modeling and experimental studies have demonstrated that lower affinity antibodies experience better tissue distribution.[389-391] This "binding site barrier" was first described in a modeling study by Fujimori *et al.* and is based on the successful binding of a ligand to tumor cells near the site of entry into the tumor; this binding then impedes ligand distribution throughout the tumor.[389] As high affinity ligands bind readily to tumor cells, there are fewer free ligands available to penetrate further into the tumor, and the high affinity ligands remain trapped in locations near where they first entered the tumor leading to heterogeneous tumor distribution. Lower affinity ligands experience faster off rates with their receptor and can therefore dissociate prior to cellular internalization and penetrate further into the tumor tissue. In contrast to these studies, the therapeutic efficacy of liposomes displaying the lower affinity H2009.1 monomeric peptide did not differ from that of liposomes displaying the higher affinity H2009.1 tetrameric peptide. However, the ability of the monomeric peptide to improve liposomal tumor distribution was likely hampered by the large size of

the liposomes. Thus, my results suggest that the nanoparticle platform and not the targeting ligand drives tumor penetration.

Other studies have demonstrated improved tumor inhibition for peptide-targeted liposomal doxorubicin compared to non-targeted liposomal doxorubicin.[154, 158-166] However, it is important to note that the majority of these peptides have targeted the tumor vasculature and not the tumor cells. As vasculature-targeting peptides reach their target cells while in the bloodstream, they are not dependent on escape from the vasculature and subsequent penetration through the tumor tissue. These liposome formulations may function more as antiangiogenic therapies.

A few tumor cell specific peptides have increased the efficacy of liposomal doxorubicin.[159, 161, 162] For two of these peptide-targeted liposomal formulations, it is unclear why they preferentially inhibited tumor growth while our H2009.1-targeted liposomes did not improve efficacy.[161, 162] The tumor accumulation and distribution of these liposome formulations have not been determined, but it is feasible that differences in tumor type and blood vessel density and leakiness improve the accumulation or penetration for these targeted formulations. Interestingly, another peptide specific for NSCLC improved the efficacy of liposomal doxorubicin.[159] When the SP5-2 peptide, which was isolated from a phage library panning against CL1-5 NSCLC cells, was conjugated to liposomal doxorubicin, it significantly inhibited tumor growth compared to both control non-targeted liposomes and liposomes conjugated to a mutant non-targeting peptide. This increased efficacy for the targeted liposomes appears to result from increased tumor accumulation of the targeted liposomes. SP5-2 peptide-targeted liposomal doxorubicin accumulated in tumors at levels at ~2-fold higher and in tumor

nuclei at levels ~2.5-fold higher than both control liposome formulations. This could be a result of the different vasculature pattern of the tumors allowing for better accumulation of the targeted liposomes. Alternatively, the SP5-2 peptide could override the EPR effect to lead to increased tumor targeting.

Other groups have reported peptide-targeted liposomal doxorubicin formulations that failed to inhibit tumor growth *in vivo*. Two separate studies failed to demonstrate *in vivo* efficacy for liposomal doxorubicin conjugated to the LyP-1 peptide.[154, 300] This peptide was isolated from an *in vivo* phage display library panning in mice bearing MDA-MB-435[95-98] tumors[99] and binds to the p32 receptor expressed on tumor cells, tumor lymphatic vessels, and tumor macrophages.[297] Of note, the LyP-1 targeted liposomes did not alter tumor growth compared to control, buffer-treated mice. However, treating mice with a combination of local hyperthermia mediated by gold nanorods and the LyP-1 targeted liposomes significantly inhibited tumor growth compared to both control mice and mice treated with hyperthermia and non-targeted liposomes.[154] This result was attributed to the ability of the gold nanorod-induced hyperthermia to improve tumor accumulation of the targeted liposomes. It would be interesting to explore whether combination with hyperthermia treatment could improve efficacy of the H2009.1-targeted liposomes. However, it is important to note that hyperthermia treatment also slightly upregulated the expression of the p32 receptor to which the LyP-1 peptide binds. Therefore, some of the improved efficacy of this combination treatment is likely due to increased receptor expression. As it is not known whether hyperthermia would increase $\alpha_v\beta_6$ expression, this type of combination treatment may not have the same benefit for our system. However, $\alpha_v\beta_6$ is already expressed at high levels throughout the H2009 tumors.

Several additional strategies can be explored to improve the tumor distribution and penetration of the H2009.1-targeted liposomes. These strategies can seek to affect the tumor vasculature or to directly affect tumor penetration. One potential method for improving liposome tumor accumulation and penetration is to combine liposome treatment with antiangiogenic therapy. While the primary design of antiangiogenic therapy has been to both inhibit new tumor blood vessel growth and to destroy existing tumor blood vessels,[392-394] combining antiangioenic therapy with systemic chemotherapy has had the surprising result of improving patient outcomes compared to chemotherapy alone.[395] This result has been attributed to the "vascular normalization" hypothesis that antiangiogenic therapy reverts tumor blood vessels back to a more normal state, allowing for more homogenous blood flow and a more uniform delivery of drugs into the tumor.[395] Accordingly, antiangiogenic treatment has been shown to increase tumor penetration of both a protein-dye conjugate[396] and chemotherapeutics.[397] Additionally, one study demonstrated that co-treatment with both tumor cell targeted antibody-functionalized liposomal doxorubicin and vasculature targeted peptide-functionalized liposomal doxorubicin improved efficacy compared to either treatment alone.[398] Therefore, a combination treatment of H2009.1 peptide targeted liposomal doxorubicin with an antiangiogenic therapy such as an antibody targeting vascular endothelial growth factor (VEGF) should be examined for *in vivo* efficacy in tumor-bearing mice to determine whether vascular normalization can improve penetration and subsequently the toxicity of H2009.1-targeted liposomes.

Recently, Ruoslahti and colleagues described a new tumor-penetrating peptide that they have dubbed the "iRGD" peptide, short for internalizing RGD peptide.[178] iRGD

is a tumor vasculature specific peptide selected from *in vivo* phage display panning in mice bearing metastatic human prostate cancer.[178] The cyclic peptide has the sequence CRGDKGPDC and contains both an integrin-binding RGD motif[399] and a neuropilin-1 (NRP-1) binding RGDK CendR motif.[291] iRGD functions via a three step mechanism: first the RGD motif binds to $\alpha_v\beta_3$ and $\alpha_v\beta_5$ on the tumor vasculature, next the peptide is cleaved by proteases to reveal the hidden RGDK CendR motif which only functions once its C-terminus is exposed, and finally the RGDK binds to NRP-1 overexpressed by both endothelial and tumor cells to stimulate penetration through the vasculature and tumor tissue.[178] Co-injection of the iRGD peptide with a variety of drug platforms, ranging from small molecules to 130 nm sized nanoparticles, demonstrates increased tumor accumulation and penetration and a subsequent increase in therapeutic efficacy for the co-injected drugs compared to treatment with the drugs alone.[179] Significantly, the iRGD peptide also increased tumor accumulation, penetration, and toxicity of liposomal doxorubicin.[179] The effects of iRGD are so promising that the CendR Inc. company has formed to test the clinical utility of this peptide.

Based on the ability of the iRGD peptide to increase the accumulation and penetration of liposomal doxorubicin in tumors, it is desirous to test the effects of co-injection of the iRGD peptide with H2009.1 peptide-targeted liposomal doxorubicin on the tumor penetration and therapeutic efficacy of the H2009.1 liposomes. Increased tumor penetration of the H2009.1 liposomes would lead to increased opportunity for targeting to $\alpha_v\beta_6$-expressing cells and could, therefore, potentiate the toxicity of the targeted liposomes compared to the non-targeted liposomes.

Other types of drug platforms may also increase the utility of the H2009.1 peptide and improve *in vivo* therapeutic efficacy. Micelles have many of the same advantages as liposomes, such as the ability to incorporate unmodified drugs and to encapsulate multiple agents at once. However, the smaller size of micelles gives them intermediate circulation times and can allow for better escape from the vasculature into the tumor tissue. Therefore, H2009.1 peptide-targeted micellular drugs may experience better tumor tissue penetration and efficacy than the H2009.1 peptide-targeted liposomes. Small ligands with high affinity are also predicted to have high accumulation and retention in tumors and better distribution throughout the tumor.[387] The H2009.1 peptide can easily be modified for direct conjugation to different chemotherapeutics, and the next chapter describes the development of two different H2009.1-drug conjugates.

The identical *in vivo* efficacy of H2009.1 peptide verses control liposomes illustrates that just because a ligand targets a tumor *in vivo* (as shown for the H2009.1 peptide in Chapter 2) and targets a nanoparticle *in vitro* (as shown for the H2009.1 peptide targeted liposomes in Chapter 4), does not necessarily lead to beneficial nanoparticle-targeting *in vivo*. It will be important to thoroughly examine different drug constructs to identify the best platform for *in vivo* delivery.

5.5 Acknowledgements

I wish to thank Dr. Michael McGuire for acting as the independent scientist for all of the tumor measurements. In addition, Dr. Shunzi Li synthesized many of the monomeric peptides used in this study. Whole tumor section images were possible due to the assistance of the UT Southwestern Live Cell Imaging Facility, a Shared Resource of

the Harold C. Simmons Cancer Center, supported in part by an NCI Cancer Center Support Grant, 1P30 CA142543-01.

CHAPTER SIX

IN VITRO AND *IN VIVO* EFFICACY OF H2009.1 PEPTIDE-DOXORUBICIN AND PACLITAXEL CONJUGATES

6.1 Introduction

Conjugation of the H2009.1 peptide to liposomal doxorubicin significantly inhibited tumor growth *in vivo* compared to control mice, but there was no therapeutic difference between mice treated with the peptide-targeted liposomes and mice treated with non-targeted liposomes (Chapter 5). These results are in stark contrast to the preferential cell toxicity of the H2009.1 peptide-liposomes compared to the non-targeted liposomes *in vitro* (Chapter 4). The failure of the H2009.1 peptide liposomes to specifically alter tumor growth *in vivo* appears to result from the identical tumor accumulation of the H2009.1 targeted and non-targeted liposome formulations coupled with the inability of the targeted liposomes to penetrate the tumor tissue beyond the area immediately adjacent to the tumor vasculature (Chapter 5). Directly conjugating the H2009.1 peptide to a drug of interest is anticipated to improve tumor penetration and *in vivo* efficacy due to the smaller size of drug conjugates compared to liposomes.

The small size of peptide-drug conjugates allows for better escape from the tumor vasculature and penetration through the tumor,[139] leading to high levels of tumor accumulation. However, only peptides with high affinity for their target are predicted to exhibit high tumor uptake as low affinity peptides are rapidly washed out of the tumor tissue.[387] The high affinity of the H2009.1 tetrameric peptide for $\alpha_v\beta_6$ coupled with the ability of a H2009.1 tetrameric peptide-dye conjugate to target tumors *in vivo* (Chapter 2)

suggests that H2009.1 tetrameric peptide-drug conjugates should specifically accumulate in tumors. Importantly, the peptide-dye conjugate was visible in tumors 24 hours after injection, indicating that the H2009.1 peptide has the required affinity for drug retention in the tumor tissue. Additionally, the small size of the H2009.1 peptide-drug should allow for extensive tumor penetration, potentially overcoming the failings of the H2009.1 peptide-targeted liposomes.

There have been several reports of tumor-specific peptides conjugated to chemotherapeutic drugs, including the widely used cytotoxic agents doxorubicin and paclitaxel, for targeted delivery to different cancer types. In particular, peptides isolated from phage display peptide libraries have been conjugated to both drugs.[112-118] While most of these conjugates, including the paclitaxel conjugates, have only been used for *in vitro* toxicity studies, several have also been shown to inhibit tumor growth *in vivo*. The NGR and RGD-4C peptides, both isolated from *in vivo* phage panning in mice bearing MDA-MB-435[95-98] breast xenografts, also both inhibited MDA-MB-435 tumor growth when conjugated to doxorubicin.[115] Of note, both of these peptides target the tumor vasculature and not the tumor cells. However, a peptide specific for tumor cells has also proven effective for drug targeting *in vivo*. The tumor cell targeting A54 peptide, isolated from *in vivo* panning in mice bearing BEL-7402 hepatocellular carcinoma xenografts, also inhibited tumor growth when conjugated to doxorubicin.[117]

To examine the ability of the H2009.1 peptide to target drugs to NSCLC tumors, we conjugated the peptide to both doxorubicin and paclitaxel. The peptide was conjugated to doxorubicin for a side-by-side comparison with the H2009.1 peptide-targeted liposomal doxorubicin formulation and was conjugated to paclitaxel due to

standard use of this drug in treating NSCLC. Despite the *in vitro* toxicity of both conjugates, neither conjugate significantly inhibited tumor growth compared to free, unmodified drugs. The lack of *in vivo* efficacy appears to result from poor drug release from the conjugates. Therefore, different linkers should be used to conjugate the drugs to the peptide or different drugs with specificity for the intracellular compartment into which they are delivered should be considered.

6.2 Materials and Methods

6.2.1 *Materials*

All Fmoc amino acids, the NovaPEG Rink Amide resin and 2-(1*H*-benzotriazole-1-yl)-1,1,3,3-tetramethyluronium hexafluorophosphate (HBTU) were purchased from Novabiochem® (EMD Millipore, Billerica, MA). The Fmoc-β-Ala-CLEAR™ Acid Resin was purchased from Peptides International (Osaka, Japan) and the Fmoc-NH-$(PEG)_{11}$-COOH ($C_{42}H_{65}NO_{16}$) from Polypure (Oslo, Norway). *N*-Methylmorpholine (NMM) and *N*,*N*'-Dicyclohexyl-carbodiimide (DCC) were purchased from ACROS Organics (Geel, Belgium). Anhydrous hydroxybenzotriazole (HOBt) was purchased from SynBioSci (Livermore, CA). Piperidine, β-maleimidopropionic acid, anhydrous methanol and Sephadex G-25 medium were purchased from Sigma-Aldrich Inc. (Livermore, CA). Doxorubicin HCl and paclitaxel were purchased from LC Laboratories (Woburn, MA). *N*-β-maleimidopropionic acid hydrazide trifluoroacetic acid salt (BMPH) was purchased from (Thermo Fisher Scientific, Rockford, IL). Sephadex G-50 Medium was purchased from GE Heatlhcare (Waukesha, WI). For cell culture, fetal bovine serum (FBS) was

purchased from Gemini Bio-Products (West Sacramento, CA) and both RPMI 1640 and Trypsin EDTA, 1x from Mediatech, Inc. (Fisher Scientific, Pittsburgh, PA).

6.2.2 *Cell Lines*

All human NSCLC cell lines were provided by the UT Southwestern Medical Center Hamon Center for Therapeutic Oncology Research and maintained according to published protocols.[334] The H2009 and H460 cell lines were all grown at 37°C and 5% CO_2 in RPMI 1640 supplemented with 5% FBS (R5).

6.2.3 *Peptide Synthesis and Purification*

Monomeric peptides were synthesized on a Symphony Synthesizer (Rainin Instruments, Protein Technologies, Inc., Woburn, MA) by Fmoc solid-phase peptide synthesis on a Rink Amide AM resin (substitution level 0.71 mmol/g). All amino acids were Fmoc-protected, and the Fmoc was removed to allow for amino acid coupling using 20% Piperidine in DMF. The amino acids were subsequently coupled at a 5-fold excess using HBTU, HOBt, and NMM coupling for 45 minutes. The PEG group added to each amino acid was purchased as Fmoc-NH-$(PEG)_{11}$-COOH and was coupled in the same manner as the amino acids, except that it was coupled at a 2.5-fold excess. The synthesized peptides were removed from the resin by shaking in a mixture of 94%:2.5%:1.0%:2.5%: triofluoroacetic acid (TFA):triisopropylsilane:H_2O:ethanediothiol (EDT) for 2-4 hours. The majority of the TFA solution was then removed by N_2 pressure before precipitation in diethyl ether at -80°C for a minimum of 2 hours. Precipitated peptide was dried under vacuum for a minimum of 12 hours.

The tetrameric cores were also synthesized on the Symphony Synthesizer using the Fmoc-β-Ala-CLEAR™ Acid Resin (substitution level 0.40 mmol/g) under the same coupling conditions as the monomeric peptides. Fmoc-Cys(Acm)-OH was first coupled to the resin followed by Fmoc-Lys(Fmoc)-OH, $[\text{Fmoc-Lys(Fmoc)-OH}]_2$, and finally $(\beta\text{-maleimidopropionic acid})_4$. The cores were removed from the resin in the same manner as the monomeric peptides.

The crude monomeric peptides and tetrameric cores were purified by reverse phase high-performance liquid chromatography (HPLC) using a SPIRIT™ Spirit Peptide C18 5 μm, 25 x 2.12 (AAPPTec®, Louisville, KY) on a Breeze™ HPLC (Waters Corporation, Milford, MA). H_20/0.1% TFA (eluent A) and acetonitrile/0.1% TFA (eluent B) were used for purification as follows: 0-1 minute, 90% A, 10% B at 10mL/minute; from 1-100 minutes, eluent B was increased from 10% to 60% at a flow rate of 10 mL/minute. The peptides were detected by ultraviolet (UV) absorbance at 220nm. Matrix-assisted laser desorption/ionization time of flight mass spectrometry was used to confirm peptide mass (Voyager-DE™ PRO, Applied Biosystems, Inc., Foster City, CA). The mass of the monomeric peptides (average mass calculated/MH+: 1843.02/1844.18) and tetrameric core (average mass calculated/MNa+: 1251.49/1274.27) were determined in reflective mode using α-cyano-4-hydroxycinnamic acid as a matrix.

The tetrameric peptides were synthesized by coupling purified monomeric peptide to purified, deprotected tetrameric core (8:1 monomeric peptide to tetrameric core) for 2 hours at room temperature in phosphate buffered saline, pH 7.4, containing 10 mM EDTA. Afterwards, excess monomeric peptide was removed by reverse phase HPLC

using the same elution method that was used for purification of the monomeric peptides and tetrameric core. The mass of the tetrameric peptides (average mass calculated/ MH+: 8629.01/8626.77) were also determined using matrix-assisted laser desorption/ionization time of flight mass spectrometry using linear mode and sinapinic acid as a matrix.

Before the tetrameric peptides could react with the maleimide-activated drugs, the unique cysteine placed before the branch point of the tetramers had to be deprotected to remove the acetamidomethyl (Acm) group protecting the thiol of the cysteine. The tetrameric peptides were deprotected by reaction of the peptide (0.35 μmol) with AgOAc (0.168 M AgOAc in 99:1 TFA:anisole to a total volume of 350 μL) for 2 hours at 4°C. The majority of the TFA solution was then removed under a slow stream of nitrogen and the peptide precipitated in diethyl ether at -80°C for a minimum of 30 minutes. After removing the ether from the precipitated peptide, the peptide was reacted with 150 μL of a 0.2 M dithiothreitol (DTT) solution (DTT dissolved in 1 M acetic acid) for a minimum of 5 hours shaking. The resulting solution was centrifuged and the supernatant taken for HPLC purification of the deprotected peptide. Additional tetrameric peptide was recovered from the pellet by shaking in 8 M guanidine HCl for an additional 5 hours. The supernatant resulting from centrifugation of this mixture was also taken for HPLC purification. The deprotected tetramers were purified using the same HPLC conditions as used for the other peptides, and the deprotection was verified by mass spectrometry, using the same method used for the protected tetramers (average mass calculated/ MH+: 8557.94/8558.38).

6.2.4 *Synthesis of Hydrazone Derivative of Doxorubicin*

A solution of doxorubicin HCl (5.8 mg, 10 μmol) and *N*-β-maleimidopropionic acid hydrazide trifluoroacetic acid salt (BMPH, 6 mg, 20.2 μmol) was prepared in 1 mL of anhydrous methanol. To this solution, 5 μL of trifluoroacetic acid (TFA) was added. The reaction mixture was stirred in the dark at room temperature for 120 hours. The methanolic solution was concentrated under nitrogen pressure to a volume of 100 μL. Acetonitrile (5 mL) was added and the resulting suspension was allowed to stand at -20°C for 24 hours. The red solid precipitate was washed three times with cold acetonitrile (3 mL) and dried for a minimum of 4 hours in a desiccator under vacuum.

6.2.5 *Conjugation of the H2009.1 Tetrameric Peptide to the Hydrazone Derivative of Doxorubicin*

A solution of the H2009.1 tetrameric peptide (8.6 mg, 1 μmol) was prepared in 1 mL of phosphate buffered saline (PBS) with 0.01 M EDTA. A solution of the doxorubicin-BMPH conjugate (3.5 mg, 5 μmol) in 0.5 mL methanol was added to the peptide. The reaction mixture was stirred in the dark at room temperature for 3 hours. At this point, the reaction mixture was purified on a Sephadex G-50 Medium column (500 mm x 18 mm) using PBS as the eluent. The proper fraction was desalted on a Sephadex G-25 column (500 mm x 18 mm) using H_2O as the eluent. Collected product was lyophilized giving a red powder (8.0 mg, 86% yield). Final product was verified by matrix-assisted laser desorption/ionization (MALDI) time of flight mass spectrometry. The mass was determined in linear mode using sinapinic acid as a matrix. (average mass

calculated/ MH+: 9267.61/9267.47). Subsequent HPLC analysis demonstrated that the product was > 96% pure.

6.2.6 *Doxorubicin Fluorescence to Monitor Accumulation of H2009.1-Doxoroubicin Conjugate in Cells*

H2009 cells were plated in 12 well plates and 48 hours later, once the cells reached 90% confluency, incubated with the H2009.1-doxorubicin conjugate for 1 hour. After washing the cells twice with PBS, PBS + 5% Triton was added and the plates were shaken for 15 minutes to lyse the cells. Doxorubicin concentration was determined by absorbance at 590 nm compared to doxorubicin standards in untreated cells using a F-7000 Fluorescence Spectrophotometer (Hitachi, Tokyo, Japan).

6.2.7 *Confocal Microscopy for Drug Release from H2009.1-Doxorubicin Conjugate*

H2009 cells were plated at 1,000 cells/plate in poly-d-lysine coated glass bottom culture dishes (MatTek Corporation, Ashland, MA). Once the cells had adhered to the plates, ~24 hours later, they were incubated with 4 μM (based on total doxorubicin concentration) of either free doxorubicin or of H2009.1-doxorubicin conjugate. After 1 hour, the cells were washed twice with R5 before the addition of fresh R5. The cells were then examined using a Nikon TE2000-E microscope (Melville, NY), observing doxorubicin fluorescence (excitation 485 nm , emission 595 nm).

6.2.8 *Synthesis of 2'-Maleimido-Paclitaxel*

Paclitaxel (8.6 mg, 10 μmol) was incubated with β-maleimidopropionic acid (1.0 mg, 6 μmol) and dicyclohexylcarbodiimide (4.1 mg, 20 μmol) in 500 μL anhydrous dichloromethane for 12 h at room temperature. Dicyclohexylurea was removed by filtration. The organic solvent was removed under vacuum and the solid was resuspended in 1 mL CH_3OH:H_2O (50:50 V/V) containing 0.1% trifluoroacetic acid. The reaction mixture was purified by reverse phase HPLC with eluents of H_2O/0.1% TFA (eluent A) and acetonitrile/0.1% TFA (eluent B). The following elution profile (referred to as Method A) was utilized: 0–1 min, 70% A, 30% B; 1–71 min, eluent B was increased from 30% to 100% at a flow rate of 10 mL/min. Elution of the conjugate was monitored by UV absorbance at 220 nM. The purified conjugate was characterized by MALDI mass spectrometry and 1H NMR. 2'-maleimido-paclitaxel ($C_{54}H_{56}N_2O_{17}$): MALDI MNa+ (monoisotopic mass calculated/ found: 1027.36/1027.19). 1H NMR reported in ppm (CDCl3): 1.82 (s, 1H, 1-OH); 5.68 (d, 1H, H-2); 3.80 (d, 1H, H-3); 2.45 (s, 3H, 4-OAc); 4.97 (d, 1H, H-5); 2.54 (m, 1H, Ha-6); 1.98 (m, 1H, Hb-6); 4.43 (m, 1H, H-7); 2.40 (d, 1H, 7-OH); 6.28 (s, 1H, H-10); 2.23 (s, 3H, 10-OAc); 6.19 (t, 1H, H13); 2.20–2.30 (band, 2H, H14); 1.24 (s, 3H, Me-16); 1.14 (s, 3H, Me-17); 1.68 (s, 3H, Me- 18); 1.93 (s, 3H, Me-19); 4.32 (d, 1H, Ha-20); 4.21 (d, 1H, Hb- 20); 5.47 (d, 1H, H-20); 6.06 (dd, 1H, H-30); 6.98 (d, 1H, 30-NH); 7.62–8.13 (m, 5H, C2-OBz); 7.32–7.52 (m, 5H, C30-Ph); 7.49– 7.77 (m, 5H, C30-NBz) and 2.75 (t, 2H); 3.84 (t, 2H); 6.51 (s, 2H) attributed to 3-maleimidopropionic acid.

6.2.9 *Conjugation of the H2009.1 Tetrameric Peptide to 2'-Maleimido-Paclitaxel*

A solution of 2'-maleimido-paclitaxel (17.1 mg, 2 μmol) was prepared in 0.8 mL Ar-purged PBS/ 0.01 M EDTA. A solution of the H2009.1 tetrameric peptide (3.0 mg, 3 μmol) in 0.2 mL DMF was added to the peptide solution. The reaction mixture was stirred at room temperature for 30 min. The product, H2009.1 tetrameric peptide–paclitaxel conjugate was then purified by HPLC using Method A and characterized by MALDI mass spectrometry. H2009.1 tetrameric peptide-paclitaxel ($C_{418}H_{708}N_{94}O_{147}S_5$): MALDI MH+ (average mass calculated/found: 9562.96/9561.75).

6.2.10 *Synthesis of H2009.1 Peptide-Paclitaxel-FITC*

The H2009.1-paclitaxel-FITC conjugate was prepared by reaction of the tetrameric core with FITC before conjugation to either the monomeric peptide or paclitaxel. The free ε-amino group of Lys on the maleimido tetrameric core was labeled with FITC. A solution of maleimido tetrameric core with Lys (ε-NH_2) (2.9 mg, 2 μmol) was prepared in 0.5 mL 0.1 M borate buffer (pH 9.3). A solution of FITC (1.2 mg, 3 μmol) in 0.5 mL DMF was added to the tetrameric core solution. The reaction mixture was stirred at room temperature in the dark for 3 hours and purified by reverse phase HPLC using Method B. The FITC labeled maleimido tetrameric core was applied for convergent synthesis of H2009.1 tetrameric peptide and paclitaxel conjugation as described above.

6.2.11 In Vitro *Release of Paclitaxel from the H2009.1-Paclitaxel Conjugate*

The H2009.1-paclitaxel conjugate was dissolved in each of the following solutions: 0.01 M PBS at pH 7.4, esterase (18 μg/mL) in PBS, or rat serum. The solutions were incubated at 37 °C. At time points of 3, 8, 24, 48, 72, and 96 hours post-incubation, aliquots were removed and mixed with 100 μL of ethanol to precipitate the serum proteins. The mixture was centrifuged at 3000 rpm for 5 min. The pellets were resuspended with 80% ethanol, followed by centrifugation at 3000 rpm again for 5 min. The pellets were rinsed and washed one more time. Then the pooled supernatants were analyzed by HPLC to determine the amounts of paclitaxel liberated from the conjugate. Paclitaxel was quantified by HPLC using a standard curve prepared with authentic paclitaxel. UV–Vis detection at 220 nm was used for data collection and analysis.

6.2.12 *Binding of H2009.1-Paclitaxel-FITC Analyzed by Flow Cytometry*

Approximately 100,000 cells were seeded per well in 12 well culture plates and allowed to adhere overnight. Cells were incubated for 1 hour with 1 μM H2009.1-paclitaxel–FITC or scH2009.1–paclitaxel–FITC. Cells were washed four times with PBS^{+} containing 0.1% BSA, followed by 2 brief rinses with 20 mM HCl–glycine, pH 2.2, 150 mM NaCl, and a final rinse with PBS. Cells were removed from the wells by incubation on ice for 30 min in 1 mL/well of Enzyme-free Cell Dissociation Buffer (Gibco®, Life Technologies™, Grand Island, NY). Cells were scraped from the plate and prepared as a single cell suspension by passage through a 27 gauge needle. Peptide-paclitaxel–FITC binding was assessed for 10,000 cells per treatment group by flow cytometry using a

CellQuanta™ flow cytometer (Beckman Coulter, Inc., Brea, CA). Cells were gated by size and side scatter properties, and FITC assayed by fluorescence in channel 1 (excitation 395 nm, emission 488 nm).

6.2.13 *Drug Competition of Free H2009.1 Peptide with H2009.1-Paclitaxel Conjugate*

H2009 cells were plated at 1000 cell/well in 96-well plates one day prior to the treatment to allow the cells to adhere to the plate. The next day, the cells were pre-incubated with 10 μM H2009.1 tetrameric peptide for 1 hour then 1 μM H2009.1-paclitaxel conjugate was added. After 10 min, cells were washed three times with 200 μL R5 before continuing culture in 100 μL R5 for 120 hours. Cell viability was determined using the ATP-based CellTiter-Glo® Luminescent Cell Viability Assay (Promega Corporation, Fitchburg, WI). Luminescence was detected using a SpectraMax M5 Multi-Mode Microplate Reader (Molecular Devices, Sunnyvale, CA).

6.2.14 *Cell Cycle Analysis for Cells Treated with the H2009.1-Paclitaxel Conjugate*

Cell cycle perturbations induced by the H2009.1–paclitaxel conjugate were analyzed by propidium iodide (PI) DNA staining with flow cytometric analysis. H2009 cells were seeded in 12 well culture plates at approximately 100,000 cells per well and allowed to adhere overnight. Cells were treated with free paclitaxel or the H2009.1–paclitaxel conjugate at different concentrations for 10 min. Drugs were removed and the cells washed with R5 three times followed by recovering for 24 or 48 hours. At the end of each treatment, cells were collected, resuspended in 0.5 mL PBS and fixed in 70%

ethanol for 12 hours at 4 °C. Ethanol-suspended cells were centrifuged at 3000 rpm for 5 min and washed twice in PBS to remove residual ethanol. Cell pellets were suspended in 1 mL of PBS containing 0.02 mg/mL of PI and 0.5 mg/mL of DNase- free RNase A and incubated at 37 °C for 1 hour. Cell cycle profiles were studied using a CellQuanta™ flow cytometer (Beckman Coulter, Inc., Brea, CA), and data were analyzed by WinMDI 2.9 software.

6.2.15 *Apoptosis Assay for Cells Treated with the H2009.1-Paclitaxel Conjugate*

Drug induced apoptosis was analyzed by Vybrant® FAM Poly Caspases Assay which detects activated caspases 1, 3, 4, 5, 6, 7, 8, and 9 (Life Technologies™, Grand Island, NY). Briefly, H2009 cells were plated and exposed to 1 μM drug for 10 min followed by different recovery times. Both suspended and adherent cells were collected and subjected to caspases/PI staining using Vybrant® FAM Poly Caspases Assay Kit according to the protocol provided by the manufacturer. Stained cells were analyzed on a CellQuanta™ flow cytometer (Beckman Coulter, Inc., Brea, CA). Data were analyzed by WinMDI 2.9 software.

6.2.16 *Cell Viability*

For the H2009.1-doxorubicin conjugate cell viability studies, H2009 cells were plated in Corning® Costar® 96-well, black, clear bottom cell culture plates (Fisher Scientific, Pittsburg, PA). The cells were seeded at 2,000 cells/well in a volume of 50 μL R5 media per well. After 24 hours, cells were treated with various concentrations of the

conjugate dissolved in 50 μL R5 to produce a final volume of 100 μL and final concentrations ranging from 10 – 20480 nM (based on total doxorubicin concentration). Untreated cells were incubated with R5 media alone. Each treatment was performed in sets of 8 replicates. After incubation with the conjugate for 1 hour, all wells were washed twice with 100 μL of R5 before the addition of 100 μL of fresh R5. The cells were maintained at 37°C and 5% CO_2 for an additional 96 hours, with one media change at 72 hours. At 120 hours, cell viability was determined using the ATP-based CellTiter-Glo® Luminescent Cell Viability Assay (Promega Corporation, Fitchburg, WI). Luminescence was detected using a SpectraMax M5 Multi-Mode Microplate Reader (Molecular Devices, Sunnyvale, CA).

For the H2009.1-paclitaxel conjugate cell viability studies, H2009 or H460 cells were plated in Corning® Costar® 96-well, black, clear bottom cell culture plates (Fisher Scientific, Pittsburg, PA). The cells were seeded at 1,000 cells/well in a volume of 50 μL media per well. After 24 hours, free paclitaxel, H2009.1-paclitaxel conjugate, or scH2009.1-paclitaxel conjugate were added to quadruplicate wells in 50 μL R5 media to produce the final concentrations indicated (ranging from 1 nM to 1 μM, all based on total paclitaxel concentration). Untreated control cells received 50 μL R5 only and were cultured as a set of eight replicate wells per plate. After 10 min of exposure to the drug, media was aspirated from all wells, and the wells were washed four times with 200 μL R5 before continuing the culture in 100 μL R5 for varying periods of time (from 24 to 120 hours). At the end of the post-treatment incubation, cell viability was assessed using the ATP-based CellTiter-Glo® Luminescent Cell Viability Assay (Promega Corporation,

Fitchburg, WI). Luminescence was detected using a SpectraMax M5 Multi-Mode Microplate Reader (Molecular Devices, Sunnyvale, CA).

6.2.17 *Establishment of Mouse Tumor Models*

Animal protocols were approved by the Institutional Animal Care and Use Committee at UT Southwestern Medical Center. Female NOD/SCID mice (from the UT Southwestern Medical Center Mouse Breeding Core Facility) were injected with 1 million H2009 cells in the right flank. All cells were injected in PBS, pH 7.4, and were prepared for injection by incubating the cells with 0.05% Trypsin-EDTA (Gibco®, Life Technologies™, Grand Island, NY) for 10 minutes, quenching the trypsin with media, and washing the cells with PBS before final suspension in PBS at a concentration of 10 million cells per mL.

6.2.18 *H2009.1-Doxorubicin Conjugate In Vivo Therapeutic Experiments*

Subcutaneous H2009 tumors were established in the flank of NOD/SCID mice. Once palpable tumors had formed, 18 days after tumor cell implantation, the mice were treated with PBS (control) or the H2009.1-doxorubicin conjugate, based on the total concentration of doxorubicin. The different treatment doses are described in detail in Section 6.3. For all experiments, mice were treated once weekly for 3 weeks, on days 18, 25, and 32, via tail vein injection. Tumors were measured by an independent scientist, and tumor volumes were calculated from the formula $V = (l \times w^2)/2$.

6.2.19 *H2009.1-Paclitaxel Conjugate In Vivo Therapeutic Experiments*

Subcutaneous H2009 tumors were established in the flank of NOD/SCID mice. Once palpable tumors had formed, 18 days after tumor cell implantation, the mice were treated with PBS (control), 5 mg/kg of free paclitaxel, or 5 mg/kg of H2009.1-pacliataxel conjugate. The mice were treated every 3 days for a total of 5 injections. Tumors were measured by an independent scientist, and tumor volumes were calculated from the formula $V = (l \times w^2)/2$.

6.2.20 *Statistical Methods*

Test for statistical significance of tumor size differences between drug treated groups and the control group were calculated using one way ANOVA with Dunnett's multiple comparison test and between different drug treated groups, using one way ANOVA with Tukey's multiple comparison test. The statistical significance of differences between survival curves were calculated from Kaplan-Meier curves with log-rank tests. All calculations were determined using GraphPad Prism.

6.3 Results

6.3.1 *Synthesis of H2009.1 Tetrameric Peptide-Doxorubicin Conjugate*

Synthesis of the H2009.1 tetrameric peptide-doxorubicin conjugate was carried out similarly to previously published procedures from our lab.[114] First, a hydrazone derivative of doxorubicin, formed by reacting doxorubicin with a β-maleimidopropinoic acid (BMPH) linker, was synthesized (Scheme 6-3). Then, the maleimide portion of the

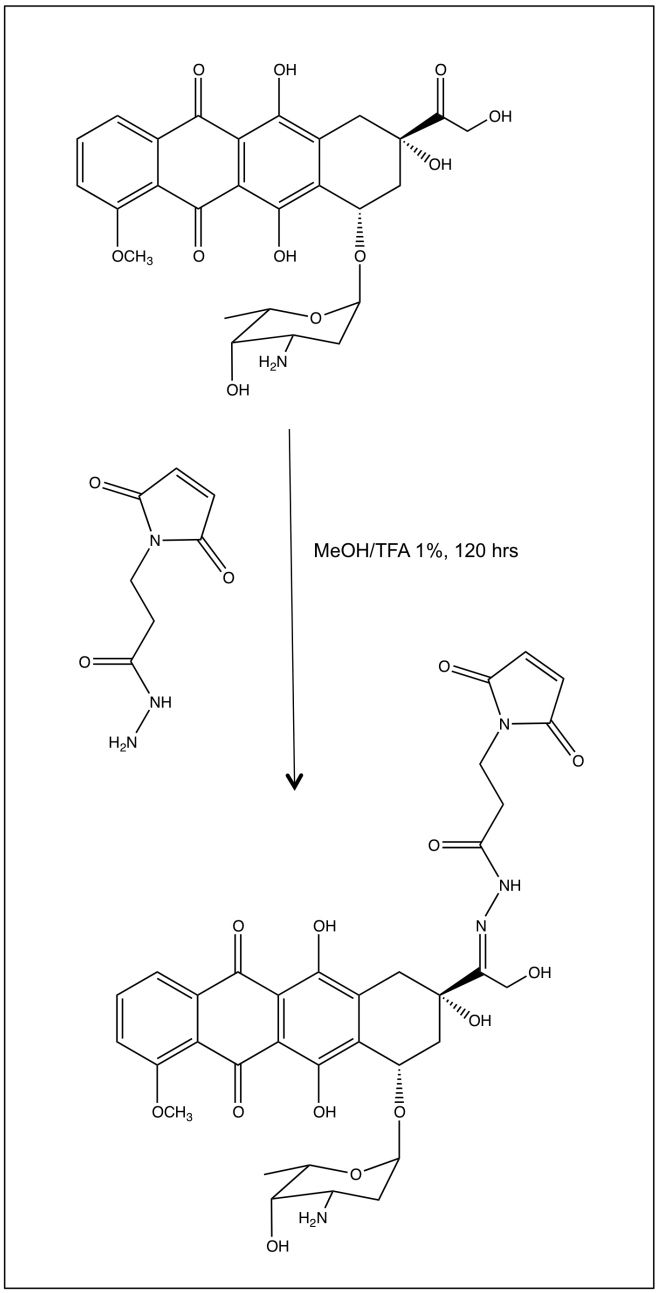

Scheme 6-1. Synthesis of hydrazone derivative of doxorubicin by reaction of doxorubicin with β-maleimidopropionic acid hydrazide.

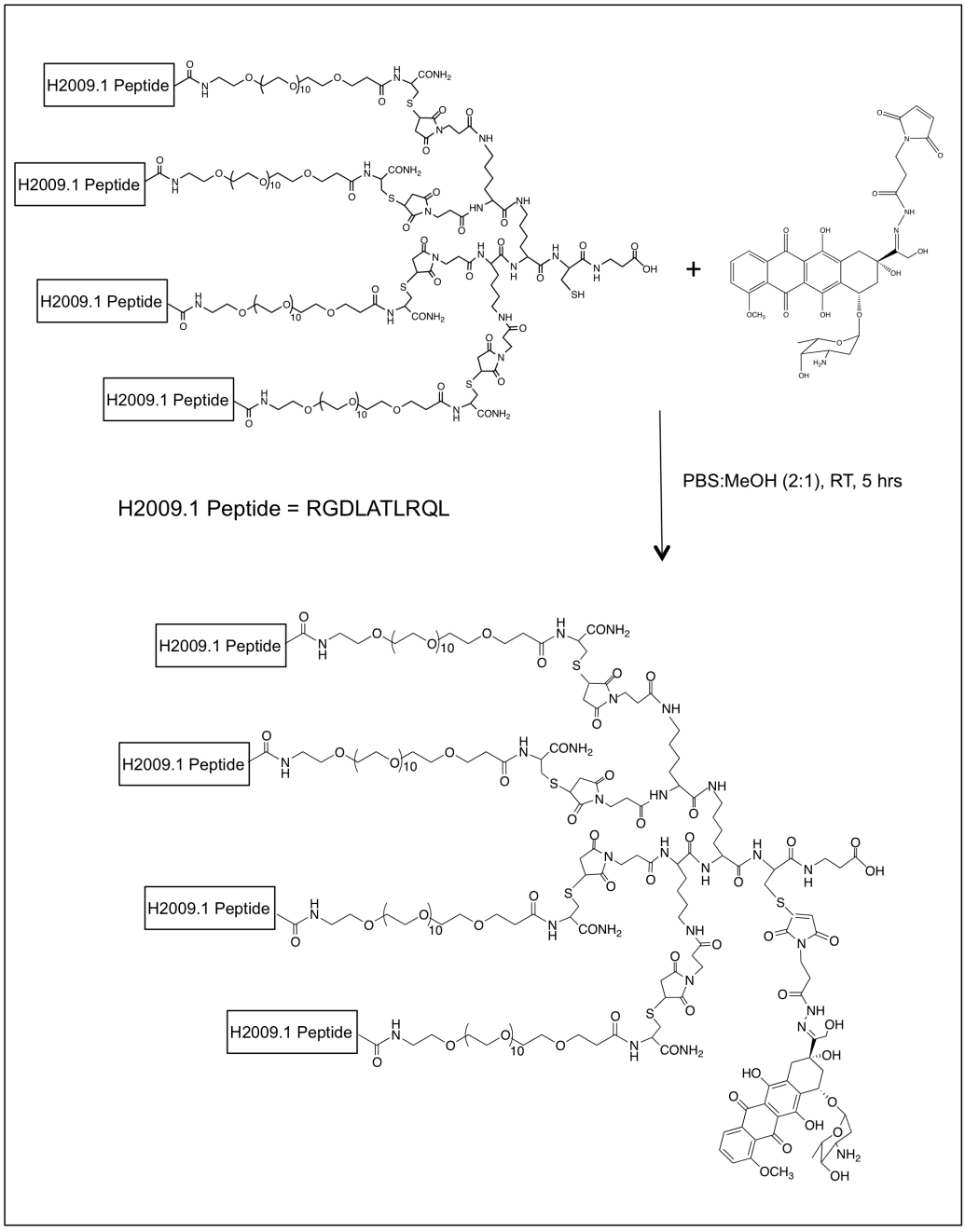

Scheme 6-2. Synthesis of H2009.1 tetramer peptide-doxorubicin conjugate by reaction of the H2009.1 tetrameric peptide with the hydrazone derivative of doxorubicin.

hydrazone drug derivative was reacted with a unique cysteine placed before the branch point of the H2009.1 tetrameric peptide to create the H2009.1-doxorubicin conjugate (Scheme 6-2). As hydrazine linkers are stable at neutral pH, this conjugate should remain intact with an inactive drug moiety until encountering lower pH compartments upon cell internalization. Thus, the H2009.1-doxorubicin conjugate is expected to internalize into $\alpha_v\beta_6$ expressing cells and release the doxorubicin cargo once inside these cells.

6.3.2 *Accumulation of the H2009.1-Doxorubicin Conjugate in $\alpha_v\beta_6$-Positive H2009 Cells*

To verify that the H2009.1-doxorubicin conjugate retains $\alpha_v\beta_6$-specificity and that the drug does not interfere with peptide binding, I incubated $\alpha_v\beta_6$-positive H2009 cells with the conjugate and measured the amount of doxorubicin internalized into the cells. After incubation with the conjugate, the cells were washed to remove unbound conjugate and then lysed with detergent to quantify the amount of cell-associated doxorubicin via total doxorubicin fluorescence. Based on a standard curve of free doxorubicin, this assay was able to detect doxorubicin amounts above ~0.4 pmole. Cells were counted prior to fluorescence measurements so that the doxorubicin concentration could be normalized on a per cell basis; therefore, the results are calculated as picomoles of doxorubicin per 10,000 cells. Figure 6-1 shows the internalization of the H2009.1-doxorubicin conjugate into H2009 cells compared to both free doxorubicin and the 1.3% H2009.1 tetrameric liposomal doxorubicin formulation over a range of doxorubicin concentrations. The cell accumulation of both the free doxorubicin and 1.3% H2009.1

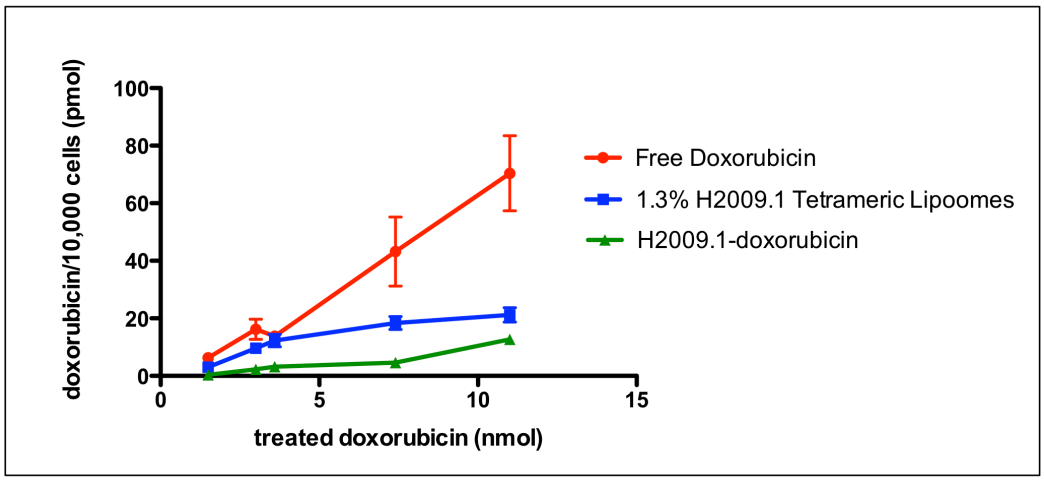

Figure 6-1. The H2009.1-doxorubicin conjugate targets and internalizes into $\alpha_v\beta_6$-expressing cells. $\alpha_v\beta_6$-expressing H2009 cells were incubated with increasing concentrations of the H2009.1-doxorubicin conjugate. Cellular doxorubicin levels were determined as pmol doxorubicin/10,000 cells.

tetrameric liposomes was described in more detail in Chapter 4. As is often observed, free doxorubicin accumulated easily in the H2009 cells. Interestingly, the H2009.1-doxorubicin conjugate internalized into H2009 cells at levels only 4-fold below those of the 1.3% H2009.1 tetrameric liposomes. This is significant because each liposome carries approximately 2.6 x 10^4 molecules of doxorubicin. Therefore, one successful targeting event initiated by the H2009.1 tetrameric peptide on a liposome surface leads to the internalization of 26,000 molecules of doxorubicin. Conversely, the 1:1 ratio of peptide:drug exhibited by the H2009.1-doxorubicin conjugate means that one successful targeting event leads to the delivery of only 1 doxorubicin molecule. To achieve levels of cell targeting 4-fold below the H2009.1 liposomes, the H2009.1-doxorubicin conjugate must initiate 6,500 targeting events for every targeting event initiated by a liposome.

Thus, the H2009.1-doxorubicin conjugate appears to target and internalize efficiently into $\alpha_v\beta_6$-expressing cells.

6.3.3 *Drug Release from the H2009.1-Doxorubicin Conjugate*

As doxorubicin must enter the cell nucleus in order to exert its effects, it is important to verify that the H2009.1-doxorubicin conjugate can release the drug, freeing it to accumulate in the nucleus. To visualize the subcellular localization of the conjugate and the entry of doxorubicin into the nucleus, H2009 cells were incubated with either free doxorubicin or the H2009.1-doxorubicin conjugate and doxorubicin fluorescence was examined by confocal microscopy (Figure 6-2). As previously demonstrated in Chapter 4, free doxorubicin was visible in the cell nucleus as early as 1 hour after incubation and began to visibly affect cell structure 48 hours after treatment. By 72 hours, cells treated with free doxorubicin began to bleb, indicative of apoptosis. In contrast, the H2009.1-doxorubicin conjugate initially appeared perinuclear and remained in this compartment of the cell at 48 hours post-treatment. Although doxorubicin was never observed primarily in the nuclei of conjugate treated cells, by 72 hours, the cells appeared bloated and abnormal, and at 96 hours they began to bleb. As nuclear drug accumulation is not visible, the conjugate likely breaks down slowly, releasing low concentrations of drug to the nucleus at levels not detectable by microscopy. Alternatively, the drug remains cytoplasmic and exerts its effects by a different mechanism.

The initial perinuclear localization of the H2009.1-doxorubicin conjugate appears almost identical to the perinuclear localization of the 1.3% H2009.1 tetrameric liposomes as demonstrated in Chapter 4. While the liposomes affected cellular structure and

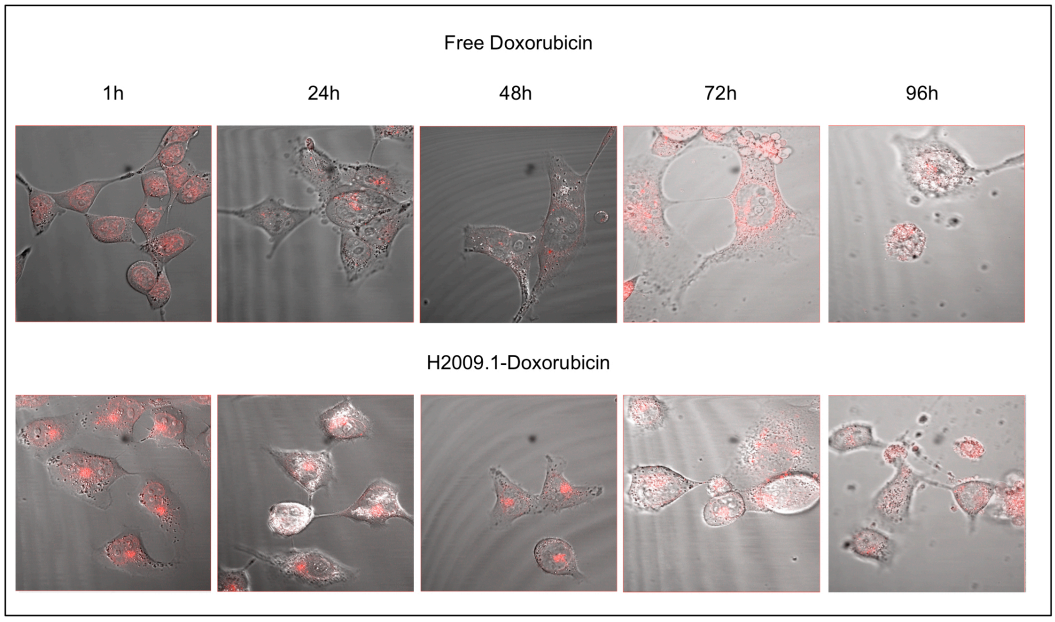

Figure 6-2. Time course for release of doxorubicin from the H2009.1-doxorubicin conjugate. Cells were treated with either free doxorubicin or H2009.1-doxorubicin for 1 hour before the drug was removed. Doxorubicin fluorescence was observed by confocal microscopy at the indicated time after initial treatment.

initiated cell death on the same time frame as the H2009.1-doxorubicin conjugate, doxorubicin was visible in the nuclei of liposome treated cells 48 hours after treatment. Therefore, while the H2009.1-doxorubicin conjugate enters cells in a manner similar to that of H2009.1-targeted liposomes, drug accumulation in the nucleus occurs at different efficiencies. However, both H2009.1-targeted constructs initiate cell death starting at 96 hours, indicating that they both release active doxorubicin around the same time.

Table 6-1. IC_{50} values of H2009.1-Doxorubicin Conjugate Compared to 1.3% H2009.1 Liposomal Doxorubicin Formulations on the $\alpha_v\beta_6$-Positive H2009 Cells.[a]

Drug Formulation	IC_{50} on H2009 cells (nM)
H2009.1-Doxorubicin	6300 ± 940
1.3% H2009.1 Monomeric Liposomes	5700 ± 120
1.3% H2009.1 Tetrameric Liposomes	970 ± 130
Free Doxorubicin	430 ± 75

a – Cells were incubated with the different drug formulations for 1 hour followed by a 120 hour recovery in media.

6.3.4 *Cytotoxicity of the H2009.1-Doxorubicin Conjugate*

To examine the ability of the H2009.1-doxorubicin conjugate to induce cell death, the IC_{50} of the conjugate was determined for the $\alpha_v\beta_6$-positive H2009 cells. As detailed in Table 6-1, the H2009.1-doxorubicin conjugate had an IC_{50} of 6300 ± 940 nM on the H2009 cells. As expected from the 4-fold lower accumulation of the conjugate compared to the liposomes in cells, the IC_{50} of the conjugate is 6-fold higher than the IC_{50} of the 1.3% H2009.1 tetrameric liposomes (970 ± 130 nM). Significantly, the IC_{50} of the H2009.1-doxorubicin conjugate is similar to the IC_{50} of the 1.3% H2009.1 monomeric peptide liposomes (5700 ± 120).

6.3.5 In vivo *Efficacy of the H2009.1-Doxorubicin Conjugate Targeting* $\alpha_v\beta_6$

In order to examine the *in vivo* toxicity of the H2009.1-doxorubicin conjugate, mice bearing $\alpha_v\beta_6$-expressing H2009 NSCLC tumors were treated with either phosphate buffered saline (PBS) as a control, free doxorubicin, or the H2009.1-doxorubicin

conjugate. As with the liposome *in vivo* experiments (Chapter 5), $\alpha_v\beta_6$-expressing H2009 cells were injected into NOD/SCID mice to form subcutaneous H2009 xenografts and treatment started at day 18, once the mice had formed palpable tumors. Mice were initially treated with 2 mg/kg (total doxorubicin concentration) once weekly for 3 weeks. As demonstrated in Figure 6-3a and previously shown in Chapter 5, 2 mg/kg of free doxorubicin inhibited tumor growth compared to growth in control mice ($p < 0.05$ at day 57). Although the H2009.1-doxorubicin conjugate slightly inhibited tumor growth compared to that in control mice, there was no statistical difference in tumor growth between these two groups. Additionally, free doxorubicin inhibited tumor growth better than the H2009.1-doxorubicin conjugate ($p < 0.01$ at day 64).

Free doxorubicin is toxic to mice at a dosing of 4 mg/kg, with the free doxorubicin mice all dying after receiving two weekly injections of 4 mg/kg. Therefore, I next examined whether mice could tolerate a 4 mg/kg dosing regimen of the H2009.1-doxorubicin conjugate and whether this higher dose of conjugate would improve tumor inhibition. Unlike a higher dose of free doxorubicin, the higher dose of the H2009.1-doxorubicin conjugate did not exhibit any obvious toxicity towards the mice. The mice gained weight throughout the study (Figure 6-4b) and were able to receive all 3 injections of the conjugate. Thus, conjugation of the H2009.1 peptide to doxorubicin reduces off target effects and toxicity of doxorubicin in non-target tissues. However, the 4 mg/kg treatment of H2009.1-doxorubicin did not improve tumor inhibition compared to the lower dose 2 mg/kg treatment of conjugate (Figure 6-3b). The 2 mg/kg and 4 mg/kg

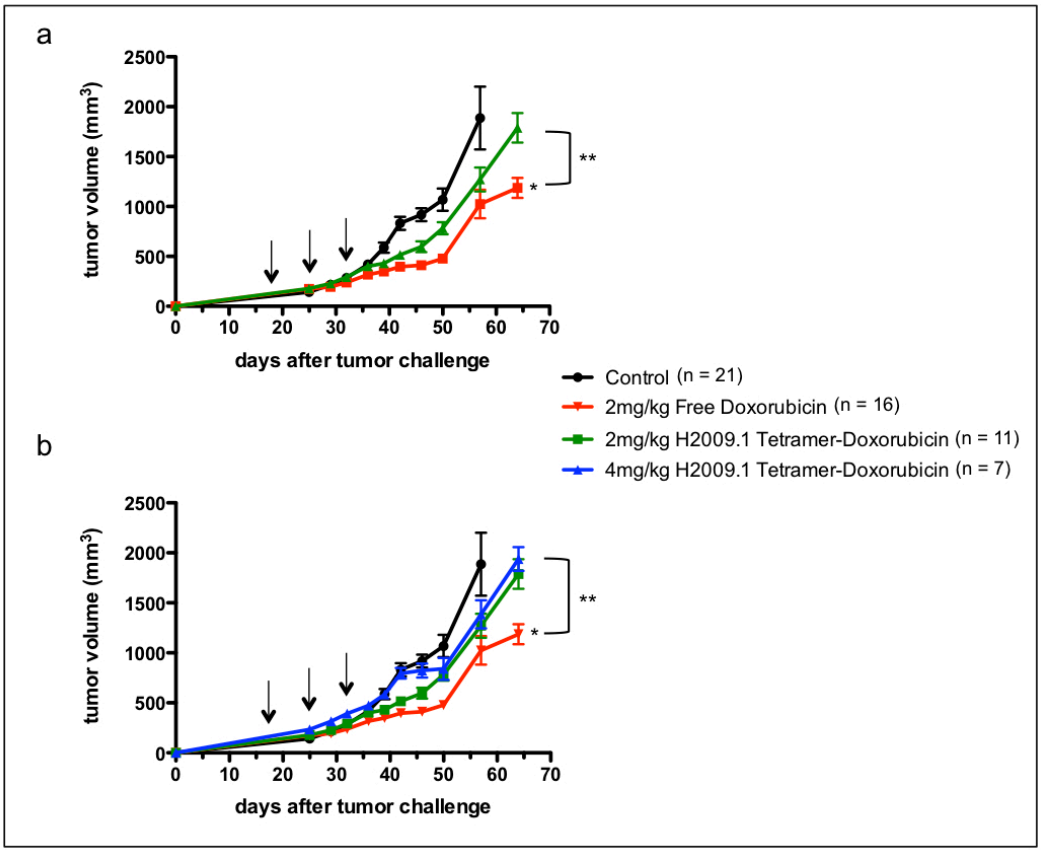

Figure 6-3. Treatment with the H2009.1-doxorubicin conjugate does not significantly inhibit tumor growth compared to control mice. Subcutaneous H2009 tumors were established in the flank of NOD/SCID mice. Once palpable tumors had formed, 18 days after tumor cell implantation, the mice were treated with PBS (control), 2 mg/kg of free doxorubicin, 2 mg/kg of H2009.1-doxorubicin, or 4 mg/kg of H2009.1-doxorubicin. Mice were treated once weekly for 3 weeks, on days 18, 25, and 32, as indicated by the arrows. Tumors were measured by an independent scientist, and tumor volumes were calculated from the formula $V = (l \times w^2)/2$. * $p < 0.05$ verses control at day 57. ** $p < 0.01$ between 2 mg/kg free doxorubicin and both treatment doses of H2009.1-doxorubicin at day 64.

conjugate tumor growth curves overlapped for the majority of the tumor measurements, and both were significantly less efficient at inhibiting tumor growth compared to 2 mg/kg treatments with free doxorubicin ($p < 0.01$ for both conjugate doses compared to free doxorubicin at day 64). Additionally, both doses of the conjugate increased survival to the same extent, although this increase was not statistically significant compared to control mice (Figure 6-4a). Interestingly, while all of the control and conjugate treated mice gained weight throughout the studies, mice treated with 2 mg/kg free doxorubicin lost weight during their treatment and did not regain the weight until more than a week after their last treatment with the drug (Figure 6-4b). It is clear that the H2009.1-doxoroubicin conjugate is less toxic to the mouse than free doxorubicin.

It is important to point out the large difference in tumor inhibition between the 1.3% H2009.1 tetramer liposomes and the H2009.1-doxorubicin at a 4 mg/kg treatment concentration. At day 64 the tumors from mice treated with 1.3% H2009.1 tetramer liposomes were 9-fold smaller than the tumors from mice treated with the H2009.1-doxorubicin conjugate (Figure 6-5). Therefore, the H2009.1 tetrameric peptide liposome inhibits tumor growth better than the direct drug conjugate, and the H2009.1-doxorubicin conjugate does not inhibit tumor growth as well as the free drug.

The ability of the free doxorubicin to inhibit tumor growth better than the H2009.1-doxorubicin conjugate is not entirely unexpected considering the higher IC_{50} of the conjugate compared to the free drug *in vitro*. However, it is surprising that the H2009.1-doxorubicin conjugate does not significantly reduce tumor growth compared to

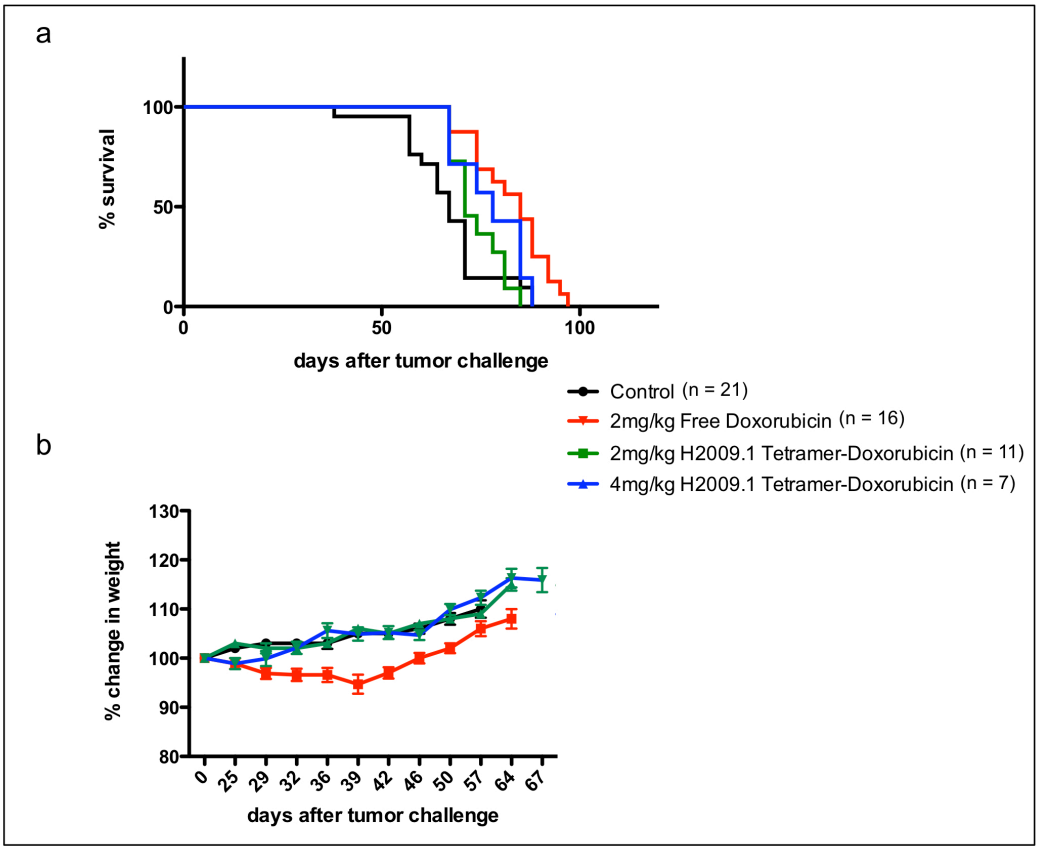

Figure 6-4. Treatment with the H2009.1-doxorubicin conjugate does not significantly increase survival or alter weight gain compared to control mice. Subcutaneous H2009 tumors were established in the flank of NOD/SCID mice. Once palpable tumors had formed, 18 days after tumor cell implantation, the mice were treated with PBS (control), 2 mg/kg of free doxorubicin, 2 mg/kg of H2009.1-doxorubicin, or 4 mg/kg of H2009.1-doxorubicin. Mice were treated once weekly for 3 weeks, on days 18, 25, and 32, as indicated by the arrows in (a). Tumors were measured by an independent scientist, and tumor volumes were calculated from the formula $V = (l \times w^2)/2$. (a) Kaplan-Meier survival curves. (b) Percent change in mouse weight.

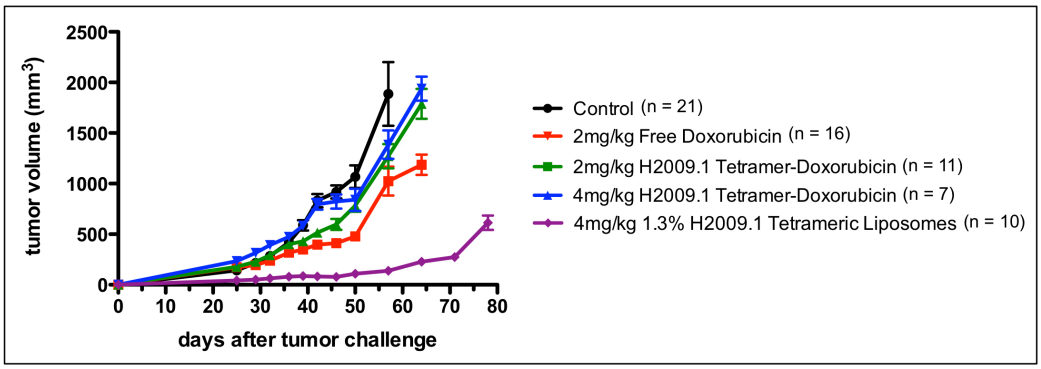

Figure 6-5. H2009.1 tetrameric liposomal doxorubicin inhibits tumor growth better than either the H2009.1-doxorubicin conjugate or free doxorubicin.

control mice as the H2009.1 tetrameric peptide specifically targets H2009 tumors *in vivo* (Chapter 2). It will be important to determine the biodistribution and pharmacokinetic profile of the H2009.1-doxorubicin conjugate to identify the reason for poor *in vivo* efficacy. Possible reasons include an inability of the conjugate to target the tumor, inefficient or premature release of the doxorubicin from the conjugate, or poor tumor penetration and distribution. However, it is encouraging that the H2009.1-doxorubicin conjugate renders the doxorubicin significantly less toxic to mice. The mice can handle a conjugate dosing regimen twice that of the free drug, suggesting that the H2009.1 peptide prevents accumulation of the drug in off-target tissues. Therefore, assuming the conjugate is found to localize to the tumor tissue, it may be possible to use a different drug linker or a different drug to improve the efficacy of a H2009.1 peptide-drug direct conjugate.

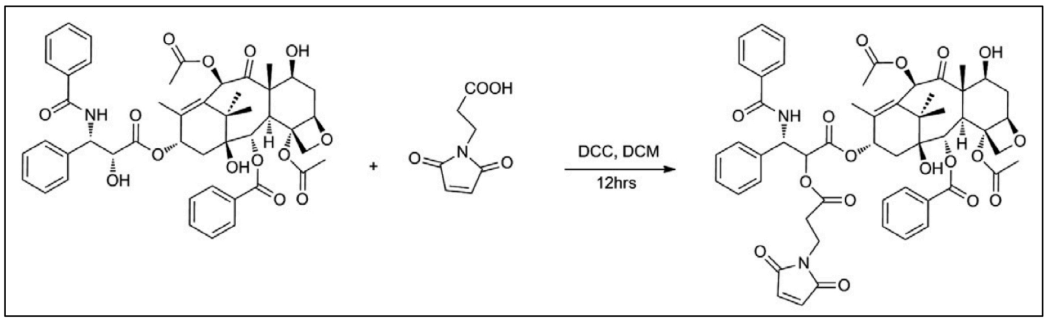

Scheme 6-3. Synthesis of 2'-maleimido-paclitaxel from reaction of paclitaxel with β-maleimidopropionic acid.

6.3.6 *Synthesis of H2009.1 Tetrameric Peptide-Paclitaxel Conjugate*

Paclitaxel might be a better drug choice for conjugation to the H2009.1 peptide. It is more toxic to cells, meaning that less drug must internalize and release to induce cell death. Additionally, paclitaxel is clinically used for the treatment of NSCLC. Although paclitaxel contains both 2'-hydroxyl and 7'-hydroxyl groups available for conjugation, the 2'-hydroxyl reacts preferentially due to steric hindrance at the 7'-hydroxyl group. Therefore, reaction of paclitaxel with β-maleimidopropionic acid resulted in a 2'-maleimide-paclitaxel conjugate (Scheme 6-3). The reaction proceeded with 68% yield, and ^{1}NMR analysis of the product demonstrated a C-2' proton shift from the 4.71 ppm seen with free paclitaxel to 5.47 ppm for the conjugate. The free paclitaxel 2'-OH proton resonance at 3.55 ppm also disappeared while the C-7' resonance remained unchanged, confirming an ester bond at the C-2' position.

The H2009.1 tetrameric peptide-paclitaxel conjugate was prepared by chemoselective reaction of the thiol in the unique cysteine of the peptide with the maleimide group of the 2'-maleimide-paclitaxel conjugate and proceeded with

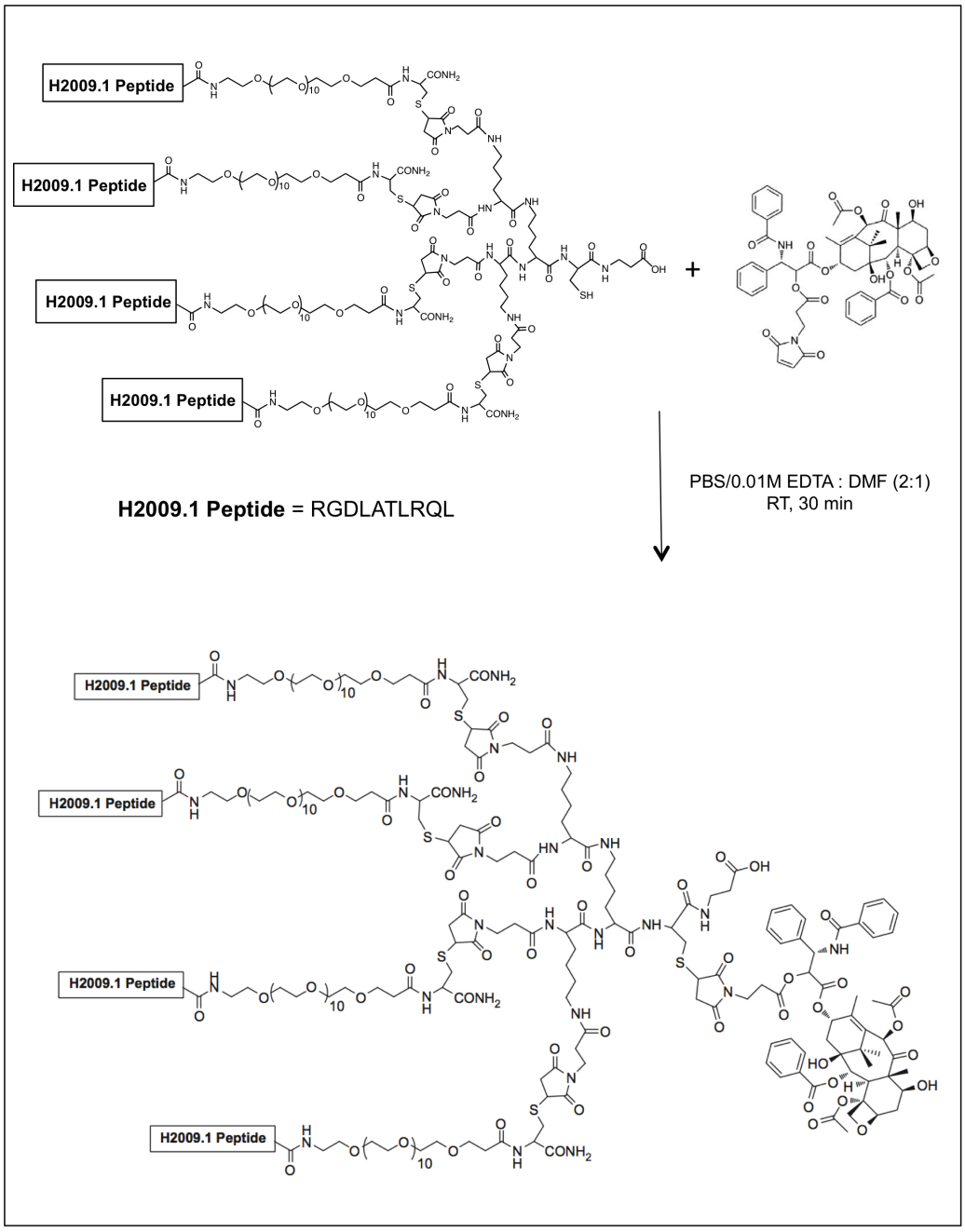

Scheme 6-4. Synthesis of H2009.1 tetrameric peptide-paclitaxel from reaction of the H2009.1 tetrameric peptide with 2'-maleimide-paclitaxel.

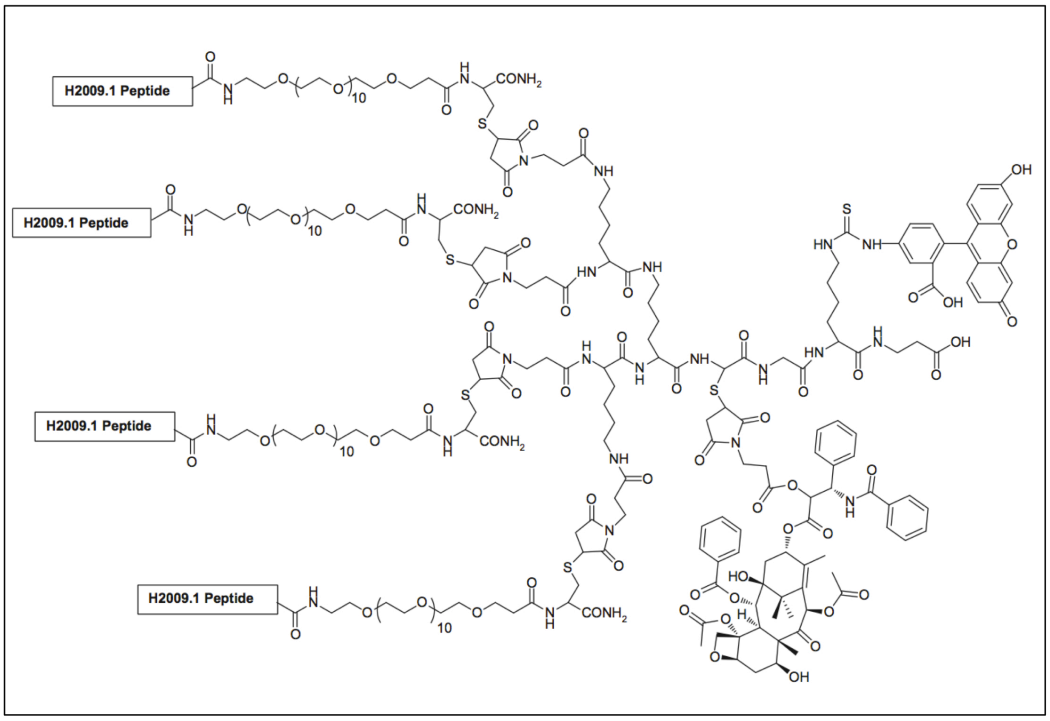

Figure 6-6. Structure of the FITC-labeled H2009.1-paclitaxel conjugate.

approximately 90% yield (Scheme 6-4). A control scH2009.1 tetrameric peptide-paclitaxel conjugate was also prepared in the same manner. The scH2009.1 tetrameric peptide is a control sequence scrambled version of the H2009.1 peptide that contains the same amino acids as the H2009.1 peptide except in a scrambled order. Both the H2009.1 and scH2009.1-paclitaxel conjugates were soluble in cold water and in most polar organic solvents, including chloroform and methanol. As free paclitaxel is insoluble in water and requires an oil-based emulsifier vehicle (Cremophor® EL) for administration to patients, the water solubility of the peptide-paclitaxel conjugates is a great advantage.

6.3.7 *Accumulation of the H2009.1-Paclitaxel Conjugate in $\alpha_v\beta_6$-Positive H2009 Cells*

It is important to verify that the H2009.1-paclitaxel conjugate retains the same $\alpha_v\beta_6$-specificity as the free H2009.1 tetrameric peptide. Although the paclitaxel is attached to the peptide away from the peptide binding domain, steric hindrance may inhibit peptide binding. Therefore both the H2009.1-paclitaxel conjugate and the control scH2009.1 paclitaxel-conjugates were labeled with the dye fluorescein (FITC) (Figure 6-6) so that the binding of the conjugates to $\alpha_v\beta_6$-positive H2009 cells could be quantified by flow cytometry. While the control scH2009.1-paclitaxel conjugate did not bind to H2009 cells, the H2009.1-paclitaxel conjugate bound the cells with a mean fluorescence intensity (MFI) 3.3-fold larger than that of the scH2009.1 conjugate (Figure 6-7). Thus the binding of the H2009.1-paclitaxel conjugate is due solely to the H2009.1 peptide and not to the presence of the paclitaxel. To verify the $\alpha_v\beta_6$-specificity of the H2009.1-paclitaxel conjugate, the H460 cells were used as a control $\alpha_v\beta_6$-negative cell line. While H460 cells express $\alpha_v\beta_3$, $\alpha_5\beta_1$, and $\alpha_v\beta_5$, they do not express $\alpha_v\beta_6$.[81] The H2009.1-paclitxel conjugate only exhibits minimal binding to the H460 cells and binds at the same level as the scH2009.1-paclitaxel conjugate, indicating that conjugation of paclitaxel to the H2009.1 peptide does not alter $\alpha_v\beta_6$-specificity by increasing binding to the $\alpha_v\beta_6$-negative H460 cells.

6.3.8 *Paclitaxel Release from the H2009.1-Paclitaxel Conjugate*

As the 2'-hydroxyl group of paclitaxel is required for tubulin binding and activity of the drug,[400, 401] paclitaxel is not expected to retain activity while conjugated to the

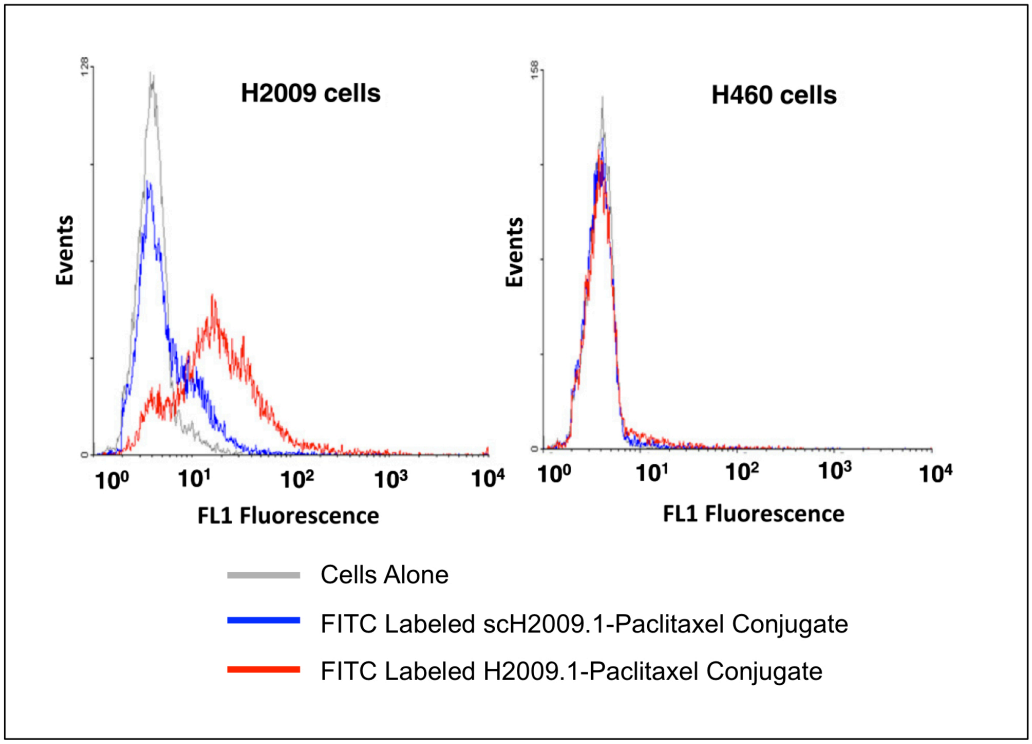

Figure 6-7. The H2009.1-paclitaxel conjugate binds specifically to $\alpha_v\beta_6$-expressing cells. $\alpha_v\beta_6$-positive H2009 or $\alpha_v\beta_6$-negative H460 cells were incubated for 1 hour with 1 M of either the H2009.1 or scH2009.1-paclitaxel conjugates labeled with FITC. Conjugate binding was measured by flow cytometry. A total of 10,000 events were evaluated for fluorescence in channel 1 (excitation at 488 nm, emission at 500 – 550 nm).

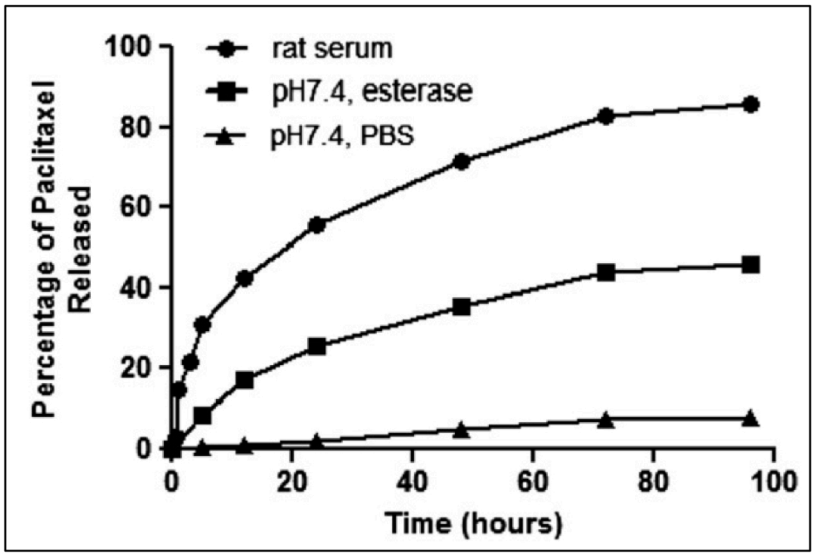

Figure 6-8. Paclitaxel releases from the H2009.1-paclitaxel conjugate in the presence of both esterase and serum. The H2009.1-paclitaxel conjugate was dissolved in either 0.01 M PBS at pH 7.4, esterase (18 μg/mL) in PBS, or rat serum. All incubations were performed at 37°C. Paclitaxel release was measured by HPLC at 3, 8, 24, 48, 72, and 96 hours.

H2009.1 peptide at the 2' position. Paclitaxel must therefore release from the H2009.1 peptide to be active. However, it is important that the H2009.1-paclitaxel conjugate remain intact until after cellular internalization so that the H2009.1 peptide can successfully carry the drug to tumors *in vivo*. The ester linkage between the H2009.1 peptide and paclitaxel is expected to remain stable until exposure to esterases and proteases inside of cells. To examine the stability of the H2009.1-paclitaxel conjugate, the release of paclitaxel from the conjugate was determined in both PBS buffer (pH 7.4) and PBS buffer containing porcine esterase. Even after 96 hours of incubation, only minimal release of paclitaxel was observed in PBS buffer (Figure 6-8). Incubation with PBS containing esterase increased the drug release 7-fold, leading to 34.1% release at 48

hours. However, the release is still inefficient. Incubation with rat serum further increased drug release, leading to 70% paclitaxel release by 48 hours and a half-life of approximately 20 hours. Other reported paclitaxel ester linkers exhibit similar serum half-lives.[402] The increased drug release in serum likely results from the presence of additional proteases or esterases in the serum. While the release of paclitaxel in serum suggests that the drug may release from the conjugate while in circulation *in vivo*, 86% of the conjugate is still intact after 1 hour in rat serum, and the conjugate is expected to clear from the bloodstream due to renal filtration within this time frame. As the free H2009.1 tetrameric peptide has a half-life of 14 hours in human serum, the peptide should also be sufficiently stable to deliver drug.

6.3.9 *In Vitro Toxicity of the H2009.1-Paclitaxel Conjugate*

To verify that the H2009.1-paclitaxel conjugate delivers paclitaxel to cells and releases the drug to exert its effects, the cytotoxicity of free paclitaxel, H2009.1-paclitaxel, and scH2009.1-paclitaxel were determined in $\alpha_v\beta_6$-positive H2009 cells. The IC_{50} values for each drug formulation are listed in Table 6-2. Importantly, the H2009.1-paclitaxel conjugate specifically killed cells compared to the control scH2009.1-paclitaxel conjugate. The H2009.1-paclitaxel conjugate had an IC_{50} of 460 nM while the IC_{50} of the scH2009.1 conjugate was never reached, even at treatment concentrations of 1 μM. These results verify that the specific sequence of H2009.1 peptide drives delivery of active paclitaxel to $\alpha_v\beta_6$-expressing cells.

Table 6-2. IC_{50} Values of Paclitaxel Conjugates in $\alpha_v\beta_6$-Positive H2009 Cells.[a]

	H2009 cells	H460 cells
Paclitaxel	14.8 ± 3.3 nM	23.6 ± 7.4 nM
H2009.1-paclitaxel	460 ± 75 nM	Not reached[b]
scH2009.1-paclitaxel	Not reached[b]	Not reached[b]

a – Cells were exposed to the drug 10 min followed by a 120 hour recovery in media. The short incubation time assures that cytotoxicity is due to the peptide conjugate and not free paclitaxel prematurely released from the conjugate.
b – Not reached at the highest concentration used, 1 μM.

Despite its paclitaxel targeting ability, the H2009.1-paclitaxel conjugate has reduced potency compared to free paclitaxel, which has an IC_{50} of 15 nM. Direct conjugates commonly reduce the efficacy of drugs compared to their unconjugated counterparts, and other peptide-paclitaxel conjugates exhibit similar reductions in paclitaxel efficacy.[402, 403] Although it is not known why the efficacy of paclitaxel decreases after conjugation to peptides, this decrease could result from reduced cellular uptake of the drug, a slow release of the drug from the peptide, delivery of the paclitaxel to an inappropriate cellular compartment, or subsequent trapping of the drug in the undesired compartment. Despite the reduced efficacy of the H2009.1-paclitaxel *in vitro*, active targeting of the drug *in vivo* may improve delivery to the tumor cells, overcoming this reduction in cell toxicity.

To examine the time dependence of H2009.1-paclitaxel conjugate induced cell death compared to that of the free paclitaxel, the $\alpha_v\beta_6$-positive H2009 cells were treated with 1 μM of the different drug constructs for 10 minutes, and cell viability was determined every 24 hours for a total of 120 hours (Figure 6-9). While free paclitaxel

began to reduce cell viability between 24 and 48 hours, neither of the peptide-paclitaxel conjugates exhibited cell toxicity at the 48 hour time point. However, a visible reduction in viability was observed for the H2009.1-paclitaxel treated cells by 72 hours post-treatment and only 40% of these conjugate treated cells remained at 120 hours. In contrast, the control scH2009.1-paclitaxel conjugate rendered very little cell death, with more than 85% of the cells remaining at 120 hours. The specificity of the H2009.1-paclitaxel conjugate and its ability to deliver active drug within the 10 minute incubation period suggests that conjugate accumulates quickly in the cells and that the delayed and reduced effects of the peptide-bound drug are not due to a lack of cell targeting or slow accumulation in the cells. Instead, the delayed toxicity effects of the H2009.1 conjugate suggest that release of paclitaxel from the conjugate is the limiting step such that the cells require sufficient time with the conjugate to hydrolyze the ester bond and release active and toxic paclitaxel. Alternatively, the drug release could occur efficiently yet the released drug could remain trapped in an intracellular compartment with the rate-limiting step being a slow shuttling of released drug to the cytoplasm.

The specificity of the H2009.1-paclitaxel conjugate was examined by comparing cytoxicity of the conjugate towards $\alpha_v\beta_6$-positive H2009 cells verses $\alpha_v\beta_6$-negative H460 cells. Once again, cells were treated with 1 μM of the different drug constructs for 10 minutes, and cell viability was determined every 24 hours for a total of 120 hours. While free paclitaxel killed both cell types, the H2009.1-paclitaxel conjugate exhibited preferential toxicity towards the $\alpha_v\beta_6$-positive H2009 cells and had very little toxicity towards the $\alpha_v\beta_6$-negative H460 cells (Figure 6-9). Therefore, conjugation of paclitaxel

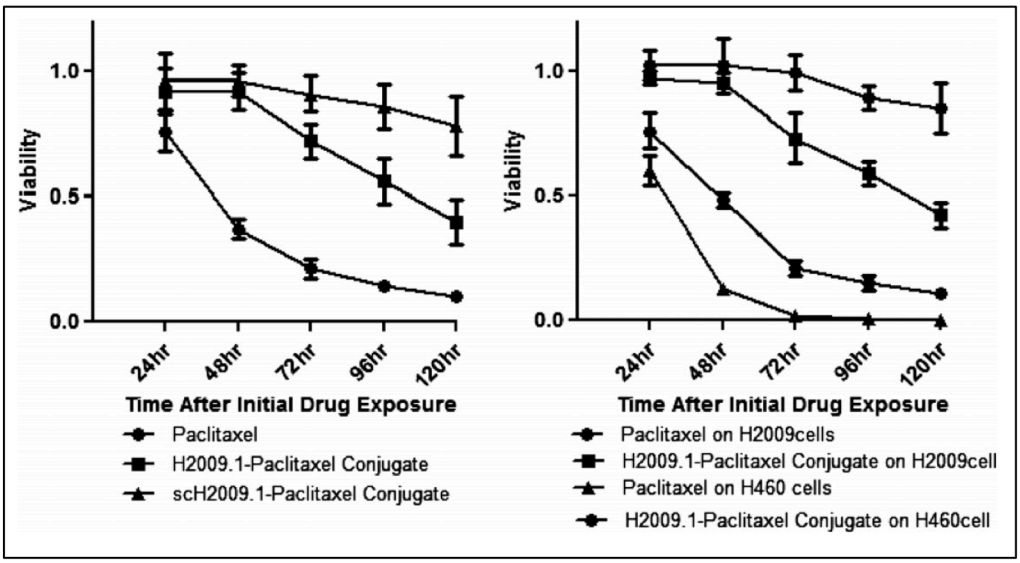

Figure 6-9. The H2009.1-paclitaxel conjugate selectively kills $\alpha_v\beta_6$-expressing cells in a time dependent manner. Cells were incubated with 1 μM the different drug formulations for 10 min, washed, and then incubated in fresh media until the time point indicated. Cell viability is normalized to untreated control cells. Left panel - H2009 cells. Right panel – H2009 and H460 cells.

to the H2009.1 peptide alters paclitaxel specificity, converting the drug from a general cytotoxic agent to an $\alpha_v\beta_6$-specific cytotoxic agent. Thus, despite the reduced *in vitro* efficacy of the H2009.1-paclitaxel conjugate compared to the free paclitaxel, the $\alpha_v\beta_6$-specificity of the conjugate widens the therapeutic window.

6.3.10 In Vitro *Toxicity of the H2009.1-Paclitaxel Conjugate Can Be Blocked By the H2009.1 Peptide*

The $\alpha_v\beta_6$-driven cellular accumulation and toxicity of the H2009.1-paclitaxel conjugate was verified by the ability of free H2009.1 peptide to block the toxicity of the

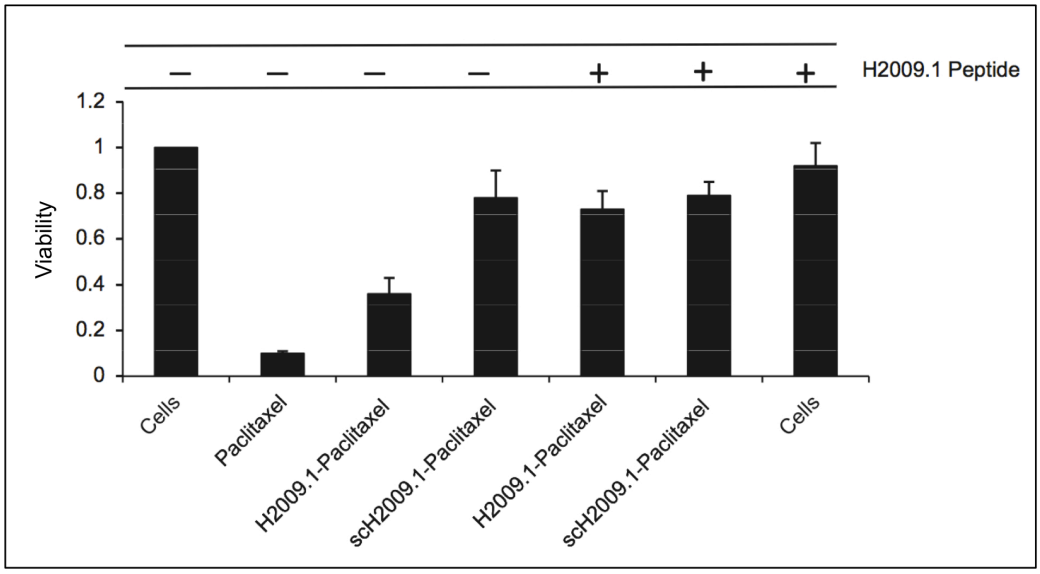

Figure 6-10. The cytotoxicity of the H2009.1-paclitaxel conjugate is blocked by pretreatment with the H2009.1 peptide. H2009 cells were treated with or without 10 μM of the H2009.1 tetrameric peptide for 1 hour, washed, and then treated with 1 μM of free paclitaxel, the H2009.1-paclitaxel conjugate, or the scH2009.1-paclitaxel conjugate. Cell viability was determined at 96 hours.

conjugate (Figure 6-10). H2009 cells were either incubated with the conjugate or pretreated with 10-fold excess of the H2009.1 peptide prior to treatment with the conjugate and tested for viability 120 hours later. While the H2009.1-paclitaxel conjugate reduced cell viability to 36 ± 0.07%, pretreatment with the free H2009.1 peptide protected cells from conjugate toxicity, restoring viability to the level of cells treated with the control scH2009.1-paclitaxel conjugate (cell viability 73 ± 0.08% for the H2009.1 conjugate and 79 ± 0.06% for the scH2009.1 conjugate). Thus, the H2009.1-paclitaxel conjugate enters cells through $\alpha_v\beta_6$-mediated internalization. While a 10-fold excess of H2009.1 peptide was required to inhibit the conjugate toxicity, this large excess in

Table 6-3. Cell Cycle Analysis of H2009 Cells Treated with the H2009.1-Paclitaxel Conjugate[a]

	No Drug		1 μM		5 μM	
	Control cells	Paclitaxel 24 hrs	Conjugate 24 hrs	Conjugate 48 hrs	Conjugate 24 hrs	Conjugate 48 hrs
G1	51	8.5	45	11	36	24
S	11	4.1	8.1	4.5	6.7	8.5
G2/M	31	73	39	57	46	54
Polyploid	6.8	14	8.0	27	12	24

a - All values represent the average of two experiments.

peptide is attributed to multivalent high avidity binding of the conjugate and/or rapid receptor recycling of $\alpha_v\beta_6$.

6.3.11 *The H2009.1-Paclitaxel Conjugate Induces Cell Cycle Arrest*

Paclitaxel functions by stabilizing microtubules and arresting cells in the G2/M phase of the cell cycle, eventually leading to apoptosis.[404] To determine whether the H2009.1-paclitaxel conjugate functions in this same manner, flow cytometry was used to follow perturbations in the cell cycle of conjugate-treated H2009 cells (Table 6-3). At 24 hours after drug treatment, cells treated with 1 μM of free paclitaxel exhibited G2/M cell cycle arrest while cells treated with 1 μM of the conjugate remained unperturbed. However, by 48 hours after treatment, the conjugate treated cells experienced a ~2-fold increase in G2/M arrested cells and a ~3-fold increase in polyploid cells. Therefore, the

H2009.1-paclitaxel functions in the same manner as free paclitaxel, although on a delayed time frame. This delay likely results from the time required to build a sufficient intracellular concentration of free paclitaxel due to the anticipated slow release of the drug from the conjugate. The conjugate also exhibits dose-dependent cell cycle arrest. Treatment with a higher 5 μM concentration of the H2009.1-paclitaxel conjugate produced G2/M arrest at 24 hours, with 50% of the cells arresting compared to the baseline of 31% arrested cells.

6.3.12 *The H2009.1-Paclitaxel Conjugate Induces Apoptosis*

Cell apoptosis is initiated by the activation of a cascade of caspase proteins. To determine the time frame of caspase activation in cells treated with the H2009.1-paclitaxel conjugate, caspase activation in cells was monitored by flow cytometry using the Vybrant® FAM Poly Caspases Assay. Additionally, propidium iodine (PI) was included to distinguish non-viable cells. Starting at 24 hours after treatment with the conjugate, 37% of the cells stained positive for caspase activation (Figure 6-11). Within this caspase-activated subpopulation, 70% of the cells were PI negative and therefore still viable, indicating that the majority of cells are in the early stages of apoptosis. By 96 hours, 43% of the cells stained positive for both caspase activation and PI, indicative of cells in late stage apoptosis with loss of cell membrane integrity. Caspase activation and the extent of apoptosis can be attributed to specific delivery of paclitaxel by the H2009.1 peptide; only 14% of cells treated with the control scH2009.1-paclitaxel conjugate exhibited caspase activation at 96 hours. Significantly, the time course for apoptosis in

the H2009.1-paclitaxel treated cells exhibits the same delay observed in the cytotoxicity and cell cycle arrest studies.

It is important to note that at 144 hours, 27% of the conjugate treated cells remained both caspase and PI negative. Thus, almost a third of the cell population is not affected by the conjugate treatment. There may exist a subpopulation of cells unable to either bind to the H2009.1 peptide or to accumulate sufficient amounts of paclitaxel during the short 10 minute incubation. This result aligns with the flow cytometry binding data of the FITC-labeled H2009.1-paclitaxel conjugate, which also demonstrated a minority subpopulation of cells that did not bind the conjugate. Such tumor cell heterogeneity can be problematic for targeting therapies and highlights the need for additional tumor targeting ligands.

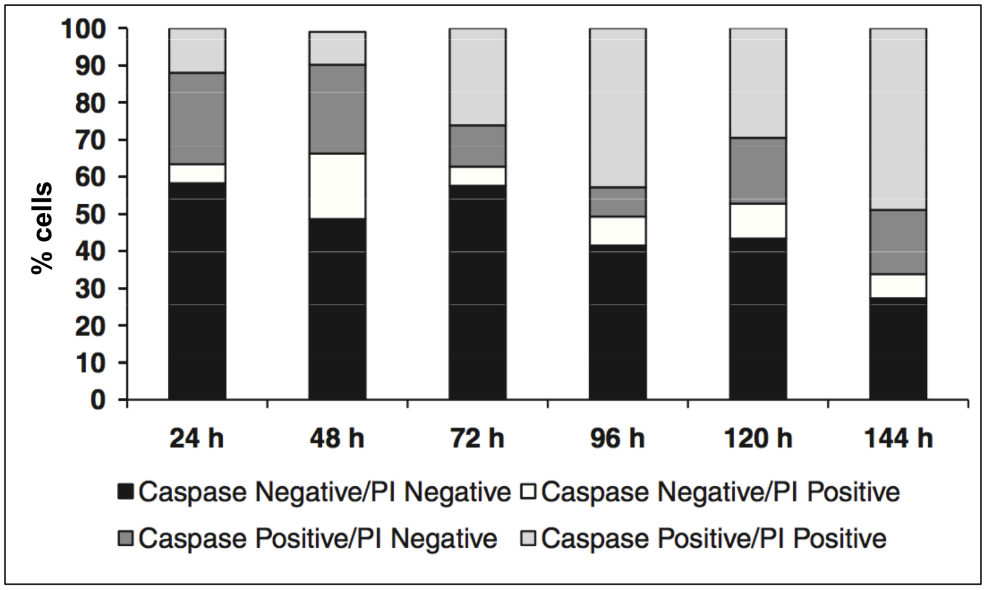

Figure 6-11. The H2009.1-paclitaxel conjugate activates caspases and initiates apoptosis. H2009 cells were exposed to 1 μM of the H2009.1-paclitaxel conjugate for 10 min, washed, and incubated with fresh media for the indicated times. All cells, both floating and attached, were collected and subjected to caspase and PI staining using the Vybrant® FAM Poly Caspases Assay before analysis by flow cytometry. A total of 10,000 events were measured using channel 1 (excitation 488 nm, emission 500 nm) and channel 3 (excitation 488 nm, emission 650 nm). The data represent the average of two experiments.

6.3.13 In Vivo *Efficacy of the H2009.1-Paclitaxel Conjugate*

While drug conjugates often have reduced efficacy *in vitro* compared to their non-conjugated partners, the opposite is often true *in vivo* as improved biodistribution of the targeted drug conjugates can overcome the loss of activity. Therefore, I determined the efficacy of the H2009.1-paclitaxel conjugate in a H2009 xenograft model. H2009 cells were implanted subcutaneously on the flank of immunocompromised mice. At day 18, once palpable tumors had formed, the animals were treated with PBS, 5 mg/kg paclitaxel or 5 mg/kg H2009.1-paclitaxel (based on the total amount of paclitaxel). A total of 5 injections per mouse were given every 3 days. While the H2009.1 paclitaxel conjugate reduced the rate of tumor growth compared to saline, there is no statistical difference between free paclitaxel and the conjugate in terms of tumor growth rate or survival (Figure 6-12). Similarly, the animal weights remained steady for both groups suggesting that no gross toxicity was observed (data not shown). Thus, conjugation to the targeting peptide did not provide any obvious benefit over the free drug *in vivo*. Interestingly, the effect of the H2009.1-paclitaxel is delayed; the growth rates for the control animals and those treated with the H2009.1-paclitaxel conjugate do not begin to diverge until day 46. This is 7 days after the free drug begins to show an effect on tumor growth. Also of note, in contrast to the H2009.1-doxorubicin conjugate, the H2009.1-paclitaxel conjugate does not decrease the performance of paclitaxel despite its higher *in vitro* IC_{50}.

Complete biodistribution and pharmacokinetic experiments are needed to determine if the observed results are due to a lack of drug targeting, inefficient drug release, premature drug release, or poor distribution throughout the tumor. As the

conjugate is below the renal filtration limit, rapid clearance by the kidneys may contribute to the lack of efficacy; however free paclitaxel is also cleared by the kidneys, and previous studies have demonstrated accumulation of the peptide in $\alpha_v\beta_6$-positive tumors despite the rapid renal filtration (Chapter 2). Additionally, maximally tolerated dosage needs to be examined; it is possible that higher doses of paclitaxel can be administered as a conjugate because of reduced off target effects.

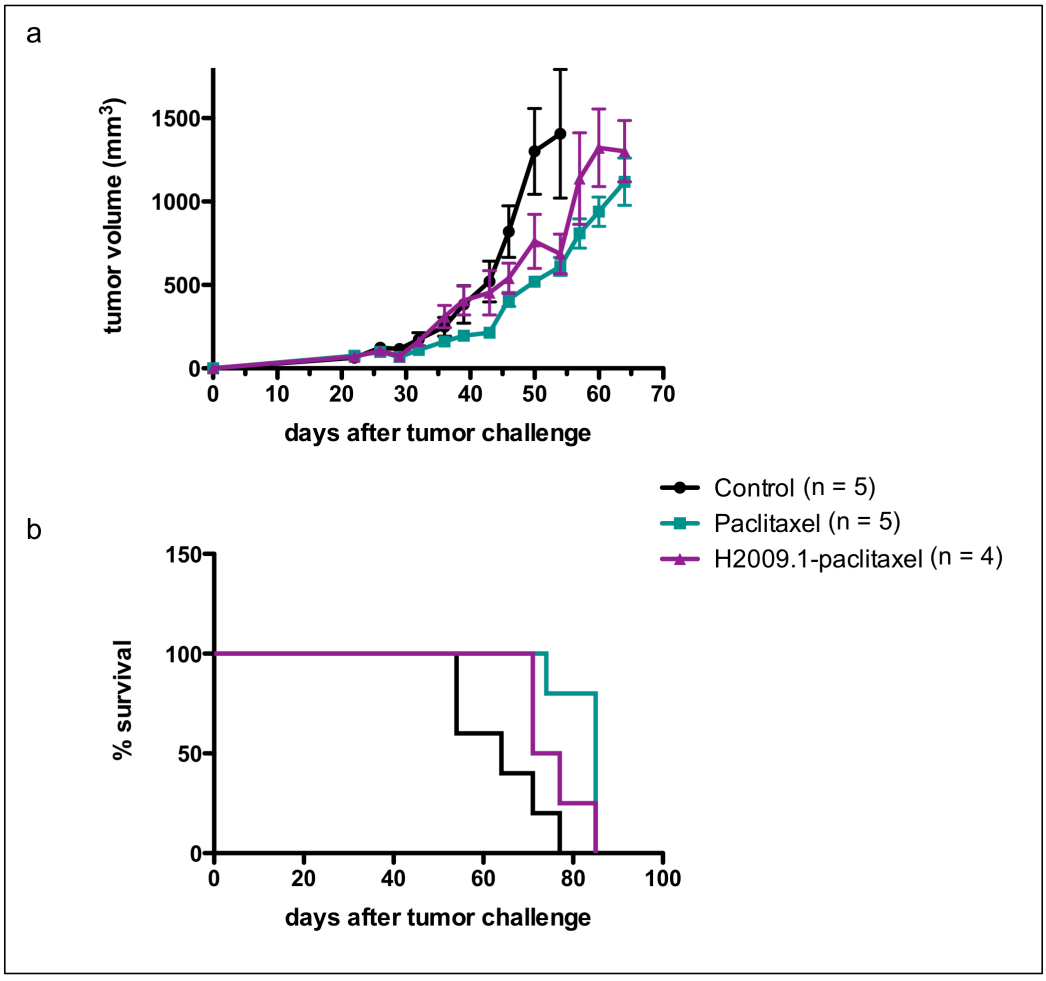

Figure 6-12. Tumor growth rate is slowed by free paclitaxel and the H2009.1-paclitaxel conjugate by similar amounts. Subcutaneous tumors were established on the flank of NOD/SCID mice. At day 18, PBS, free paclitaxel, and the H2009.1-paclitaxel conjugate were injected intravenously via the tail vein at 5 mg/kg, based on paclitaxel weight. Animals were treated at days 18, 21, 24, 27, and 30. Tumor measurements were made with calipers by an independent scientist and tumor volumes were calculated as $V= (l \times w^2)/2$. a – Tumor growth curves. b – Kaplan-Meier survival curves.

6.4 Discussion

Tumor targeting therapies that specifically deliver drugs to the tumor, reducing accumulation and toxicity in non-target tissues, are a promising niche in cancer treatment development. Such therapies include a tumor specific ligand conjugated to a drug or drug carrier, although most attention has been focused on ligand-drug direct conjugates. Peptides are attractive targeting ligands and can be easily chemically modified for conjugation to chemotherapeutics. The small size of peptide-drug conjugates allows for escape from the tumor vasculature and penetration through the tumor,[139] and peptides with high affinity for their target are predicted to have high levels of accumulation in the tumor and to remain in the tumor tissue, both important characteristics for drug delivery.[387]

To examine the therapeutic potential of H2009.1 peptide-drug conjugates, the H2009.1 tetrameric peptide was conjugated to both doxorubicin and paclitaxel for *in vitro* and *in vivo* studies. Both the H2009.1-doxrubicin and H2009.1-paclitaxel conjugates specifically delivered drug to $\alpha_v\beta_6$-positive cells *in vitro*, inducing cell death. However, both conjugates were less toxic than the respective free drugs *in vitro* and exerted their effects on a later time frame than the free drugs. Microscopy of cells treated with the H2009.1-doxorubicin conjugate revealed that the conjugate localizes to a perinuclear region within cells. Although doxorubicin release and accumulation in its site of action in the nucleus was not observed in the doxorubicin conjugate treated cells, the conjugate began to affect cell structure in the same manner as the free doxorubicin at a time point 24 hours later than the free drug. Cell blebbing indicative of cell death also began only 24 hours after that of the free drug treated cells. Therefore, the H2009.1-doxorubicin

conjugate appears to accumulate in a perinuclear compartment and slowly release the doxorubicin cargo. The H2009.1-paclitaxel conjugate induced cell death via the same G2/M cell cycle arrest and caspase activated apoptosis pathway as free paclitaxel. However, just as with the doxorubicin-conjugate, the H2009.1-paclitaxel conjugate exerted its effects on a delayed time frame 24 hours later than the free drug. While free paclitaxel induced cell cycle arrest at 24 hours and toxicity at 48 hours, the H2009.1-paclitaxel conjugate did not induce cell cycle arrest until 48 hours, or induce toxicity until 72 hours. The 24 hour delay exhibited by both conjugates suggests that they require time to slowly release their conjugated drug to produce active drug. Alternatively, the drugs are released quickly but are delayed in exiting the cellular compartment in which they reside, taking time to accumulate in either the nucleus (for doxorubicin) or the cytoplasm (for paclitaxel).

While both the H2009.1-doxouribicin and paclitaxel conjugates have reduced efficacy *in vitro* compared to the non-conjugated, free, drugs, improved *in vivo* biodistribution of targeted drug conjugates often overcomes such loss of activity. Therefore, the activity of both conjugates was examined in a NSCLC H2009 xenograft model. Tumor growth was significantly inhibited by treatment with 2 mg/kg of free doxorubicin compared to control mice. While treatment with 2 mg/kg of the H2009.1-doxorubicin conjugate inhibited tumor growth compared to the control mice, this inhibition was not statistically significant. Additionally, free doxorubicin was significantly better at inhibiting tumor growth compared to the H2009.1-doxorubicin conjugate at the 2 mg/kg concentration. Treatment with 4 mg/kg of the conjugate did not alter targeting, resulting in tumor inhibition identical to the lower dose of conjugate

treatment. However, as free doxorubicin is toxic to mice at this 4 mg/kg dosing, the H2009.1-doxorubicin conjugate is significantly less toxic than the free drug. Importantly, the mice did not exhibit any signs of toxicity at this higher dose of conjugate treatment and continued to gain weight throughout the experiment. The reduced toxicity of the H2009.1-doxorubicn conjugate compared to the free drug indicates that the peptide is able to prevent off target drug effects and provides a promising beginning for the development of H2009.1-targeted therapies.

Of note, the H2009.1-doxorubicin conjugate was significantly less efficient at inhibiting tumor growth compared to the 1.3% H2009.1-tetrameric liposomal doxorubicin formulation examined in detail in Chapter 5. While we originally predicted that the better tumor penetration of the H2009.1-doxorubicin conjugate would improve tumor growth inhibition compared to the liposomes, the opposite proved true. However, as the levels of tumor accumulation and penetration of the conjugate are unknown, it is not clear whether this is the result of poor tumor targeting, poor tumor penetration, or poor drug release.

The H2009.1-paclitaxel conjugate exhibited tumor inhibition effects that closely resembled those of the doxorubicin conjugate, except that the paclitaxel conjugate and free paclitaxel exhibited similar tumor inhibition. Both the H2009.1-paclitaxel conjugate and free paclitaxel appeared to inhibit tumor growth compared to control mice, but this inhibition did not reach statistical significance. However, despite the >30-fold higher IC_{50} of the paclitaxel conjugate compared to the free drug *in vitro*, both drugs exhibited the same *in vivo* toxicity. As higher concentrations of drug treatment have not been tested for

either the H2009.1-paclitaxel conjugate or free paclitaxel, it is unknown whether this conjugate is less toxic than the free drug.

It is unclear why both the H2009.1-doxorubicin and paclitaxel conjugates fail to significantly alter tumor growth *in vivo*. Comprehensive biodistribution and pharmacokinetic studies are needed to clarify whether these results are due to a lack of drug targeting, inefficient drug release, premature drug release, or poor tumor penetration and distribution. As dye-conjugated H2009.1 tetrameric peptide targets H2009 tumors *in vivo* and is still visible in the tumors 24 hours after injection, it is unlikely that the conjugates fail to accumulate in the tumor tissue. Based on the reduced *in vitro* toxicity of both conjugates compared to the free drugs and the 24 hour delay in drug efficacy after treatment with either conjugate, it is probable that slow release of the drugs from the conjugates tempers the *in vivo* activity of these drug formulations. Therefore, the use of different linkers that allowed for better drug release could potentially improve the *in vivo* efficacy of these H2009.1 peptide conjugates. Para-aminobenzylalcohol and ethylenediamine based self-immolative linkers that undergo spontaneous release are an attractive linker alternative and have recently been used successfully for both *in vitro* and *in vivo* studies.[112, 405-407]

While other peptide-doxorubicin conjugates have shown improved *in vivo* activity compared to free doxorubicin, it is difficult to determine why these conjugates improved drug efficacy and the H2009.1 conjugate did not. Many experimental parameters that would help clarify the differences between the H2009.1 conjugate and the other peptide conjugates, such as the pathways of conjugate cellular internalization, time course of drug release, and levels of tumor accumulation and penetration for the various

peptide-drug conjugates are unknown. In some cases, such as for the heptacellular carcinoma targeting peptide, A54, it is not even clear what chemistry was used to conjugate doxorubicin to the peptide, making it difficult to determine how this peptide-drug platform compares to the H2009.1-doxorubicn conjugate.[117] Additionally, the RGD-4C-doxorubicin conjugate targets both the tumor vasculature cells and the tumor cells;[115] therefore this peptide can exert both vasculature and tumor cell-specific toxicity, making it difficult to make a side-by-side comparison with our conjugate.

Although tumor vasculature targeting platforms are not dependent upon tumor penetration as are tumor cell targeting platforms such as the H2009.1 peptide conjugates, several interesting studies with the tumor vasculature targeting NGR-doxorubicin are of interest. The first report of a NGR-doxorubicin conjugate demonstrated that the conjugate inhibited tumor growth and improved survival for mice bearing either MDA-MB-435[95-98] or MDA-MB-231 xenografts.[115] Subsequent studies with the ester-linked NGR-doxorubicin conjugate demonstrated that this conjugate localizes to the cytoplasm after cellular internalization and releases doxorubicin to the nucleus within 30 minutes after drug exposure.[110] Therefore, this conjugate both exhibits a very different pattern of intracellular accumulation than our H2009.1-conjugate and releases free doxorubicin on a much faster time frame, suggesting that improving drug release from our conjugate by use of a different drug linker could improve *in vivo* efficacy. However, it is interesting to note that while the NGR-doxorubicin conjugate inhibited tumor growth and improved survival for mice bearing either MDA-MB-435 or MDA-MB-231 xenografts,[115] it did not alter tumor growth for mice bearing OVCAR-3 xenografts.[110] Much like the results with our H2009.1-doxorubicin conjugate, free doxorubicin inhibited tumor growth better than

the NGR-doxorubicin conjugate in mice bearing OVCAR-3 xenografts. Interestingly, while we saw some tumor inhibition with the H2009.1-doxorubicin conjugate compared to control mice, the NGR-doxorubicin conjugate did not alter tumor growth compared to the control mice in the OVCAR-3 tumor model.

Similar results were observed with two closely related peptide-paclitaxel conjugates targeting the integrin $\alpha_v\beta_3$, which is expressed by both the tumor vasculature and some tumor cells. A dimeric form of the $\alpha_v\beta_3$-targeting peptide c(RGDyK), the E-[c(RGDyK)$_2$] peptide, conjugated to paclitaxel inhibited tumor growth better than free paclitaxel in a mouse MDA-MB-435 xenograft model.[408] However, a similar peptide conjugate with *in vitro* activity, formed from conjugation of the dimeric E-[c(RGDfK)$_2$] peptide to paclitaxel, did not alter tumor growth compared to control treated mice in a OVCAR-3 tumor model.[403] In this same tumor model, the free paclitaxel did inhibit tumor growth. As both MDA-MB-435 and OVCAR-3 tumor cells express $\alpha_v\beta_3$,[409, 410] both of these tumor models should allow for peptide targeting to both the tumor vasculature and the tumor cells. It is interesting to note that for both the NGR-doxorubicin conjugate and the dimeric RGD peptide-doxorubicin conjugates, the conjugates inhibited tumor growth in a MDA-MB-435 tumor model but not a OVCAR-3 tumor model. The OVCAR-3 tumor model may not have a vasculature pattern that allows for efficient drug delivery. These results highlight the difficulties of tumor targeting and demonstrate that peptide-drug conjugate efficacy can vary between different tumor types, suggesting that future studies with H2009.1 peptide-drug conjugates should include multiple $\alpha_v\beta_6$-expressing tumor models for comparison of drug efficacy in different tumor types.

The H2009.1 peptide may also benefit from design of a conjugate tailored to the perinuclear compartment to which the peptide localizes. Recent data from Dr. Michael McGuire in our lab suggest that the H2009.1 peptide binds to $\alpha_v\beta_6$ and internalizes via a caveolar mechanism, carrying its cargo to the endoplasmic reticulum (ER) and Golgi apparatus (Golgi) of the cell (data not shown). This is significant as most drug conjugates are designed with the assumption that ligands internalize via clatherin mediated endocytosis. The clatherin mediated endocytotic pathway is the primary method by which macromolecules enter the cell and involves a pathway of vesicle transport.[411, 412] Ligands initially internalize into the cell in a vesicle formed by membrane invagination. This vesicle becomes an endosome and follows a pathway from early endosome to late endosome to lysosome. At each point in the vesicle pathway the pH drops, moving from a pH of 5.5-6.0 in the early endosome, to a pH of 5.5 in the late endosome, and finally as low as a of pH 4.5 in the lysosome. This acidic environment is ideal for drug linkers such as the acid-labile hydrazone linker incorporated into the H2009.1-doxorubicin conjugate. Under acidic pH, the hydrazone linker cleaves, releasing active drug. In addition, lysosomes contain a variety of enzymes that can degrade other linkers.[413] These include esterases and proteases capable of hydrolyzing the ester linkage in the H2009.1-paclitaxel conjugate to release free and active paclitaxel.

In contrast to clatherin mediated endocytosis, caveolar endocytosis involves ligand encapsulation in a caveolar carrier that can deliver its cargo to either an endosome or a caveosome.[414] The caveosome, which does not experience a low pH, then delivers its cargo to either the ER or the Golgi. As our recent data indicates that the H2009.1 peptide never localizes to or delivers its cargo to the lysosome and instead delivers its cargo to

the ER and Golgi, it likely transports through the caveosome. Therefore, the acid-labile hydrazone linker used in the H2009.1-doxorubicin conjugate and the ester linkage used in the H2009.1-paclitaxel conjugate may not be ideal drug linkers for use with the H2009.1 peptide. A linker better designed for localization to either the ER or Golgi could be of benefit. One such strategy could be to incorporate a furin-cleavable linker into either of the H2009.1 drug conjugates. Furin is an endoprotease responsible for proteolytically activating numerous secreted proteins and is localized to the Golgi.[415] The peptide cleavage sites of furin are known and can be incorporated into proteins to induce specific furin cleavage. Two such peptides, the TRHRQPRGWE cleavage site from *Pseudomonas* exotoxin A and the AGNRVRRSVG cleavage site from diphtheria toxin induced furin specific cleavage of recombinant HER2 immunotoxins leading to HER2-mediated cell specific death.[416] Therefore, inclusion of either of these furin cleavage sites might allow for better drug release from the H2009.1 conjugates.

Alternatively, the H2009.1 peptide may benefit from conjugation to a different drug that is able to easily exit the ER or Golgi, simplifying the steps of drug release from these compartments and transport into the drug's site of action within the cell. One class of such drugs is the plant toxins, including the toxin gelonin (rGel). Like other plant toxins, gelonin induces cell apoptosis by enzymatically inhibiting 28s rRNA.[417] Although only a few molecules of gelonin are needed to initiate cell death, free gelonin does not easily cross cell membranes. However, once inside the Golgi of a cell, gelonin is able to cross the Golgi membrane and enter the cytoplasm to exert its toxicity against ribosomal RNA. Conjugation of rGel to the H2009.1 peptide could both internalize the toxin into cells and localize the toxin to the Golgi, allowing for release to its site of action in the

cytoplasm. Preliminary data from our lab showed that conjugation of the H2009.1 tetrameric peptide to rGel via a disulfide bond demonstrated $\alpha_v\beta_6$-specific rGel targeting, resulting in cell death (data not shown). Further study is needed to determine whether the H2009.1-rGel construct will exhibit $\alpha_v\beta_6$-specific toxicity *in vivo*.

6.5 Acknowledgements

Dr. Shunzi Li worked on optimizing the synthesis protocol for the doxorubicin conjugate, synthesized the paclitaxel conjugate, and performed all of the paclitaxel *in vitro* experiments. I wish to thank her for tireless contributions to these experiments. I also wish to thank Dr. Michael McGuire and Dorothy Cupka for helping with tumor measurements.

CHAPTER SEVEN

CONCLUSIONS AND FUTURE DIRECTIONS

The primary goal of this study was to translate the H2009.1 peptide from a phage display selected peptide to a viable tumor targeting ligand for the selective delivery of therapeutics to $\alpha_v\beta_6$-expressing NSCLC cells. The integrin $\alpha_v\beta_6$ in an ideal tumor target; it is only rarely expressed in normal tissue[346, 355] but is expressed by numerous cancers of the epithelium,[342-352] including NSCLC.[81] As the H2009.1 peptide displays high affinity for $\alpha_v\beta_6$, specifically binding and internalizing into $\alpha_v\beta_6$-positive cells and also targets $\alpha_v\beta_6$-positive tumors *in vivo*, it is anticipated to have great utility as a therapeutic targeting agent.

To examine the ability of the H2009.1 peptide to specifically deliver drugs to NSCLC cells, the peptide was used as a targeting ligand for three different drug platforms: liposomal doxorubicin and direct drug conjugates of both doxorubicin and paclitaxel. Conjugation of the H2009.1 peptide to all three of these drug platforms led to $\alpha_v\beta_6$-specific targeting and toxicity *in vitro*. However, each targeted formulation failed to improve tumor growth inhibition compared to the untargeted drugs *in vivo*. These results highlight the complexity of drug delivery and targeting *in vivo* and provide a basis for the design of optimized H2009.1 targeting therapies.

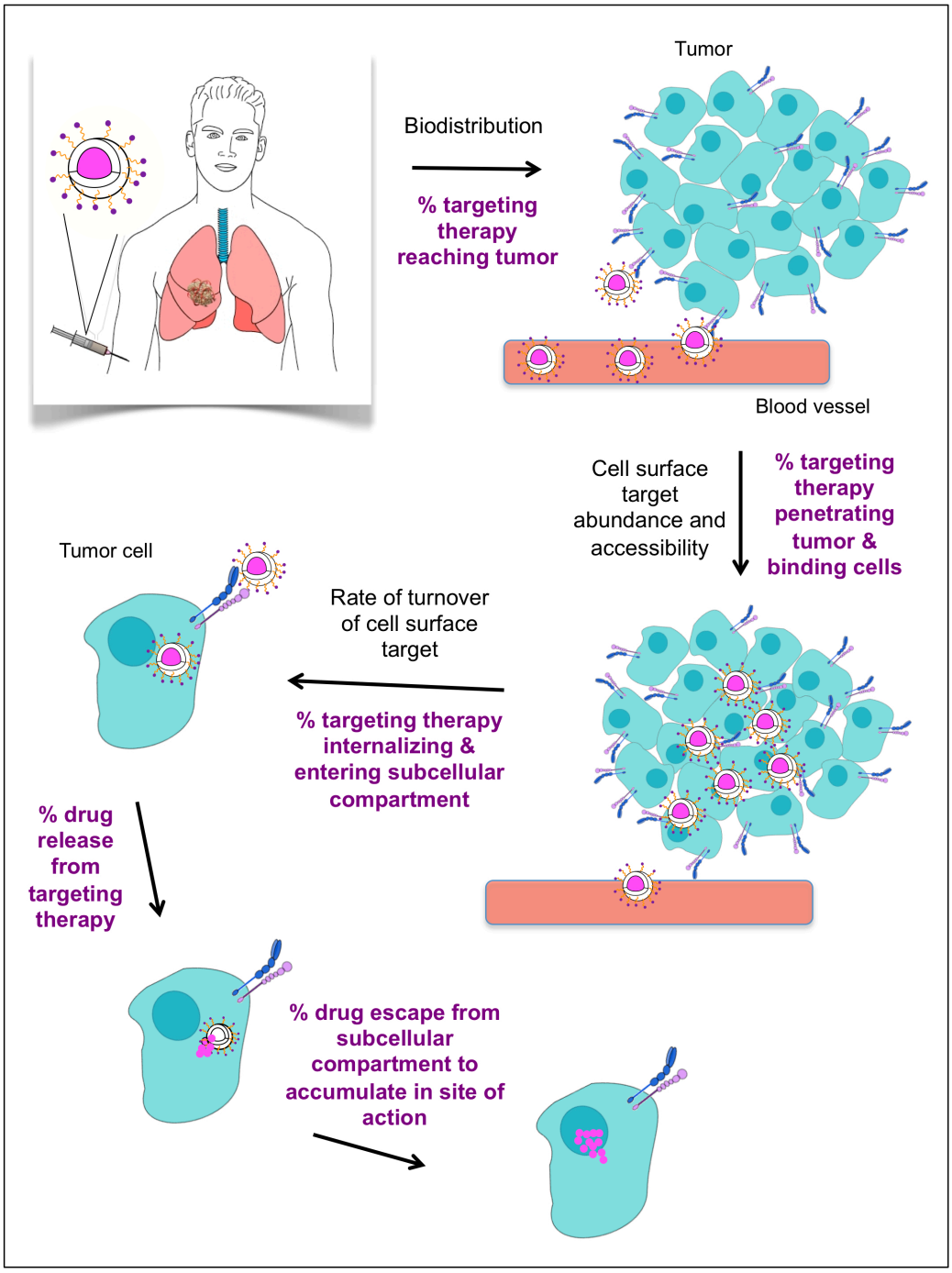

Figure 7-1. Diagram of the steps required for targeting therapeutics to tumor cells, from injection into the patient to accumulation of the drug in its cellular site of action.

7.1 Requirements for and Complexity of *In Vivo* Tumor Targeting Therapies

Drug targeting *in vitro* is a relatively simplistic system involving primarily the therapeutic agent and the cancer cells. Targeted delivery of therapeutics to cancer cells *in vivo* is a much more complex process, involving many different steps (Figure 7-1). At each step there is potential for drug loss. Even if a targeting agent specifically delivers its cargo to the tumor, only a fraction of the injected drug will reach its site of action in tumor cells.

After initial injection into the bloodstream, the targeted drug must circulate and escape the vasculature to enter the tumor. A number of factors, including the size and type of therapy, the affinity of the targeting ligand, and the vasculature pattern of the tumor, determine biodistribution and subsequent tumor accumulation. Once in the tumor, the targeted drug must penetrate the tumor tissue and bind to the tumor cells. This requires that the target receptor have an appropriate abundance in the tumor cells and be accessible for binding. In addition, the size and type of drug construct and the affinity of the targeting ligand for its receptor affect both tumor penetration and binding to tumor cells. After binding to the tumor cells, the targeting ligand must also internalize into the cells. This depends on both the affinity of the ligand and the rate of receptor recycling. Even after the targeting ligand has delivered its drug cargo inside the tumor cell, the cargo is still trapped within the targeting drug platform and remains inactive. The drug must release from the targeting scaffold to regain activity. Additionally, targeting ligands usually carry drugs to a different subcellular compartment than the compartment where the drugs exert their effects. Therefore, another step is required to transport or release the drug to its site of action. Then, the drug is finally ready and able to act.

Together these steps inevitably result in a significant reduction of the amount of drug reaching each cell compared to the amount of drug originally injected. Assuming a 50% success rate for each step, including the ability of the drug to exert its cytotoxic effects, only 1.56% of the original dose reaches the final cellular target in an active, toxic state.[418] Clearly the *in vivo* delivery of targeted therapies is not trivial and involves numerous steps, each of which can require optimization. Although complex, *in vivo* targeted drug delivery ultimately requires one thing: the ability to deliver a therapeutically effective amount of active drug to its cellular site of action.

7.2 Improving Tumor Penetration

The inability of the different H2009.1 targeted drug platforms to improve therapeutic efficacy compared to the untargeted drugs *in vivo* could hypothetically arise from difficultly with any of the steps required for *in vivo* delivery. However, my data indicate that the H2009.1 targeted liposomes suffer from poor tumor penetration and very heterogeneous tumor distribution. The liposomes remain closely associated with highly vascularized regions primarily on the periphery of the tumor leaving the majority of the tumor unaffected. As both the H2009.1 targeted and untargeted liposomes accumulate in tumors to the same extent based on the EPR effect, the targeted liposomes must exhibit a different pattern of tumor distribution to improve drug efficacy. This requires access to the bulk tumor cells so that the H2009.1 peptide can bind $\alpha_v\beta_6$ and specifically deliver liposomal doxorubicin into cells. As described in Chapter 5, several strategies involving combination treatments can be employed to improve tumor penetration and distribution

of the H2009.1 targeted liposomes; these strategies can seek to affect the tumor vasculature or to directly affect tumor penetration.

One potential method for improving liposome tumor accumulation and penetration is to induce "vascular normalization" by combining liposome treatment with antiangiogenic therapy. Combination therapy with both antiangioenic therapy and systemic chemotherapy has had the surprising result of improving patient outcomes compared to chemotherapy alone,[395] and this has been attributed to vascular normalization by the antiangiogenic therapy. Tumor blood vessels revert back to a more normal and less disordered state, allowing for more homogenous blood flow and a more uniform delivery of chemotherapeutic drugs into the tumor.[395] This results in better drug penetration into the tumor tissue.[397] Therefore, combining H2009.1 peptide targeted liposomal doxorubicin with an antiangiogenic therapy such as an antibody targeting vascular endothelial growth factor (VEGF) may improve liposome tumor penetration and allow the H2009.1 peptide to actively target cells and induce $\alpha_v\beta_6$-specific toxicity.

The cyclic iRGD peptide, CRGDKGPDC, also improves drug tumor penetration.[178] This peptide has a very unique mechanism and contains two different peptide motifs, each of which contributes to its effects. The accessible RGD motif first binds to $\alpha_v\beta_3$ and $\alpha_v\beta_5$ on the tumor vasculature. Once the peptide is localized to the tumor vasculature, it is cleaved by proteases to reveal the previously hidden RGDK motif. As this motif only functions once its C-terminus is exposed, it is then able to bind NRP-1 overexpressed by both endothelial and tumor cells. Binding to NRP-1 stimulates penetration through the vasculature and tumor tissue.[178] Co-injection of the iRGD peptide with a variety of drug platforms, ranging from small molecules to 130 nm sized

nanoparticles, demonstrates increased tumor accumulation and penetration, and a subsequent increase in therapeutic efficacy, for the co-injected drugs compared to treatment with the drugs alone.[179] Significantly, the iRGD peptide also increased tumor accumulation, penetration, and toxicity of liposomal doxorubicin,[179] suggesting that it should be able to improve tumor penetration of H2009.1 peptide-targeted liposomal doxorubicin. Increased tumor penetration of the H2009.1 liposomes would lead to increased opportunity for targeting to $\alpha_v\beta_6$-expressing cells and could, therefore, potentiate the toxicity of the targeted liposomes compared to the non-targeted liposomes.

Another method for improving tumor penetration is the use of a different, smaller type of drug platform. Micelles have many of the same advantages as liposomes, such as the ability to incorporate unmodified drugs and to encapsulate multiple agents at once. However, the smaller size of micelles can allow for better escape from the vasculature into the tumor tissue. Therefore, H2009.1 peptide-targeted micellular drugs may experience better tumor tissue penetration and efficacy than the H2009.1 peptide-targeted liposomes. The use of any of these methods to improve tumor penetration should allow the H2009.1 peptide to reach the majority of the tumor cells, bind $\alpha_v\beta_6$, and carry its drug cargo into the cells, increasing the intracellular accumulation of drug and moving the drug one step closer to its cellular site of action.

7.3 Improving Drug Release

Further study is required to determine the exact mechanism for the failure of the H2009.1-doxorubicin and paclitaxel conjugates to improve therapeutic efficacy *in vivo*. Comprehensive biodistribution and pharmacokinetic studies are needed to determine the

levels of conjugate tumor accumulation and penetration and to clarify whether the therapeutic results are due to a lack of drug targeting, inefficient drug release, premature drug release, or poor tumor penetration and distribution. *In vitro*, both the H2009.1-doxorubicin and paclitaxel conjugates exhibited reduced toxicity compared to the free drugs and experienced a 24 hour delay in drug efficacy, consistent with a phenotype of slow drug release from the conjugates. These results coupled with the ability of the H2009.1-dye conjugate to target and retain in tumors *in vivo*, suggest that the H2009.1 drug conjugates are able to target the tumor but suffer from slow drug release. As the H2009.1 drug conjugates are similar in size to the H2009.1-dye conjugate, they likely exhibit similar tumor accumulation and retention. Therefore, the use of different linkers that allowed for better drug release could potentially improve *in vivo* efficacy of H2009.1 peptide conjugates. Para-aminobenzylalcohol and ethylenediamine based self-immolative linkers that undergo spontaneous release are an attractive linker alternative and have recently been used successfully for both *in vitro* and *in vivo* studies.[112, 405-407]

Recent data from Dr. Michael McGuire in lab suggest that our future studies should focus on conjugates that specifically release in either the ER or the Golgi. The H2009.1 peptide does not follow a traditional clatherin mediated route of endocytosis or localize with lyososomes. Instead, it binds to $\alpha_v\beta_6$ and internalizes into cells via a caveolar mechanism, carrying its cargo to the ER and Golgi of the cell (data not shown). As both the hydrazone and ester linkages used for the doxorubicin and paclitaxel conjugates are optimized for a clatherin mediated endocytotic pathway that terminates in the lysosome, linkers better designed for the caveole pathway should improve conjugate drug release. During clatherin mediated endocytosis, ligands internalize into the cell in a

vesicle formed by membrane invagination; this vesicle subsequently becomes an endosome and follows a pathway from early endosome to late endosome to lysosome.[411, 412] At each point in the vesicle pathway the pH drops, moving from a pH of 5.5-6.0 in the early endosome, to a pH of 5.5 in the late endosome, and finally as low as a of pH 4.5 in the lysosome. The acidic environment of the lysosome is ideal for drug release from the acid-labile hydrazone linker in the H2009.1-doxorubicin conjugate. Additionally, lysosomes contain a variety of esterases and proteases that can hydrolyze the ester linkage in the H2009.1-paclitaxel conjugate to release free pacltiaxel.[413]

A caveolar pathway of endocytosis is consistent with the predicted inefficient release of drug from both H2009.1 peptide conjugates. In contrast to clatherin mediated endocytosis, caveolar endocytosis involves ligand encapsulation in a caveolar carrier that can deliver its cargo to either an endosome or a caveosome.[414] The caveosome, which does not experience a low pH, then delivers its cargo to either the ER or the Golgi. As the H2009.1 peptide does not localize to the lysosome and instead delivers its cargo to the ER and Golgi, it likely transports through the caveosome. Therefore, the H2009.1-doxorubicin conjugate is never exposed to low pH conditions and cannot efficiently release drug. Additionally, the H2009.1-pacltaxel conjugate does not reach the esterase-rich cytosol or lysosome and must release drug within the ER or Golgi. Both conjugates are still clearly capable of drug release under these sub-optimal conditions, but it is anticipated that rational design of a drug linker suited for the caveolar pathway will improve drug release and efficacy for H2009.1 peptide conjugates.

Furin-cleavable linkers are optimal for ligands that localize to the Golgi. Furin is an endoprotease responsible for proteolytically activating numerous secreted proteins and

is localized to the Golgi.[415] Two peptides with furin-cleavage sites, the TRHRQPRGWE peptide from *Pseudomonas* exotoxin A and the AGNRVRRSVG peptide from diphtheria toxin, induce furin specific cleavage when incorporated into recombinant immunotoxins, releasing the toxins to exert cell specific death.[416] Therefore, inclusion of either of these furin cleavage sites might allow for better drug release from the H2009.1 conjugates.

As drugs conjugated to the H2009.1 peptide are inactive while they remain bound to the peptide, the conjugate must release the drug to produce an active drug that can accumulate in the required cellular compartment and exert cytotoxic effects. It is important to note that while drug release is likely a limiting factor for peptide-drug direct conjugates, inefficient drug release from a nanoparticle such as a liposome is less likely to be as problematic. As each liposome carries thousands of drug molecules, even if the liposome degrades slowly to release the encapsulated drug, it will still release a large payload of drug. Accordingly, while H2009.1 peptide-targeted liposomal doxorubicin and the H2009.1-doxorubicin conjugate both localized to the same subcellular compartment and were both able to exert cell toxicity, only the targeted liposomes released a drug payload that could be visualized in the nucleus. This could help account for the significantly lower IC_{50} of the H2009.1 tetrameric peptide-targeted liposomes compared to the H2009.1 tetrameric peptide-doxorubicin conjugate.

7.4 Directed Design of H2009.1 Peptide Therapeutics

Based on lessons learned with the H2009.1 peptide targeted liposomes and direct drug conjugates, H2009.1 peptide therapeutics can be rationally designed to improve efficacy. One primary focus of these next-generation H2009.1 conjugates should be

conjugation of the peptide to highly potent cytotoxic agents that do not need a high intracellular concentration to induce their toxic effects. As such drugs do not need a high level of accumulation in the cell, even if the conjugate or drug platform suffers from low levels of tumor accumulation or from slow drug release, enough drug should accumulate in cells and release to exert potent activity. Additionally, the reduced nonspecific toxicity of the H2009.1-doxorubicin conjugate compared to the free doxorubicin, which was toxic at a 4 mg/kg treatment regimen that was tolerated for the conjugate, indicates that the H2009.1 peptide alters drug distribution and prevents unwanted toxicities. This is a particularly attractive trait for a ligand conjugated to a highly toxic drug.

One potent cytotoxic agent worth pursuing is the microtubule-disrupting agent monomethyl auristatin E. Auristatin E is a synthetic analogue of dolastatin 10, a marine natural product, and is ~200-fold more potent than doxorubicin.[419] Adcetris™ (brentuximab vedotin), the only clinically approved antibody-drug conjugate, is an anti-CD30 antibody conjugated auristatin E.[30] Thus, aurostatin E has a proven track record of success with conjugation to antibodies.

The plant toxin gelonin (rGel) is also highly toxic. Like other plant toxins, gelonin induces cell apoptosis by enzymatically inhibiting 28s rRNA, and only a few molecules of gelonin are needed to initiate cell death.[417] As free gelonin does not easily cross cell membranes, conjugation of gelonin to the H2009.1 peptide would overcome this limitation. Additionally, gelonin easily crosses the Golgi membrane, the same compartment to which the H2009.1 localizes. A H2009.1 peptide-rGel conjugate would deliver the toxin to the Golgi; once the toxin released from the peptide, it would then exit the Golgi and enter the cytoplasm to exert its effects. Preliminary data from Dr. Michael

McGuire in our lab demonstrated $\alpha_v\beta_6$-specific rGel-induced cell death from a H2009.1 tetrameric peptide-rGel conjugate (data not shown). It will be exciting to test this peptide-drug construct *in vivo*.

Notably, the H2009.1 peptide is a versatile targeting ligand that can be altered to change affinity and valency by synthesizing monomeric or tetrameric versions of the peptide. The H2009.1 peptide is also amenable to conjugation to a variety of drug platforms without alteration of peptide binding affinity. These characteristics will allow for the use of an assortment of optimization techniques during the design of future H2009.1-therapeutics. Of particular interest, if a H2009.1 tetrameric peptide therapeutic exerts effects reflective of a "binding site barrier," with accumulation in sites near the entry of the tumor and a failure to distribute throughout the tumor,[389] the lower affinity H2009.1 peptide can be conjugated to the therapeutic and tested for better tumor penetration.

7.5 Use of the H2009.1 Peptide for Imaging Applications

Irrespective of its therapeutic targeting abilities, the H2009.1 peptide appears perfectly primed for imaging applications. As demonstrated in Chapter 2, a H2009.1-near infrared dye conjugate localized to tumors *in vivo*, emitting an easily-detected fluorescent signal from the tumor during whole mouse fluorescent imaging. Additionally, a collaboratorion between our lab and Dr. Xiankai Sun's lab has demonstrated that the H2009.1 peptide is an ideal ligand for position emission tomography (PET) imaging of NSCLC tumors (data not shown). As most NSCLC patients present to the clinic with late stage disease,[3] development of agents that could identify tumors at an earlier stage is

warranted. Early stage squamous cell carcinoma NSCLC tumors express $\alpha_v\beta_6$ (Chapter 3), implying that H2009.1 peptide-targeted imaging agents will detect these early lesions.

7.6 Conclusion

This study highlights the challenges of *in vivo* drug targeting. Targeted therapies that work well *in vitro* do not always maintain specific efficacy *in vivo*, even when the targeting ligand itself homes to tumors. Tumor targeting *in vivo* depends on many aspects not present in the *in vitro* context that can be difficult to predict prior to *in vivo* experiments. While H2009.1 peptide-targeted doxorubicin and paclitaxel conjugates and H2009.1 peptide-targeted liposomal doxorubicin induced specific toxicity towards $\alpha_v\beta_6$-expressing NSCLC cells *in vitro*, these constructs did not improve upon *in vivo* efficacy compared to the non-targeted drugs. However, these studies provide several drug platforms for optimization of an $\alpha_v\beta_6$-specific therapeutic. Additionally, the H2009.1 peptide appears well suited for imaging applications.

In addition, we have the tools in place for the development of other NSCLC-targeting therapeutics. Our lab isolated a panel of 11 different NSCLC-targeting peptides and demonstrated that 5 of these peptides home to tumors in mice. While the broad-binding H2009.1 peptide was the focus of this dissertation, future studies will involve the development of additional NSCLC-targeting therapies using the other peptides. As these peptides combined target 85% of the NSCLC cell lines tested, it is anticipated that therapies based on these peptides will target the majority of NSCLC cases presenting in the clinic.

For each peptide it will be important to examine the method of cellular internalization and the intracellular localization upon cell entry to determine how to best design therapeutics. Additionally, future treatments are expected to include a cocktail of different tumor targeting drugs given in combination with traditional chemotherapy or antiangiogenic therapy, much as chemotherapeutic agents are given in combination today. This cocktail of drugs could include different targeting ligands conjugated to the same drug construct or the same tumor targeting ligand conjugated to different drug constructs. The simultaneous use of different peptides would allow for targeting of multiple receptors at the same time, while the use of the same peptide with different drug constructs would allow for different levels of tumor accumulation and distribution.

7.7 Acknowledgements

I wish to thank Chase Kessinger for drawing the impressive illustration of the patient with a lung tumor.

BIBLIOGRAPHY

1. Jemal, A.; Bray, F.; Center, M. M.; Ferlay, J.; Ward, E.*, et al.*, Global cancer statistics. *CA-Cancer J. Clin.* 2011, *61* (2), 69-90.
2. Murphy, S. L.; Xu, J.; Kochanek, K. D., Deaths: preliminary data for 2010. *Natl. Vital Stat. Rep.* 2012, *60* (4), 1-68.
3. Siegel, R.; Ward, E.; Brawley, O.; Jemal, A., Cancer statistics, 2011. *CA-Cancer J. Clin.* 2011, *61* (4), 212-236.
4. Sun, S.; Schiller, J. H.; Spinola, M.; Minna, J. D., New molecularly targeted therapies for lung cancer. *J. Clin. Invest.* 2007, *117* (10), 2740-2750.
5. Lung Cancer Prevention (PDQ) Health Professional Version 2012. HTTP://WWW.CANCER.GOV (accessed 01/25/2012).
6. Ettinger, D. S.; Akerley, W.; Borghael, H.; Chang, A.; Cheney, R. T.*, et al.* Non-Small Cell Lung Cancer *NCCN Guidelines* [Online], 2012, p. 1-112. HTTP://BOOKS.GOOGLE.COM/BOOKS?ID=T3TPCQAACAAJ&DQ=NCCN+CLINICAL+PRACTICE+GUIDELINES+IN+ONCOLOGY&CD=1&SOURCE=GBS_API.
7. Herbst, R. S.; Heymach, J. V.; Lippman, S. M., Lung Cancer. *N. Engl. J. Med.* 2008, *359* (13), 1367-1380.
8. Travis, W.; Brambilla, E.; Muller-Hermelink, H.; Harris, C., *Pathology & Genetics: Tumors of the Lung, Pleura, Thymus and Heart*. Lyon, France: IARC Press: 2004.
9. Bhattacharjee, A.; Richards, W. G.; Staunton, J.; Li, C.; Monti, S.*, et al.*, Classification of human lung carcinomas by mRNA expression profiling reveals distinct adenocarcinoma subclasses. *Proc. Natl. Acad. Sci. U. S. A.* 2001, *98* (24), 13790-5.
10. Edge, S.; Byrd, D.; Compton, C.; al, e., *AJCC Cancer Staging Manual, 7th Edition*. 7th ed.; Springer: New York, 2010.
11. Detterbeck, F. C.; Boffa, D. J.; Tanoue, L. T., The new lung cancer staging system. *Chest* 2009, *136* (1), 260-271.
12. . Stages of Non-Small Cell Lung Cancer *General Information About Non-Small Cell Lung Cancer* [Online], 2012. HTTP://WWW.CANCER.GOV/CANCERTOPICS/PDQ/TREATMENT/NON-SMALL-CELL-LUNG/PATIENT/PAGE2 (accessed 1/20/2012).
13. NCCN Guidelines. In *Non-Small Cell Lung Cancer* [Online] National Comprehensive Cancer Network: 2012. HTTP://BOOKS.GOOGLE.COM/BOOKS?ID=T3TPCQAACAAJ&AMP

;DQ=NCCN+CLINICAL+PRACTICE+GUIDELINES+IN+ONCOLOGY&CD=1&SOURCE=GBS_API.

14. Scott, W. J.; Howington, J.; Feigenberg, S.; Movsas, B.; Pisters, K., Treatment of non-small cell lung cancer stage I and stage II: ACCP evidence-based clinical practice guidelines (2nd edition). *Chest* 2007, *132* (3 Suppl), 234S-242S.
15. Ou, S. H. I.; Zell, J. A.; Ziogas, A.; Anton-Culver, H., Prognostic factors for survival of stage I nonsmall cell lung cancer patients. *Cancer* 2007, *110* (7), 1532-1541.
16. Dahele, M.; Senan, S., The Role of Stereotactic Ablative Radiotherapy for Early-Stage and Oligometastatic Non-small Cell Lung Cancer: Evidence for Changing Paradigms. *Cancer Res. Treat.* 2011, *43* (2), 75.
17. Aupérin, A.; Le Péchoux, C.; Rolland, E.; Curran, W. J.; Furuse, K.*, et al.*, Meta-analysis of concomitant versus sequential radiochemotherapy in locally advanced non-small-cell lung cancer. *J. Clin. Oncol.* 2010, *28* (13), 2181-2190.
18. Shirvani, S. M.; Chang, J. Y., Scalpel or SABR for Treatment of Early-Stage Lung Cancer: Clinical Considerations for the Multidisciplinary Team. *Cancers* 2011, *3* (3), 3432-3448.
19. Timmerman, R.; McGarry, R.; Yiannoutsos, C.; Papiez, L.; Tudor, K.*, et al.*, Excessive toxicity when treating central tumors in a phase II study of stereotactic body radiation therapy for medically inoperable early-stage lung cancer. *J. Clin. Oncol.* 2006, *24* (30), 4833-9.
20. Forquer, J. A.; Fakiris, A. J.; Timmerman, R. D.; Lo, S. S.; Perkins, S. M.*, et al.*, Brachial plexopathy from stereotactic body radiotherapy in early-stage NSCLC: dose-limiting toxicity in apical tumor sites. *Radiother. Oncol.* 2009, *93* (3), 408-13.
21. Johnson, D. H., Evolution of cisplatin-based chemotherapy in non-small cell lung cancer: a historical perspective and the eastern cooperative oncology group experience. *Chest* 2000, *117* (4 Suppl 1), 133S-137S.
22. Schiller, J. H.; Harrington, D.; Belani, C. P.; Langer, C.; Sandler, A.*, et al.*, Comparison of four chemotherapy regimens for advanced non-small-cell lung cancer. *N. Engl. J. Med.* 2002, *346* (2), 92-98.
23. Kris, M. G.; Gralla, R. J.; Kalman, L. A.; Kelsen, D. P.; Casper, E. S.*, et al.*, Randomized trial comparing vindesine plus cisplatin with vinblastine plus cisplatin in patients with non-small cell lung cancer, with an analysis of methods of response assessment. *Cancer Treat. Rep.* 1985, *69* (4), 387-95.
24. Franklin, W. A.; Veve, R.; Hirsch, F. R.; Helfrich, B. A.; Bunn, P. A., Jr., Epidermal growth factor receptor family in lung cancer and premalignancy. *Semin. Oncol.* 2002, *29* (1 Suppl 4), 3-14.

25. Mok, T. S.; Wu, Y. L.; Thongprasert, S.; Yang, C. H.; Chu, D. T.*, et al.*, Gefitinib or carboplatin–paclitaxel in pulmonary adenocarcinoma. *N. Engl. J. Med.* 2009, *361* (10), 947-957.
26. Soda, M.; Choi, Y. L.; Enomoto, M.; Takada, S.; Yamashita, Y.*, et al.*, Identification of the transforming EML4–ALK fusion gene in non-small-cell lung cancer. *Nature* 2007, *448* (7153), 561-566.
27. Winau, F.; Westphal, O.; Winau, R., Paul Ehrlich — in search of the magic bullet. *Microbes Infect.* 2004, *6* (8), 786-789.
28. Canal, P.; Gamelin, E.; Vassal, G.; Robert, J., Benefits of pharmacological knowledge in the design and monitoring of cancer chemotherapy. *Pathol. Oncol. Res.* 1998, *4* (3), 171-178.
29. Reichert, J. M.; Valge-Archer, V. E., Development trends for monoclonal antibody cancer therapeutics. *Nat. Rev. Drug Discovery* 2007, *6* (5), 349-356.
30. Pazdur, R. FDA Approval for Brentuximab Vedotin 2011. HTTP://WWW.CANCER.GOV (accessed June 28, 2012).
31. Adams, G. P.; Weiner, L. M., Monoclonal antibody therapy of cancer. *Nat. Biotechnol.* 2005, *23* (9), 1147-1157.
32. Dvorak, H. F.; Nagy, J. A.; Dvorak, A. M., Structure of solid tumors and their vasculature: implications for therapy with monoclonal antibodies. *Cancer Cells* 1991, *3* (3), 77-85.
33. Tabrizi, M. A.; Tseng, C.-M. L.; Roskos, L. K., Elimination mechanisms of therapeutic monoclonal antibodies. *Drug Discovery Today* 2006, *11* (1-2), 81-88.
34. Neumeister, P.; Eibl, M.; Zinke-Cerwenka, W.; Scarpatetti, M.; Sill, H.*, et al.*, Hepatic veno-occlusive disease in two patients with relapsed acute myeloid leukemia treated with anti-CD33 calicheamicin (CMA-676) immunoconjugate. *Ann. Hematol.* 2001, *80* (2), 119-120.
35. Bray, B. L., Innovation: Large-scale manufacture of peptide therapeutics by chemical synthesis. *Nat. Rev. Drug Discovery* 2003, *2* (7), 587-593.
36. Schally, A. V.; Nagy, A., New approaches to treatment of various cancers based on cytotoxic analogs of LHRH, somatostatin and bombesin. *Life Sciences* 2003, *72* (21), 2305-2320.
37. Smith, G. P., Filamentous fusion phage: novel expression vectors that display cloned antigens on the virion surface. *Science* 1985, *228* (4705), 1315-7.
38. Aina, O. H.; Liu, R.; Sutcliffe, J. L.; Marik, J.; Pan, C. X.*, et al.*, From combinatorial chemistry to cancer-targeting peptides. *Mol. Pharm.* 2007, *4* (5), 631-51.

39. Barbas, C. F., 3rd; Kang, A. S.; Lerner, R. A.; Benkovic, S. J., Assembly of combinatorial antibody libraries on phage surfaces: the gene III site. *Proc. Natl. Acad. Sci. U. S. A.* 1991, *88* (18), 7978-82.
40. Smith, G. P.; Petrenko, V. A., Phage Display. *Chem. Rev.* 1997, *97* (2), 391-410.
41. Gao, C.; Mao, S.; Lo, C. H.; Wirsching, P.; Lerner, R. A.*, et al.*, Making artificial antibodies: a format for phage display of combinatorial heterodimeric arrays. *Proc. Natl. Acad. Sci. U. S. A.* 1999, *96* (11), 6025-30.
42. Kehoe, J. W.; Kay, B. K., Filamentous phage display in the new millennium. *Chem. Rev.* 2005, *105* (11), 4056-72.
43. Scott, J. K.; Smith, G. P., Searching for peptide ligands with an epitope library. *Science* 1990, *249* (4967), 386-90.
44. Cwirla, S. E.; Peters, E. A.; Barrett, R. W.; Dower, W. J., Peptides on phage: a vast library of peptides for identifying ligands. *Proc. Natl. Acad. Sci. U. S. A.* 1990, *87* (16), 6378-82.
45. Mazzucchelli, L.; Burritt, J. B.; Jesaitis, A. J.; Nusrat, A.; Liang, T. W.*, et al.*, Cell-specific peptide binding by human neutrophils. *Blood* 1999, *93* (5), 1738-48.
46. Ph.D. Phage Dispaly Libraries Instruction Manual. In *Protein Tools*, New England Biolabs: pp i - 42.
47. Zhong, G.; Smith, G. P.; Berry, J.; Brunham, R. C., Conformational mimicry of a chlamydial neutralization epitope on filamentous phage. *J. Biol. Chem.* 1994, *269* (39), 24183-8.
48. Kuzmicheva, G. A.; Jayanna, P. K.; Sorokulova, I. B.; Petrenko, V. A., Diversity and censoring of landscape phage libraries. *Protein Eng. Des. Sel.* 2009, *22* (1), 9-18.
49. Phage Display Discovery Tool. HTTP://WWW.DYAX.COM/RESEARCH/PHAGE-DISPLAY-DISCOVERY-TOOL.HTML (accessed 5-26).
50. . Explanation of the Smith Lab Phage Display Vectors 2012, p. 1-8. http://WWW.BIOSCI.MISSOURI.EDU/SMITHGP/PHAGEDISPLAYWEBSITE/VECTORS.DOC (accessed 5-26-12).
51. Serwer, P.; Wright, E. T.; Hakala, K. W.; Weintraub, S. T., Evidence for bacteriophage T7 tail extension during DNA injection. *BMC Res. Notes* 2008, *1*, 36.
52. Felici, F.; Castagnoli, L.; Musacchio, A.; Jappelli, R.; Cesareni, G., Selection of antibody ligands from a large library of oligopeptides expressed on a multivalent exposition vector. *J. Mol. Biol.* 1991, *222* (2), 301-10.

53. Gao, C.; Mao, S.; Ditzel, H. J.; Farnaes, L.; Wirsching, P.*, et al.*, A cell-penetrating peptide from a novel pVII-pIX phage-displayed random peptide library. *Bioorg. Med. Chem.* 2002, *10* (12), 4057-65.
54. Steven, A. C.; Trus, B. L., The structure of bacteriophage T7. In *Electron Microscopy of Proteins*, Academic Press: New York, 1986; Vol. 5, pp 2-35.
55. Condron, B. G.; Atkins, J. F.; Gesteland, R. F., Frameshifting in gene 10 of bacteriophage T7. *J. Bacteriol.* 1991, *173* (21), 6998-2003.
56. T7Select System Manual. Novagen, Ed. 2011; pp 1-24.
57. Liu, C. C.; Mack, A. V.; Tsao, M. L.; Mills, J. H.; Lee, H. S.*, et al.*, Protein evolution with an expanded genetic code. *Proc. Natl. Acad. Sci. U. S. A.* 2008, *105* (46), 17688-93.
58. Daugherty, P. S., Protein engineering with bacterial display. *Curr. Opin. Struct. Biol.* 2007, *17* (4), 474-80.
59. Georgiou, G.; Stathopoulos, C.; Daugherty, P. S.; Nayak, A. R.; Iverson, B. L.*, et al.*, Display of heterologous proteins on the surface of microorganisms: from the screening of combinatorial libraries to live recombinant vaccines. *Nat. Biotechnol.* 1997, *15* (1), 29-34.
60. Lu, Z.; Murray, K. S.; Van Cleave, V.; LaVallie, E. R.; Stahl, M. L.*, et al.*, Expression of thioredoxin random peptide libraries on the Escherichia coli cell surface as functional fusions to flagellin: a system designed for exploring protein-protein interactions. *Biotechnology (N Y)* 1995, *13* (4), 366-72.
61. Bessette, P. H.; Rice, J. J.; Daugherty, P. S., Rapid isolation of high-affinity protein binding peptides using bacterial display. *Protein Eng. Des. Sel.* 2004, *17* (10), 731-9.
62. Rice, J. J.; Schohn, A.; Bessette, P. H.; Boulware, K. T.; Daugherty, P. S., Bacterial display using circularly permuted outer membrane protein OmpX yields high affinity peptide ligands. *Protein Sci.* 2006, *15* (4), 825-36.
63. Nakajima, H.; Shimbara, N.; Shimonishi, Y.; Mimori, T.; Niwa, S.*, et al.*, Expression of random peptide fused to invasin on bacterial cell surface for selection of cell-targeting peptides. *Gene* 2000, *260* (1-2), 121-31.
64. Chen, W.; Georgiou, G., Cell-Surface display of heterologous proteins: From high-throughput screening to environmental applications. *Biotechnol. Bioeng.* 2002, *79* (5), 496-503.
65. Lam, K. S.; Lebl, M.; Krchnak, V., The "One-Bead-One-Compound" Combinatorial Library Method. *Chem. Rev.* 1997, *97* (2), 411-448.
66. Lam, K. S.; Salmon, S. E.; Hersh, E. M.; Hruby, V. J.; Kazmierski, W. M.*, et al.*, A new type of synthetic peptide library for identifying ligand-binding activity. *Nature* 1991, *354* (6348), 82-4.

67. Liu, R.; Marik, J.; Lam, K. S., A novel peptide-based encoding system for "one-bead one-compound" peptidomimetic and small molecule combinatorial libraries. *J. Am. Chem. Soc.* 2002, *124* (26), 7678-80.
68. Wang, X.; Peng, L.; Liu, R.; Gill, S. S.; Lam, K. S., Partial alloc-deprotection approach for ladder synthesis of "one-bead one-compound" combinatorial libraries. *J. Comb. Chem.* 2005, *7* (2), 197-209.
69. Aggarwal, S.; Janssen, S.; Wadkins, R. M.; Harden, J. L.; Denmeade, S. R., A combinatorial approach to the selective capture of circulating malignant epithelial cells by peptide ligands. *Biomaterials* 2005, *26* (30), 6077-86.
70. Aggarwal, S.; Harden, J. L.; Denmeade, S. R., Synthesis and screening of a random dimeric peptide library using the one-bead-one-dimer combinatorial approach. *Bioconjug. Chem.* 2006, *17* (2), 335-40.
71. Dooley, C. T.; Houghten, R. A., The use of positional scanning synthetic peptide combinatorial libraries for the rapid determination of opioid receptor ligands. *Life Sci.* 1993, *52* (18), 1509-17.
72. Dooley, C. T.; Houghten, R. A., Synthesis and screening of positional scanning combinatorial libraries. *Methods Mol. Biol.* 1998, *87*, 13-24.
73. Pinilla, C.; Appel, J. R.; Blanc, P.; Houghten, R. A., Rapid identification of high affinity peptide ligands using positional scanning synthetic peptide combinatorial libraries. *Biotechniques* 1992, *13* (6), 901-5.
74. Rothman, R. B.; Baumann, M. H.; Dersch, C. M.; Appel, J.; Houghten, R. A., Discovery of novel peptidic dopamine transporter ligands by screening a positional scanning combinatorial hexapeptide library. *Synapse* 1999, *33* (3), 239-46.
75. Lee, Y.; Kang, D. K.; Chang, S. I.; Han, M. H.; Kang, I. C., High-throughput screening of novel peptide inhibitors of an integrin receptor from the hexapeptide library by using a protein microarray chip. *J. Biomol. Screen* 2004, *9* (8), 687-94.
76. Kim, E. Y.; Bang, J. Y.; Chang, S. I.; Kang, I. C., A novel integrin alpha5beta1 antagonistic peptide, A5-1, screened by Protein Chip system as a potent angiogenesis inhibitor. *Biochem. Biophys. Res. Commun.* 2008, *377* (4), 1288-93.
77. Liu, R.; Enstrom, A. M.; Lam, K. S., Combinatorial peptide library methods for immunobiology research. *Exp. Hematol.* 2003, *31* (1), 11-30.
78. Brown, K. C., Peptidic tumor targeting agents: the road from phage display peptide selections to clinical applications. *Curr. Pharm. Des.* 2010, *16* (9), 1040-54.
79. Pasqualini, R.; Ruoslahti, E., Organ targeting in vivo using phage display peptide libraries. *Nature* 1996, *380* (6572), 364-6.

80. Barry, M. A.; Dower, W. J.; Johnston, S. A., Toward cell-targeting gene therapy vectors: selection of cell-binding peptides from random peptide-presenting phage libraries. *Nat. Med.* 1996, *2* (3), 299-305.
81. Elayadi, A. N.; Samli, K. N.; Prudkin, L.; Liu, Y.-H.; Bian, A.*, et al.*, A peptide selected by biopanning identifies the integrin alphavbeta6 as a prognostic biomarker for nonsmall cell lung cancer. *Cancer Res.* 2007, *67* (12), 5889-5895.
82. Bausch, D.; Thomas, S.; Mino-Kenudson, M.; Fernandez-del, C. C.; Bauer, T. W.*, et al.*, Plectin-1 as a novel biomarker for pancreatic cancer. *Clin. Cancer Res.* 2011, *17* (2), 302-9.
83. Kubo, N.; Akita, N.; Shimizu, A.; Kitahara, H.; Parker, A. L.*, et al.*, Identification of oligopeptide binding to colon cancer cells separated from patients using laser capture microdissection. *J. Drug Target.* 2008, *16* (5), 396-404.
84. Kolonin, M. G.; Bover, L.; Sun, J.; Zurita, A. J.; Do, K. A.*, et al.*, Ligand-directed surface profiling of human cancer cells with combinatorial peptide libraries. *Cancer Res.* 2006, *66* (1), 34-40.
85. Shukla, G. S.; Krag, D. N., Selection of tumor-targeting agents on freshly excised human breast tumors using a phage display library. *Oncol. Rep.* 2005, *13* (4), 757-64.
86. Arap, W.; Kolonin, M. G.; Trepel, M.; Lahdenranta, J.; Cardo-Vila, M.*, et al.*, Steps toward mapping the human vasculature by phage display. *Nat. Med.* 2002, *8* (2), 121-7.
87. Cardo-Vila, M.; Zurita, A. J.; Giordano, R. J.; Sun, J.; Rangel, R.*, et al.*, A ligand peptide motif selected from a cancer patient is a receptor-interacting site within human interleukin-11. *PLoS One* 2008, *3* (10), e3452.
88. Zurita, A. J.; Troncoso, P.; Cardo-Vila, M.; Logothetis, C. J.; Pasqualini, R.*, et al.*, Combinatorial screenings in patients: the interleukin-11 receptor alpha as a candidate target in the progression of human prostate cancer. *Cancer Res.* 2004, *64* (2), 435-9.
89. Pasqualini, R.; Moeller, B. J.; Arap, W., Leveraging molecular heterogeneity of the vascular endothelium for targeted drug delivery and imaging. *Semin. Thromb. Hemost.* 2010, *36* (3), 343-51.
90. Krag, D. N.; Shukla, G. S.; Shen, G. P.; Pero, S.; Ashikaga, T.*, et al.*, Selection of tumor-binding ligands in cancer patients with phage display libraries. *Cancer Res.* 2006, *66* (15), 7724-33.
91. Cao, Q.; Liu, S.; Niu, G.; Chen, K.; Yan, Y.*, et al.*, Phage display peptide probes for imaging early response to bevacizumab treatment. *Amino Acids* 2011, *41* (5), 1103-12.

92. Passarella, R. J.; Zhou, L.; Phillips, J. G.; Wu, H.; Hallahan, D. E.*, et al.*, Recombinant peptides as biomarkers for tumor response to molecular targeted therapy. *Clin. Cancer Res.* 2009, *15* (20), 6421-9.
93. Han, Z.; Fu, A.; Wang, H.; Diaz, R.; Geng, L.*, et al.*, Noninvasive assessment of cancer response to therapy. *Nat. Med.* 2008, *14* (3), 343-9.
94. Bussolati, B.; Grange, C.; Tei, L.; Deregibus, M. C.; Ercolani, M.*, et al.*, Targeting of human renal tumor-derived endothelial cells with peptides obtained by phage display. *J. Mol. Med. (Berl.)* 2007, *85* (8), 897-906.
95. There is debate about whether this cell line is a breast cancer cell line or a melanoma cell line. See references 96-98 for details.
96. Rae, J. M.; Creighton, C. J.; Meck, J. M.; Haddad, B. R.; Johnson, M. D., MDA-MB-435 cells are derived from M14 melanoma cells--a loss for breast cancer, but a boon for melanoma research. *Breast Cancer Res. Treat.* 2007, *104* (1), 13-9.
97. Chambers, A. F., MDA-MB-435 and M14 cell lines: identical but not M14 melanoma? *Cancer Res.* 2009, *69* (13), 5292-3.
98. Hollestelle, A.; Schutte, M., Comment Re: MDA-MB-435 and M14 cell lines: identical but not M14 Melanoma? *Cancer Res.* 2009, *69* (19), 7893.
99. Laakkonen, P.; Porkka, K.; Hoffman, J. A.; Ruoslahti, E., A tumor-homing peptide with a targeting specificity related to lymphatic vessels. *Nat. Med.* 2002, *8* (7), 751-5.
100. Laakkonen, P.; Akerman, M. E.; Biliran, H.; Yang, M.; Ferrer, F.*, et al.*, Antitumor activity of a homing peptide that targets tumor lymphatics and tumor cells. *Proc. Natl. Acad. Sci. U. S. A.* 2004, *101* (25), 9381-6.
101. Zhang, L.; Giraudo, E.; Hoffman, J. A.; Hanahan, D.; Ruoslahti, E., Lymphatic zip codes in premalignant lesions and tumors. *Cancer Res.* 2006, *66* (11), 5696-706.
102. Laakkonen, P.; Zhang, L.; Ruoslahti, E., Peptide targeting of tumor lymph vessels. *Ann. N. Y. Acad. Sci.* 2008, *1131*, 37-43.
103. Dane, K. Y.; Chan, L. A.; Rice, J. J.; Daugherty, P. S., Isolation of cell specific peptide ligands using fluorescent bacterial display libraries. *J. Immunol. Methods* 2006, *309* (1-2), 120-9.
104. Pennington, M. E.; Lam, K. S.; Cress, A. E., The use of a combinatorial library method to isolate human tumor cell adhesion peptides. *Mol. Divers.* 1996, *2* (1-2), 19-28.
105. Aina, O. H.; Sroka, T. C.; Chen, M. L.; Lam, K. S., Therapeutic cancer targeting peptides. *Biopolymers* 2002, *66* (3), 184-99.
106. Lam, K. S.; Lou, Q.; Zhao, Z. G.; Smith, J.; Chen, M. L.*, et al.*, Idiotype specific peptides bind to the surface immunoglobulins of two murine B-cell lymphoma lines, inducing signal transduction. *Biomed. Pept. Proteins Nucleic Acids* 1995, *1* (3), 205-10.

107. Denholt, C. L.; Hansen, P. R.; Pedersen, N.; Poulsen, H. S.; Gillings, N.*, et al.*, Identification of novel peptide ligands for the cancer-specific receptor mutation EFGRvIII using a mixture-based synthetic combinatorial library. *Biopolymers* 2009, *91* (3), 201-6.
108. Gazdar, A. F.; Girard, L.; Lockwood, W. W.; Lam, W. L.; Minna, J. D., Lung cancer cell lines as tools for biomedical discovery and research. *J. Natl. Cancer Inst.* 2010, *102* (17), 1310-21.
109. Nair, R. R.; Emmons, M. F.; Cress, A. E.; Argilagos, R. F.; Lam, K.*, et al.*, HYD1-induced increase in reactive oxygen species leads to autophagy and necrotic cell death in multiple myeloma cells. *Mol. Cancer Ther.* 2009, *8* (8), 2441-51.
110. van Hensbergen, Y.; Broxterman, H. J.; Elderkamp, Y. W.; Lankelma, J.; Beers, J. C.*, et al.*, A doxorubicin-CNGRC-peptide conjugate with prodrug properties. *Biochem. Pharmacol.* 2002, *63* (5), 897-908.
111. Meyer-Losic, F.; Quinonero, J.; Dubois, V.; Alluis, B.; Dechambre, M.*, et al.*, Improved therapeutic efficacy of doxorubicin through conjugation with a novel peptide drug delivery technology (Vectocell). *J. Med. Chem.* 2006, *49* (23), 6908-16.
112. Yoneda, Y.; Steiniger, S. C.; Capkova, K.; Mee, J. M.; Liu, Y.*, et al.*, A cell-penetrating peptidic GRP78 ligand for tumor cell-specific prodrug therapy. *Bioorg. Med. Chem. Lett.* 2008, *18* (5), 1632-6.
113. Min, K.; Jo, H.; Song, K.; Cho, M.; Chun, Y. S.*, et al.*, Dual-aptamer-based delivery vehicle of doxorubicin to both PSMA (+) and PSMA (-) prostate cancers. *Biomaterials* 2011, *32* (8), 2124-32.
114. Zhou, X.; Chang, Y. C.; Oyama, T.; McGuire, M. J.; Brown, K. C., Cell-specific delivery of a chemotherapeutic to lung cancer cells. *J. Am. Chem. Soc.* 2004, *126* (48), 15656-7.
115. Arap, W.; Pasqualini, R.; Ruoslahti, E., Cancer treatment by targeted drug delivery to tumor vasculature in a mouse model. *Science* 1998, *279* (5349), 377-80.
116. Kim, J. W.; Lee, H. S., Tumor targeting by doxorubicin-RGD-4C peptide conjugate in an orthotopic mouse hepatoma model. *Int. J. Mol. Med.* 2004, *14* (4), 529-35.
117. Du, B.; Han, H.; Wang, Z.; Kuang, L.; Wang, L.*, et al.*, targeted drug delivery to hepatocarcinoma in vivo by phage-displayed specific binding peptide. *Mol. Cancer Res.* 2010, *8* (2), 135-44.
118. Kim, Y.; Lillo, A. M.; Steiniger, S. C.; Liu, Y.; Ballatore, C.*, et al.*, Targeting heat shock proteins on cancer cells: selection, characterization, and cell-penetrating properties of a peptidic GRP78 ligand. *Biochemistry* 2006, *45* (31), 9434-44.

119. Wang, X. F.; Birringer, M.; Dong, L. F.; Veprek, P.; Low, P.*, et al.*, A peptide conjugate of vitamin E succinate targets breast cancer cells with high ErbB2 expression. *Cancer Res.* 2007, *67* (7), 3337-44.
120. Kohno, M.; Horibe, T.; Haramoto, M.; Yano, Y.; Ohara, K.*, et al.*, A novel hybrid peptide targeting EGFR-expressing cancers. *Eur. J. Cancer* 2011, *47* (5), 773-83.
121. Kelly, K. A.; Jones, D. A., Isolation of a colon tumor specific binding peptide using phage display selection. *Neoplasia* 2003, *5* (5), 437-44.
122. Nishimura, S.; Takahashi, S.; Kamikatahira, H.; Kuroki, Y.; Jaalouk, D. E.*, et al.*, Combinatorial targeting of the macropinocytotic pathway in leukemia and lymphoma cells. *J. Biol. Chem.* 2008, *283* (17), 11752-62.
123. Karjalainen, K.; Jaalouk, D. E.; Bueso-Ramos, C. E.; Zurita, A. J.; Kuniyasu, A.*, et al.*, Targeting neuropilin-1 in human leukemia and lymphoma. *Blood* 2011, *117* (3), 920-7.
124. Mintz, P. J.; Cardo-Vila, M.; Ozawa, M. G.; Hajitou, A.; Rangel, R.*, et al.*, An unrecognized extracellular function for an intracellular adapter protein released from the cytoplasm into the tumor microenvironment. *Proc. Natl. Acad. Sci. U. S. A.* 2009, *106* (7), 2182-7.
125. Jiang, Y. Q.; Wang, H. R.; Li, H. P.; Hao, H. J.; Zheng, Y. L.*, et al.*, Targeting of hepatoma cell and suppression of tumor growth by a novel 12mer peptide fused to superantigen TSST-1. *Mol. Med.* 2006, *12* (4-6), 81-7.
126. Cai, J.; Wei, R.; Cheng, J., Preparation and characterization of a novel chimeric protein VEGI-CTT in Escherichia coli. *J. Biomed. Biotechnol.* 2008, *2008*, 564969.
127. Zou, Y.; Chen, Y.; Jiang, Y.; Gao, J.; Gu, J., Targeting matrix metalloproteinases and endothelial cells with a fusion peptide against tumor. *Cancer Res.* 2007, *67* (15), 7295-300.
128. Meng, J.; Ma, N.; Yan, Z.; Han, W.; Zhang, Y., NGR enhanced the anti-angiogenic activity of tum-5. *J. Biochem.* 2006, *140* (2), 299-304.
129. Meng, J.; Yan, Z.; Wu, J.; Li, L.; Xue, X.*, et al.*, High-yield expression, purification and characterization of tumor-targeted IFN-alpha2a. *Cytotherapy* 2007, *9* (1), 60-8.
130. Zhang, B.; Gao, B.; Dong, S.; Zhang, Y.; Wu, Y., Anti-tumor efficacy and pre-clinical immunogenicity of IFNalpha2a-NGR. *Regul. Toxicol. Pharmacol.* 2011, *60* (1), 73-8.
131. Hamzah, J.; Nelson, D.; Moldenhauer, G.; Arnold, B.; Hammerling, G. J.*, et al.*, Vascular targeting of anti-CD40 antibodies and IL-2 into autochthonous tumors enhances immunotherapy in mice. *J. Clin. Invest.* 2008, *118* (5), 1691-9.

132. Chen, B.; Cao, S.; Zhang, Y.; Wang, X.; Liu, J.*, et al.*, A novel peptide (GX1) homing to gastric cancer vasculature inhibits angiogenesis and cooperates with TNF alpha in anti-tumor therapy. *BMC Cell Biol.* 2009, *10*, 63.
133. Curnis, F.; Sacchi, A.; Borgna, L.; Magni, F.; Gasparri, A.*, et al.*, Enhancement of tumor necrosis factor alpha antitumor immunotherapeutic properties by targeted delivery to aminopeptidase N (CD13). *Nat. Biotechnol.* 2000, *18* (11), 1185-90.
134. Curnis, F.; Sacchi, A.; Corti, A., Improving chemotherapeutic drug penetration in tumors by vascular targeting and barrier alteration. *J. Clin. Invest.* 2002, *110* (4), 475-82.
135. Sacchi, A.; Gasparri, A.; Curnis, F.; Bellone, M.; Corti, A., Crucial role for interferon gamma in the synergism between tumor vasculature-targeted tumor necrosis factor alpha (NGR-TNF) and doxorubicin. *Cancer Res.* 2004, *64* (19), 7150-5.
136. Sacchi, A.; Gasparri, A.; Gallo-Stampino, C.; Toma, S.; Curnis, F.*, et al.*, Synergistic antitumor activity of cisplatin, paclitaxel, and gemcitabine with tumor vasculature-targeted tumor necrosis factor-alpha. *Clin. Cancer. Res.* 2006, *12* (1), 175-82.
137. Wang, H.; Chen, K.; Cai, W.; Li, Z.; He, L.*, et al.*, Integrin-targeted imaging and therapy with RGD4C-TNF fusion protein. *Mol. Cancer Ther.* 2008, *7* (5), 1044-53.
138. Corti, A.; Pastorino, F.; Curnis, F.; Arap, W.; Ponzoni, M.*, et al.*, Targeted drug delivery and penetration into solid tumors. *Med. Res. Rev.* 2011.
139. Jain, R. K., Delivery of molecular and cellular medicine to solid tumors. *J. Control. Release* 1998, *53* (1-3), 49-67.
140. Torchilin, V. P.; Lukyanov, A. N., Peptide and protein drug delivery to and into tumors: challenges and solutions. *Drug Discovery Today* 2003, *8* (6), 259-266.
141. Allen, T. M.; Cheng, W. W.; Hare, J. I.; Laginha, K. M., Pharmacokinetics and pharmacodynamics of lipidic nano-particles in cancer. *Anticancer Agents Med. Chem.* 2006, *6* (6), 513-23.
142. Torchilin, V. P., Recent advances with liposomes as pharmaceutical carriers. *Nat. Rev. Drug Discov.* 2005, *4* (2), 145-60.
143. Owens, D. E., 3rd; Peppas, N. A., Opsonization, biodistribution, and pharmacokinetics of polymeric nanoparticles. *Int. J. Pharm.* 2006, *307* (1), 93-102.
144. Tollemar, J.; Andersson, S.; Ringden, O.; Tyden, G., A retrospective clinical comparison between antifungal treatment with liposomal amphotericin B (AmBisome) and conventional amphotericin B in transplant recipients. *Mycoses* 1992, *35* (9-10), 215-20.

145. Gordon, A. N.; Fleagle, J. T.; Guthrie, D.; Parkin, D. E.; Gore, M. E.*, et al.*, Recurrent epithelial ovarian carcinoma: a randomized phase III study of pegylated liposomal doxorubicin versus topotecan. *J. Clin. Oncol.* 2001, *19* (14), 3312-22.
146. Orlowski, R. Z.; Nagler, A.; Sonneveld, P.; Blade, J.; Hajek, R.*, et al.*, Randomized phase III study of pegylated liposomal doxorubicin plus bortezomib compared with bortezomib alone in relapsed or refractory multiple myeloma: combination therapy improves time to progression. *J. Clin. Oncol.* 2007, *25* (25), 3892-901.
147. Northfelt, D. W.; Dezube, B. J.; Thommes, J. A.; Levine, R.; Von Roenn, J. H.*, et al.*, Efficacy of pegylated-liposomal doxorubicin in the treatment of AIDS-related Kaposi's sarcoma after failure of standard chemotherapy. *J. Clin. Oncol.* 1997, *15* (2), 653-9.
148. Duggan, S. T.; Keating, G. M., Pegylated liposomal doxorubicin: a review of its use in metastatic breast cancer, ovarian cancer, multiple myeloma and AIDS-related Kaposi's sarcoma. *Drugs* 2011, *71* (18), 2531-58.
149. Pegylated Liposomal Doxorubicin and Carboplatin as First Line Treatment for Patients With Advanced Non-small Cell Lung Cancer. HTTP://CLINICALTRIALS.GOV/CT2/SHOW/NCT01051362?TERM=DOXIL&COND=NON-SMALL+CELL+LUNG+CANCER&RANK=1.
150. Taatjes, D. J.; Koch, T. H., Nuclear targeting and retention of anthracycline antitumor drugs in sensitive and resistant tumor cells. *Curr. Med. Chem.* 2001, *8* (1), 15-29.
151. Tewey, K. M.; Rowe, T. C.; Yang, L.; Halligan, B. D.; Liu, L. F., Adriamycin-induced DNA damage mediated by mammalian DNA topoisomerase II. *Science* 1984, *226* (4673), 466-8.
152. Drummond, D. C.; Meyer, O.; Hong, K.; Kirpotin, D. B.; Papahadjopoulos, D., Optimizing liposomes for delivery of chemotherapeutic agents to solid tumors. *Pharmacol. Rev.* 1999, *51* (4), 691-743.
153. Akita, N.; Maruta, F.; Seymour, L. W.; Kerr, D. J.; Parker, A. L.*, et al.*, Identification of oligopeptides binding to peritoneal tumors of gastric cancer. *Cancer Sci.* 2006, *97* (10), 1075-81.
154. Park, J. H.; von Maltzahn, G.; Xu, M. J.; Fogal, V.; Kotamraju, V. R.*, et al.*, Cooperative nanomaterial system to sensitize, target, and treat tumors. *Proc. Natl. Acad. Sci. U. S. A.* 2010, *107* (3), 981-6.
155. Song, S.; Liu, D.; Peng, J.; Sun, Y.; Li, Z.*, et al.*, Peptide ligand-mediated liposome distribution and targeting to EGFR expressing tumor in vivo. *Int. J. Pharm.* 2008, *363* (1-2), 155-61.

156. Staquicini, F. I.; Dias-Neto, E.; Li, J.; Snyder, E. Y.; Sidman, R. L.*, et al.*, Discovery of a functional protein complex of netrin-4, laminin gamma1 chain, and integrin alpha6beta1 in mouse neural stem cells. *Proc. Natl. Acad. Sci. U. S. A.* 2009, *106* (8), 2903-8.
157. Jayanna, P. K.; Bedi, D.; Gillespie, J. W.; DeInnocentes, P.; Wang, T.*, et al.*, Landscape phage fusion protein-mediated targeting of nanomedicines enhances their prostate tumor cell association and cytotoxic efficiency. *Nanomedicine* 2010, *6* (4), 538-46.
158. Chang, D. K.; Chiu, C. Y.; Kuo, S. Y.; Lin, W. C.; Lo, A.*, et al.*, Antiangiogenic targeting liposomes increase therapeutic efficacy for solid tumors. *J. Biol. Chem.* 2009, *284* (19), 12905-16.
159. Chang, D. K.; Lin, C. T.; Wu, C. H.; Wu, H. C., A novel peptide enhances therapeutic efficacy of liposomal anti-cancer drugs in mice models of human lung cancer. *PLoS One* 2009, *4* (1), e4171.
160. Lee, T. Y.; Lin, C. T.; Kuo, S. Y.; Chang, D. K.; Wu, H. C., Peptide-mediated targeting to tumor blood vessels of lung cancer for drug delivery. *Cancer Res.* 2007, *67* (22), 10958-65.
161. Lee, T. Y.; Wu, H. C.; Tseng, Y. L.; Lin, C. T., A novel peptide specifically binding to nasopharyngeal carcinoma for targeted drug delivery. *Cancer Res.* 2004, *64* (21), 8002-8.
162. Lo, A.; Lin, C. T.; Wu, H. C., Hepatocellular carcinoma cell-specific peptide ligand for targeted drug delivery. *Mol. Cancer Ther.* 2008, *7* (3), 579-89.
163. Lowery, A.; Onishko, H.; Hallahan, D. E.; Han, Z., Tumor-targeted delivery of liposome-encapsulated doxorubicin by use of a peptide that selectively binds to irradiated tumors. *J. Control. Release* 2011, *150* (1), 117-24.
164. Penate Medina, O.; Haikola, M.; Tahtinen, M.; Simpura, I.; Kaukinen, S.*, et al.*, Liposomal Tumor Targeting in Drug Delivery Utilizing MMP-2- and MMP-9-Binding Ligands. *J. Drug Deliv.* 2011, *2011*, 160515.
165. Pastorino, F.; Brignole, C.; Marimpietri, D.; Cilli, M.; Gambini, C.*, et al.*, Vascular damage and anti-angiogenic effects of tumor vessel-targeted liposomal chemotherapy. *Cancer Res.* 2003, *63* (21), 7400-9.
166. Pastorino, F.; Di Paolo, D.; Piccardi, F.; Nico, B.; Ribatti, D.*, et al.*, Enhanced antitumor efficacy of clinical-grade vasculature-targeted liposomal doxorubicin. *Clin. Cancer Res.* 2008, *14* (22), 7320-9.
167. Garde, S. V.; Forte, A. J.; Ge, M.; Lepekhin, E. A.; Panchal, C. J.*, et al.*, Binding and internalization of NGR-peptide-targeted liposomal doxorubicin (TVT-DOX) in CD13-expressing cells and its antitumor effects. *Anticancer Drugs* 2007, *18* (10), 1189-200.

168. Yuan, F.; Leunig, M.; Huang, S. K.; Berk, D. A.; Papahadjopoulos, D.*, et al.*, Microvascular permeability and interstitial penetration of sterically stabilized (stealth) liposomes in a human tumor xenograft. *Cancer Res.* 1994, *54* (13), 3352-6.
169. Vicent, M. J.; Duncan, R., Polymer conjugates: nanosized medicines for treating cancer. *Trends Biotechnol.* 2006, *24* (1), 39-47.
170. Sutton, D.; Nasongkla, N.; Blanco, E.; Gao, J., Functionalized micellar systems for cancer targeted drug delivery. *Pharm. Res.* 2007, *24* (6), 1029-46.
171. Torchilin, V. P., Structure and design of polymeric surfactant-based drug delivery systems. *J. Control. Release* 2001, *73* (2-3), 137-72.
172. Matsumura, Y.; Kataoka, K., Preclinical and clinical studies of anticancer agent-incorporating polymer micelles. *Cancer Sci.* 2009, *100* (4), 572-9.
173. Guthi, J. S.; Yang, S. G.; Huang, G.; Li, S.; Khemtong, C.*, et al.*, MRI-visible micellar nanomedicine for targeted drug delivery to lung cancer cells. *Mol. Pharm.* 2010, *7* (1), 32-40.
174. Cheng, Y.; Meyers, J. D.; Agnes, R. S.; Doane, T. L.; Kenney, M. E.*, et al.*, Addressing Brain Tumors with Targeted Gold Nanoparticles: A New Gold Standard for Hydrophobic Drug Delivery? *Small* 2011.
175. Agemy, L.; Friedmann-Morvinski, D.; Kotamraju, V. R.; Roth, L.; Sugahara, K. N.*, et al.*, Targeted nanoparticle enhanced proapoptotic peptide as potential therapy for glioblastoma. *Proc. Natl. Acad. Sci. U. S. A.* 2011, *108* (42), 17450-5.
176. Ashley, C. E.; Carnes, E. C.; Phillips, G. K.; Durfee, P. N.; Buley, M. D.*, et al.*, Cell-specific delivery of diverse cargos by bacteriophage MS2 virus-like particles. *ACS Nano* 2011, *5* (7), 5729-45.
177. Hariri, G.; Yan, H.; Wang, H.; Han, Z.; Hallahan, D. E., Radiation-guided drug delivery to mouse models of lung cancer. *Clin. Cancer. Res.* 2010, *16* (20), 4968-77.
178. Sugahara, K. N.; Teesalu, T.; Karmali, P. P.; Kotamraju, V. R.; Agemy, L.*, et al.*, Tissue-penetrating delivery of compounds and nanoparticles into tumors. *Cancer Cell* 2009, *16* (6), 510-20.
179. Sugahara, K. N.; Teesalu, T.; Karmali, P. P.; Kotamraju, V. R.; Agemy, L.*, et al.*, Coadministration of a tumor-penetrating peptide enhances the efficacy of cancer drugs. *Science* 2010, *328* (5981), 1031-5.
180. Karmali, P. P.; Kotamraju, V. R.; Kastantin, M.; Black, M.; Missirlis, D.*, et al.*, Targeting of albumin-embedded paclitaxel nanoparticles to tumors. *Nanomedicine* 2009, *5* (1), 73-82.
181. Yan, F.; Li, X.; Jin, Q.; Jiang, C.; Zhang, Z.*, et al.*, Therapeutic ultrasonic microbubbles carrying paclitaxel and LyP-1 peptide: preparation,

characterization and application to ultrasound-assisted chemotherapy in breast cancer cells. *Ultrasound Med. Biol.* 2011, *37* (5), 768-79.
182. Passarella, R. J.; Spratt, D. E.; van der Ende, A. E.; Phillips, J. G.; Wu, H.*, et al.*, Targeted nanoparticles that deliver a sustained, specific release of Paclitaxel to irradiated tumors. *Cancer Res.* 2010, *70* (11), 4550-9.
183. Matsumura, Y.; Maeda, H., A new concept for macromolecular therapeutics in cancer chemotherapy: mechanism of tumoritropic accumulation of proteins and the antitumor agent smancs. *Cancer Res.* 1986, *46* (12 Pt 1), 6387-92.
184. Bae, Y. H.; Park, K., Targeted drug delivery to tumors: myths, reality and possibility. *J. Control Release* 2011, *153* (3), 198-205.
185. Kirpotin, D. B.; Drummond, D. C.; Shao, Y.; Shalaby, M. R.; Hong, K.*, et al.*, Antibody targeting of long-circulating lipidic nanoparticles does not increase tumor localization but does increase internalization in animal models. *Cancer Res.* 2006, *66* (13), 6732-40.
186. Mamot, C.; Drummond, D. C.; Noble, C. O.; Kallab, V.; Guo, Z.*, et al.*, Epidermal growth factor receptor-targeted immunoliposomes significantly enhance the efficacy of multiple anticancer drugs in vivo. *Cancer Res.* 2005, *65* (24), 11631-8.
187. Pero, S. C.; Shukla, G. S.; Armstrong, A. L.; Peterson, D.; Fuller, S. P.*, et al.*, Identification of a small peptide that inhibits the phosphorylation of ErbB2 and proliferation of ErbB2 overexpressing breast cancer cells. *Int. J. Cancer* 2004, *111* (6), 951-60.
188. Karasseva, N. G.; Glinsky, V. V.; Chen, N. X.; Komatireddy, R.; Quinn, T. P., Identification and characterization of peptides that bind human ErbB-2 selected from a bacteriophage display library. *J. Protein Chem.* 2002, *21* (4), 287-96.
189. Kumar, S. R.; Gallazzi, F. A.; Ferdani, R.; Anderson, C. J.; Quinn, T. P.*, et al.*, In vitro and in vivo evaluation of (6)(4)Cu-radiolabeled KCCYSL peptides for targeting epidermal growth factor receptor-2 in breast carcinomas. *Cancer Biother. Radiopharm.* 2010, *25* (6), 693-703.
190. Kumar, S. R.; Quinn, T. P.; Deutscher, S. L., Evaluation of an 111In-radiolabeled peptide as a targeting and imaging agent for ErbB-2 receptor expressing breast carcinomas. *Clin. Cancer Res.* 2007, *13* (20), 6070-9.
191. Deutscher, S. L.; Figueroa, S. D.; Kumar, S. R., In-labeled KCCYSL peptide as an imaging probe for ErbB-2-expressing ovarian carcinomas. *J. Labelled Compd. Radiopharm.* 2009, *52* (14), 583-590.
192. Li, Z.; Zhao, R.; Wu, X.; Sun, Y.; Yao, M.*, et al.*, Identification and characterization of a novel peptide ligand of epidermal growth factor receptor for targeted delivery of therapeutics. *FASEB J.* 2005, *19* (14), 1978-85.

193. Klutz, K.; Schaffert, D.; Willhauck, M. J.; Grunwald, G. K.; Haase, R.*, et al.*, Epidermal growth factor receptor-targeted (131)I-therapy of liver cancer following systemic delivery of the sodium iodide symporter gene. *Mol. Ther.* 2011, *19* (4), 676-85.
194. Kelly, K. A.; Setlur, S. R.; Ross, R.; Anbazhagan, R.; Waterman, P.*, et al.*, Detection of early prostate cancer using a hepsin-targeted imaging agent. *Cancer Res.* 2008, *68* (7), 2286-91.
195. Wu, X.; Li, Z.; Yao, M.; Wang, H.; Qu, S.*, et al.*, Identification and characterization of a novel peptide ligand of Tie2 for targeting gene therapy. *Acta Biochim. Biophys. Sin. (Shanghai)* 2008, *40* (3), 217-25.
196. Mai, J.; Song, S.; Rui, M.; Liu, D.; Ding, Q.*, et al.*, A synthetic peptide mediated active targeting of cisplatin liposomes to Tie2 expressing cells. *J. Control. Release* 2009, *139* (3), 174-81.
197. Su, J. L.; Lai, K. P.; Chen, C. A.; Yang, C. Y.; Chen, P. S.*, et al.*, A novel peptide specifically binding to interleukin-6 receptor (gp80) inhibits angiogenesis and tumor growth. *Cancer Res.* 2005, *65* (11), 4827-35.
198. Koivunen, E.; Gay, D. A.; Ruoslahti, E., Selection of peptides binding to the alpha 5 beta 1 integrin from phage display library. *J. Biol. Chem.* 1993, *268* (27), 20205-10.
199. Murayama, O.; Nishida, H.; Sekiguchi, K., Novel peptide ligands for integrin alpha 6 beta 1 selected from a phage display library. *J. Biochem.* 1996, *120* (2), 445-51.
200. Koolpe, M.; Dail, M.; Pasquale, E. B., An ephrin mimetic peptide that selectively targets the EphA2 receptor. *J. Biol. Chem.* 2002, *277* (49), 46974-9.
201. Blackburn, W. H.; Dickerson, E. B.; Smith, M. H.; McDonald, J. F.; Lyon, L. A., Peptide-functionalized nanogels for targeted siRNA delivery. *Bioconjug. Chem.* 2009, *20* (5), 960-8.
202. van Geer, M. A.; Bakker, C. T.; Koizumi, N.; Mizuguchi, H.; Wesseling, J. G.*, et al.*, Ephrin A2 receptor targeting does not increase adenoviral pancreatic cancer transduction in vivo. *World J. Gastroenterol.* 2009, *15* (22), 2754-62.
203. Scarberry, K. E.; Dickerson, E. B.; McDonald, J. F.; Zhang, Z. J., Magnetic nanoparticle-peptide conjugates for in vitro and in vivo targeting and extraction of cancer cells. *J. Am. Chem. Soc.* 2008, *130* (31), 10258-62.
204. Koivunen, E.; Arap, W.; Valtanen, H.; Rainisalo, A.; Medina, O. P.*, et al.*, Tumor targeting with a selective gelatinase inhibitor. *Nat. Biotechnol.* 1999, *17* (8), 768-74.

205. Heikkila, P.; Suojanen, J.; Pirila, E.; Vaananen, A.; Koivunen, E.*, et al.*, Human tongue carcinoma growth is inhibited by selective antigelatinolytic peptides. *Int. J. Cancer* 2006, *118* (9), 2202-9.
206. Medina, O. P.; Soderlund, T.; Laakkonen, L. J.; Tuominen, E. K.; Koivunen, E.*, et al.*, Binding of novel peptide inhibitors of type IV collagenases to phospholipid membranes and use in liposome targeting to tumor cells in vitro. *Cancer Res.* 2001, *61* (10), 3978-85.
207. Kuhnast, B.; Bodenstein, C.; Haubner, R.; Wester, H. J.; Senekowitsch-Schmidtke, R.*, et al.*, Targeting of gelatinase activity with a radiolabeled cyclic HWGF peptide. *Nucl. Med. Biol.* 2004, *31* (3), 337-44.
208. Medina, O. P.; Kairemo, K.; Valtanen, H.; Kangasniemi, A.; Kaukinen, S.*, et al.*, Radionuclide imaging of tumor xenografts in mice using a gelatinase-targeting peptide. *Anticancer Res.* 2005, *25* (1A), 33-42.
209. Sprague, J. E.; Li, W. P.; Liang, K.; Achilefu, S.; Anderson, C. J., In vitro and in vivo investigation of matrix metalloproteinase expression in metastatic tumor models. *Nucl. Med. Biol.* 2006, *33* (2), 227-37.
210. Hanaoka, H.; Mukai, T.; Habashita, S.; Asano, D.; Ogawa, K.*, et al.*, Chemical design of a radiolabeled gelatinase inhibitor peptide for the imaging of gelatinase activity in tumors. *Nucl. Med. Biol.* 2007, *34* (5), 503-10.
211. Xiao, N.; Cheng, D.; Wang, Y.; Chen, L.; Liu, X.*, et al.*, Identification of a high affinity TAG-72 binding peptide by phage display selection. *Cancer Biol. Ther.* 2011, *11* (1), 22-31.
212. Rusckowski, M.; Gupta, S.; Liu, G.; Dou, S.; Hnatowich, D. J., Evidence of specificity of radiolabeled phage display peptides for the TAG-72 antigen. *Cancer Biother. Radiopharm.* 2007, *22* (4), 564-72.
213. Chen, L.; Wang, Y.; Liu, X.; Dou, S.; Liu, G.*, et al.*, A new TAG-72 cancer marker peptide identified by phage display. *Cancer Lett.* 2008, *272* (1), 122-32.
214. Devemy, E.; Blaschuk, O. W., Identification of a novel dual E- and N-cadherin antagonist. *Peptides* 2009, *30* (8), 1539-47.
215. Devemy, E.; Blaschuk, O. W., Identification of a novel N-cadherin antagonist. *Peptides* 2008, *29* (11), 1853-61.
216. Askoxylakis, V.; Garcia-Boy, R.; Rana, S.; Kramer, S.; Hebling, U.*, et al.*, A new peptide ligand for targeting human carbonic anhydrase IX, identified through the phage display technology. *PLoS One* 2010, *5* (12), e15962.
217. Zou, J.; Glinsky, V. V.; Landon, L. A.; Matthews, L.; Deutscher, S. L., Peptides specific to the galectin-3 carbohydrate recognition domain inhibit metastasis-associated cancer cell adhesion. *Carcinogenesis* 2005, *26* (2), 309-18.

218. Kumar, S. R.; Deutscher, S. L., 111In-labeled galectin-3-targeting peptide as a SPECT agent for imaging breast tumors. *J. Nucl. Med.* 2008, *49* (5), 796-803.
219. Deutscher, S. L.; Figueroa, S. D.; Kumar, S. R., Tumor targeting and SPECT imaging properties of an (111)In-labeled galectin-3 binding peptide in prostate carcinoma. *Nucl. Med. Biol.* 2009, *36* (2), 137-46.
220. Thapa, N.; Kim, S.; So, I. S.; Lee, B. H.; Kwon, I. C.*, et al.*, Discovery of a phosphatidylserine-recognizing peptide and its utility in molecular imaging of tumour apoptosis. *J. Cell. Mol. Med.* 2008, *12* (5A), 1649-60.
221. Zhao, P.; Grabinski, T.; Gao, C.; Skinner, R. S.; Giambernardi, T.*, et al.*, Identification of a met-binding peptide from a phage display library. *Clin. Cancer Res.* 2007, *13* (20), 6049-55.
222. Aggarwal, S.; Singh, P.; Topaloglu, O.; Isaacs, J. T.; Denmeade, S. R., A dimeric peptide that binds selectively to prostate-specific membrane antigen and inhibits its enzymatic activity. *Cancer Res.* 2006, *66* (18), 9171-7.
223. Qin, X.; Wan, Y.; Li, M.; Xue, X.; Wu, S.*, et al.*, Identification of a novel peptide ligand of human vascular endothelia growth factor receptor 3 for targeted tumour diagnosis and therapy. *J. Biochem.* 2007, *142* (1), 79-85.
224. Du, B.; Qian, M.; Zhou, Z.; Wang, P.; Wang, L.*, et al.*, In vitro panning of a targeting peptide to hepatocarcinoma from a phage display peptide library. *Biochem. Biophys. Res. Commun.* 2006, *342* (3), 956-62.
225. Eriksson, F.; Culp, W. D.; Massey, R.; Egevad, L.; Garland, D.*, et al.*, Tumor specific phage particles promote tumor regression in a mouse melanoma model. *Cancer Immunol. Immunother.* 2007, *56* (5), 677-87.
226. Matsuo, A. L.; Tanaka, A. S.; Juliano, M. A.; Rodrigues, E. G.; Travassos, L. R., A novel melanoma-targeting peptide screened by phage display exhibits antitumor activity. *J. Mol. Med. (Berl.)* 2010, *88* (12), 1255-64.
227. Staquicini, F. I.; Tandle, A.; Libutti, S. K.; Sun, J.; Zigler, M.*, et al.*, A subset of host B lymphocytes controls melanoma metastasis through a melanoma cell adhesion molecule/MUC18-dependent interaction: evidence from mice and humans. *Cancer Res.* 2008, *68* (20), 8419-28.
228. Huang, C.; Liu, X. Y.; Rehemtulla, A.; Lawrence, T. S., Identification of peptides that bind to irradiated pancreatic tumor cells. *Int. J. Radiat. Oncol. Biol. Phys.* 2005, *62* (5), 1497-503.
229. Romanov, V. I.; Durand, D. B.; Petrenko, V. A., Phage display selection of peptides that affect prostate carcinoma cells attachment and invasion. *Prostate* 2001, *47* (4), 239-51.
230. Zitzmann, S.; Mier, W.; Schad, A.; Kinscherf, R.; Askoxylakis, V.*, et al.*, A new prostate carcinoma binding peptide (DUP-1) for tumor imaging and therapy. *Clin. Cancer Res.* 2005, *11* (1), 139-46.

231. Askoxylakis, V.; Zitzmann-Kolbe, S.; Zoller, F.; Altmann, A.; Markert, A.*, et al.*, Challenges in optimizing a prostate carcinoma binding peptide, identified through the phage display technology. *Molecules* 2011, *16* (2), 1559-78.
232. Jayanna, P. K.; Bedi, D.; Deinnocentes, P.; Bird, R. C.; Petrenko, V. A., Landscape phage ligands for PC3 prostate carcinoma cells. *Protein Eng. Des. Sel.* 2010, *23* (6), 423-30.
233. Wang, J.; Liu, Y.; Teesalu, T.; Sugahara, K. N.; Kotamrajua, V. R.*, et al.*, Selection of phage-displayed peptides on live adherent cells in microfluidic channels. *Proc. Natl. Acad. Sci. U. S. A.* 2011, *108* (17), 6909-14.
234. Hu, S.; Guo, X.; Xie, H.; Du, Y.; Pan, Y.*, et al.*, Phage display selection of peptides that inhibit metastasis ability of gastric cancer cells with high liver-metastatic potential. *Biochem. Biophys. Res. Commun.* 2006, *341* (4), 964-72.
235. Bai, F.; Liang, J.; Wang, J.; Shi, Y.; Zhang, K.*, et al.*, Inhibitory effects of a specific phage-displayed peptide on high peritoneal metastasis of gastric cancer. *J. Mol. Med. (Berl.)* 2007, *85* (2), 169-80.
236. Liang, S.; Lin, T.; Ding, J.; Pan, Y.; Dang, D.*, et al.*, Screening and identification of vascular-endothelial-cell-specific binding peptide in gastric cancer. *J. Mol. Med. (Berl.)* 2006, *84* (9), 764-73.
237. Kelly, K.; Alencar, H.; Funovics, M.; Mahmood, U.; Weissleder, R., Detection of invasive colon cancer using a novel, targeted, library-derived fluorescent peptide. *Cancer Res.* 2004, *64* (17), 6247-51.
238. Rasmussen, U. B.; Schreiber, V.; Schultz, H.; Mischler, F.; Schughart, K., Tumor cell-targeting by phage-displayed peptides. *Cancer Gene Ther.* 2002, *9* (7), 606-12.
239. Rittner, K.; Schreiber, V.; Erbs, P.; Lusky, M., Targeting of adenovirus vectors carrying a tumor cell-specific peptide: in vitro and in vivo studies. *Cancer Gene Ther.* 2007, *14* (5), 509-18.
240. Zhang, Y.; Chen, J.; Zhang, Y.; Hu, Z.; Hu, D.*, et al.*, Panning and identification of a colon tumor binding peptide from a phage display peptide library. *J. Biomol. Screen.* 2007, *12* (3), 429-35.
241. Odermatt, A.; Audige, A.; Frick, C.; Vogt, B.; Frey, B. M.*, et al.*, Identification of receptor ligands by screening phage-display peptide libraries ex vivo on microdissected kidney tubules. *J. Am. Soc. Nephrol.* 2001, *12* (2), 308-16.
242. Hong, F. D.; Clayman, G. L., Isolation of a peptide for targeted drug delivery into human head and neck solid tumors. *Cancer Res.* 2000, *60* (23), 6551-6.

243. Bao, L.; Gorin, M. A.; Zhang, M.; Ventura, A. C.; Pomerantz, W. C.*, et al.*, Preclinical development of a bifunctional cancer cell homing, PKCepsilon inhibitory peptide for the treatment of head and neck cancer. *Cancer Res.* 2009, *69* (14), 5829-34.
244. Nothelfer, E. M.; Zitzmann-Kolbe, S.; Garcia-Boy, R.; Kramer, S.; Herold-Mende, C.*, et al.*, Identification and characterization of a peptide with affinity to head and neck cancer. *J. Nucl. Med.* 2009, *50* (3), 426-34.
245. Ivanenkov, V. V.; Felici, F.; Menon, A. G., Targeted delivery of multivalent phage display vectors into mammalian cells. *Biochim. Biophys. Acta* 1999, *1448* (3), 463-72.
246. Shadidi, M.; Sioud, M., Identification of novel carrier peptides for the specific delivery of therapeutics into cancer cells. *FASEB J.* 2003, *17* (2), 256-8.
247. Luo, H.; Yang, J.; Jin, H.; Huang, C.; Fu, J.*, et al.*, Tetrameric far-red fluorescent protein as a scaffold to assemble an octavalent peptide nanoprobe for enhanced tumor targeting and intracellular uptake in vivo. *FASEB J.* 2011, *25* (6), 1865-73.
248. Wang, T.; D'Souza, G. G.; Bedi, D.; Fagbohun, O. A.; Potturi, L. P.*, et al.*, Enhanced binding and killing of target tumor cells by drug-loaded liposomes modified with tumor-specific phage fusion coat protein. *Nanomedicine (Lond.)* 2010, *5* (4), 563-74.
249. Bedi, D.; Musacchio, T.; Fagbohun, O. A.; Gillespie, J. W.; Deinnocentes, P.*, et al.*, Delivery of siRNA into breast cancer cells via phage fusion protein-targeted liposomes. *Nanomedicine* 2011, *7* (3), 315-23.
250. Zhang, J.; Spring, H.; Schwab, M., Neuroblastoma tumor cell-binding peptides identified through random peptide phage display. *Cancer Lett.* 2001, *171* (2), 153-64.
251. Shahin, M.; Ahmed, S.; Kaur, K.; Lavasanifar, A., Decoration of polymeric micelles with cancer-specific peptide ligands for active targeting of paclitaxel. *Biomaterials* 2011, *32* (22), 5123-33.
252. Askoxylakis, V.; Zitzmann, S.; Mier, W.; Graham, K.; Kramer, S.*, et al.*, Preclinical evaluation of the breast cancer cell-binding peptide, p160. *Clin. Cancer Res.* 2005, *11* (18), 6705-12.
253. Askoxylakis, V.; Mier, W.; Zitzmann, S.; Ehemann, V.; Zhang, J.*, et al.*, Characterization and development of a peptide (p160) with affinity for neuroblastoma cells. *J. Nucl. Med.* 2006, *47* (6), 981-8.
254. Samoylova, T. I.; Petrenko, V. A.; Morrison, N. E.; Globa, L. P.; Baker, H. J.*, et al.*, Phage probes for malignant glial cells. *Mol. Cancer Ther.* 2003, *2* (11), 1129-37.
255. Spear, M. A.; Breakefield, X. O.; Beltzer, J.; Schuback, D.; Weissleder, R.*, et al.*, Isolation, characterization, and recovery of small peptide phage

display epitopes selected against viable malignant glioma cells. *Cancer Gene Ther.* 2001, *8* (7), 506-11.
256. Wu, C.; Lo, S. L.; Boulaire, J.; Hong, M. L.; Beh, H. M.*, et al.*, A peptide-based carrier for intracellular delivery of proteins into malignant glial cells in vitro. *J. Control. Release* 2008, *130* (2), 140-5.
257. Ho, I. A.; Hui, K. M.; Lam, P. Y., Isolation of peptide ligands that interact specifically with human glioma cells. *Peptides* 2010, *31* (4), 644-50.
258. Ho, I. A.; Lam, P. Y.; Hui, K. M., Identification and characterization of novel human glioma-specific peptides to potentiate tumor-specific gene delivery. *Hum. Gene Ther.* 2004, *15* (8), 719-32.
259. Robinson, P.; Stuber, D.; Deryckere, F.; Tedbury, P.; Lagrange, M.*, et al.*, Identification using phage display of peptides promoting targeting and internalization into HPV-transformed cell lines. *J. Mol. Recognit.* 2005, *18* (2), 175-82.
260. Morpurgo, M.; Kirschner, M.; Radu, A., An approach to increased polyplex gene delivery by peptides selected from a phage display library. *J. Biochem. Biophys. Methods* 2002, *52* (1), 31-43.
261. Bockmann, M.; Drosten, M.; Putzer, B. M., Discovery of targeting peptides for selective therapy of medullary thyroid carcinoma. *J. Gene Med.* 2005, *7* (2), 179-88.
262. Zitzmann, S.; Kramer, S.; Mier, W.; Hebling, U.; Altmann, A.*, et al.*, Identification and evaluation of a new tumor cell-binding peptide, FROP-1. *J. Nucl. Med.* 2007, *48* (6), 965-72.
263. Witt, H.; Hajdin, K.; Iljin, K.; Greiner, O.; Niggli, F. K.*, et al.*, Identification of a rhabdomyosarcoma targeting peptide by phage display with sequence similarities to the tumour lymphatic-homing peptide LyP-1. *Int. J. Cancer* 2009, *124* (9), 2026-32.
264. McGuire, M. J.; Samli, K. N.; Chang, Y.-C.; Brown, K. C., Novel ligands for cancer diagnosis: selection of peptide ligands for identification and isolation of B-cell lymphomas. *Exp. Hematol.* 2006, *34* (4), 443-452.
265. Jager, S.; Jahnke, A.; Wilmes, T.; Adebahr, S.; Vogtle, F. N.*, et al.*, Leukemia-targeting ligands isolated from phage-display peptide libraries. *Leukemia* 2007, *21* (3), 411-20.
266. Oyama, T.; Sykes, K. F.; Samli, K. N.; Minna, J. D.; Johnston, S. A.*, et al.*, Isolation of lung tumor specific peptides from a random peptide library: generation of diagnostic and cell-targeting reagents. *Cancer Lett.* 2003, *202* (2), 219-230.
267. Oyama, T.; Rombel, I. T.; Samli, K. N.; Zhou, X.; Brown, K. C., Isolation of multiple cell-binding ligands from different phage displayed-peptide libraries. *Biosens. Bioelectron.* 2006, *21* (10), 1867-1875.

268. Zang, L.; Shi, L.; Guo, J.; Pan, Q.; Wu, W.*, et al.*, Screening and identification of a peptide specifically targeted to NCI-H1299 from a phage display peptide library. *Cancer Lett.* 2009, *281* (1), 64-70.
269. Tu, X.; Zang, L.; Lan, D.; Liang, W., Screening and identification of a peptide specifically targeted to NCI-H1299 cells from a phage display peptide library. *Mol. Med. Report* 2009, *2* (6), 1005-10.
270. Guan, H.; McGuire, M. J.; Li, S.; Brown, K. C., Peptide-targeted polyglutamic acid doxorubicin conjugates for the treatment of alpha(v)beta(6)-positive cancers. *Bioconjug. Chem.* 2008, *19* (9), 1813-21.
271. Li, S.; McGuire, M. J.; Lin, M.; Liu, Y.-H.; Oyama, T.*, et al.*, Synthesis and characterization of a high-affinity {alpha}v{beta}6-specific ligand for in vitro and in vivo applications. *Mol. Cancer Ther.* 2009, *8* (5), 1239-1249.
272. Zhang, L.; Yin, G.; Yan, D.; Wei, Y.; Ma, C.*, et al.*, In vitro screening of ovarian tumor specific peptides from a phage display peptide library. *Biotechnol. Lett.* 2011, *33* (9), 1729-35.
273. Li, M.; Anastassiades, C. P.; Joshi, B.; Komarck, C. M.; Piraka, C.*, et al.*, Affinity peptide for targeted detection of dysplasia in Barrett's esophagus. *Gastroenterology* 2010, *139* (5), 1472-80.
274. Sun, X.; Niu, G.; Yan, Y.; Yang, M.; Chen, K.*, et al.*, Phage display-derived peptides for osteosarcoma imaging. *Clin. Cancer Res.* 2010, *16* (16), 4268-77.
275. Choi, J. H.; Lee, W. K.; Han, S. H.; Ha, S.; Ahn, S. M.*, et al.*, Identification and characterization of nonapeptide targeting a human B cell lymphoma, Raji. *Int. Immunopharmacol.* 2008, *8* (6), 852-8.
276. Hsiung, P. L.; Hardy, J.; Friedland, S.; Soetikno, R.; Du, C. B.*, et al.*, Detection of colonic dysplasia in vivo using a targeted heptapeptide and confocal microendoscopy. *Nat. Med.* 2008, *14* (4), 454-8.
277. Lee, S. M.; Lee, E. J.; Hong, H. Y.; Kwon, M. K.; Kwon, T. H.*, et al.*, Targeting bladder tumor cells in vivo and in the urine with a peptide identified by phage display. *Mol. Cancer Res.* 2007, *5* (1), 11-9.
278. Kelly, K. A.; Bardeesy, N.; Anbazhagan, R.; Gurumurthy, S.; Berger, J.*, et al.*, Targeted nanoparticles for imaging incipient pancreatic ductal adenocarcinoma. *PLoS Med* 2008, *5* (4), e85.
279. Zhi, M.; Wu, K. C.; Dong, L.; Hao, Z. M.; Deng, T. Z.*, et al.*, Characterization of a specific phage-displayed Peptide binding to vasculature of human gastric cancer. *Cancer. Biol. Ther.* 2004, *3* (12), 1232-5.
280. Hui, X.; Han, Y.; Liang, S.; Liu, Z.; Liu, J.*, et al.*, Specific targeting of the vasculature of gastric cancer by a new tumor-homing peptide CGNSNPKSC. *J. Control. Release* 2008, *131* (2), 86-93.

281. Cao, S.; Liu, Y.; Li, X.; Zhang, Y.; Wang, J.*, et al.*, Expression, purification, and characterization of recombinant protein GX1-rmhTNFalpha. *Mol. Biotechnol.* 2009, *43* (1), 1-7.
282. Chen, K.; Yap, L. P.; Park, R.; Hui, X.; Wu, K.*, et al.*, A Cy5.5-labeled phage-displayed peptide probe for near-infrared fluorescence imaging of tumor vasculature in living mice. *Amino Acids* 2012, *42* (4), 1329-37.
283. Chen, K.; Sun, X.; Niu, G.; Ma, Y.; Yap, L. P.*, et al.*, Evaluation of (6)(4)Cu labeled GX1: a phage display peptide probe for PET imaging of tumor vasculature. *Mol. Imaging Biol.* 2012, *14* (1), 96-105.
284. Wang, H.; Yan, H.; Fu, A.; Han, M.; Hallahan, D.*, et al.*, TIP-1 translocation onto the cell plasma membrane is a molecular biomarker of tumor response to ionizing radiation. *PLoS One* 2010, *5* (8), e12051.
285. Hariri, G.; Wellons, M. S.; Morris, W. H., 3rd; Lukehart, C. M.; Hallahan, D. E., Multifunctional FePt nanoparticles for radiation-guided targeting and imaging of cancer. *Ann. Biomed. Eng.* 2011, *39* (3), 946-52.
286. Liu, J.; Liu, J.; Chu, L.; Wang, Y.; Duan, Y.*, et al.*, Novel peptide-dendrimer conjugates as drug carriers for targeting nonsmall cell lung cancer. *Int. J. Nanomedicine* 2011, *6*, 59-69.
287. Sun, L.; Chu, T.; Wang, Y.; Wang, X., Radiolabeling and biodistribution of a nasopharyngeal carcinoma-targeting peptide identified by in vivo phage display. *Acta Biochim. Biophys. Sin. (Shanghai)* 2007, *39* (8), 624-32.
288. Newton, J. R.; Kelly, K. A.; Mahmood, U.; Weissleder, R.; Deutscher, S. L., In vivo selection of phage for the optical imaging of PC-3 human prostate carcinoma in mice. *Neoplasia* 2006, *8* (9), 772-80.
289. Newton-Northup, J. R.; Figueroa, S. D.; Deutscher, S. L., Streamlined in vivo selection and screening of human prostate carcinoma avid phage particles for development of peptide based in vivo tumor imaging agents. *Comb. Chem. High Throughput Screen* 2011, *14* (1), 9-21.
290. Ye, Y.; Zhu, L.; Ma, Y.; Niu, G.; Chen, X., Synthesis and evaluation of new iRGD peptide analogs for tumor optical imaging. *Bioorg. Med. Chem. Lett.* 2011, *21* (4), 1146-50.
291. Teesalu, T.; Sugahara, K. N.; Kotamraju, V. R.; Ruoslahti, E., C-end rule peptides mediate neuropilin-1-dependent cell, vascular, and tissue penetration. *Proc. Natl. Acad. Sci. U. S. A.* 2009, *106* (38), 16157-62.
292. Haspel, N.; Zanuy, D.; Nussinov, R.; Teesalu, T.; Ruoslahti, E.*, et al.*, Binding of a C-end rule peptide to the neuropilin-1 receptor: a molecular modeling approach. *Biochemistry* 2011, *50* (10), 1755-62.
293. Pasqualini, R.; Koivunen, E.; Kain, R.; Lahdenranta, J.; Sakamoto, M.*, et al.*, Aminopeptidase N is a receptor for tumor-homing peptides and a target for inhibiting angiogenesis. *Cancer Res.* 2000, *60* (3), 722-7.

294. Hajitou, A.; Trepel, M.; Lilley, C. E.; Soghomonyan, S.; Alauddin, M. M.*, et al.*, A hybrid vector for ligand-directed tumor targeting and molecular imaging. *Cell* 2006, *125* (2), 385-98.
295. Fueyo, J.; Alemany, R.; Gomez-Manzano, C.; Fuller, G. N.; Khan, A.*, et al.*, Preclinical characterization of the antiglioma activity of a tropism-enhanced adenovirus targeted to the retinoblastoma pathway. *J. Natl. Cancer Inst.* 2003, *95* (9), 652-60.
296. Line, B. R.; Mitra, A.; Nan, A.; Ghandehari, H., Targeting tumor angiogenesis: comparison of peptide and polymer-peptide conjugates. *J. Nucl. Med.* 2005, *46* (9), 1552-60.
297. Fogal, V.; Zhang, L.; Krajewski, S.; Ruoslahti, E., Mitochondrial/cell-surface protein p32/gC1qR as a molecular target in tumor cells and tumor stroma. *Cancer Res.* 2008, *68* (17), 7210-8.
298. Makela, A. R.; Matilainen, H.; White, D. J.; Ruoslahti, E.; Oker-Blom, C., Enhanced baculovirus-mediated transduction of human cancer cells by tumor-homing peptides. *J. Virol.* 2006, *80* (13), 6603-11.
299. Makela, A. R.; Enback, J.; Laakkonen, J. P.; Vihinen-Ranta, M.; Laakkonen, P.*, et al.*, Tumor targeting of baculovirus displaying a lymphatic homing peptide. *J. Gene Med.* 2008, *10* (9), 1019-31.
300. Herringson, T. P.; Altin, J. G., Effective tumor targeting and enhanced anti-tumor effect of liposomes engrafted with peptides specific for tumor lymphatics and vasculature. *Int. J. Pharm.* 2011, *411* (1-2), 206-14.
301. Zhang, F.; Niu, G.; Lin, X.; Jacobson, O.; Ma, Y.*, et al.*, Imaging tumor-induced sentinel lymph node lymphangiogenesis with LyP-1 peptide. *Amino Acids* 2012, *42* (6), 2343-51.
302. Bockmann, M.; Hilken, G.; Schmidt, A.; Cranston, A. N.; Tannapfel, A.*, et al.*, Novel SRESPHP peptide mediates specific binding to primary medullary thyroid carcinoma after systemic injection. *Hum. Gene Ther.* 2005, *16* (11), 1267-75.
303. Schmidt, A.; Eipel, C.; Furst, K.; Sommer, N.; Pahnke, J.*, et al.*, Evaluation of systemic targeting of RET oncogene-based MTC with tumor-selective peptide-tagged Ad vectors in clinical mouse models. *Gene Ther.* 2011, *18* (4), 418-23.
304. Hoffman, J. A.; Giraudo, E.; Singh, M.; Zhang, L.; Inoue, M.*, et al.*, Progressive vascular changes in a transgenic mouse model of squamous cell carcinoma. *Cancer Cell* 2003, *4* (5), 383-91.
305. Numata, K.; Reagan, M. R.; Goldstein, R. H.; Rosenblatt, M.; Kaplan, D. L., Spider silk-based gene carriers for tumor cell-specific delivery. *Bioconjug. Chem.* 2011, *22* (8), 1605-10.

306. Agemy, L.; Sugahara, K. N.; Kotamraju, V. R.; Gujraty, K.; Girard, O. M.*, et al.*, Nanoparticle-induced vascular blockade in human prostate cancer. *Blood* 2010, *116* (15), 2847-56.
307. Joyce, J. A.; Laakkonen, P.; Bernasconi, M.; Bergers, G.; Ruoslahti, E.*, et al.*, Stage-specific vascular markers revealed by phage display in a mouse model of pancreatic islet tumorigenesis. *Cancer Cell* 2003, *4* (5), 393-403.
308. Wang, W.; Ke, S.; Kwon, S.; Yallampalli, S.; Cameron, A. G.*, et al.*, A new optical and nuclear dual-labeled imaging agent targeting interleukin 11 receptor alpha-chain. *Bioconjug. Chem.* 2007, *18* (2), 397-402.
309. Miller, S. J.; Joshi, B. P.; Feng, Y.; Gaustad, A.; Fearon, E. R.*, et al.*, In vivo fluorescence-based endoscopic detection of colon dysplasia in the mouse using a novel peptide probe. *PLoS One* 2011, *6* (3), e17384.
310. Elahi, S. F.; Miller, S. J.; Joshi, B.; Wang, T. D., Targeted imaging of colorectal dysplasia in living mice with fluorescence microendoscopy. *Biomed. Opt. Express* 2011, *2* (4), 981-6.
311. Yang, W.; Luo, D.; Wang, S.; Wang, R.; Chen, R.*, et al.*, TMTP1, a novel tumor-homing peptide specifically targeting metastasis. *Clin. Cancer Res.* 2008, *14* (17), 5494-502.
312. Zitzmann, S.; Kramer, S.; Mier, W.; Mahmut, M.; Fleig, J.*, et al.*, Identification of a new prostate-specific cyclic peptide with the bacterial FliTrx system. *J. Nucl. Med.* 2005, *46* (5), 782-5.
313. Dane, K. Y.; Gottstein, C.; Daugherty, P. S., Cell surface profiling with peptide libraries yields ligand arrays that classify breast tumor subtypes. *Mol. Cancer Ther.* 2009, *8* (5), 1312-8.
314. Li, W.; Lei, P.; Yu, B.; Wu, S.; Peng, J.*, et al.*, Screening and identification of a novel target specific for hepatoma cell line HepG2 from the FliTrx bacterial peptide library. *Acta Biochim. Biophys. Sin. (Shanghai)* 2008, *40* (5), 443-51.
315. Brown, C. K.; Modzelewski, R. A.; Johnson, C. S.; Wong, M. K., A novel approach for the identification of unique tumor vasculature binding peptides using an E. coli peptide display library. *Ann. Surg. Oncol.* 2000, *7* (10), 743-9.
316. Weller, G. E.; Wong, M. K.; Modzelewski, R. A.; Lu, E.; Klibanov, A. L.*, et al.*, Ultrasonic imaging of tumor angiogenesis using contrast microbubbles targeted via the tumor-binding peptide arginine-arginine-leucine. *Cancer Res.* 2005, *65* (2), 533-9.
317. Yao, N.; Xiao, W.; Wang, X.; Marik, J.; Park, S. H.*, et al.*, Discovery of targeting ligands for breast cancer cells using the one-bead one-compound combinatorial method. *J. Med. Chem.* 2009, *52* (1), 126-33.

318. Xiao, W.; Yao, N.; Peng, L.; Liu, R.; Lam, K. S., Near-infrared optical imaging in glioblastoma xenograft with ligand-targeting alpha 3 integrin. *Eur. J. Nucl. Med. Mol. Imaging* 2009, *36* (1), 94-103.
319. Xiao, W.; Wang, Y.; Lau, E. Y.; Luo, J.; Yao, N.*, et al.*, The use of one-bead one-compound combinatorial library technology to discover high-affinity alphavbeta3 integrin and cancer targeting arginine-glycine-aspartic acid ligands with a built-in handle. *Mol. Cancer Ther.* 2010, *9* (10), 2714-23.
320. Park, S. I.; Renil, M.; Vikstrom, B.; Amro, N.; Song, L.-w.*, et al.*, The use of one-bead one-compound combinatorial library method to identify peptide ligands for alpha-4 beta-1 integrin receptor in non-Hodgkin's lymphoma. *Pept. Res. Ther.* 2002, *8*, 171-178.
321. Aina, O. H.; Marik, J.; Liu, R.; Lau, D. H.; Lam, K. S., Identification of novel targeting peptides for human ovarian cancer cells using "one-bead one-compound" combinatorial libraries. *Mol. Cancer Ther.* 2005, *4* (5), 806-13.
322. Aina, O. H.; Marik, J.; Gandour-Edwards, R.; Lam, K. S., Near-infrared optical imaging of ovarian cancer xenografts with novel alpha 3-integrin binding peptide "OA02". *Mol. Imaging* 2005, *4* (4), 439-47.
323. Lau, D.; Guo, L.; Liu, R.; Marik, J.; Lam, K., Peptide ligands targeting integrin alpha3beta1 in non-small cell lung cancer. *Lung Cancer* 2006, *52* (3), 291-7.
324. Mikawa, M.; Wang, H.; Guo, L.; Liu, R.; Marik, J.*, et al.*, Novel peptide ligands for integrin alpha 4 beta 1 overexpressed in cancer cells. *Mol. Cancer Ther.* 2004, *3* (10), 1329-34.
325. DeRoock, I. B.; Pennington, M. E.; Sroka, T. C.; Lam, K. S.; Bowden, G. T.*, et al.*, Synthetic peptides inhibit adhesion of human tumor cells to extracellular matrix proteins. *Cancer Res.* 2001, *61* (8), 3308-13.
326. Sroka, T. C.; Pennington, M. E.; Cress, A. E., Synthetic D-amino acid peptide inhibits tumor cell motility on laminin-5. *Carcinogenesis* 2006, *27* (9), 1748-57.
327. Zhang, H.; Aina, O. H.; Lam, K. S.; de Vere White, R.; Evans, C.*, et al.*, Identification of a bladder cancer-specific ligand using a combinatorial chemistry approach. *Urol. Oncol.* 2010.
328. Denholt, C. L.; Binderup, T.; Stockhausen, M. T.; Poulsen, H. S.; Spang-Thomsen, M.*, et al.*, Evaluation of 4-[18F]fluorobenzoyl-FALGEA-NH2 as a positron emission tomography tracer for epidermal growth factor receptor mutation variant III imaging in cancer. *Nucl. Med. Biol.* 2011, *38* (4), 509-15.
329. Choi, Y.; Kim, E.; Lee, Y.; Han, M. H.; Kang, I. C., Site-specific inhibition of integrin alpha v beta 3-vitronectin association by a ser-asp-

val sequence through an Arg-Gly-Asp-binding site of the integrin. *Proteomics* 2010, *10* (1), 72-80.
330. Bang, J. Y.; Kim, E. Y.; Kang, D. K.; Chang, S. I.; Han, M. H.*, et al.*, Pharmacoproteomic analysis of a novel cell-permeable peptide inhibitor of tumor-induced angiogenesis. *Mol. Cell. Proteomics* 2011, *10* (8), M110 005264.
331. Baek, S. H.; Seo, J. K.; Chae, C. B.; Suh, P. G.; Ryu, S. H., Identification of the peptides that stimulate the phosphoinositide hydrolysis in lymphocyte cell lines from peptide libraries. *J. Biol. Chem.* 1996, *271* (14), 8170-5.
332. Christophe, T.; Karlsson, A.; Dugave, C.; Rabiet, M. J.; Boulay, F.*, et al.*, The synthetic peptide Trp-Lys-Tyr-Met-Val-Met-NH2 specifically activates neutrophils through FPRL1/lipoxin A4 receptors and is an agonist for the orphan monocyte-expressed chemoattractant receptor FPRL2. *J. Biol. Chem.* 2001, *276* (24), 21585-93.
333. Le, Y.; Gong, W.; Li, B.; Dunlop, N. M.; Shen, W.*, et al.*, Utilization of two seven-transmembrane, G protein-coupled receptors, formyl peptide receptor-like 1 and formyl peptide receptor, by the synthetic hexapeptide WKYMVm for human phagocyte activation. *J. Immunol.* 1999, *163* (12), 6777-84.
334. Phelps, R. M.; Johnson, B. E.; Ihde, D. C.; Gazdar, A. F.; Carbone, D. P.*, et al.*, NCI-Navy Medical Oncology Branch cell line data base. *J. Cell Biochem. Suppl.* 1996, *24*, 32-91.
335. De, J.; Chang, Y.-C.; Samli, K. N.; Schisler, J. C.; Newgard, C. B.*, et al.*, Isolation of a mycoplasma-specific binding peptide from an unbiased phage-displayed peptide library. *Mol. BioSyst.* 2005, *1* (2), 149-157.
336. McGuire, M. J.; Sykes, K. F.; Samli, K. N.; Timares, L.; Barry, M. A.*, et al.*, A library-selected, Langerhans cell-targeting peptide enhances an immune response. *DNA Cell Biol.* 2004, *23* (11), 742-752.
337. Slamon, D. J.; Godolphin, W.; Jones, L. A.; Holt, J. A.; Wong, S. G.*, et al.*, Studies of the HER-2/neu proto-oncogene in human breast and ovarian cancer. *Science* 1989, *244* (4905), 707-12.
338. Lu, Y.; Yang, J.; Sega, E., Issues related to targeted delivery of proteins and peptides. *AAPS J.* 2006, *8* (3), E466-78.
339. McGregor, D. P., Discovering and improving novel peptide therapeutics. *Curr. Opin. Pharmacol.* 2008, *8* (5), 616-9.
340. Otvos, L., Jr., Peptide-based drug design: here and now. *Methods Mol. Biol.* 2008, *494*, 1-8.
341. Nestor, J. J., 2.14 - Peptide and Protein Drugs: Issues and Solutions. In *Comprehensive Medicinal Chemistry II*, Editors-in-Chief: John, B. T.; David, J. T., Eds. Elsevier: Oxford, 2007; pp 573-601.

342. Ahmed, N.; Riley, C.; Rice, G. E.; Quinn, M. A.; Baker, M. S., Alpha(v)beta(6) integrin-A marker for the malignant potential of epithelial ovarian cancer. *J. Histochem. Cytochem.* 2002, *50* (10), 1371-80.
343. Arihiro, K.; Kaneko, M.; Fujii, S.; Inai, K.; Yokosaki, Y., Significance of alpha 9 beta 1 and alpha v beta 6 integrin expression in breast carcinoma. *Breast Cancer* 2000, *7* (1), 19-26.
344. Bates, R. C.; Bellovin, D. I.; Brown, C.; Maynard, E.; Wu, B.*, et al.*, Transcriptional activation of integrin beta6 during the epithelial-mesenchymal transition defines a novel prognostic indicator of aggressive colon carcinoma. *J. Clin. Invest.* 2005, *115* (2), 339-47.
345. Hamidi, S.; Salo, T.; Kainulainen, T.; Epstein, J.; Lerner, K.*, et al.*, Expression of alpha(v)beta6 integrin in oral leukoplakia. *Br. J. Cancer* 2000, *82* (8), 1433-40.
346. Breuss, J.; Gallo, J.; DeLisser, H.; Klimanskaya, I.; Folkesson, H.*, et al.*, Expression of the beta 6 integrin subunit in development, neoplasia and tissue repair suggests a role in epithelial remodeling. *J. Cell Sci.* 1995, *108* (6), 2241-2251.
347. Kawashima, A.; Tsugawa, S.; Boku, A.; Kobayashi, M.; Minamoto, T.*, et al.*, Expression of alphav integrin family in gastric carcinomas: increased alphavbeta6 is associated with lymph node metastasis. *Pathol. Res. Pract.* 2003, *199* (2), 57-64.
348. Hazelbag, S.; Kenter, G.; Gorter, A.; Dreef, E.; Koopman, L.*, et al.*, Overexpression of the αvβ6 integrin in cervical squamous cell carcinoma is a prognostic factor for decreased survival. *J. Pathol.* 2007, *212* (3), 316-324.
349. Hecht, J. L.; Dolinski, B. M.; Gardner, H. A.; Violette, S. M.; Weinreb, P. H., Overexpression of the alphavbeta6 integrin in endometrial cancer. *Appl. Immunohistochem. Mol. Morphol.* 2008, *16* (6), 543-7.
350. Jones, J.; Watt, F. M.; Speight, P. M., Changes in the expression of alpha v integrins in oral squamous cell carcinomas. *J. Oral Pathol. Med.* 1997, *26* (2), 63-8.
351. Regezi, J. A.; Ramos, D. M.; Pytela, R.; Dekker, N. P.; Jordan, R. C., Tenascin and beta 6 integrin are overexpressed in floor of mouth in situ carcinomas and invasive squamous cell carcinomas. *Oral Oncol.* 2002, *38* (4), 332-6.
352. Thomas, G. J.; Nystrom, M. L.; Marshall, J. F., Alphavbeta6 integrin in wound healing and cancer of the oral cavity. *J. Oral Pathol. Med.* 2006, *35* (1), 1-10.
353. Hynes, R. O., Integrins: bidirectional, allosteric signaling machines. *Cell* 2002, *110* (6), 673-87.

354. Sheppard, D.; Rozzo, C.; Starr, L.; Quaranta, V.; Erle, D. J.*, et al.*, Complete amino acid sequence of a novel integrin beta subunit (beta 6) identified in epithelial cells using the polymerase chain reaction. *J. Biol. Chem.* 1990, *265* (20), 11502-7.
355. Haapasalmi, K.; Zhang, K.; Tonnesen, M.; Olerud, J.; Sheppard, D.*, et al.*, Keratinocytes in human wounds express alpha v beta 6 integrin. *J. Invest. Dermatol.* 1996, *106* (1), 42-8.
356. Yang, G. Y.; Xu, K. S.; Pan, Z. Q.; Zhang, Z. Y.; Mi, Y. T.*, et al.*, Integrin alpha v beta 6 mediates the potential for colon cancer cells to colonize in and metastasize to the liver. *Cancer Sci.* 2008, *99* (5), 879-87.
357. Marsh, D.; Dickinson, S.; Neill, G. W.; Marshall, J. F.; Hart, I. R.*, et al.*, alpha vbeta 6 Integrin promotes the invasion of morphoeic basal cell carcinoma through stromal modulation. *Cancer Res.* 2008, *68* (9), 3295-303.
358. Hausner, S. H.; DiCara, D.; Marik, J.; Marshall, J. F.; Sutcliffe, J. L., Use of a peptide derived from foot-and-mouth disease virus for the noninvasive imaging of human cancer: generation and evaluation of 4-[18F]fluorobenzoyl A20FMDV2 for in vivo imaging of integrin alphavbeta6 expression with positron emission tomography. *Cancer Res.* 2007, *67* (16), 7833-40.
359. Hausner, S. H.; Abbey, C. K.; Bold, R. J.; Gagnon, M. K.; Marik, J.*, et al.*, Targeted in vivo imaging of integrin alphavbeta6 with an improved radiotracer and its relevance in a pancreatic tumor model. *Cancer Res.* 2009, *69* (14), 5843-50.
360. Ruoslahti, E., RGD and other recognition sequences for integrins. *Annu. Rev. Cell Dev. Biol.* 1996, *12*, 697-715.
361. Jackson, T.; Sharma, A.; Ghazaleh, R. A.; Blakemore, W. E.; Ellard, F. M.*, et al.*, Arginine-glycine-aspartic acid-specific binding by foot-and-mouth disease viruses to the purified integrin alpha(v)beta3 in vitro. *J. Virol.* 1997, *71* (11), 8357-61.
362. Jackson, T.; Blakemore, W.; Newman, J. W.; Knowles, N. J.; Mould, A. P.*, et al.*, Foot-and-mouth disease virus is a ligand for the high-affinity binding conformation of integrin alpha5beta1: influence of the leucine residue within the RGDL motif on selectivity of integrin binding. *J. Gen. Virol.* 2000, *81* (Pt 5), 1383-91.
363. Jackson, T.; Sheppard, D.; Denyer, M.; Blakemore, W.; King, A. M. Q., The Epithelial Integrin alphav beta6 is Receptor for Foot-and-Mouth Disease Virus. *J. Virol.* 2000, *74* (11), 4949-4956.
364. Jackson, T.; Mould, A. P.; Sheppard, D.; King, A. M., Integrin alphavbeta1 is a receptor for foot-and-mouth disease virus. *J. Virol.* 2002, *76* (3), 935-41.

365. Villaverde, A.; Feliu, J. X.; Harbottle, R. P.; Benito, A.; Coutelle, C., A recombinant, arginine-glycine-aspartic acid (RGD) motif from foot-and-mouth disease virus binds mammalian cells through vitronectin and, to a lower extent, fibronectin receptors. *Gene* 1996, *180* (1-2), 101-6.
366. Prudkin, L.; Liu, D. D.; Ozburn, N. C.; Sun, M.; Behrens, C.*, et al.*, Epithelial-to-mesenchymal transition in the development and progression of adenocarcinoma and squamous cell carcinoma of the lung. *Modern Pathol.* 2009, *22* (5), 668-678.
367. Alley, S. C.; Okeley, N. M.; Senter, P. D., Antibody-drug conjugates: targeted drug delivery for cancer. *Curr. Opin. Chem. Biol.* 2010, *14* (4), 529-537.
368. Mammen, M.; Choi, S. K.; Whitesides, G. M., Polyvalent interactions in biological systems: implications for design and use of multivalent ligands and inhibitors. *Angew. Chem., Int. Ed.* 1998, *37* (20), 2754-2794.
369. Kiessling, L. L.; Gestwicki, J. E.; Strong, L. E., Synthetic multivalent ligands in the exploration of cell-surface interactions. *Curr. Opin. Chem. Biol.* 2000, *4* (6), 696-703.
370. Helms, B. A.; Reulen, S. W. A.; Nijhuis, S.; Graaf-Heuvelmans, P. T. H. M. d.; Merkx, M.*, et al.*, High-Affinity Peptide-Based Collagen Targeting Using Synthetic Phage Mimics: From Phage Display to Dendrimer Display. *J. Am. Chem. Soc.* 2009, *131* (33), 11683-11685.
371. Bastings, M. M. C.; Helms, B. A.; van Baal, I.; Hackeng, T. M.; Merkx, M.*, et al.*, From Phage Display to Dendrimer Display: Insights into Multivalent Binding. *J. Am. Chem. Soc.* 2011, *133* (17), 6636-6641.
372. Loi, M.; Marchio, S.; Becherini, P.; Di Paolo, D.; Soster, M.*, et al.*, Combined targeting of perivascular and endothelial tumor cells enhances anti-tumor efficacy of liposomal chemotherapy in neuroblastoma. *J. Control. Release* 2010, *145* (1), 66-73.
373. Akinc, A.; Querbes, W.; De, S.; Qin, J.; Frank-Kamenetsky, M.*, et al.*, Targeted Delivery of RNAi Therapeutics With Endogenous and Exogenous Ligand-Based Mechanisms. *Mol. Ther.* 2010, *18* (7), 1357-1364.
374. Copland, M. J.; Baird, M. A.; Rades, T.; McKenzie, J. L.; Becker, B.*, et al.*, Liposomal delivery of antigen to human dendritic cells. *Vaccine* 2003, *21* (9-10), 883-890.
375. Espuelas, S.; Haller, P.; Schuber, F.; Frisch, B., Synthesis of an Amphiphilic Tetraantennary Mannosyl Conjugate and Incorporation into Liposome Carriers. *Bioorg. Med. Chem. Lett.* 2003, *13* (15), 2557-2560.
376. Heurtault, B.; Gentine, P.; Thomann, J.-S.; Baehr, C.; Frisch, B.*, et al.*, Design of a Liposomal Candidate Vaccine Against Pseudomonas

aeruginosa and its Evaluation in Triggering Systemic and Lung Mucosal Immunity. *Pharm. Res.* 2008, *26* (2), 276-285.
377. Martin, A. L.; Li, B.; Gillies, E. R., Surface Functionalization of Nanomaterials with Dendritic Groups: Toward Enhanced Binding to Biological Targets. *J. Am. Chem. Soc.* 2009, *131* (2), 734-741.
378. Shmeeda, H.; Even-Chen, S.; Honen, R.; Cohen, R.; Weintraub, C.*, et al.*, Enzymatic Assays for Quality Control and Pharmacokinetics of Liposome Formulations: Comparison with Nonenzymatic Conventional Methodologies. In *Method. Enzymology*, Elsevier: 2003; Vol. 367.
379. Abraham, S. A.; Waterhouse, D. N.; Mayer, L. D.; Cullis, P. R.; Madden, T. D.*, et al.*, The Liposomal Formulation of Doxorubicin. In *Method. Enzymology*, Elsevier: 2005; Vol. 391.
380. Dubey, P. K.; Mishra, V.; Jain, S.; Mahor, S.; Vyas, S., Liposomes modified with cyclic RGD peptide for tumor targeting. *J. Drug Targeting* 2004, *12* (5), 257-264.
381. Moore, N. W.; Kuhl, T. L., The role of flexible tethers in multiple ligand-receptor bond formation between curved surfaces. *Biophys. J.* 2006, *91* (5), 1675-87.
382. Allen, T. M.; Mumbengegwi, D. R.; Charrois, G. J., Anti-CD19-targeted liposomal doxorubicin improves the therapeutic efficacy in murine B-cell lymphoma and ameliorates the toxicity of liposomes with varying drug release rates. *Clin. Cancer Res.* 2005, *11* (9), 3567-73.
383. Pastorino, F.; Brignole, C.; Marimpietri, D.; Sapra, P.; Moase, E. H.*, et al.*, Doxorubicin-loaded Fab' fragments of anti-disialoganglioside immunoliposomes selectively inhibit the growth and dissemination of human neuroblastoma in nude mice. *Cancer Res.* 2003, *63* (1), 86-92.
384. Lopes de Menezes, D. E.; Pilarski, L. M.; Allen, T. M., In vitro and in vivo targeting of immunoliposomal doxorubicin to human B-cell lymphoma. *Cancer Res.* 1998, *58* (15), 3320-30.
385. Park, J. W., Liposome-based drug delivery in breast cancer treatment. *Breast Cancer Res.* 2002, *4* (3), 95-9.
386. Mamot, C.; Ritschard, R.; Vogel, B.; Dieterle, T.; Bubendorf, L.*, et al.* In *A Phase I Study of Doxorubicin-loaded anti-EGFR Immunoliposomes in Patients with Advanced Solid Tumors*, 2011 ASCO Annual Meeting, Chicago, IL, Chicago, IL, 2011.
387. Schmidt, M. M.; Wittrup, K. D., A modeling analysis of the effects of molecular size and binding affinity on tumor targeting. *Mol. Cancer Ther.* 2009, *8* (10), 2861-71.
388. Perrault, S. D.; Walkey, C.; Jennings, T.; Fischer, H. C.; Chan, W. C., Mediating tumor targeting efficiency of nanoparticles through design. *Nano Lett.* 2009, *9* (5), 1909-15.

389. Fujimori, K.; Covell, D. G.; Fletcher, J. E.; Weinstein, J. N., A modeling analysis of monoclonal antibody percolation through tumors: a binding-site barrier. *J. Nucl. Med.* 1990, *31* (7), 1191-8.
390. Thurber, G. M.; Schmidt, M. M.; Wittrup, K. D., Antibody tumor penetration: transport opposed by systemic and antigen-mediated clearance. *Adv. Drug Deliv. Rev.* 2008, *60* (12), 1421-34.
391. Rudnick, S. I.; Lou, J.; Shaller, C. C.; Tang, Y.; Klein-Szanto, A. J.*, et al.*, Influence of affinity and antigen internalization on the uptake and penetration of Anti-HER2 antibodies in solid tumors. *Cancer Res.* 2011, *71* (6), 2250-9.
392. Alon, T.; Hemo, I.; Itin, A.; Pe'er, J.; Stone, J.*, et al.*, Vascular endothelial growth factor acts as a survival factor for newly formed retinal vessels and has implications for retinopathy of prematurity. *Nat. Med.* 1995, *1* (10), 1024-8.
393. Benjamin, L. E.; Keshet, E., Conditional switching of vascular endothelial growth factor (VEGF) expression in tumors: induction of endothelial cell shedding and regression of hemangioblastoma-like vessels by VEGF withdrawal. *Proc. Natl. Acad. Sci. U. S. A.* 1997, *94* (16), 8761-6.
394. Kerbel, R.; Folkman, J., Clinical translation of angiogenesis inhibitors. *Nat. Rev. Cancer* 2002, *2* (10), 727-39.
395. Goel, S.; Wong, A. H.; Jain, R. K., Vascular normalization as a therapeutic strategy for malignant and nonmalignant disease. *Cold Spring Harb. Perspect. Med.* 2012, *2* (3), a006486.
396. Tong, R. T.; Boucher, Y.; Kozin, S. V.; Winkler, F.; Hicklin, D. J.*, et al.*, Vascular normalization by vascular endothelial growth factor receptor 2 blockade induces a pressure gradient across the vasculature and improves drug penetration in tumors. *Cancer Res.* 2004, *64* (11), 3731-6.
397. Dickson, P. V.; Hamner, J. B.; Sims, T. L.; Fraga, C. H.; Ng, C. Y.*, et al.*, Bevacizumab-induced transient remodeling of the vasculature in neuroblastoma xenografts results in improved delivery and efficacy of systemically administered chemotherapy. *Clin. Cancer Res.* 2007, *13* (13), 3942-50.
398. Pastorino, F.; Brignole, C.; Di Paolo, D.; Nico, B.; Pezzolo, A.*, et al.*, Targeting liposomal chemotherapy via both tumor cell-specific and tumor vasculature-specific ligands potentiates therapeutic efficacy. *Cancer Res.* 2006, *66* (20), 10073-82.
399. Ruoslahti, E., The RGD story: a personal account. *Matrix Biol.* 2003, *22* (6), 459-65.
400. Deutsch, H. M.; Glinski, J. A.; Hernandez, M.; Haugwitz, R. D.; Narayanan, V. L.*, et al.*, Synthesis of congeners and prodrugs. 3. Water-

soluble prodrugs of taxol with potent antitumor activity. *J. Med. Chem.* 1989, *32* (4), 788-92.
401. Mathew, A. E.; Mejillano, M. R.; Nath, J. P.; Himes, R. H.; Stella, V. J., Synthesis and evaluation of some water-soluble prodrugs and derivatives of taxol with antitumor activity. *J. Med. Chem.* 1992, *35* (1), 145-51.
402. Wang, S.; Zhelev, N. Z.; Duff, S.; Fischer, P. M., Synthesis and biological activity of conjugates between paclitaxel and the cell delivery vector penetratin. *Bioorg. Med. Chem. Lett.* 2006, *16* (10), 2628-31.
403. Ryppa, C.; Mann-Steinberg, H.; Biniossek, M. L.; Satchi-Fainaro, R.; Kratz, F., In vitro and in vivo evaluation of a paclitaxel conjugate with the divalent peptide E-[c(RGDfK)2] that targets integrin alpha v beta 3. *Int. J. Pharm.* 2009, *368* (1-2), 89-97.
404. Horwitz, S. B., Taxol (paclitaxel): mechanisms of action. *Ann. Oncol.* 1994, *5 Suppl 6*, S3-6.
405. Abu Ajaj, K.; Biniossek, M. L.; Kratz, F., Development of protein-binding bifunctional linkers for a new generation of dual-acting prodrugs. *Bioconjug. Chem.* 2009, *20* (2), 390-6.
406. Dubikovskaya, E. A.; Thorne, S. H.; Pillow, T. H.; Contag, C. H.; Wender, P. A., Overcoming multidrug resistance of small-molecule therapeutics through conjugation with releasable octaarginine transporters. *Proc. Natl. Acad. Sci. U. S. A.* 2008, *105* (34), 12128-33.
407. Kumar, S. K.; Williams, S. A.; Isaacs, J. T.; Denmeade, S. R.; Khan, S. R., Modulating paclitaxel bioavailability for targeting prostate cancer. *Bioorg. Med. Chem.* 2007, *15* (14), 4973-84.
408. Cao, Q.; Li, Z. B.; Chen, K.; Wu, Z.; He, L.*, et al.*, Evaluation of biodistribution and anti-tumor effect of a dimeric RGD peptide-paclitaxel conjugate in mice with breast cancer. *Eur. J. Nucl. Med. Mol. Imaging* 2008, *35* (8), 1489-98.
409. Taherian, A.; Li, X.; Liu, Y.; Haas, T. A., Differences in integrin expression and signaling within human breast cancer cells. *BMC Cancer* 2011, *11*, 293.
410. Cannistra, S. A.; Ottensmeier, C.; Niloff, J.; Orta, B.; DiCarlo, J., Expression and function of beta 1 and alpha v beta 3 integrins in ovarian cancer. *Gynecol. Oncol.* 1995, *58* (2), 216-25.
411. Bareford, L. M.; Swaan, P. W., Endocytic mechanisms for targeted drug delivery. *Adv. Drug Deliv. Rev.* 2007, *59* (8), 748-58.
412. Conner, S. D.; Schmid, S. L., Regulated portals of entry into the cell. *Nature* 2003, *422* (6927), 37-44.
413. Christie, R. J.; Grainger, D. W., Design strategies to improve soluble macromolecular delivery constructs. *Adv. Drug Deliv. Rev.* 2003, *55* (3), 421-37.

414. Parton, R. G.; Simons, K., The multiple faces of caveolae. *Nat. Rev. Mol. Cell. Biol.* 2007, *8* (3), 185-94.
415. Thomas, G., Furin at the cutting edge: from protein traffic to embryogenesis and disease. *Nat. Rev. Mol. Cell Biol.* 2002, *3* (10), 753-66.
416. Wang, T.; Zhao, J.; Ren, J. L.; Zhang, L.; Wen, W. H.*, et al.*, Recombinant immunoproapoptotic proteins with furin site can translocate and kill HER2-positive cancer cells. *Cancer Res.* 2007, *67* (24), 11830-9.
417. Kreitman, R. J., Immunotoxins for targeted cancer therapy. *AAPS J.* 2006, *8* (3), E532-51.
418. Teicher, B. A.; Chari, R. V., Antibody conjugate therapeutics: challenges and potential. *Clin. Cancer Res.* 2011, *17* (20), 6389-97.
419. Doronina, S. O.; Toki, B. E.; Torgov, M. Y.; Mendelsohn, B. A.; Cerveny, C. G.*, et al.*, Development of potent monoclonal antibody auristatin conjugates for cancer therapy. *Nat. Biotechnol.* 2003, *21* (7), 778-84.